



Memòria presentada per optar al títol de doctor dins el

**Programa de doctorat en Enginyeria i Tecnologies Avançades**

# Smart Chemical Sensors: Concepts and Application

---

**Author:** Sergi Udina Oliva

**Director:** Dr. Santiago Marco

Barcelona, May 2012



*Al meu pare,*

---

## ABBREVIATIONS

## ACKNOWLEDGEMENT

## *PREFACI*

---

---

## 1. INTRODUCTION

---

1.1 Smart sensors basics.....	1
1.2 Chemical sensors.....	4
1.3 Current trends in chemical sensing.....	7
1.4 Overview of smart sensor standards.....	8
1.4.1 The IEEE-1451 family of standards.....	9
1.4.2 IEEE-1451.2.....	14
1.4.3 BS-7986.....	17
1.5 Selected examples.....	19
1.5.1 IEEE 1451 Environmental monitor.....	20
1.5.2 IEEE 1451.2 Gas measurement system.....	21
1.5.3 Self-validating dissolved oxygen sensor.....	22
1.5.4 Self-validating pressure sensor.....	22
1.6 Smart sensors outlook .....	24

---

## 2. A SELECTED APPLICATION: NATURAL GAS QUALITY CONTROL

---

2.1 Natural gas significance.....	27
2.2 The importance of quality control.....	28
2.3 Instruments and techniques for natural gas quality control.....	29
2.3.1 Combustion calorimeters.....	30
2.3.2 The process gas chromatograph (PGC).....	32
2.3.3 Correlative methods.....	33
2.3.3.1 Dielectric permittivity method.....	33
2.3.3.2 IR spectrometry.....	34
2.3.3.3 VOS-Meter.....	34
2.3.3.4 WOM 2000.....	35
2.3.3.5 EMC 500.....	36
2.3.3.6 Gas-PT.....	37

2.3.3.7. Gas-Las Q1.....	37
2.3.3.8. Methane number microsensor.....	38
2.3.3.9. ANGus.....	39
2.3.3.10. Research approaches based on thermal conductivity.....	40
2.4. Gas sensing technologies.....	41
2.4.1. Conducting polymer sensors.....	41
2.4.2. Quartz crystal sensors.....	41
2.4.3. Electrochemical sensors.....	43
2.4.4. Infrared based gas sensors.....	43
2.4.4.1. NDIR.....	44
2.4.4.2. Photoacoustic devices.....	46
2.4.5. Colorimetric gas sensors.....	48
2.4.6. Fiber optic based gas sensors.....	48
2.4.7. Pellistors.....	49
2.4.8. Thermal conductivity sensors.....	49
2.4.9. Metal-oxide semiconductor sensors.....	51
2.4.10. Velocity of sound sensors.....	52
2.4.11. Microfluidic oscillator sensors.....	52
2.4.12. Dielectric permittivity sensors.....	53
2.5. Comparison of considered technologies.....	53

### 3. OBJECTIVES

3. Objectives.....	55
--------------------	----

## 4. STUDY OF A NOVEL APPROACH:A MICROMACHINED THERMOELECTRIC GAS SENSOR FOR NATURAL GAS ANALYSIS

4.1. Introduction.....	58
4.2. Sensor fabrication and operating principle.....	59
4.3. Sensor characterization.....	62
4.4. Thermal conductivity of gas mixtures .....	63
4.5. Physical model .....	66
4.6. Model results and validation.....	68
4.6.1. Laboratory testbench and validation results.....	69
4.6.2. IR imaging and discussion.....	73
4.7. Estimation of the sensor sensitivity.....	73
4.8. Chapter conclusions.....	77

## 5. MICROMACHINED THERMOELECTRIC GAS SENSOR FOR NATURAL GAS ANALYSIS: CALIBRATION

---

5.1. Introduction.....	79
5.2. Multivariate calibration: methodology.....	80
5.2.1. Simulation setup.....	80
5.2.2. Experimental setup.....	81
5.2.3. Signal processing.....	85
5.2.4. Uncertainty analysis.....	86
5.2.5. Validation.....	88
5.2.6. Performance limits estimation.....	89
5.3. Multivariate calibration results and discussion.....	90
5.3.1. Calibration and validation results.....	90
5.3.2. Uncertainty analysis results.....	94
5.3.3. Performance limits estimation results.....	97
5.4. Chapter conclusions.....	100

## 6. SMART CHEMICAL SENSOR DESIGN: THE NATURAL GAS ANALYZER PROTOTYPE

---

6.1. Introduction.....	102
6.2. Description of the electronic instrumentation.....	103
6.2.1. Sensor excitation.....	105
6.2.2. Sensor reading.....	107
6.2.3. Combined implementation of IEEE-1451 and BS-7986 standards.....	109
6.2.4. Communications.....	113
6.2.5. PC data-logging software.....	114
6.3. Signal processing.....	115
6.3.1. Signal pre-processing and temperature correction.....	116
6.3.2. PLS regression.....	118
6.3.3. Fault detection.....	119
6.3.3.1. Univariate fault detection.....	119
6.3.3.2. Multivariate fault detection.....	123
6.3.4. Training and operation modes.....	123
6.4. Experimental.....	124
6.4.1. Sensor chamber and sampling.....	124
6.4.2. Design of experiments.....	125
6.4.3. Validation measurements.....	126
6.5. Test results.....	127
6.6. Chapter conclusions.....	130

---

## 7. CONCLUSIONS

---

7. Conclusions.....	131
---------------------	-----

---

## REFERENCES

---

References .....	133
------------------	-----

---

## APPENDIX A: UNCERTAINTY ANALYSIS DETAILS

## APPENDIX B: LIST OF PUBLICATIONS

## APPENDIX C: RESUM EN CATALÀ

---

## ABBREVIATIONS

---

AC	Alternating current
ADC	Analog to digital converter
BSI	British standards institute
CHEMFET	Chemically sensitized field effect transistor
CMOS	Complementary metal oxide semiconductor
CORBA	Common Object Request Broker Architecture
DAC	Digital to analog converter
DC	Direct current
FET	Field effect transistor
FID	Flame ionization detector
FPGA	Field programmable gate array
FS	Full scale
FTIR	Fourier transform infrared
GC	Gas chromatograph/y
GPS	Global Positioning System
IEEE	Institute of Electrical and Electronics Engineers
IR	Infrared
LEL	Lower explosive level
MEMS	Micro-electromechanical system
MOSFET	Metal oxide semiconductor field effect transistor
MOX	Metal oxide
MS	Mass spectroscopy
MTGS	Micromachined thermoelectric gas sensor
NCAP	Network capable application processor
NDIR	Non-dispersive infra-red
NIR	Near infra-red

NIST	National Institute for Standards and Testing
NMR	Nuclear magnetic resonance
PDF	Probablity distribution function
PEL	Permissible exposure limit
PGC	Process gas chromatograph/y
PLS	Partial least squares (aka Projection to latent structures)
QMB	Quartz crystal microbalance
RMS	Root mean square
SAW	Surface acoustic wave
SEVA	Self-validating
SHV	Superior heating value
SNR	Signal to noise ratio
STIM	Smart transducer interface module
TEDS	Transducer electronic data sheets
TGS	Taguchi gas sensor
TII	Transducer independent interface
TIM	Transducer interface module
UEL	Upper explosive level
USB	Universal serial bus
VCSEL	Vertical cavity surface emitting laser
VHDL	VHSIC hardware description language
VHSIC	Very high-speed integrated circuits
VU	Validated uncertainty
VV	Validated value

## ACKNOWLEDGEMENT

---

Many people have contributed to help me build this PhD thesis at many different levels, I wish to acknowledge people and institutions who have contributed in the scientific, technical, funding, and management aspects.

Dr. Carlos Calaza, Dr. Guillem Carles and Dr. Manuel Carmona have crucially contributed to the FEM simulation tasks with ANSYS. Dr. Jose Bosch contributed strongly in the implementation of IEEE-1451.2 protocols, communications, and acquisition software. And also for his supervision of this work. Dr. Antonio Pardo provided essential background information and endless support throughout the thesis. He is also acknowledged for the supervision of this work. Dr. Pere Miribel is also acknowledged for his supervision. Dr. Eva Martin provided wonderful project managing and communication with the university patent center. Dr. Alex Perera is acknowledged for his necessary feedback to build the SIGMA-STS labview gas sensor test station. M.Sc. Luis Fernandez is acknowledged for joining his efforts to mine in rebuilding gas test station. Dr. Ricardo Gutierrez-Osuna is acknowledged for his excellent course in pattern recognition, and his annoying ICA exercise. Dr. Zeev Karpas is acknowledged for his kind paper revision. Dr. Ricardo Leardi is acknowledged for his interesting course on design of experiments and for allowing the use of his response surface software for the sensitivity analysis in chapter 4. Prof. Pascual Segura and Montserrat Jané from the centre de patents de la UB are acknowledged for their assistance in composing the patent proposals. Manuel Mena at ENAGAS regasification plant in Barcelona is acknowledged for his kind guidance and knowledgeable feedback throughout the visit to the center in 2008. Prof. Santiago Marco, director of this PhD thesis, is also acknowledged and recognised for his never-ending support and commitment to making this PhD thesis as good as possible. The people at the Departament d'electrònica de la Universitat de Barcelona are acknowledged, and particularly the people at administration and workshop, for their help on paperwork, and prototyping respectively. Special thanks to Paco Udina for his assistance in the cover design.

ISP group is a consolidated Grup de Recerca de la Generalitat de Catalunya and has support from the *Departament d'Universitats, Recerca i Societat de la Informació de la Generalitat de Catalunya* (*expedient 2009 SGR 0753*). This work has received support from the *Comissionat per a Universitats i Recerca del DIUE de la Generalitat de Catalunya* and the European Social Fund (ESF). Project TEC2004-07853-C02-01 is also acknowledged for funding the research, and also the Spanish ministry of education and science for bestowing the FPI PhD grant on the author.

## PREFACI

Era la tardor de l'any 2005, estàvem asseguts davant l'ordinador, jo estava encara mastegant i remastegant tota la informació reunida en l'estudi de l'estat de l'art. Tot donant voltes a com podriem tenir un sensor basat en conductivitat tèrmica que fos prou ràpid i fiable, en Santi va dir "podríamos utilizar las termopilas de Carlos". Probablement la contribució més important d'aquest treball ven prendre forma en els cinc segons que van seguir aquesta frase.

Cinc segons... que s'han extès en gairebé set anys de treballs. Aquest llarg trajecte ha estat gràcies a la oportunitat que va sorgir al final dels 4 anys corresponents a la beca predoctoral, de valoritzar les patents presentades amb el projecte VALTEC08-2-0043 (abreviat VALTEC) concedit pel CIDEM-ACCIO (Generalitat de Catalunya). Tot i així, els resultats aquí ressenyats corresponen en un 99% a experiments i enginyeria elaborada durant els quatre anys primers corresponents a la beca FPI. Ha estat precisament degut a les tasques del projecte VALTEC, que no ha estat possible finalitzar la redacció d'aquest tesi fins al cap de gairebé 7 anys del seu inici.

A part dels aspects tècnics, científics i de gestió, hi ha sens dubte una vessant personal molt important en l'elaboració d'una tesi doctoral. Aquest prefaci està dedicat a aquesta gent que ha incidit de forma fonamental en el pla personal. Durant aquest set anys he viscut moments excel·lents, i també moments molt difícils. Aquesta tesi no seria tal com és si no fos per les persones que han estat al meu voltant durant aquests anys.

Vull agrair molt especialment al Dr. Jordi Paretas, la Dra. Anna Isart, l'Aina Margenat i a la Maria Jorba el seu suport en els moments difícils d'aquesta tesi. Vull també agrair a Marta Pigem i Idoya Agudo la seva paciència i confiança. Així com al Dr. Fèlix Casanova i a Sonia Maestre pel seu consell i les bones estones.

Als Arreplegats de la Zona Universitària els he d'agrair el haver-me demostrat la irrealitat de l'impossible, i la meravellosa sublimació dels somnis. Als Castellers de Barcelona els he d'agrair el haver-me donat la oportunitat de donar-ho tot per fer crèixer la història de l'entitat. A Albert Arjona, Oriol Martinez, Sergi Argenton, Sergio Norte i Victor Garcia els he d'agrair les bones estones de creació, composició grabació del que ha acabat sent una bona col·lecció musical.

Finalment agrair a la meva mare tots els esforços i ajut que m'ha donat durant aquests anys.

# 1. INTRODUCTION

---

1.1 Smart sensors basics.....	1
1.2 Chemical sensors.....	4
1.3 Current trends in chemical sensing.....	7
1.4 Overview of smart sensor standards.....	8
1.4.1    The IEEE-1451 family of standards.....	9
1.4.2    IEEE-1451.2.....	14
1.4.3    BS-7986.....	17
1.5 Selected examples.....	19
1.5.1    IEEE 1451 Environmental monitor.....	20
1.5.2    IEEE 1451.2 Gas measurement system.....	21
1.5.3    Self-validating dissolved oxygen sensor.....	22
1.5.4    Self-validating pressure sensor.....	22
1.6 Smart sensors outlook .....	24

## 1.1 SMART SENSORS BASICS

**D**evelopments in the miniaturization of sensors and actuators, fostered by mature micromachining technologies and parallel improvements in microelectronics and packaging, have led to new generation sensors which have been usually termed *smart sensors*. However, there is often confusion about the term *smart sensor*. The term has been used differently throughout the literature [KoFung1982, IEEE1997, Song2008, Henry1993, Karatzas2007], making reference to sensors incorporating different new functionalities. In practice, the term *smart sensor* has been generally used to refer to a sensor which basically “does something more” than a conventional or traditional sensor. This “something more” can in most cases be described as the combined integration of different functionalities as shown in Fig. 1.1.

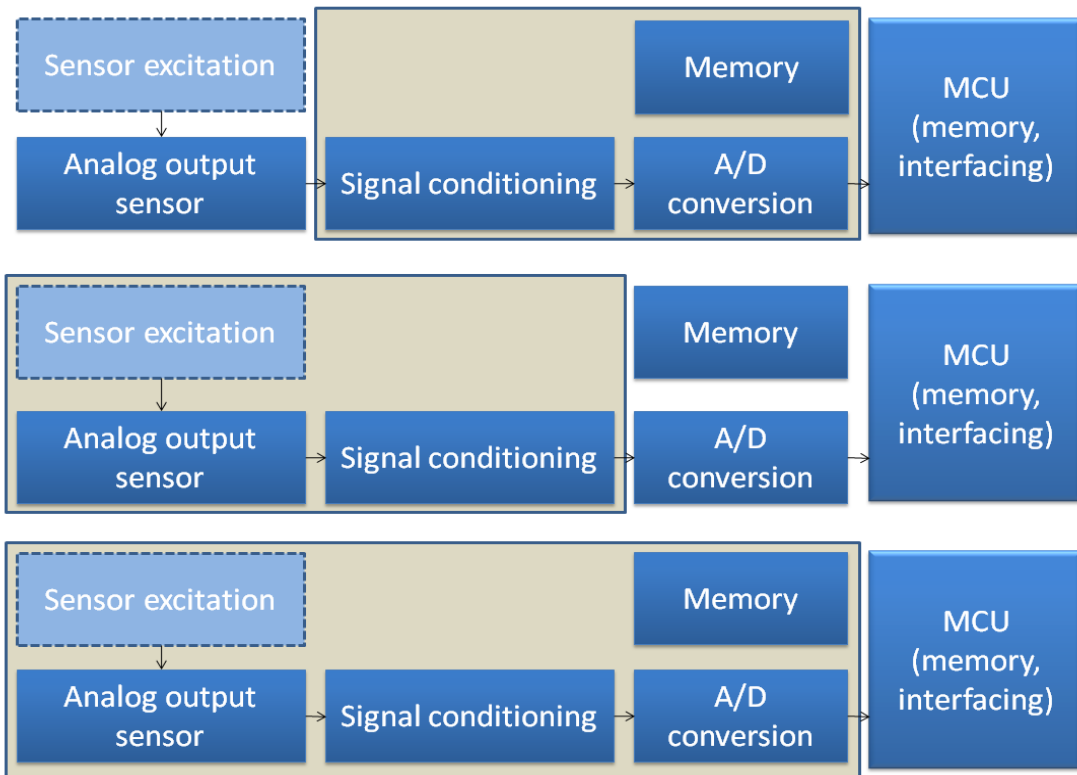


**Figure 1.1 Integration possibilities for smart sensors**

Several commercially available smart sensor examples can be found, such as the MEMS sensors line by Analog Devices Inc. (Boston, USA) including Gyroscopes, accelerometers, inertial sensors, temperature sensors and microphones with integrated analog to digital conversion. Also worth noting is the MEMS product line by the relatively new company Sensirion AG (Staefa, Switzerland) including temperature and humidity sensors, as well as flow and pressure sensors with again integrated calibration possibilities and digital conversion. According to the information by the latter

company, their proprietary technology CMOSens® is now in its fourth generation (see table 1.1) also Texas Instruments Inc. (Dallas, USA) commercializes a large number of smart temperature sensors with integrated calibration features and digital output.

**TABLE 1.1 GENERATIONS OF THE SMART SENSOR (CMOSSENS®) TECHNOLOGY BY SENSIIRION AG**

CMOSens technology	Features
<b>1<sup>st</sup> generation</b>	miniaturized sensor component
<b>2<sup>nd</sup> generation</b>	1st generation plus amplifier and A/D converter
<b>3<sup>rd</sup> generation</b>	2nd generation plus intelligence for linearization and temperature compensation
<b>4<sup>th</sup> generation</b>	3rd generation plus memory to hold calibration data

Source: [www.sensirion.com](http://www.sensirion.com) (Feb 2012)

For chip-sized sensors intended for PCB implementation, typical microelectronics digital interfaces such as SPI, I<sup>2</sup>C, or similar proprietary interfaces are common. In these particular cases where the chip sensor typically becomes part of an embedded system including a microcontroller, the adaptation to different interfaces is not extremely limiting. However, in many other cases the smart sensor may interface to other host systems and processors which might not be as flexible as a bare microcontroller. As a consequence the overall progress of this technology is often hindered by the need to choose between the many existing sensor networks and interfaces. This either restricts the connectivity of the equipment, or increases costs in case many networks protocols and interfaces are implemented.

In an effort to improve this situation the IEEE released the IEEE-1451 family of standards starting with the IEEE-1451.2 in 1997 [IEEE1997, Song2008], which intended to rationalize the design of smart sensors and provide a defined framework for smart sensors. IEEE-1451 is aimed generally to transducers, which include actuators as well as sensors, and defines the *smart transducer* as “a transducer that provides functions beyond those necessary for generating a correct representation of a sensed or controlled quantity.” but also pointing out that “This functionality typically simplifies the integration of the transducer into applications in a networked environment”, which provides some clarification of the “something more” that may be expected from a smart sensor. IEEE-1451 focuses mainly on the advanced features of self-identification to networks, availability of integrated calibration and status data, hot-plug capability and standard interfacing. An overview of the standard is provided in section 1.4.1. Another standard of current interest [Karatzas2001, Feng2009] is the BS-7986 for self-validating (SEVA) sensors, which focuses mainly in data quality self-assessment of the sensors, the formatting of standard status flags and data quality indicators as

well as expressing reliable uncertainty estimations in order to improve the reliability of sensors. This approach is highly relevant especially in critical process control applications, but can have wide applicability through most sensing applications. The standard is overviewed in section 1.4.2.

Both IEEE-1451 and BS-7986 are in some way complementary in the sense that they have a main focus on different advanced sensor functionalities. The combination of both standards was already suggested by Karatzas et al. [Karatzas2007] and is explored in this thesis by implementing this combination into a smart sensor prototype, which is described in chapter 6.

This introduction to smart sensors has so far considered smart sensors in general regardless of the type of primary sensor. However, chemical sensors are increasingly becoming a special case. Chemical sensing is in general a highly demanding task, typically involving the resolution of high dynamic ranges in presence of huge amounts of interfering factors such as environmental effects and cross-sensitivity to undesired chemical species. In most cases, the reactive nature of the sensors leads to slow degradation of the sensor and in general stability problems such as drift or even poisoning, which increase the need for sensor replacement with respect to other sensors. Going smart is a convenient way to deal with this replacement. Besides, there is a strong trend to chemical sensor arrays as a means of improving chemical instruments and as a consequence they usually require more complex signal analysis and processing than other types of sensors. These characteristics make them particularly suited candidates for smart sensors. Next section intends to briefly introduce the characteristics of chemical sensors.

## 1.2 CHEMICAL SENSORS

A chemical sensor can be defined as “a device that transforms chemical information, ranging from the concentration of a specific sample component to total composition analysis, into an analytically useful signal. In particular, said chemical information may originate from a chemical reaction of the analyte or from a physical property of the investigated system” [Hulanicki1991].

As described by [Hulanicki1991], chemical sensors consist of two parts, a receptor part and a transducer part. Some sensors may include a separator between the parts, for instance a membrane.

In the **receptor** part of a sensor the chemical information is transformed into a form of energy, or modulation of a property which can be converted to a signal by the transducer.

The **transducer** part is a device capable of transforming the energy carrying the chemical information about the sample into a useful analytical signal. The transducer as such does not show selectivity.

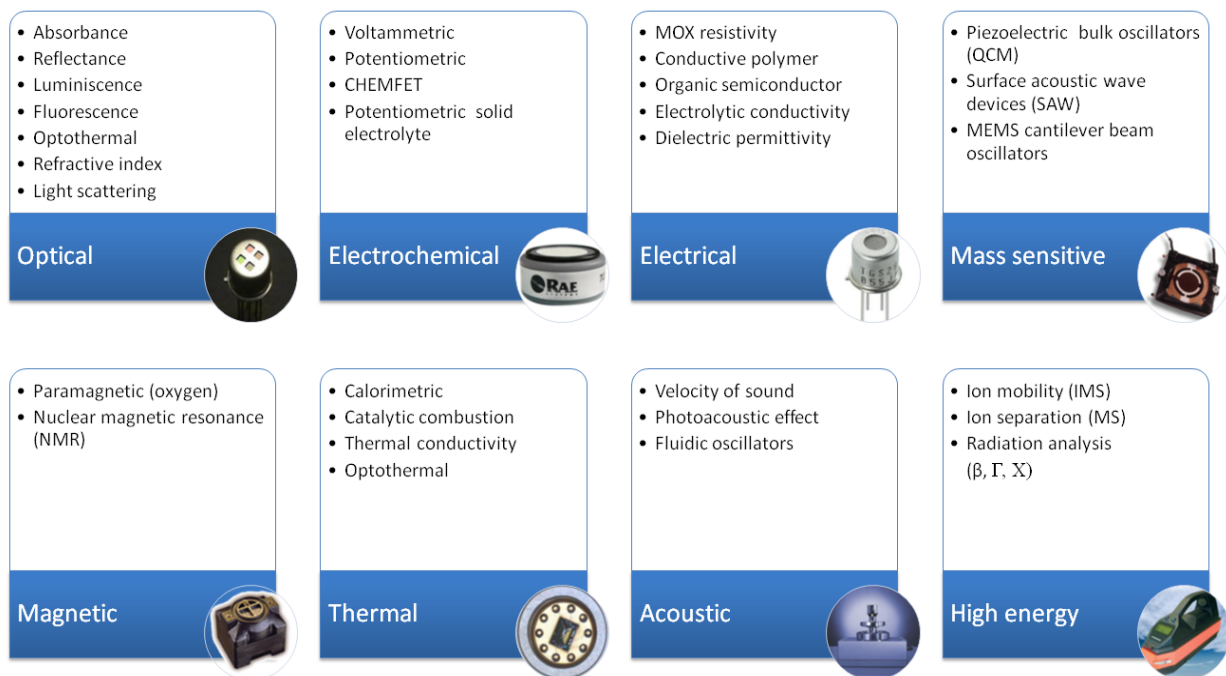


**Figure 1.2 A possible classification of chemical sensors<sup>1</sup>**

The receptor part of chemical sensors may be based upon various principles:

- **Physical**, where no chemical reaction takes place. Typical examples are those based upon measurement of absorbance, refractive index, conductivity, temperature or mass change. And in particular the thermal sensing approach finally adopted in this thesis.
- **Chemical**, in which a chemical reaction with participation of the analyte gives rise to the analytical signal. Typical examples are the electrochemical sensors and Metal-oxide semiconductor (MOX) sensors.
- **Biochemical**, in which a biochemical process is the source of the analytical signal. Typical examples are microbial potentiometric sensors or immunosensors. They may **be** regarded as a subgroup of the chemical ones. Such sensors are called **biosensors**.

<sup>1</sup> Miniature images correspond to: Quadruple Pyroelectric detector with integrated filters from pyreos, Edinburgh; Electrochemical sensor from RAE systems, USA; Taguchi gas sensor (MOX) from Figaro engineering Inc., Japan; Polymer coated QCM from ProTech scientific (Masscal corp.), USA; Paracube sensor, Servomex, USA; TCG-3880 sensor from Xensor inc., The Netherlands; Velocity of sound sensor from Anton Paar GmbH, Austria; IMS portable instrument from Elmulab Ltd., South Africa

In some cases it is not possible to decide unequivocally whether a sensor operates on a chemical or on a physical principle. This is, for example, the case when the signal is due to an adsorption process.

Chemical sensors are basic components of chemical instruments, together with the sampling, sample transport, signal processing and interfacing subsystems and any other additional ones that the instrument may incorporate. A visual review of the types of chemical sensors is shown in Fig. 1.2.

Note that Figure 1.2 does not consider one of the main techniques of analytical chemistry, chromatography, within the types of sensors, since it is a *separation* technique rather than a chemical sensing technique. Another example for this could be, for instance, a selective membrane which allowed only part of the components of a mixture through it. After the separation, a chemical sensor or detector is placed which can in most cases be attributed to one of the reported types in Fig. 1.2. For instance, considering the two most common gas chromatography (GC) detectors, the flame ionization detector (FID) and the thermal conductivity detector (TCD), would be adscribed to the high energy categories due to the ion producing pyrolysis that takes place at the high temperature flame of the detector; and to the thermal type of sensors respectively.

In general, separation techniques such as chromatography are compatible with any other kind of chemical sensor working as a detector. Examples of these are the GC setups proposed by Heberle et al. [Heberle2000] indenting the GC separation with a metal-oxide sensor detector, and Ruzsanyi et al. [Ruzsanyi2005] who proposed indenting the GC separation with an Ion mobility spectrometer (IMS).

In many current applications, a single chemical sensor is used to obtain an equilibrium or steady-state response which is more or less specific to a single analyte of interest [Janata1989, Janata2001, Gopel1991, Hierlemann2007]. This approach is analogous to that of most other types of sensors (e.g. temperature, light, humidity, pressure, flow, acceleration...). However, the single chemical sensor approach is typically highly vulnerable to interference, as the sensor specificity is never high enough as to reject all the vast numbers of chemical species which may appear undesirably in a measured sample, even immunosensors, particularly aimed for extremely high specificity, are known to show cross-sensitivity to similarly structured molecules [Calvo2011]. The high dimensionality of the chemical space is thus a problem for the single sensor approach.

A trend to sensor arrays and multisensor approaches as a means to increase the dimensionality of the sensor space and to be able to compensate or even measure the presence of interfering chemical species has been an ongoing research goal during the last three decades as reviewed by Hierlemann and Gutierrez-Osuna in 2007 [Hierlemann2007]. The field of electronic noses which conceptually started in 1982 with a work by Persaud et al. [Persaud1982] deserves a special

mention for two reasons. In first place it gave birth to a new topic in chemical instrument research, from which much has been learned about technology, signal processing and analysis, performance and limitations of chemical sensor arrays. In second place, it has been a long running research line in this research group where this thesis has been produced, and as a consequence it has influenced the strategy and methods selected in this work.

### 1.3 CURRENT TRENDS IN CHEMICAL SENSING

---

The current and many advances in Microsystems and materials technology are a strong technological push in the development of chemical sensors. Examples can be found in the development of chemical sensor arrays as reported by two exhaustive reviews by Hierlemann and Gutierrez-Osuna [Hierlemann2007, Gutierrez2010]. Other relevant examples can also be found in other technologies like the Micro Mass [Diaz2002, Sillon2002], Infrared [Pan2004, Hulme2004], and nuclear magnetic resonance (NMR) spectrometers [Kakuta2003], Micro Gas Chromatographs [Ohira2008] and more generally sensor systems belonging to the Micro-Total analysis systems (TAS) or lab-on-a-chip categories as reviewed by Arora and previously by Vilkner [Arora2010, Vilkner2004]. All of these approaches are subjects of intense investigation and development in the field of chemical and biochemical sensing.

Simultaneously, a second technological push is favouring the advances in chemical sensing - particularly chemical data analysis - over the last 40 years. Developments in signal and data processing associated with chemical instrumentation and sensing systems have consolidated the field of chemometrics as a well established area within chemistry, despite its relative youth (the field started around the 70s with the onset of computer processing) [Frank1982]. Among the whole set of available techniques, a group of *de facto* standards exists [Hierlemann2007, Jurs2000, Ramos1986]. These techniques such as Principal Component Regression or Partial Least Squares allow operating with huge data flows and high dimensionality spaces, and generating compact and practical (in the sense of useful) multivariable calibration models for sensor arrays, hyphenated instrumentation, or multisensor systems (either homogeneous or heterogeneous) [Jurs2000, Hierlemann2007].

This combined technological push is yet reinforced with the arising possibilities of solving historical industrial problems (olfactometric panels) or new ones (i.e.: medical diagnosis, chemical warfare) using new chemical instruments and sensors.

However, common problems of chemical sensors and instrumentation are often short time stability due to drift, high vulnerability to interference, and limited operational lifespan due to aging or poisoning. These problems can be dealt either from a sensor technology approach as reviewed by

Comini et al. [Comini2009(6.1)] or a data analysis approach [Padilla2010], as reviewed by Gutierrez-Osuna and Hierlemann [Gutierrez2010].

Electronic noses, Micro-Spectrometry and Micro-TAS, the latter two based on more established approaches of analytical chemistry – spectrometry and chromatography -, are of great interest in the hopes that chemical analysis which nowadays must be performed in the laboratory will be performed *in situ* or even *in vivo* –for biomedical applications-, with the obvious impact in medicine, security, food industry, etc...

Examples of the latest relevant achievements include works by the ETH institute (Zurich, Switzerland) such as the monolithic gas sensor arrays with integrated electronics [Frey2007], and also new approaches such as the fabrication of monolithic multiple quartz crystal microbalances as reviewed by Tuantranont et al. [Tuantranont2011], or monolithic immunofluorescence chips by another swiss institute, the EPFL (Lausane, Switzerland) [Dupont2010].

The approach in this work stands slightly apart from current trends towards high sensitivity and improved selectivity. The requirements for the selected application, natural gas analysis, are particularly stringent in regards to sensor stability and reliability, as explained in section 2. In addition, instrumentation in the field of natural gas analysis is characterized by a high conservatism and the selection of reliable and well-established technologies in most cases, what brings the field typically apart from the latest chemical sensing trends and applications. For this reason, the sensing approach was carefully considered and studied in order to solve the selected application reliably. Chapter 2 and in particular section 2.3 offer a detailed discussion on this subject.

## 1.4 OVERVIEW OF SMART SENSOR STANDARDS

Smart sensors can provide many advanced features, and the ways of implementing them can vary largely between different designs. This often leads to unnecessary recurrent engineering efforts. Standard proposals for implementing smart sensor features were issued since late 1990s, being the IEEE-1451.2 the first of these standards to appear. From that on, different IEEE-1451 standards appeared progressively, as shown in Figure 1.3, and explained in the next section.

Another standard worth mentioning was issued at the beginning of 2003 by the Object Management Group (OMG). It was a specification for a smart transducer interface standard [OMG2003] looking for a world-wide standard that satisfied the following needs: (i) real-time characteristics and functionalities for the smart transducer network (ii) online diagnostic service capability (iii) support for start-up and dynamic configuration (iv) a uniform naming and addressing scheme for all relevant data in the smart transducer system (v) a generic interface

enabling the smart transducer system to interact with other systems via a CORBA (Common Object Request Broker Architecture) gateway, and (vi) the support of communication interfaces available on current low-cost microcontrollers, e. g., UART ports.

Basically OMG is an organization issuing standards for software modelling strategies, object oriented system integration and embedded systems with a rather general scope. Adoption of this standard has been very modest at least in the public research scenario, though it is clear that many relevant IEEE-1451.1 implementations clearly rely on concepts proposed by the OMG standard and in particular the use of unified modelling language (UML) and CORBA middleware [Lee2005, Lee2006].

The OMG proposal covers basically the same area as IEEE-1451.1, defining a standard software interface with common objects and common functions to be implemented in a network in order to access the networked transducers. Considering the scientific literature in general, both standards seem to have shared their little success in finding widespread adoption. Their similarities regarding software complexity are probably a reason for that, as indicated for IEEE-1451.1 in the next section.

Finally Another relevant standard was issued in close relation to the Self-validating sensors concept (SEVA) first proposed by Clarke [Clarke1996]. The SEVA concept introduces the quality self-assessment of measurements, which outputs a set of validity codes and estimated uncertainties of a measurement. The standardization of these codes and procedures was addressed by the British Standards Institute (BSI) by issuing the BS-7986 standard [BSI2005].

---

#### 1.4.1 IEEE-1451 family of standards

---

In 1993, the IEEE and the NIST initiated an activity which led to the development of the IEEE-1451.1 and 1451.2 standards, the first standards in the IEEE-1451 family [Lee1998]. A visual summary of the current status of the family of standards is shown in Fig. 1.3.

The main idea in the standard is decoupling all sensor related electronics in a sensor module called (Smart) Transducer Independent Module (TIM, or STIM) from a high-level communication instance which provides advanced network access to the sensor termed the Network Capable Application Processor (NCAP). The original definition of both was initially covered by 1451.2 and 1451.1 standards respectively. The initial first TIM – NCAP partition was defined by IEEE-1451.2 in 1997 is shown in figure 1.4.

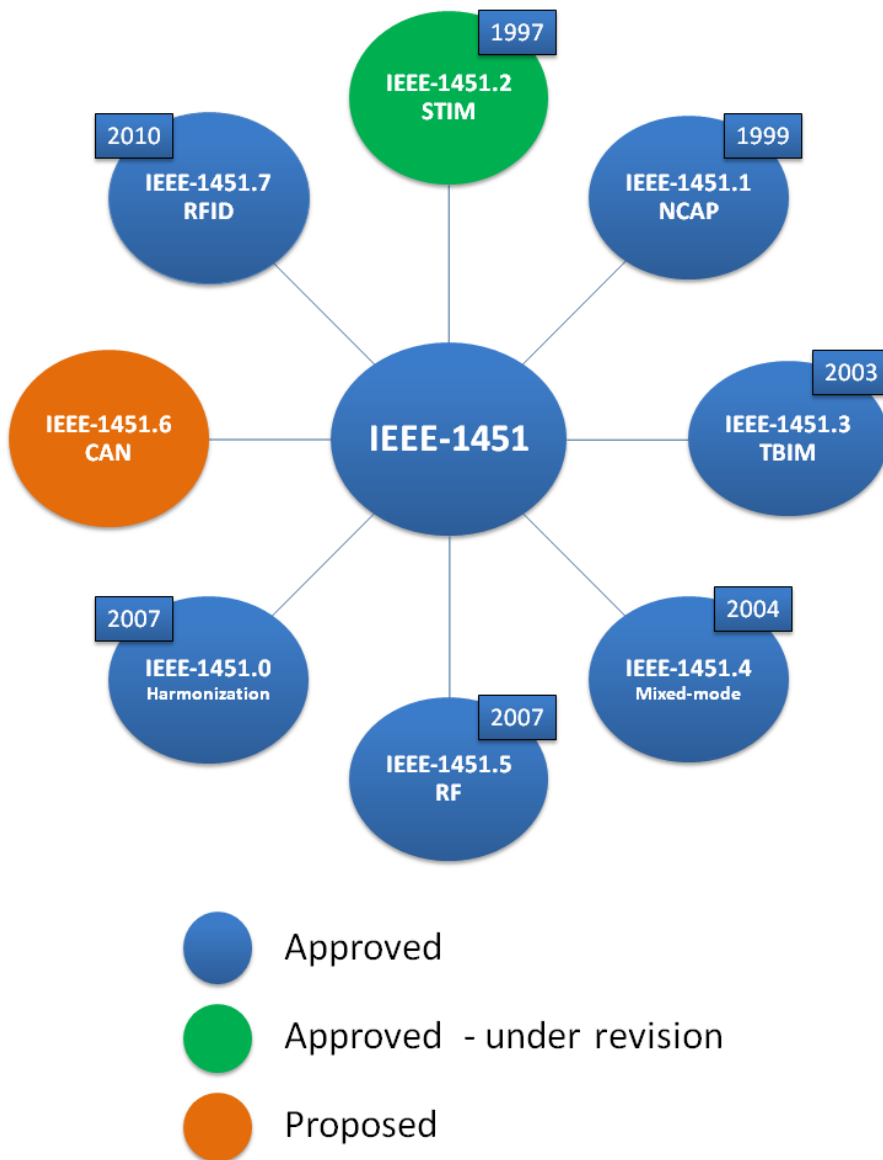


*Figure 1.3 IEEE-1451 family of standards*

In the proposed partition, IEEE 1451.2 defines the structure of the STIM (Smart Transducer Interface which finally lost the S to IEEE 1451.0 to become TIM) and the NCAP was defined in IEEE 1451.1, in the form of a common software object model with a modular structure to be implemented in a processor with network connectivity. The idea of modules or blocks is shown in figure 1.5. Code modules are added as needed, in the form of function blocks. The NCAP block “glues” the system and communication facilities together. Communications to the network using publish/subscribe and client/server interfaces are viewed by the NCAP as ports.

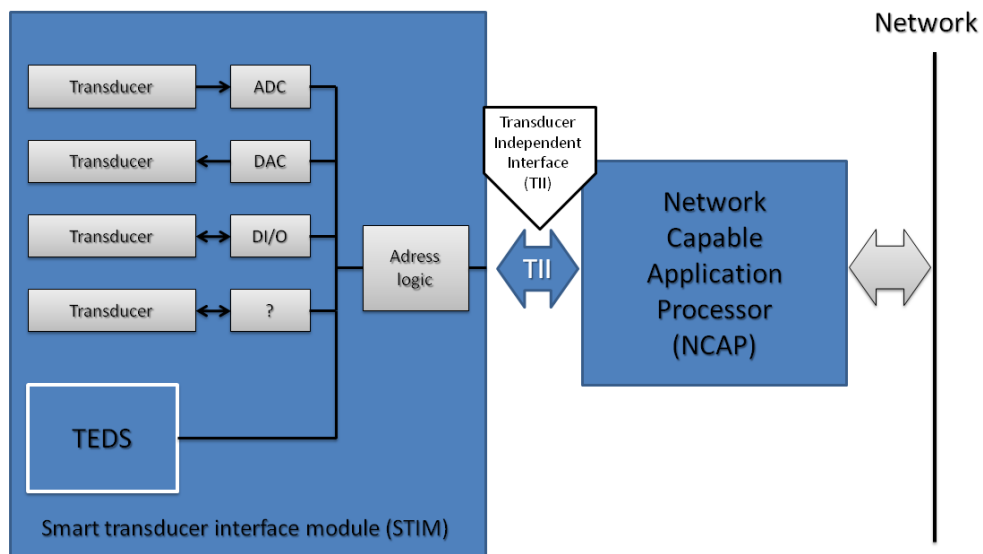


**Figure 1.4 IEEE-1451.2 context diagram (initial reference model), based on [IEEE1997].**

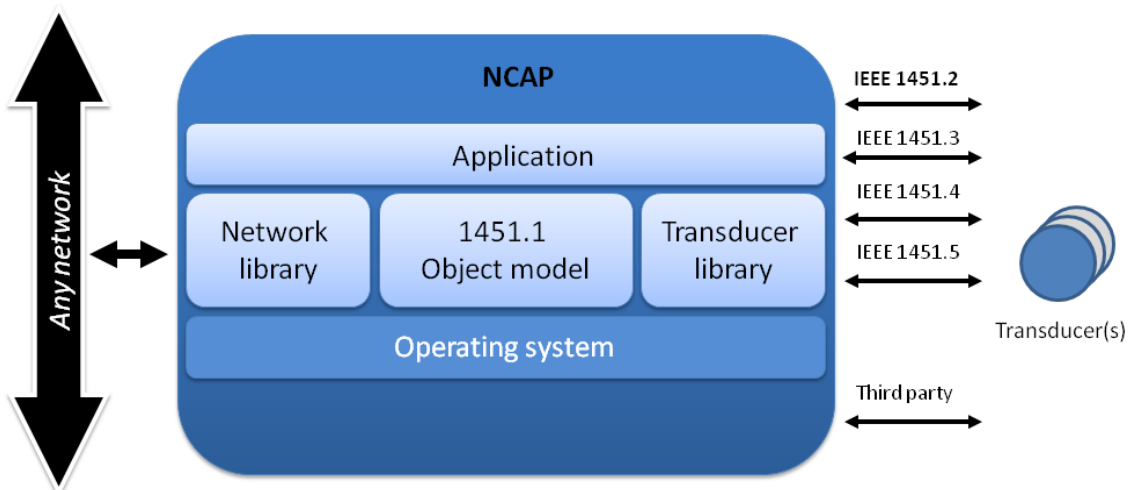


**Figure 1.5. Model layout of 1451.1 NCAP, based on [Viegas2007]**

After 1451.1 and 1451.2 were released, other standards followed which in general covered different communication options between TIM and NCAP:

- IEEE 1451.3 (2003) covers the multidrop connection of TIMs using a communications bus.
- IEEE 1451.4 (2004) covers the connection of analog sensors incorporating TEDS and a mixed-mode interface, it is a singular standard which was created as a kind of bridge between traditional analog sensors and IEEE-1451 fully based smart sensors.
- IEEE 1451.5 (2007) covers the wireless connection of the TIM (WiFi, Bluetooth and ZigBee).

- IEEE P1451.6 (draft proposal) covers the communication using CANopen interface.
- IEEE 1451.7 (2010) covers the radio frequency identification (RFID) communications.

The comprehensive overview of the IEEE 1451 family of standards by Song and Lee is recommended [Song2008].

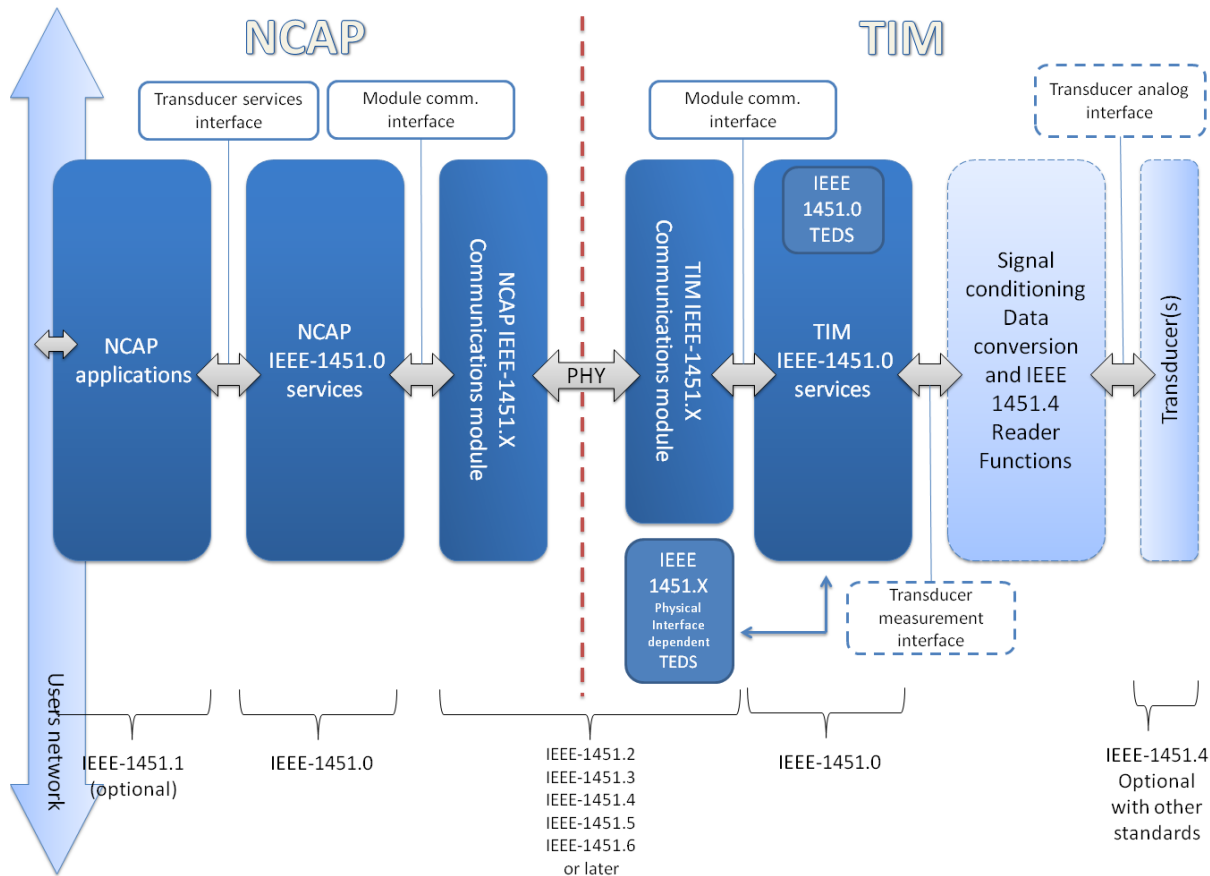


**Figure 1.6 IEEE-1451.0 reference model (revised model), based on [IEEE2007]**

As more IEEE 1451 standards were released, a need for unified data structures and common high level interfaces was evident. In order to define a set of common structures and functions for all IEEE 1451 standards, IEEE 1451.0 was released in 2007 together with IEEE 1451.5. After the release of 1451.0, IEEE 1451.1 became explicitly optional, and the reference model of IEEE 1451 changed in order to place the common IEEE-1451.0 instances and structures as shown in Fig. 1.6, which is based on figure 1 of the IEEE 1451.0 standard definition [IEEE2007].

Differences between the models from figure 1.4 and 1.6 are clear at first sight. The effort of defining common structures has resulted in a more complex model in which IEEE 1451.0 decouples the physical interface communicating TIM and NCAP from the common set of data, functions and

interfaces on the higher levels. In effect, IEEE 1451.2 and IEEE 1451.0 are not truly compatible but they have been made so by adding a flag in the IEEE 1451.0 standard which states if the TEDS are in “old” 1451.2 format or “new” 1451.0 format.

Adoption by the industry of this set of standards has so far been reduced. Citing Bissi et al. [Bissi2007]:

*“A few prototypes of NCAPs and STIMs have been proposed in the past. The EDI520 CogniSense module from electronics development corporation (EDC) combining a PIC microcontroller and signal-conditioning ASIC could be programmed to work as a 1451.2 STIM. A small piezoresistive accelerometer manufactured by IC Sensors was directly connected to the EDI520. A development kit was produced by EDC to get started with 1451.2. It included an NCAP and two STIMs as well as software. The NCAP interfaced with a RS485 network. National Instruments advertised a 1451 interface in Labview. Hewlett-Packard produced an Embedded web server (HP BFOOT 66501) that was soon discontinued. In 2002, the company Esensors produced a “websensor” with a 1451.2 prototyping kit composed by a EM04a NCAP (with ES00r for configuration) and a EI02 STIM with cables [10], [11] and [12]. Esensors wanted to anticipate changes to the IEEE 1451 standard which may include changing the sensor interface to another serial bus such as the RS232. The EM04a could be switched to interface with any of 7 different bus standards (RS232, RS485, TII, 1-wire, IEEE 1451.4, Ebus, I2C and a general bus)”*

Most of the commercial systems compliant with the IEEE 1451 standard and in particular with the TII interface were discontinued. As shown in section 1.4.2 there are several implementations of the IEEE 1451.2 but many of them refuse to implement the TII interface while maintain the TEDS and the NCAP – TIM division in most cases. Comments by Wobschall [Wobschall2002] and Bissi et al. [Bissi2007] among others, indicate the TII as a limiting factor for IEEE 1451.2 implementation. These factors along with the new TEDS coding in IEEE 1451.0 have been the main motivations of the revision of IEEE 1451.2 (IEEE P1451.2) still under way. The problem with IEEE 1451 adoption is further worsened by the fact that no off-the-shelf component that straightforwardly emulates an NCAP is available in the market [Ramos2004].

Regarding NCAPs, some confusion involved IEEE 1451.1, when after approval of IEEE 1451.0 the standard was removed from active state for a time just to be restored shortly after. The object model defined by IEEE 1451.1 is extensive (the standard is 349 pages long) [IEEE1999] and despite there have been efforts to ease the implementation of IEEE 1451.1 [Lee2005], its adoption has been very modest, and only some examples are truly compliant with it such as the implementations by Lee and Song in the same NIST group which promoted IEEE 1451 [Lee2005, Lee2006, Song2008], and also by Viegas et al. including a useful tutorial published in 2008 for operating system based NCAPs [Viegas2005,Viegas2006,Viegas2008] , and Stepanenko et al. with again K. Lee as author for approaches of IEEE 1451.1 NCAP without an operating system [Stepanenko2006]. These few

implementations already give an idea of the complexity of implementing IEEE 1451.1 and show the difficulties of a full implementation with limited hardware resources [Stepanenko2006] and also the efforts needed to build a complete IEEE 1451.1 NCAP for commercial purposes as intended by the group of V. Viegas et al. [Viegas2005, Viegas2006, Viegas2008].

So far the standard is still in a maturing process after 15 years of its first light, and it will probably remain in this status until some of the *big players* in the instrumentation field make a decided bet on it. Nevertheless, in the field of academia and research, the standard is a very valuable tool when facing the design of a smart sensor from scratch or teaching the basics of smart sensors, thanks to the extensive availability of documentation and the open nature of the standard.

#### 1.4.2 IEEE-1451.2

IEEE1451.2 Standard was devised to provide an open architecture for the networking of smart sensors, as well as transducer plug-and-play capability. As previously stated, IEEE-1451 proposes a division of a smart sensor into two hardware instances, a Transducer Interface Module (TIM) (one or many) and a Network Capable Application Processor as defined in 1451.1, or a more generic host processor (see Figure 1.4).

- The TIM (Transducer Interface Module) carries out all the functions related with the transducers (signal conditioning, measuring sensors and drive actuators), and also contains the information about the transducers used in a normalized format in the TEDS (Transducer Electronic Data Sheets). The term TIM makes reference to either the Smart Transducer Interface Module (STIM) defined in 1451.2, the Transducer Bus Interface Module (TBIM) defined in 1451.3, the Wireless Transducer Interface Module (WTIM) defined in 1451.5. The TIMs can be regarded as slave measurement devices, which are basically idle until commands from a master device are received. A 1451.2 STIM may be used to sense or control multiple physical phenomena. Each phenomenon sensed or controlled shall be associated with a STIM transducer channel. A channel may be a virtual transducer in the sense that it behaves as a sensor or actuator, even though nothing outside of the STIM is sensed or changed [IEEE1997]. The STIM building blocks are transducer channels.

- The NCAP (Network Capable Application Processor) is the second module and has different functions: It communicates with the TIM using any 1451.2-7 interface; it post-processes the data measured by the TIM if necessary; it controls the activity of the TIM (acts as the master device) and it may communicate with the outer world via a digital network. It will probably implement user applications or interfaces, or it may also be a slave device receiving commands from the network.

IEEE 1451.2 defines a point to point interfacing between a STIM and an NCAP as described by Fig 1.4., the interface is defined in the standard as the Transducer Independent Interface (TII) signal

lines defined as shown in Fig. 1.7. The physical connector is not defined and left open for the manufacturer's choice.

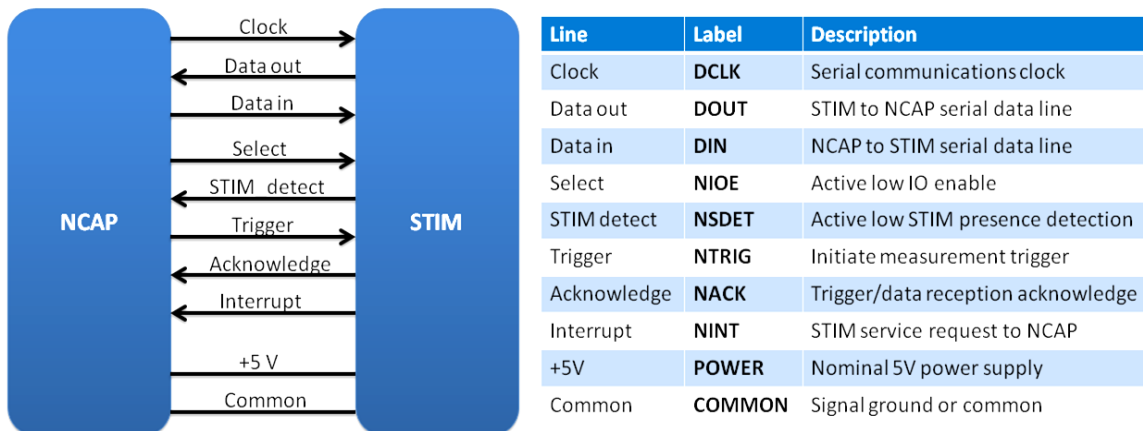


**Figure 1.7 TII signals, as defined in IEEE 1451.2 [IEEE1997]**

Eight different TEDS blocks are defined in IEEE 1451.2. The types of TEDS are either for use by the NCAP or host processor (machine readable) or for operators (human readable). There are two mandatory and four optional TEDS blocks. A summary of the TEDS data blocks is shown in table 1.1.

**Table 1.1 TEDS data blocks overview in IEEE 1451.2 standard**

Type	Readable by	IEEE 1451.2 Mandate
<b>Meta TEDS</b>	Machine	Mandatory
<b>Channel TEDS</b>	Machine	Mandatory
<b>Calibration TEDS</b>	Machine	Optional
<b>Generic-extension TEDS</b>	Machine	Optional
<b>Meta ID TEDS</b>	Human	Mandatory
<b>Channel ID TEDS</b>	Human	Mandatory
<b>Calibration ID TEDS</b>	Human	Optional
<b>End-user application specific TEDS</b>	Human	Optional

The Meta TEDS provide overall system description and TEDS structure information, the Channel TEDS provide information of the available transducers such as units, timing, accuracy and other specifications. Calibration TEDS are for use by the specific IEEE 1451.2 correction engine. Identification (ID) TEDS provide in general text labeling and signaling for user interfacing.

Examples of IEEE 1451.2 implementations are numerous in the gas sensing and environmental monitoring fields such as implementations by Kularatna and Sudantha [Kularatna2008] featuring four metal-oxide gas sensors and a buzzer actuator for a total of five transducer channels; a similar, more recent one is by Kumar et al. [Kumar2011] featuring a number of gas sensors for environmental monitoring which used a USB 2.0 interface instead of a 1451.2 TII; the environmental monitoring system by Bissi et al. [Bissi2007] implemented RS-232 instead of TII, and also featured an array of metal-oxide gas sensors; another STIM featuring an array of metal oxide gas sensors was previously reported by Pardo et al. [Pardo2006]. Simpler STIMs include Wang et al. [Wang2005] whose STIM included one thermistor based temperature sensor and a relative humidity sensor; the early example implementation by Conway et al. [Conway2000] featuring an AD590 temperature sensor and a fan actuator; or temperature sensor implementations by Xu et al. [Xu2006], Zhaochun et al. [Zhaochun2009] and Song and Lee [Song2008b], this last one featuring IEEE 1451.0 and IEEE P1451.2 (revision of IEEE 1451.2).

Diverse implementations can be found in other fields of application such as an early electronic energy smart meter based on IEEE 1451.2 before it was even approved by Nagaraju and Kumar [Nagaraju1998]; the implementation for agriculture applications (weed detection) by J. Wei et al. [Wei2005]; or a STIM for motor actuation including pressure and temperature sensors which was reported by Petru and Mircea [Petru2010].

Many of the implementations have relied on an ASIC approach for STIM implementation, such as the VHSIC Hardware description language (VHDL) STIM based implementation by de Castro et al. [Castro2002] which was tested in a Virtex (Xilinx, USA) field programmable gate array (FPGA); the one by Cheng and Qin [Cheng2005] which was implemented in a Nios (Altera, USA) FPGA; the Apex FPGA (Altera, USA) implementation by Girerd et al. for high energy physics application [Girerd2000]; and the more recent one by Depari et al. [Depari2007] showing an interesting comparison of timing performances in microcontroller and ASIC based STIMs, as well as reporting an example substitution of the TII by a USB interface. Also worth mentioning is the more recent work by Batista et al. [Batista2012] reporting a considerable size prototype TIM which is based on IEEE 1451.2 and IEEE 1451.5 using a Cyclone II FPGA with NIOS II processor (Altera, USA).

Many implementations disregard particular parts of the standard and are inspired in some parts of it without being fully compliant, in general proposing some kind of enhancement. The most common of these modifications is the substitution of the TII interface by other interfaces but there are also other different implementations such as a singular implementation by Wall and Ekpruke

[Wall2003] which claims the implementation of a STIM and NCAP in physically the same microprocessor (though details of these are not profusely documented), and used it as a network interface for ultrasonic sensors. Another implementation based on IEEE 1451.2 reporting the implementation of STIM and NCAP in the same microprocessor was reported by Ding et al. [Ding2007] for a smart power sensor with internet connectivity. In general several modified IEEE-1451 proposals have been reported, most are listed next. A proposal for a modified IEEE 1451.2 designed for deterministic, synchronous real-time operation was proposed by Doyle et al. [Doyle2004]. A water turbidity smart transducer based in IEEE 1451.2 with a RS-485 interface replacing the TII that was reported by Tai et al. [Tai2012]. Another implementation inspired on IEEE 1451.2 for robot control which implemented a CAN interface for the STIM instead of TII was reported by G. Song et al. [Song2005]. An ISA dual-port buffered interface (DPBI) was used to connect a generic IEEE 1451.2 STIM structure to a minimalistic host processor providing Internet Protocol (IP) connectivity in the work by Tao et al. [Tao2005]. Also works by Wobschall et al. in general propose the adaptation of IEEE-1451.2 to an RS-232 interface [Wobschall2002, Wobschall2004, Wobschall2009]. In practice, many of these implementations have not clearly transcended the research environment into industrial applications. This is partly because of the low adoption of the IEEE-1451 standard by industrial sensor manufacturers up to date.

---

#### 1.4.3 BS-7986 AND SEVA

---

BS-7986 Standard specifies functional requirements, example applications and data quality metrics to be used in industrial measurement and control systems [BSI2005]. The standard is based in the SEVA (self-validating) sensor approach proposed by Henry and Clarke in 1993 [Henry1993]. These data quality metrics cover three aspects which are measurement, actuation and maintenance, and are based in the definition of the following quantities:

- The Validated Value (VV) which is the measured quantity (or an estimation of it) and
- the Validated Uncertainty (VU) which is the measured uncertainty of the measurement (or an estimation of it).

Both values are accompanied by status flags (1 byte long) termed VVstatus and VUstatus which are bytes providing information on how the VV and VU values were generated. VVstatus and VUstatus effectively provide a standard reliability and quality metrics for the VV and V values by using a set of predefined byte flags. An additional flag VDstatus (Validated Device status) is also defined to communicate the device operating condition and maintenance needs to high level instances, for instance an application or an operator.

BS-7986 provides a standard encoding for the various status flags as well as device architecture guidelines and specifications to enable a standard implementation of SEVA.

Examples exist of the design of self-validating sensors and algorithms which exploit the redundancy of the sensors at different levels to produce self-assessed quality metrics variables. Despite not all of them conform to BS-7986, it is interesting to overview the different self-validating approaches reported since the late 1990s. The examples may be classified according to different categories depending on the source of the redundant information used as proposed by Feng et al. [Feng2007], as those based in Hardware redundancy, those based in analytical redundancy (where the redundancy is already present without the addition of hardware) and finally statistical (often historical) signal characteristics basically meaning some kind of time domain or frequency domain constraints that bound the signal variations in some way during normal sensor operation.

Hardware redundancy is probably the more straightforward way of exploiting sensor redundancy. It is achieved by duplicating measurements using different sensor elements such as the examples by Barberree [Barberree2002, Barberree2003]. In this approach, the primary sensor was complemented with a combination of thermally sensitive materials or thermo-elements selected to generate multiple independent signals representing the temperature at the tip of a probe, and enabled the monitoring of the condition of each element. A recent work by Taymanov also proposes several elaborated ways of exploiting some degrees of hardware redundancy to compensate critical ageing defects in pressure, temperature and electrical conductivity sensors [Taymanov2011]. Also Feng et al. reported a SEVA pressure sensor partially based on hardware redundancy [Feng2009].

Analytical redundancy is a particularly interesting method, since it does not involve an increase on the number of parts, but rather the intrinsic correlation and redundancy present in multisensor systems is used. Wang and Chen reported in 2004 the detection, diagnosis and reconstruction of faulty sensors of the central chilling systems in a building [Wang2004] using principal component analysis (PCA). In another example Qin proposed a self-validating inferential sensor approach based also on PCA, and applied it in the air emission monitoring [Qin1997]. Liu et al. (2001) used neural network to correct the readings of a digital coriolis mass flow meter for two-phase flow effects, based entirely on internally observed parameters [Liu2001]. Frolik and Abdelrahman used fuzzy logic rules for self-validation and confidence intervals assessment. The approach was used for the reconstruction of lost and poor data. Data fusion allowed the determination of the single measurements and its confidence [Frolik2001, Abdelrahman2000]. Extensive work on sensor fault detection and correction based on analytical sensor redundancy can be found in Padilla's thesis [Padilla2010], mainly applied to polymer sensor arrays.

Other methods exploit time and frequency domain distribution constraints in the signal waveform in order to predict if the sensor is behaving correctly or not. Examples of this are the proposals by Zhang et al. [Zhang2001a, Zhang2001b] in which the wavelet transform is used to characterize a

signal in both time and frequency domains, allowing to detect abnormal events in a sensor output signal. After that, the signal energy distribution, on all decomposed wavelet levels of this signal before and after these instants, is used to validate the status of the sensor. Three different approaches largely based in signal statistics were developed by Moran et al. [Moran2001], Stochastic Approximation, reduced bias estimate and the Bayesian self-organizing map using Gaussian kernels. Simulation studies showed that the Gaussian kernels based method gave superior results when compared to the reduced bias estimate algorithm. It was demonstrated that the Gaussian kernels method was more computationally and memory efficient. The techniques were demonstrated using data from a thermocouple sensor.

Other more recent approaches include work by Tsang and Chang who proposed the use of polynomial predictive FIR filtering and fuzzy logic for abnormal events detection in thermistor readings [Tsang2010]; and also work by Feng et al. [Feng2009] reporting a self-validating pressure sensor based on hardware redundancy but also exploiting the wavelet decomposition of real time measurements to obtain a fingerprint of diverse types of errors. The combination of hardware redundancy and signal analysis seems powerful, though in the proposed approaches the computing resources invested were considerable (2 DSPs running in parallel).

An interesting approach is also reported by Karatzas et al. [Karatzas2007] which relies on local regularization sparse density estimation to approximate a probability distribution function (PDF) of a non-linear sensor signal. The orthogonal forward regression with leave-one-out was proposed to obtain the sparse probabilistic model of the sensor, and an example application which intended to use the algorithm as an uncertainty estimator, and drift/fault detector. One of the first SEVA approaches was presented by Clarke and Fraher implemented SEVA in a D0x sensor, in which a test procedure based on a physical model of the diffusion processes in the sensor, provided fault detection and correction capability [Clarke1996].

---

## 1.5 SELECTED EXAMPLES

---

As summarized in section 1.4.2, a number of environmental metering devices based on gas sensor arrays have been implemented using the IEEE-1451.2 standard. It was also previously mentioned that chemical sensors and in particular gas sensor arrays are exceptional candidates for smart sensors, due to the need of advanced signal processing (or preprocessing) as close as possible to the sensors. A number of examples which are particularly relevant for the implementation in this work are discussed in the next subsections.

### 1.5.1 IEEE 1451 ENVIRONMENTAL MONITOR [Bissi2007]

The smart sensor implementation by Bissi et al. [Bissi2007] featured an array of microfabricated metal oxide sensors, the work described the structure of a multiprocessor control system for the gas sensing array, which was inspired in the IEEE 1451 standard. The system is basically a STIM compliant with IEEE-1451.2 but the TII interface was substituted by a three-wire RS-232 interface providing asynchronous communication.

The system was designed with high modularity, as a cluster of identical monosensor subsystems managed by a central Controller. A block diagram of the system can be seen in Fig. 1.8. There is an internal interfacing between the main controller and the monosensor modules based in I<sup>2</sup>C. This structure provided improved scalability possibilities to the system. Each monosensor subsystem consisted of a sensor together with the excitation, readout, and signal conditioning electronics including digital to analog converters (DAC) and a microcontroller as shown in Fig.4 of reference [Bissi2007].

A dedicated PC software named STIM-tester was programmed in place of an NCAP in order to test the STIM functions. The response of the different sensors to environmental pollutants was reported, using constant temperature excitation and pulsed excitation modes. Brief considerations were made on the sensor sensitivities; no multivariate data manipulation was reported.

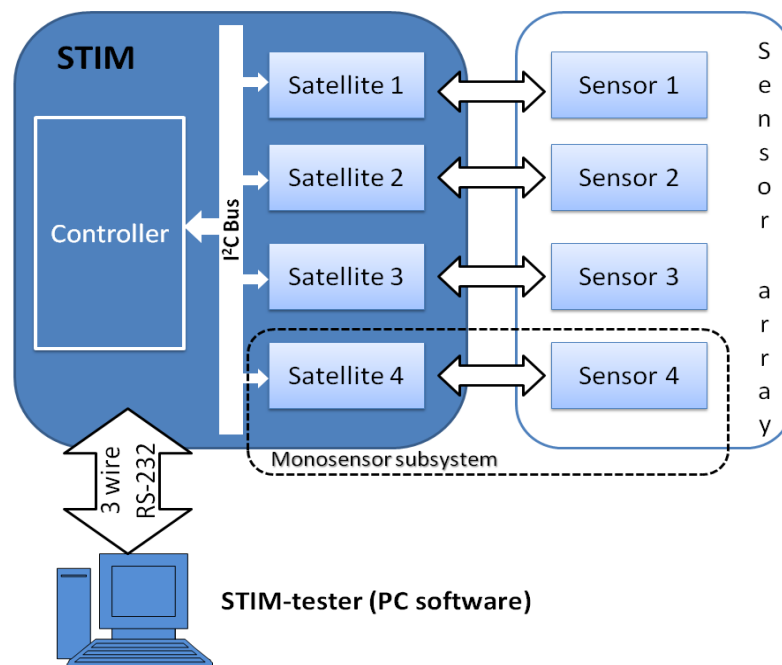


**Figure 1.8 Block diagram of the system implemented by Bissi et al. [Bissi2007]**

### 1.5.2 IEEE 1451.2 GAS MEASUREMENT SYSTEM [PARD02006]

Pardo et al. [Pardo2006] reported a compact electronic-nose inspired system based on the IEEE-1451.2 standard, a STIM. The reported STIM consisted of four commercial (discrete) tin oxide gas sensors, a temperature sensor and a humidity sensor as sensor channels, as well as two actuators for controlling a pump and an electrovalve. The STIM was divided in two blocks, a transducer module in charge of sensor excitation and readout, and a control module which drives the actuators, acquires the sensor signals, and implements the TEDS and the TII protocol. In this sense, the implementation is fully compliant with the IEEE-1451.2:1997 standard specification. The control module was programmed in an ADuC812 microcontroller, and the transducer module was implemented using a Z86E04 microcontroller, a block diagram of both modules can be seen in Figure 1.9.

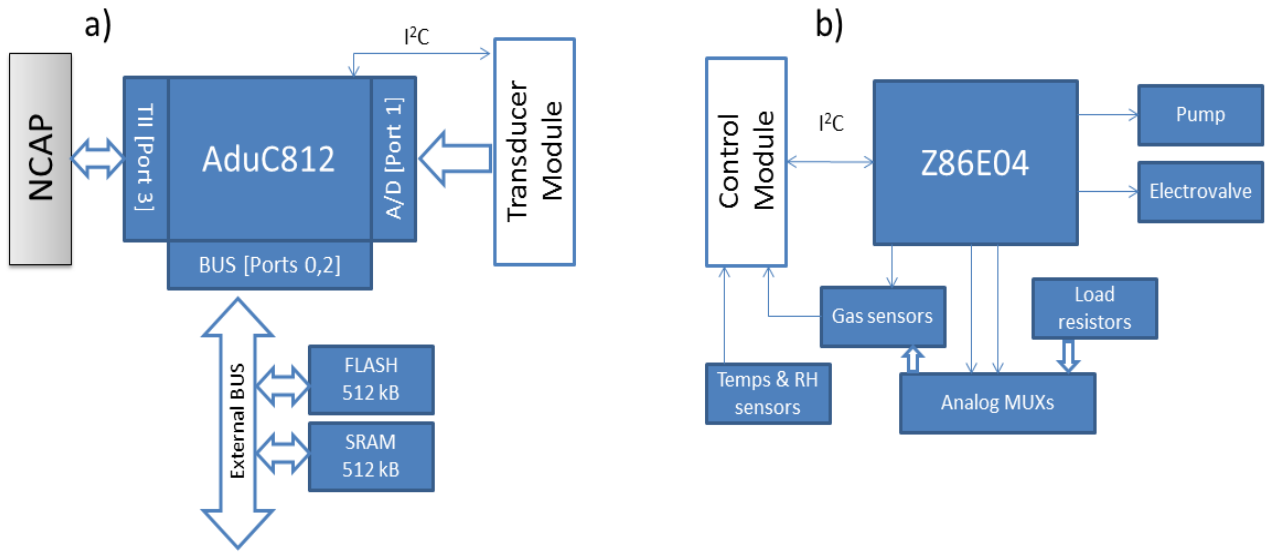


**Figure 1.9 a) Block diagram of the STIM control module, b) block diagram of the STIM transducer module. After [Pardo2006].**

The paper reported a test of the sensors, without further data analysis. The implementation differs basically from 1.5.1 in that this is fully IEEE-1451.2 compliant, and that the implemented gas sensors were commercial sensors. On the other hand it is worth noting the architectural similarities between both implementations featuring a central control unit and an independent microcontroller managed transducer module.

### 1.5.3 SELF-VALIDATING DISSOLVED OXYGEN SENSOR [CLARKE1996]

Despite the application by Clarke and Fraher is somewhat old, it provides the foundations of SEVA technology and its related standard BS-7986. The work elaborates on the need of quality metrics, in particular for sensors being part of a control system. Ways of reporting faults and uncertainty, to 'upper levels' of the control system hierarchy are proposed, and an example is provided of its application in a dissolved oxygen sensor.

The well-known process of the diffusion across the membrane present in the sensor was used to obtain a mathematical model describing the sensor response time. The transient response after sensor switching was measured and used for sensor validation. Changes in the sensor response time were detected and interpreted as a measure of sensor fouling. These changes in time constant were used to detect, quantify, and correct the sensor fault.

### 1.5.4 SELF-VALIDATING PRESSURE SENSOR [FENG2009]

Feng et al. [Feng2009] reported an interesting approach for a self-validating pressure sensor. The sensor was based on a circular-flat diaphragm structure for the elastic body and was fabricated in 1Cr18Ni9Ti stainless steel, which allowed the sensor to work in the 0-10 MPa range, and in harsh environments.

The sensor implemented several more than the typical group of four strain gauges. Eight groups of four strain gauges were implemented, which provided signal redundancy for error detection and correction. The additional information was used not only to identify fault conditions but also to classify them according to the available fault patterns. Faults are initially identified by performing a consistency check among the sensor groups, in the paper it is described as solving a maximum clique problem. While the primary sensor (group 1) is highly consistent with the rest, it is determined to be working normally, in case it is not, the fault diagnosis procedure is triggered. The diagnosis is based in a wavelet composition for extracting the fault features, and a support vector machine (SVM) is used for its classification. An example of fault patterns obtained with wavelet decomposition is shown in Fig. 1.10.

According to the detected failure, the validated uncertainty (VU) values and validated value status (VVstatus) are adjusted for precise indication of the failure.

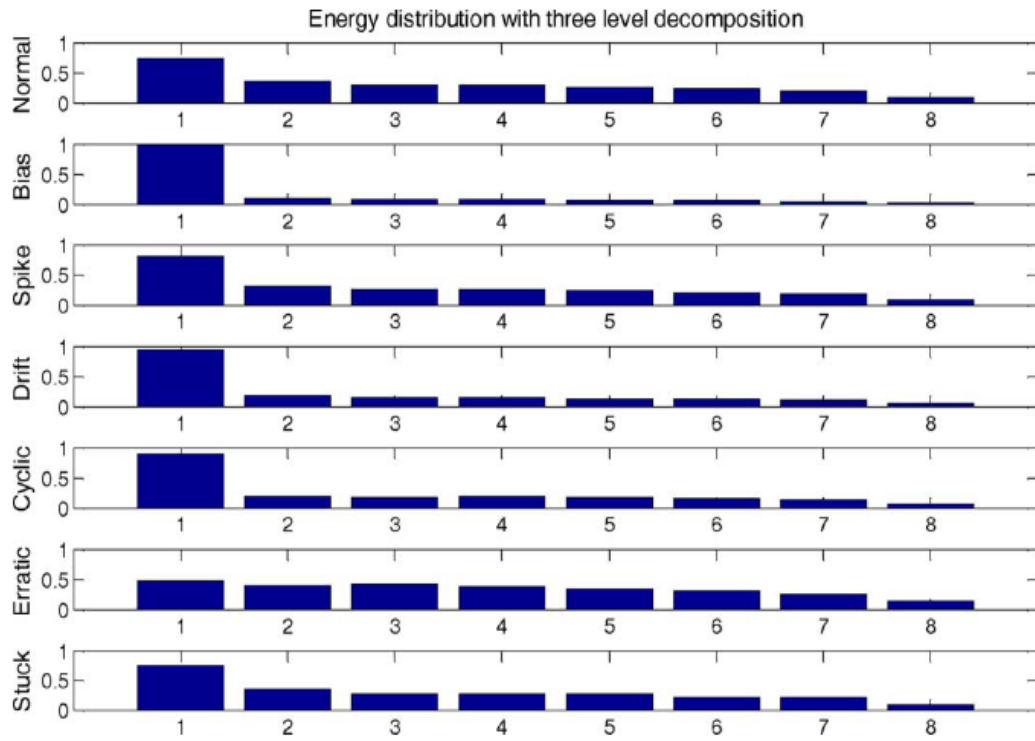


**Figure 1.10** Bar plot showing energy distribution for the seven signal patterns obtained with three-level decomposition wavelet packet. Table shows correspondence of patterns with identified fault types, based on [PENG2009].

## 1.6 SMART SENSORS OUTLOOK

The significant ambiguity of the term smart sensor itself makes it unclear if the term will be semantically successful in designating the upcoming generations of sensors. In the current scenario, the precise use of the smart sensor term is strongly linked to standards, and in particular IEEE-1451. This is so despite there are a lot of examples found in the industry and research which do not adhere to IEEE-1451 and are considered smart sensors. But, perhaps as has happened with SEVA sensors (which are indeed smart sensors as well according to its definition) other terminologies will be used which describe more specifically why that sensor is smart.

Regardless of semantic considerations, there is indeed a long way to walk in the improvement of actual sensing technologies. The exploitation of hardware redundancies and multisensor correlations or analytical redundancies for sensor fault detection and self-validation, as well as the increasing use of sensor networks, and in particular the wireless ones, ensure that smart sensing technologies will become a trending topic of instrumentation research.

It is definitely tough to envision a future where all fieldbus solutions may be replaced by a IEEE-1451 interface or a newly defined standard, though probably IEEE-1451 will slowly find its applicability and markets, likely within the most modern sensor network concepts and in particular IEEE-1451.5 and IEEE-1451.7 for wireless communications; and possibly in the context of smartphones and tablets which can be programmed as NCAPs interfacing to 3G networks. However, the experience in industrial markets so far indicates that penetration will be a slow process, and unless one or some of the big players in the instrumentation field bet on IEEE-1451, it is hard to imagine that it will reach a diffusion comparable to that of standard fieldbuses, remaining more or less like today, as a kind of research exercise.

In my opinion, a different evolution may await the SEVA sensors approach, despite the research in SEVA so far has been very modest considering its onset on 1993, this kind of approach is highly compatible with, and basically independent of, the different interfaces. The SEVA can be combined with many other technologies, and in the case of critical systems, the possibility of integrating self-validation, or self-test. This is indeed what happened in its day with car accelerometers for airbag triggering, with integrated self-test, even not bearing the SEVA terminology this kind of self-validating sensor will very possibly find new successful applications in the safety and medical fields.

## 2. NATURAL GAS QUALITY CONTROL: BACKGROUND AND OPEN ISSUES

---

1.1. Natural gas significance.....	27
1.2. The importance of quality control.....	28
1.3. Instruments and techniques for natural gas quality control.....	29
1.3.1. Combustion calorimeters.....	30
1.3.2. The process gas chromatograph (PGC).....	32
1.3.3. Correlative methods.....	33
1.3.3.1. Dielectric permittivity method.....	33
1.3.3.2. IR spectrometry.....	34
1.3.3.3. VOS-Meter.....	34
1.3.3.4. WOM 2000.....	35
1.3.3.5. EMC 500.....	36
1.3.3.6. Gas-PT.....	37
1.3.3.7. Gas-Las Q1.....	37
1.3.3.8. Methane number microsensor.....	38
1.3.3.9. ANGus.....	39
1.3.3.10. Research approaches based on thermal conductivity.....	40
1.4. Gas sensing technologies.....	41
1.4.1. Conducting polymer sensors.....	41
1.4.2. Quartz crystal sensors.....	41
1.4.3. Electrochemical sensors.....	43
1.4.4. Infrared based gas sensors.....	43
1.4.4.1. NDIR.....	44
1.4.4.2. Photoacoustic devices.....	46

---

1.4.5. Colorimetric gas sensors.....	48
1.4.6. Fiber optic based gas sensors.....	48
1.4.7. PELLISTORS.....	49
1.4.8. Thermal conductivity sensors.....	49
1.4.9. Metal-oxide semiconductor sensors.....	51
1.4.10. Velocity of sound sensors.....	52
1.4.11. Microfluidic oscillator sensors.....	52
1.4.12. Dielectric permittivity sensors.....	53
1.5. Comparison of considered technologies.....	53

## 2.1 NATURAL GAS SIGNIFICANCE

---

**E**nergy supply is unarguably a key factor to national economic development and political well-being. The arithmetic of energy dependency among countries is currently pivotal in the international relations background, including armed conflicts. There is an unambiguous relationship between energy consumption (per capita) and national wealth [Economides2009, IEA2009].

Natural gas is the name given to the hydrocarbon mixture found in natural fossil fuel reservoirs, often associated with coal beds or oil reservoirs. It consists mostly of methane with lesser amounts of ethane and propane. Non-combustible components such as carbon dioxide and nitrogen may also be present. The higher hydrocarbons (C4 and greater) typically comprise less than 1.5 mol% of the total. In general, methane does not fall below 86 mol% while ethane and propane do not exceed 10 and 2 mol%, respectively [Makhoukhi2005]. Carbon dioxide and nitrogen typically do not exceed 2 and 12 mol% respectively [Brown2004, Rahmouni2003a].

Natural Gas has seen a strong consumption increase over the last 30 years of 156% [IEA2009]. Only China has based its energy supply increase in coal, while most other important energy consumers have increased their energy supply basically with natural gas. Currently, natural gas is the third primary energy source [IEA2009]. The high availability of fossil fuels, and long established distribution and exploitation technologies make of them a commercially attractive energy source. Among them, natural gas is considered the cleaner energy source; this emplaces natural gas as an advantageous alternative which (to some extent) can address environmental concerns while still maintaining a high commercial attractiveness. On the other hand, Natural gas has also a high degree of interchangeability with the other fossil fuels [Economides2009] which increases its interest as an alternative. The ever-present concerns on nuclear energy, strongly stirred by the accident at Chernobyl (Ukraine) nuclear plant in 1986, and recently awoken by the catastrophe at Fukushima Daiichi nuclear plant in Japan in March 2011, will probably increase the reluctance of governments and society towards an increase of nuclear energy in the energy production scenario.

These considerations together with the apparent current loss of interest in the renewable energies due to its relative expensiveness seem to ensure a place of privilege for the fossil fuels, and particularly natural gas, in the next years.

## 2.2 THE IMPORTANCE OF NATURAL GAS QUALITY CONTROL

The properties of natural gas can vary strongly, according to its origin-dependent composition. These properties must be closely monitored in several scenarios, for instance, in commercial transactions of the gas, gas processing and storage, and also in process and engine control. In these applications, measurements of the calorific values (superior and lower), density, specific gravity, compressibility factor, Wobbe Index or Methane number among other magnitudes, are needed. Some important properties are briefly described next.

**Calorific value:** Also termed the heat of combustion, the heating value or the energy value of a substance or fuel, it is a measurement of the amount of heat released by the combustion of a volume equal to unity (std m<sup>3</sup> for the IS). It typically ranges from 33 to 44 MJ/m<sup>3</sup> [IEA2010] the m<sup>3</sup> units are typically expressed for this and other magnitudes as m<sup>3</sup> at IUPAC standard temperature and pressure (STP) conditions (0°C, 1 bar), this convention is used hence forward if not otherwise specified.

**Wobbe index:** is an indicator of the interchangeability of fuel gases, it is used to compare the combustion energy output of different composition fuel gases in a given gas appliance (burner, cooker, etc...). It is calculated as the ratio of the higher calorific value to the square root of the specific gravity of the gas. For natural gas it typically ranges from 39 to 56 MJ/m<sup>3</sup>.

**Methane number:** A formal definition would state that it indicates a regulated anti-detonation number representing the fuel anti-detonation performance of ignition type engine. However perhaps the definition stated in [Puente2005] which states "methane volume percentage of a mixture with hydrogen that provokes the same knocking intensity than the considered gas", is more comprehensible. In a practical way it is a measurement of the knocking tendency of a gas when an engine is fueled with it. Knocking occurs when the peak of the combustion process no longer occurs at the optimum moment for the motor cycle. The shock wave creates the characteristic metallic "pinging" sound, and cylinder pressure increases dramatically. Effects of engine knocking range from inconsequential to completely destructive. Typical range for natural gases is 75-95 MN [Malenshek2009].

**Compressibility factor:** The volume of a real gas is usually less than that of an ideal gas, and hence a real gas is said to be supercompressible. The ratio of the real volume to the ideal volume, which is a measure of the amount the gas deviates from perfect behavior, is called the supercompressibility factor, sometimes shortened to the compressibility factor. It is also called the gas deviation factor and is denoted by the symbol Z. The gas deviation factor is, by definition, the ratio of the volume actually occupied by a gas at a given pressure and temperature to the volume it would occupy if it behaved ideally [Bahadori2007].

Among the natural gas properties, the calorific value (in its various definitions [ISO1995]) is probably the most important one, for its economic implications in energy trading. Composition variability produces significant variations in the natural gas properties, for instance a variation of up to 25% for calorific value (33-44 MJ/m<sup>3</sup> [IEA2010]); Wobbe Index (42-56 MJ/m<sup>3</sup>); and normal density (0.7-0.93 Kg/m<sup>3</sup>). These properties are usually calculated from the concentrations by use of the ISO6976 standard [ISO1995] set specifically for this purpose. These variations in the natural gas composition are highly depending on its origin, as summarized in Table 1. Regarding the international energy distribution and supply market, this origin dependent variability implies that natural gas quality (calorific value) must be accurately measured and ideally closely monitored throughout the distribution process.

**TABLE 2.1. TYPICAL COUNTRY SPECIFIC GROSS CALORIFIC VALUES OF NG [IEA2010]**

COUNTRY	CALORIFIC VALUE (MJ/m <sup>3</sup> )
United States	38.267
Russian federation	37.578
Canada	38.320
Iran	39.356
Norway	39.720
China	38.931
Qatar	41.400
Algeria	42.000
Netherlands	33.339
Indonesia	40.600

## 2.3 INSTRUMENTS AND TECHNIQUES FOR NATURAL GAS QUALITY CONTROL

Along natural gas history, several methods have been proposed to monitor the heating value of natural gas [Ulbig2001], as briefly reviewed in this section. Only a portion of the proposed technologies has found wide acceptance in the industry, given its typically stringent reliability requirements and regulations. Three distinct generations of instruments can be identified, a first generation of industrial devices comprising diverse types of combustion calorimeters [Ulbig2001] a

second generation consisting of the Process Gas Chromatographs (PGCs) [Stufkens1975], which largely substituted the combustion calorimeters and are the current standard in industrial NG instrumentation; and finally a recent third generation of faster and lower-cost devices which is being progressively introduced in the industry [Schley2001]. These devices are based in the so-called ‘correlative methods’ and represent a more affordable alternative which may progressively complement the use of PGCs. Basic characteristics of these third generation devices are high sampling and analysis speed, lowered maintenance and acquisition cost and in general lower accuracy compared to PGC. These three generations of devices are reviewed next.

### 2.3.1 COMBUSTION CALORIMETERS

A first generation of industrial devices for measuring the calorific value of natural gas in gaseous state comprised diverse types of combustion calorimeters [Ulbig2001]. These type of devices burn the gas in predetermined conditions in order to measure directly the energy of the combustion. Three different families of combustion calorimeters can typically be found:

- **Combustion inside a calorimetric bomb**

The determination of the calorific value of solid and liquid samples, using bomb calorimetry has been a standard procedure in laboratory practice for decades. The use of a calorimetric bomb to determine the calorific value of gases is rare. The reason is that the as a consequence of the design of the calorimetric bombs, solid and liquid samples burn completely, while combustion of gaseous samples is incomplete, which implies the need of a correction calculation. This added complication results in a very reduced use of this kind of calorimeters for gaseous samples.

- **Open flame combustion**

Calorimetric methods with open flames for the determination of the calorific values of gaseous samples have been used for decades as a subset of cases for bomb calorimetry [Kolesov1979]. The first gas calorimeter, was presented by Hartley in the year 1882 [ASTM1958]. Following that, various instruments were developed, e.g. the Boys calorimeter, the Hyde–Saville calorimeter and the Fairweather calorimeter [Hyde1960].

The basic principle of most open flame calorimeters is the same: a specific amount of gas is metered and completely burnt. By use of a heat exchanger, the heat of combustion released by the burner is transferred to a heat absorbing fluid (water or air). As a consequence, the temperature of the fluid increases. The temperature increase is a measure of the calorific value. A more recent [Alexandrov2002]calorimeter architectures include an electrical

heater, and its power is controlled in close loop to maintain a constant temperature in the heated fluid, in this way a power balance is established, and the heater signal is directly an electrical measure of the calorific value of the gas. This kind of implementation is fully consistent with the ISO6976 [ISO1995] definition of calorific value. An example combustion calorimeter is shown in Figure 2.1.

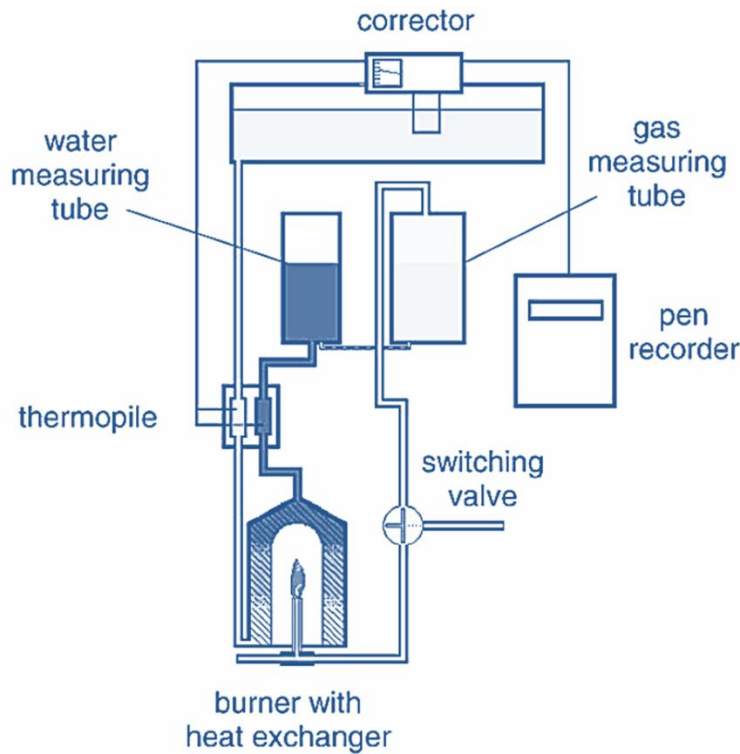


*Figure 2.1 Principle of a Reineke calorimeter, from [Ulbig2001]*

- **Oxidation by catalytic combustion**

It is possible to burn the gas in a so-called “cold combustion” by catalytic combustion. For this purpose, gas and air are led through a packed bed made of catalyst pellets. There, the gas is oxidized and the released heat of combustion rises the temperature of the catalyst bed. Measurement methods include the measurement of the temperature increase, or otherwise the change in the needed power to keep the catalyst bed at a constant temperature between 150°C and 400°C needed for the catalytic combustion to occur.

Typical accuracies of combustion calorimeter are in the range of 0.4 MJ/m<sup>3</sup> to 0.6 MJ/m<sup>3</sup> (1% to 1.5%) [Stufkens1975, Lewis1989], and their usage was greatly reduced after the development of natural gas analysers based on PGC.

### 2.3.2 THE PROCESS GAS CHROMATOGRAPH (PGC)

Gas chromatography (GC) is a common type of laboratory technique for the separation of gas mixtures used in analytic chemistry for separating and analysing gaseous compounds. GC is based on the interaction of two different "phases" which are described next:

- the mobile phase (or "moving phase") is a carrier gas, usually an inert gas such as helium or an unreactive gas such as nitrogen.
- The stationary phase is a microscopic layer of liquid or polymer on an inert solid support, inside a piece of glass or metal tubing called a column.

The gaseous compounds being analysed are driven by the mobile phase through the column and interact with the walls, which is coated with different stationary phases. This causes each compound to elute at a different time, known as the retention time of the compound. The comparison of retention times allows the identification and quantification of the compounds in the analysed sample. The use of chromatography to determine the composition of natural gas was first proposed by Stufkens and Bogaard in 1975 [Stufkens1975]. With this method the calorific value can be easily determined as a weighed sum of the calorific values of the pure components by their molar fraction, as detailed in the ISO6976 standard [ISO1995].

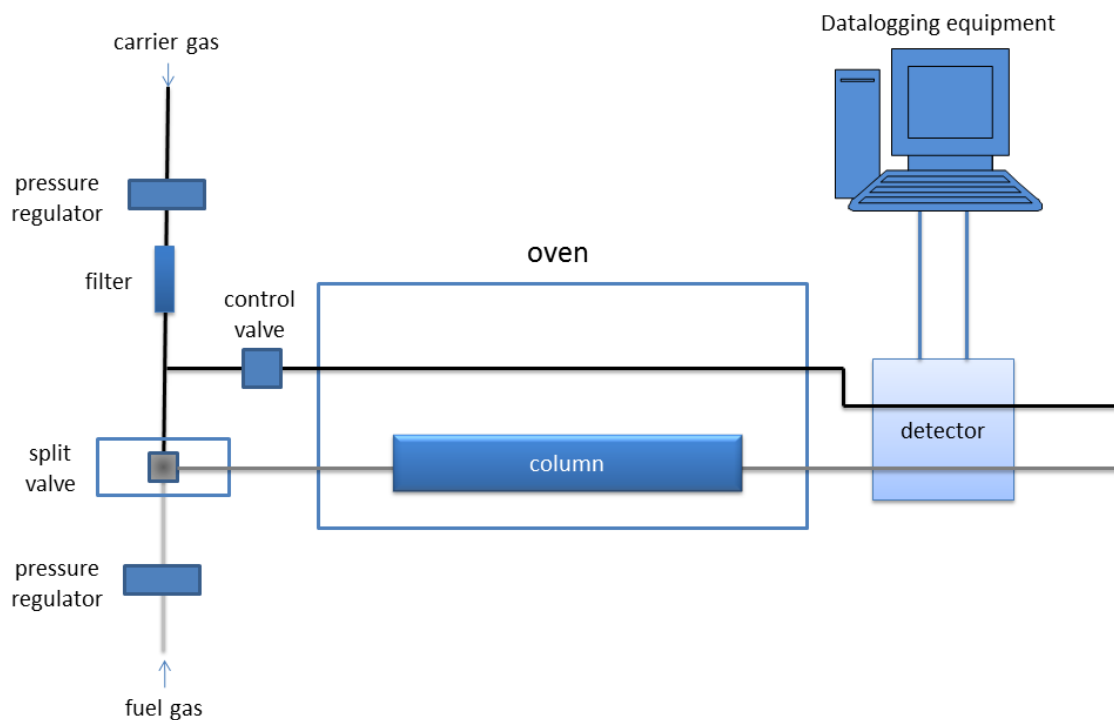


**Figure 2.2. Principle of a process gas chromatograph (based on [Ulbig2001])**

The term process gas chromatography makes reference to the fact that this kind of chromatographs can work in a continuous way with little supervision apart from the regular recalibrations of the system. A diagram of the design of a typical process gas chromatograph for natural gas analysis can be seen in Figure 2.2.

Nowadays, PGCs have substituted the use of combustion calorimeters as the reference technology for natural gas quality metering, its increased accuracy of up to 0.1% or 0,04 MJ/m<sup>3</sup>, is the main reason for this, though the intrinsic safety of the procedure as no combustion takes place, an its lower consumption of the metered gas can be pointed as other advantages.

### 2.3.3 CORRELATIVE METHODS

---

Despite the improvement of PGCs with respect to combustion calorimeters, still the instrumentation for natural gas quality monitoring is far from ideal. PGCs are costly to acquire and maintain, they require the use of a carrier gas, and calibration patterns. Also frequent recalibrations of the instrument are needed, and the instrument itself is bulky and typically requires expensive expert handling for its operation and maintenance [Schley2001].

For all these reasons, instrumentation companies and gas distributors have been looking for measurement alternatives which may overcome or minimize these problems. This research has seen a strong increase over the last decade due to increasing liberalization of the natural gas market within europe, triggered by the so-called "EU gas directive" with a first version issued in 2003 and has been followed by subsequent directives.

Several alternative instruments have been presented, some of which have been reviewed by Schley in 2001 at the world gas conference [Schley2001]. All of them are based on the measurement of a set of physical or chemical properties of the gas, which are relatively easy to measure, and correlate these set of properties to other properties of interest, such as the calorific value. Hence, they have been termed 'correlative methods'. This strong onset of new instruments in a short period of time around 2000 can be regarded as a third generation of natural gas analysers.

A brief description of proposed correlative methods, alternative systems and microsystems is provided next. Table 2.2 at the end of the section provides a summary of the relevant features of the described instruments.

---

#### 2.3.3.1 DIELECTRIC PERMITTIVITY METHOD

---

Jaeschke [Jaeschke2002] selected in this approach five magnitudes to be measured, temperature, pressure, CO<sub>2</sub> molar fraction, speed of sound and dielectric permittivity. A laboratory prototype was designed based in which attained a remarkably low uncertainty agreeing to within 0.1% of the GC

reference results in  $H_s$  (superior heating value). It has not so far reached the market, though apparently its feasibility as a reference calorimetric device traceable to established metrological standards was in 2002 under negotiation with a number of partners [Jaeschke2002].

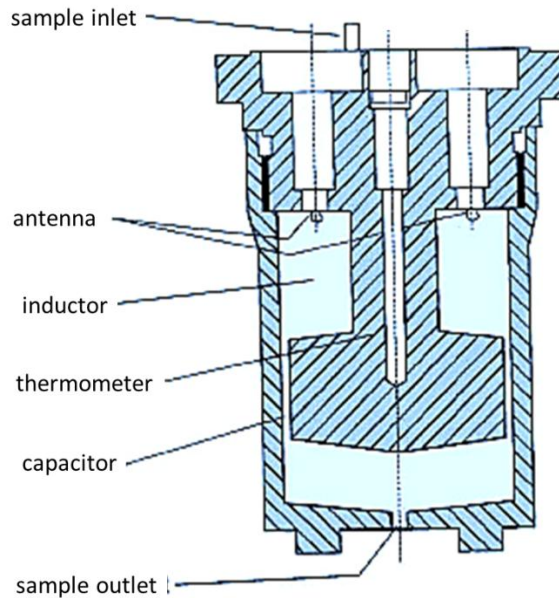


**Figure 2.3. Reentrant cavity for dielectric permittivity measurement, from [Jaeschke2002]**

#### 2.3.3.2 IR SPECTROMETRY

J. Kastner working for FlowComp Systemtechnik developed a method based in a scanning high resolution IR spectrometer [Kastner2002]. Despite promising results, development was abandoned to focus in a system more suitable for lower cost series production, the Gas-Lab Q1 [Kastner2005].

#### 2.3.3.3 VoS-METER

Panneman et al. reported in 2001 a method based in measurement of the speed of sound at two different pressures (5 bar and 40 bar) combined with CO<sub>2</sub> mole fraction [Pannemann2001]. The method made use of ultrasonic sensors, which are a common and well-known technology in gas flow sensing. A remarkable uncertainty of 0.3% was reported with an outstanding response time T90 of 4 seconds. The sensor setup was quite complex as it was enclosed in a temperature controlled box and pressure was regulated with two regulators. After initial marketing attempts, it seems that the device is no longer commercialized, as its formerly promoter company Elster-

Instromet (Essen, Germany) is now commercializing the more compact Gas-Lab Q1 [Kastner2005].

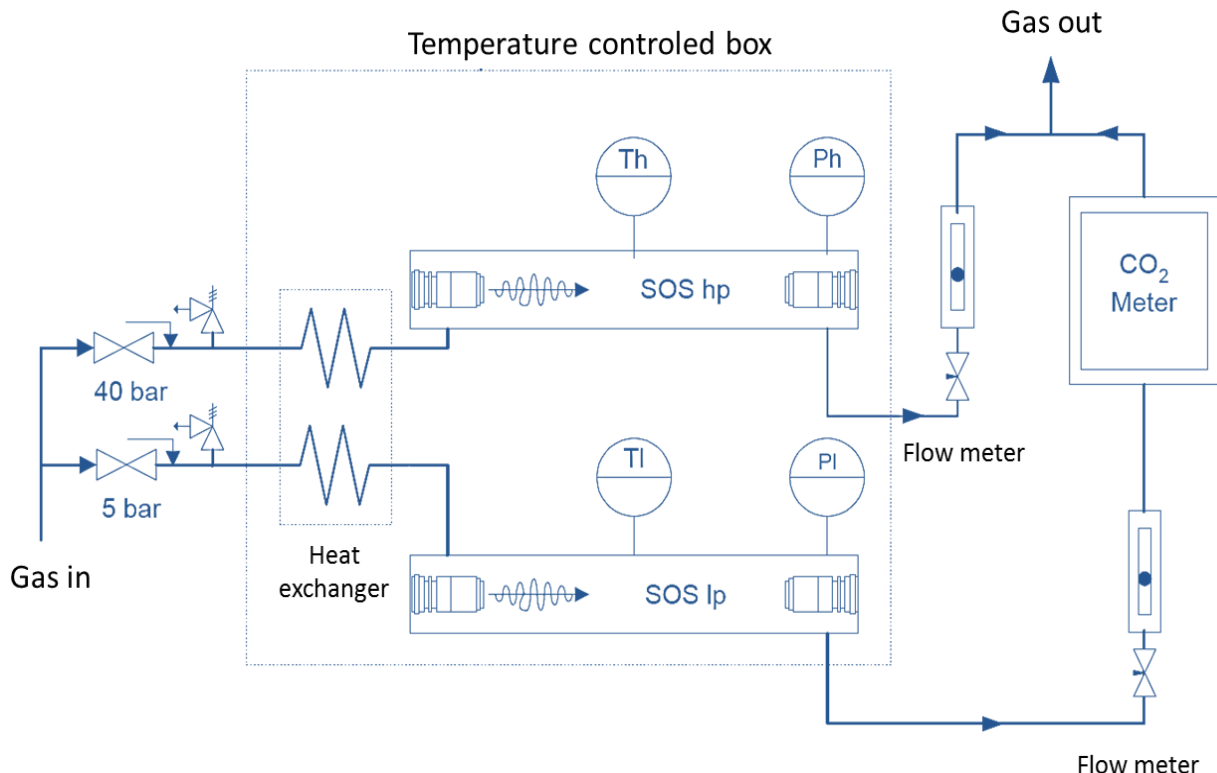


**Figure 2.4 Schematic diagram of the 2VOS-meter energy meter based on two speed of sound measurements and CO<sub>2</sub> content metering, from [Pannemann2001].**

#### 2.3.3.4 WOM 2000

The WOM 2000 was developed by RMG Meßtechnik GmbH (Kassel, Germany). According to publicly available technical data [RMG7111] it consists of two thermal sensors measuring thermal conductivity, thermal capacity and viscosity of the gas. Which correlate well with H<sub>s</sub>, and standard density ( $\rho_n$ ) is obtained by measuring pressure drop in a flow resistor. Both magnitudes are used to calculate the Wobbe index. Specifications report uncertainty better than 1% for H<sub>s</sub> and  $\rho_n$ , together with a T90 response time of 28 seconds. The instrument seems to be no longer commercialized probably due to the commercialization of its evolution, the EMC 500. A photograph of the WOM2000 is shown in Figure 2.5.

### 2.3.3.5 EMC 500

The EMC 500 device is an evolution of the WOM 2000 system [RMG7121,RMG7111]. The unit complements the sensors in WOM 2000, which measured heat capacity, heat conductivity and gas viscosity, with a CO<sub>2</sub> mole fraction IR sensor. Accuracy in measurements for standard density and superior heating value is reported to be better than 0.5%, sensibly improving the 1% specification of the WOM 2000. However, response time is slightly impaired with a T90 specification of 90 seconds. The instrument is currently commercialized; an installation diagram is shown in Fig. 2.6.



**Figure 2.5 Photograph of the WOM2000 commercial device from RMG (source: WOM 2000 datasheet [RMG7111]).**

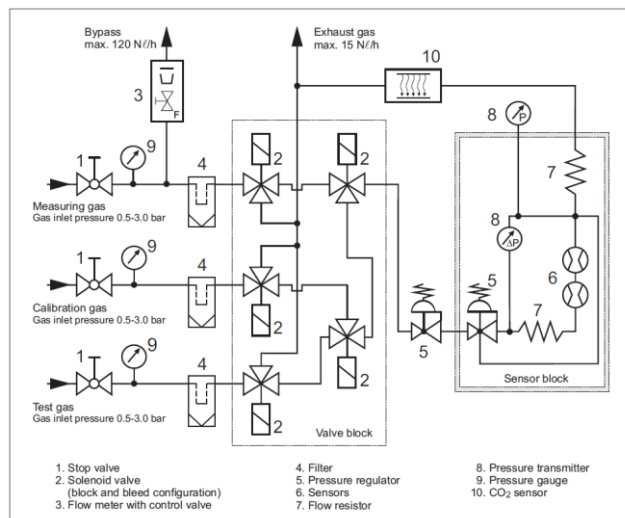


**Figure 2.6 Diagram of the EMC500 measurement setup (source: EMC500 datasheet [RMG7121])**

### 2.3.3.6 GAS-PT

This device based its operation on complementing speed of sound measurements with thermal conductivity measurements at two different temperatures using a commercial sensor [Wild2001]. It reported an uncertainty of 0.5% in SHV for the typical natural gas compositions found in UK. It must be noted that for an extended range of compositions (not specified), uncertainties slightly above 1 % were reported. Response time is specified for a sensor response change of 10% to 90% which is a more optimistic specification than the T90, a 50 seconds response time is reported. In 2010 a second version of the device, the GasPT2 has been certified and has begun to be commercialized. Improvements in this second device rely on the complementation of the GasPT measurements with an external IR CO<sub>2</sub> concentration sensor. Strong investment by CUI global (Tualatin, USA) intends to achieve high market penetration in the natural gas metering scenario, information is available through the company website ([www.cuiglobal.com](http://www.cuiglobal.com)).

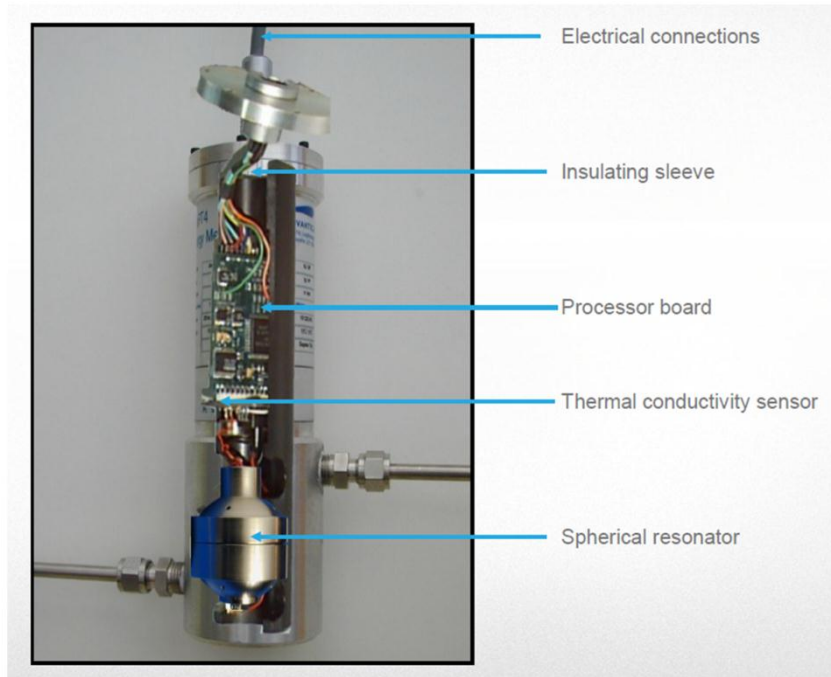


**Figure 2.6 Photograph of a Gas-PT2 device, displaying internal construction.**

### 2.3.3.7 GAS-LAB Q1

This Gas-lab Q1 instrument is available in the market since 2003, and is currently commercialized by Elster-instromet (Essen, Germany) according to the company website ([www.elster-instromet.com](http://www.elster-instromet.com)). The instrument is based on three main measurements: Two NDIR sensors determining absorption due to carbon dioxide and hydrocarbons, and a thermal conductivity sensor [Kastner2005]. Results show fast response with remarkable accuracy, including field test

results reporting differences within 0.25% of a reference Gas Chromatograph (see figure 8 in ref [Kastner2005]). The Gas-lab Q1 exhibits a fast response time ( $T_{90} < 15\text{s}$ ) and has probably been one of the most successful instruments based on correlative methods to date as it is starting to be installed as redundant instrumentation at measurement sites in the German natural gas network. The sensor block construction of the Gas-lab Q1 is shown in Figure 2.8.

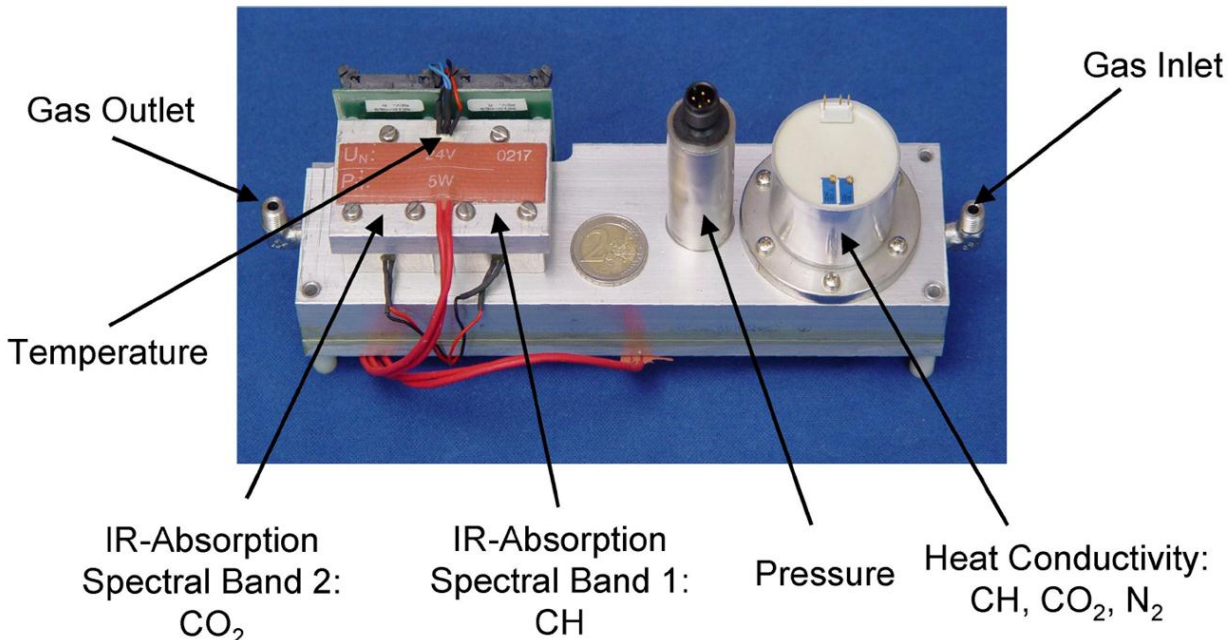


**Figure 2.8 Photograph of the Gas-Lab Q1 sensor setup (from [Kastner2005])**

### 2.3.3.8 METHANE NUMBER MICROSENSOR

An innovative microsensor to determine the methane number of natural gas was developed at Ikerlan (Mondragon, Basque country) around 2004 [Puente2005]. The device provided a single sensor (univariate) sensing approach based on the high correlation of the thermal conductivity of natural gas with the methane number. Field tests were reported showing interesting initial results, but slow response time limited the applicability of the device. Non-negligible thermal couplings of the heated resistor with other regions of the sensor or the walls of the fluidic channel is suspected to be the cause of it, as has been observed in other thermal Microsystems [Fonollosa2009a]

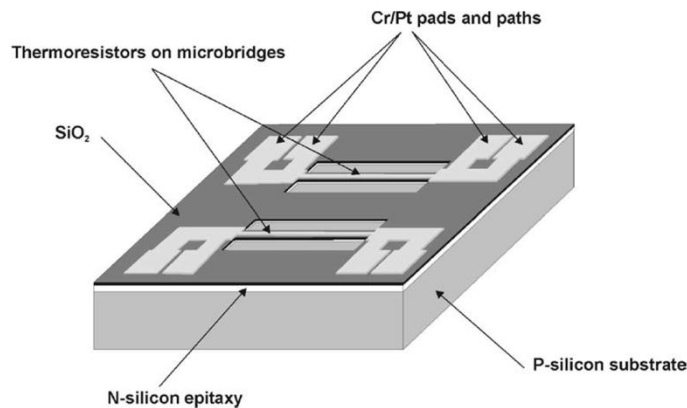


**Figure 2.9 Methane number thermal-based microsensor design from [Puente2005]**

#### 2.3.3.9 ANGus

The company Itron Inc. (Liberty lake, USA) released in 2009 the ANGus device based on the combined measurement of CO<sub>2</sub> molar fraction and thermal conductivity with a correlative inferential method ([www.itron.com/productsAndServices/Pages/ANGus.aspx](http://www.itron.com/productsAndServices/Pages/ANGus.aspx)). The device is compact and provides digital communications. A separate probe for sampling the gas line is required. Reported accuracies are of 1% of measurement point for SHV, W, inferior heating value (IHV) and specific gravity. The instrument presents a low drift which according to manufacturer data is of 0.5% of measurement point per year. Figure 2.10 shows the available connections diagram of an ANGus device.

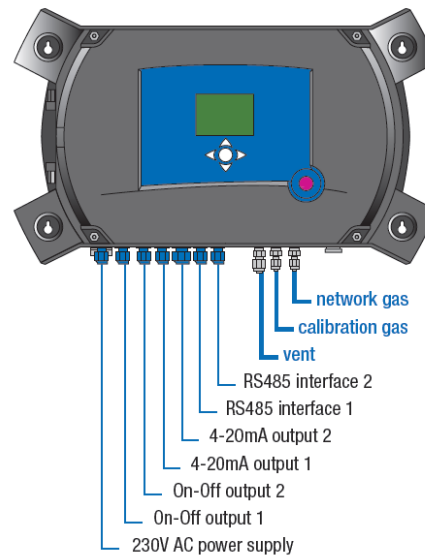


**Figure 2.10 Diagram showing the available connections of an ANGus natural gas quality analyser from Itron. Source: ANGus datasheet**

### 2.3.3.10 RESEARCH APPROACHES BASED ON THERMAL CONDUCTIVITY

The group of M. Tazerout have worked on the analysis of natural gas based in thermal conductivity measurements. First Rahmouni et al. [Rahmouni2003a, Rahmouni2003b] used discrete thermal conductivity sensors and reported accuracies better than 1% of measured value for superior calorific value determination in limited ranges of CO<sub>2</sub> content variation. The concept was further evolved in the same group by K. Loubar [Loubar2007], by adding a velocity of sound sensor and a CO<sub>2</sub> sensor. The new setup reported accuracies better than 0.5% of measured value for superior heating value.

**TABLE 2.2** OVERVIEW OF CORRELATIVE AND ALTERNATIVE METHODS FOR NATURAL GAS ANALYSIS

Nº	DEVICE	DEVELOPED BY	INPUTS	OUTPUTS	UNCERTAINTY $\Delta H_s(\%)$	STATUS	RESP. TIME
1	<b><math>\epsilon</math> method</b>	Rurhgas AG / Gasunie	$\epsilon, V_s, X_{CO_2}, P, T$	$H_s, H_i, W, \rho_n, X_{CO_2}$	0.2	Lab prototype	-
2	<b>IR Spectrometer</b>	FlowComp	$A_{IR}(CH), A_{IR}(CO_2), P, T$	$H_s, H_i, W, \rho_n, X_{CO_2}$	0.2	Lab prototype	-
3	<b>2VOS-meter</b>	Gasunie/Instromet	$V_s(HP), V_s(LP), A_{IR}(CO_2), T, P$	$H_s, H_i, W, \rho_n, X_{CO_2}$	0.3	Available	4 s
4	<b>WOM 2000</b>	RMG	$C_p, Th, \eta, P, T$	$H_s, H_i, W, \rho_n$	1.0	Relegated	28s
5	<b>EMC 500</b>	RMG	$C_p, Th, \eta, P, T, A_{IR}(CO_2)$	$H_s, H_i, W, \rho_n, X_{CO_2}$	0.5	Available	<60 s
6	<b>GasPT / GasPT2</b>	Advantica	$V_s, Th(T1), Th(T2), T, P$	$H_s, H_i, W, \rho_n, MN$	0.5	Available	(2 s) 50 s
7	<b>Gas-lab Q1</b>	Ruhrgas AG, FlowComp	$Th, A_{IR}(CH), A_{IR}(CO_2), T, P$	$H_s, H_i, W, \rho_n, X_{CO_2}, MN$	0.4	Available	15 s
8	<b>MN microsensor</b>	Ikerlan	$Th$	$MN$	-	Lab prototype	30 min
9	<b>ANGus</b>	Ittron	$Th, A_{IR}(CO_2), T, P$	$H_s, H_i, W, \rho_n, X_{CO_2}, MN, SG$	1.0	Available	2 min
10	<b>Laboratory setup</b>	CRPE research centre (Rahmouni et al.)	$Th(T1), Th(T2), T$	$H_i, W, AFR$	1.0	Lab prototype	-
11	<b>Laboratory setup</b>	CRPE research centre (Loubar et al.)	$Th(T1), Th(T2), V_s, X_{CO_2}, T$	$H_s, W, AFR$	0.5	Lab prototype	-

**$\epsilon$ :** relative permittivity;  **$A_{IR}$ :** infrared absorption;  **$V_s$ :** velocity of sound;  **$C_p$ :** heat capacity;  **$Th$ :** Thermal conductivity;  **$\eta$ :** viscosity;  **$x$ :** molar fraction;  **$H_s$ :** superior calorific value;  **$H_i$ :** inferior calorific value;  **$W$ :** Wobbe index;  **$\rho_n$ :** normal density;  **$MN$ :** Methane number;  **$SG$ :** Specific gravity;  **$AFR$ :** Air-fuel ratio;  **$T$ :** Temperature;  **$P$ :** Pressure

## 2.4 GAS SENSING TECHNOLOGIES .

---

Before selecting a suitable technology to face the particular application of natural gas analysis, the field of gas sensing was broadly considered and several technologies were overviewed. This chapter provides an overview of candidate technologies considered and provides the initial ground for the research in this thesis. Gas sensors are often combined as for instance in the devices presented in section 2.3, but combinations are virtually unlimited. The current benchmark for gas analysis is GC, often combined (hyphenated is the technical term) with mass spectroscopy (MS). However, this section is mainly focused on compact sensors which are or might be suitable for reliable integration in microsystems technology given the current state-of-the art. A table is included after each section which summarizes the relevant characteristics of each technology and its advantages and drawbacks with respect to the particular application of natural gas analysis.

### 2.4.1 CONDUCTING POLYMER SENSORS

---

Conducting polymer sensors are sensors coated with a polymeric layer aimed to adsorb certain molecular species. Once adsorbed, the volatile components modulate the electrical conduction of the polymer, which materializes as changes in the resistance of the layer. The studies of conducting polymers assume that reversible charge transferences occur between volatile organic compounds (VOCs) and the polymer, inducing changes to the electric conductivity of the sensor [Persaud1996] [Gardner1994]. Despite the conductivity is the most frequent measurement of this kind of sensors, also AC parameters can be collected. Accordingly, its electric model includes resistance, inductance and capacitance. Many application examples are found in the literature, as reported by several available review articles including Adhikari and Mjudmar [Adhikari2004], Lange et al. [Lange2008] and Bai and Shi [Bai2007]. Applications oriented to odor recognition have been common [Gardner1994, Lonergan1996, Kim2005], using not only resistivity but also changes in mass, optical properties or other electrical properties [Bai2007]. Main disadvantages are their relatively low time stability and manufacturing reproducibility. Polymer sensors can also be designed as capacitive sensors.

### 2.4.2 QUARTZ CRYSTAL SENSORS

---

Two different kind of sensors are included in this category, the surface acoustic wave (SAW) and the quartz crystal microbalance (QMB or QCM) devices which can also be classified as bulk acoustic wave (BAW) devices.

SAW and BAW devices are piezoelectric quartz crystals are normally covered with a sensitive layer usually consisting of a selective coating which adsorbs species of molecules. The adsorbed molecules increase the mass of the sensor producing a decrease of the resonance frequency of the

crystal. This principle dates back to 1964 when King used it to measure the resonance frequency shift to estimate a concentration of odorants [King1964]. From them on, the applications of quartz resonators to chemical sensing have been numerous [Chang2000], and the latest trends include the use of QCM monolithic sensor arrays [Tuantranont2011]. Of particular interest for the considered application is the alternative of using uncoated crystal resonators as gas densitometers as reported by previous works [Zeisel1999], in this configuration, the crystal oscillator works in a principle similar to the microfluidic oscillators discussed in section 2.4.11, but in a much higher frequency range (MHz).

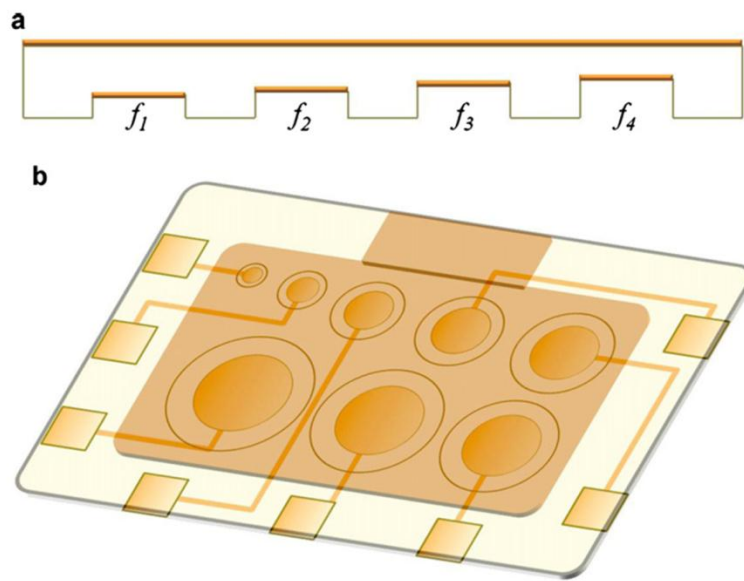


**Figure 2.11 Multi-QCM platform based on varying oscillators thickness and surface area. Multiple sensitivities and improved dynamic range are intended. Source: [Tuantranont2011].**

Both SAW/BAW structures consist of a piezoelectric substrate, a thin layer of single-crystal piezoelectric quartz, where usually a coating adsorbent layer is deposited. The difference between them is that SAW devices present two planar electrodes while BAW devices present two metal electrodes on both sides of a quartz disk as can be seen in Figure 2.11 (b). The operation principle for a SAW device is the propagation of a deformation wave over the sensor surface, while in BAW devices the acoustic wave propagates across the crystal bulk [Moseley1997]. The transmission of the wave is affected by the mass that the crystal displaces, allowing detection of volatiles adsorbed on the sensitive layer, but also changes in the density of the surrounding gas. Typical resonant frequencies for BAW devices are in the range of 5-100 MHz [Tuantranont2011] while SAW devices operate in the typical range of 100-1000 MHz [Nagle1998]. A recent review on gravimetric gas sensors showing the last works involving BAW and SAW devices is available [Fanget2011]. There is a high availability of uncoated BAW devices, but coated devices are not commercially well

established. Recent trends in QCM are the use of multiple integrated oscillators in one device. An example of this is shown in Figure 2.11.

#### 2.4.3 ELECTROCHEMICAL SENSORS

---

The oldest electrochemical sensors date back to the 1950s and were used for oxygen monitoring. Currently, a variety of electrochemical sensors are being used extensively in many applications for personal safety and also environmental monitoring. Despite similarities in construction, size and connection, the operating principles of electrochemical sensors is extremely diverse.

The key point in electrochemical sensor design is material selection. The electrolyte composition and the sensing electrode material are selected based on the chemical reactivity of the target gas. By careful selection of the electrolyte and/or the sensing electrode, one can achieve the selectivity towards the target gas, but the sensitivity may be reduced. Also the porosity of the hydrophobic barriers and other filtering membranes is an important design parameter. Additionally, some electrochemical sensors use external electrical energy to make them reactive to the target gas. Some sensors operate at considerably high temperatures. All components of the sensors play a crucial role in determining the overall characteristics of the sensors.

Electrochemical sensors operate by reacting with the gas of interest and producing an electrical signal proportional to the gas concentration. Typically the reactive processes involve reduction or oxidation of the sensed gases, for this reason most electrochemical sensors are designed for sensing in the presence of oxygen. Thus, they are in general not suitable for this particular application.

#### 2.4.4 INFRARED BASED GAS SENSORS

---

Latest trends in MEMS research and development have established over the last years a complete field of infrared (IR) microsensors for gas sensing. Expertise in this same research group from the Universitat de Barcelona can be found thanks to previous PhD thesis by Calaza, Rubio and Fonollosa among others. [Calaza2003b, Fonollosa2009c, Rubio2007]. A brief description of the sensing principle for infrared based sensors follows.

Electromagnetic radiation interacts with different molecular species in different ways, depending also on the wavelength of the radiation. IR radiation is a low energy radiation which does not change the electron energies of the atom, but it interacts with the bonds holding the atoms of a molecule together, which are in constant vibration at a characteristic frequency that depends upon the strength of the bond and the masses of the atoms or group of atoms it is holding together. These vibrating bonds may absorb IR radiation, thus attenuating the outgoing radiation. Attenuation will be greater depending on the number of molecules that the IR radiation irradiates, thus the attenuation of the radiation is an indirect measurement of the density or concentration of a given

molecular species or set of species. This is the basis of gas detection using IR detectors. Other alternative measurement methods try to measure the energy absorption instead of the radiation transmission. The photo-acoustic detectors which will be discussed in the next sections are such type of detectors. Three kind of IR sensor systems will be described, the non-dispersive IR (NDIR) systems , the Fourier transform IR (FTIR) systems, and the photo-acoustic effect based systems.

#### 2.4.4.1 NDIR

NDIR systems are a common approach based in the absorption of IR radiation at selected wavelengths by the analyzed sample. While in DIR systems, the wavelength is selected by dispersing the different wavelengths of the IR radiation with the use of a prism or a diffraction grating, in NDIR the wavelength selection is performed by using a narrowband transmission filter. An example setup of such system can be seen in Fig. 15.

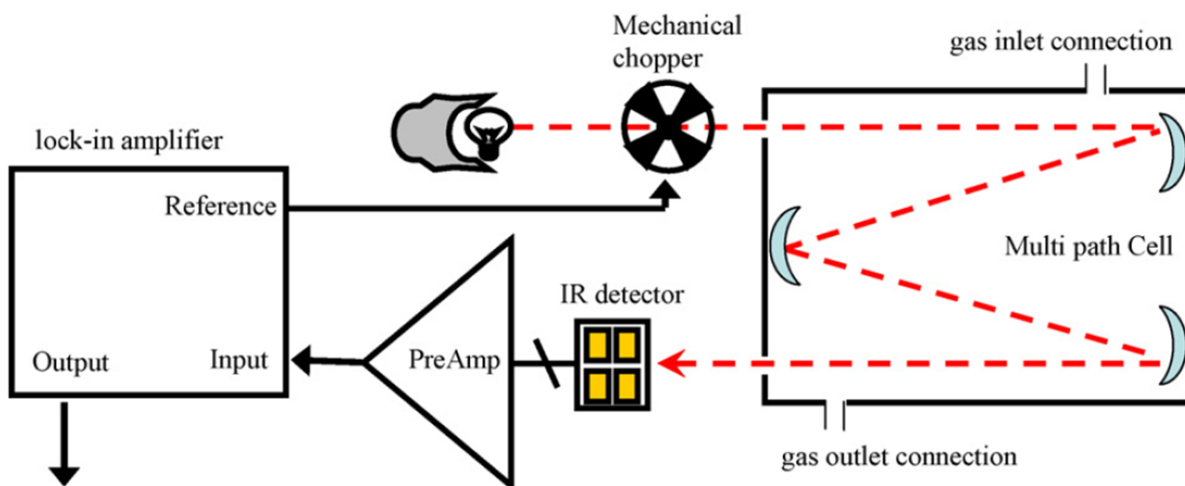


**Figure 2.12 NDIR optical detection system consisting of an IR source, a mechanical chopper, a White cell and a detector. From [Fonollosa2009b].**

The basic NDIR setup consists of:

- **An infrared source**

Absorption regions of interst in common target gases are in the wavelength band of  $3\mu\text{m}$  to  $10\mu\text{m}$ . The IR emission shall ideally concentrate its emission power in this band. Additionally, modulation of the IR emission is desirable since synchronous detection techniques provide improved signal recovery in presence of noise.

The most common type of IR source are the thermal emitters. They produce a spectral irradiance similar to the ideal black-body radiator. Traditional thermal emitters consist of a heated incandescent tungsten filament, however micromachined alternatives have been proposed though there are still problems associated with emitting in the band of interest [Cozzani2007]. Other IR sources used are Mid-IR LEDs and vertical cavity surface emitting lasers (VCSEL) which emit in the near IR. The narrowband emissions of these IR sources avoid the need of a filter. However these IR sources exhibit large power and spectral temperature dependencies, and its cost is significantly higher.

- **An IR detector**

The detector in this applications shall be sensitive to much longer wavelengths than those of the visible spectrum. An ideal detector should have a flat spectral response curve in all the range of interest which is usually not the case. There are basically two main technologies for IR detectors, the quantum detectors and the thermal detectors.

Quantum type detectors are based on photon absorption which directly excites an electron-hole pair in the detector and changes its electrical properties. An example of quantum detector is the photoconductive detector. It consists of a high-resistivity semiconductor material, the resistance of which is reduced when it is exposed to IR radiation. A second example are the photovoltaic effect based detectors, where the incident radiation causes a current to flow in the p-n junction of a semiconductor.

Quantum detectors show excellent detectivity in the IR range and fast response, but they are strongly wavelength dependent and, they need to be cooled for accurate measurement.

In thermal detectors the absorbed photons result in a temperature increase of the active part of the detector, which is transduced into an electric signal. Despite having a lower detectivity compared to quantum detectors, thermal detectors are widely used due to its uncooled operation, their small wavelength dependency and flat response [Noda2005]. Thermal detectors can be split into three large categories:, the bolometers which are resistive detectors; the pyroelectric detectors which rely in the pyroelectric effect, and the thermoelectric detectors or thermopiles which rely on the Seebeck effect. Of the three, thermopiles are the most sensitive ones, and they also exhibit a flat spectral response.

The IR detectors based in thermopiles are of particular relevance for this work since a previous PhD dissertation from Calaza in this subject [Calaza2003b] provided the necessary expertise and technology for the initial development of the work. The section on thermal sensors will further describe the operation principles some of this sensors.

- **Optics**

NDIR gas sensors use one specific detector for each gas to measure. To select the suitable wavelength for each gas, specific optical narrowband filters are needed. They are usually

placed directly upon the IR detector set or on a rotating filter roulette, though this second approach implies the complexity of additional mechanics. Other innovative approaches regarding filters have been reported by Rubio et al. [Rubio2006, Rubio2007] who suggested the use of less specific filters defining a filter array providing a pattern response to different gas mixtures or odours, and Sabaté et al. [Sabate2005] who proposed electrostatic mid-IR filter tuning using a micromachined Fabry-Perot interferometer.

A conventional bandpass optical filter consists on a number of dielectric layers on a substrate. The thickness, the number and the material of the deposited layers on the substrate determine the transmission characteristics of the filter [Rancourt1996, Schilz2000], usually silicon is used as the substrate to take advantage of its associated manufacturing technologies.

Sometimes a focusing element may be placed to increase the amount of radiation reaching the detector. Relevant work on in this field was reported by Fonollosa et al. in 2008 [Fonollosa2008, Fonollosa2009b].

- **A measuring chamber (absorption cell)**

The absorption cell provides the interaction between sample and radiation, the optical path of the radiation across the sample is a critical and size-limiting design parameter. The design of the absorption cell has direct influence in performance parameters like sensitivity, selectivity and stability. The usual design consists on a tubular cell that allows light to enter on one side and to exit on the other, with inlet and outlet gas ports [Chou2000]. Other more complex designs look for multiple reflections inside the cell to increase the optical path length without increasing the size as first proposed by White in 1942 [White1942].

The main advantages of this technology are good selectivity and repeatability, together with high manufacturing reproducibility and fast response times (mainly dependent on fluidic dynamics at the measurement chamber). However there are limitations regarding size reduction due requirement of a minimum optical path available. In general the sensor setup is more complex than in solid state sensors.

---

#### 2.4.4.2 PHOTOACOUSTIC DEVICES

---

In this case the IR radiation measured is the absorbed energy, as opposed to the NDIR devices where the transmitted energy is measured. In order to measure the absorbed energy, the incident IR radiation is modulated at high frequencies in the order of KHz, the radiation is absorbed by the gas present in the measurement chamber and causes small and fast changes in the gas temperature and pressure, which can be measured as acoustic waves. A typical microphone or pressure transducer can be used to detect these pressure fluctuations in the acoustic range ( $\sim 20\text{Hz} - 20$

KHz). The sample may be irradiated at different IR wavelengths to obtain a full IR absorption spectrum. However, since high optical powers are desired, it is common to use IR lasers or LEDs at the wavelengths of interest. Extremely sensitive devices have been reported with this approach. An example device is shown in Fig. 2.13.

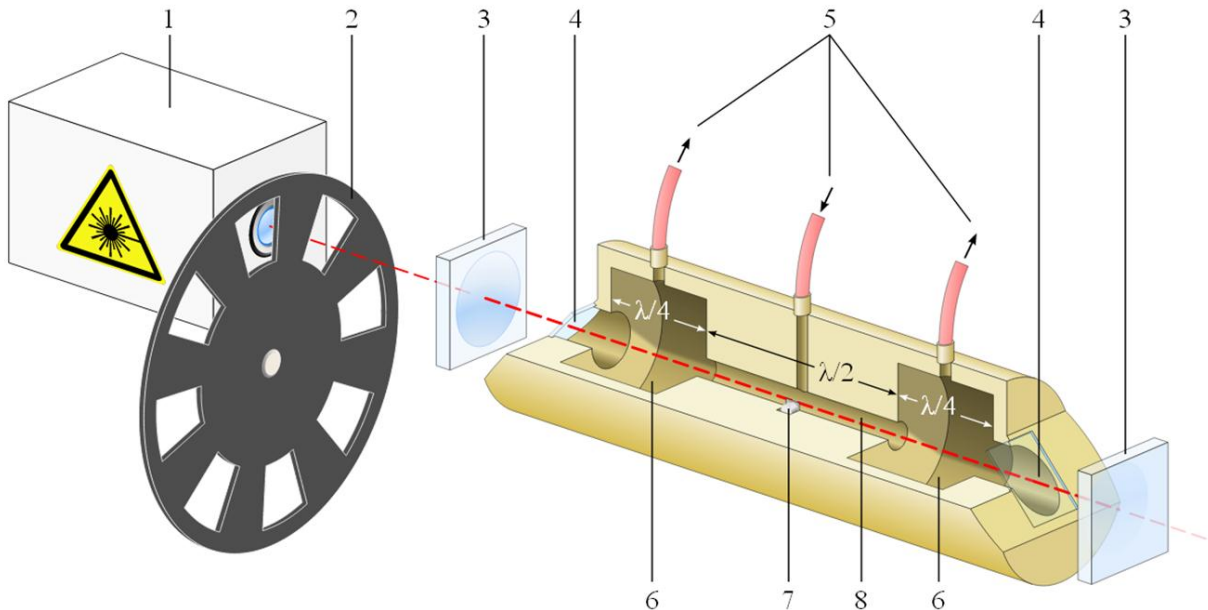


**Figure 2.13. Photoacoustic spectrometer example setup. Source: wikipedia (photoacoustic spectroscopy)**

In the example device of figure 2.13, acoustic resonance occurs at a sound wavelength of double the resonator length. Instead of a chopper wheel, variation of the absorption could also be achieved with a tunable laser, modulating its frequency across absorption wavelength. Additional  $\lambda/4$  tube elements could be added for example in the gas inlet to prevent unwanted flow noises. Electronic control elements, especially a lock-in amplifier, are not shown.

1. Light source (e. g. Laser)
2. Chopper wheel
3. semipermeable mirrors form an optical resonance system
4. cell windows (tilted for polarisation)
5. gas flow inlet and outlets
6. buffer gas volumes
7. acoustic sensor (e. g. microphone or transducer)
8. resonator

Photoacoustic sensing can in some applications provide significantly higher sensitivities than the more extended NDIR approach. If a very high sensitivity is not needed, photoacoustic devices can have a simplified design, without the need of extremely precise optics.

#### 2.4.5 COLORIMETRIC GAS SENSORS

These devices are based on the color change of a reactive substance as a consequence of the presence of a certain gas [Zdankiewicz1997].

There are two different configurations:

- **Glass pipe.** The reactive is introduced into a glass pipe, with a calibrated scale to indicate the gas concentration
- **Paper tape.** A paper tape is impregnated with the reactive which will change its color in the presence of the target gas.

In order to make electronic devices based on colorimetric sensors, a color detector must be used. This implies the need of an optical source and a color sensor. The key element of the detector is the reactive which modifies its optical properties after reaction with the target gas. Very often there is a strong chemical interaction between the sensing layer and the analyte, making the sensing reaction irreversible. Suslick et al. [Suslick2004] report an interesting application claiming a high insensitivity to changes in environmental conditions (humidity and temperature), which was often attributed as a limitation for these sensors. More importantly, Suslick proposed a matrix of colorimetric sensor arrays which provided individual color patterns when exposed to different chemical samples, which could afterwards be “readed” with low cost optics. Its main limitation in regards to the considered application remains to be the slow or/and irreversible reaction dynamics.

#### 2.4.6 FIBER OPTIC BASED GAS SENSORS

The structure of a fiber optic sensor commonly consists of a conventional optical glass fiber covered with a thin fluorescent coating on the sides or the ends of the fiber, which interacts with the gases or odorant molecules, the approach was given great interest in the late 1990s and it was proposed as a suitable approach for distributed measurement [Stewart1997]. However, development of optical fibers has continued, in particular in the field of biosensors [Leung2007], though other types of optical fibers have also been developed which are relevant for the detection of methane [Frey2011, Tao2011]. These approaches show in general a rather low sensitivity, and typically involve a complex optical setup. However, the approach has advantages regarding safety, ruggedness and stability. More generally, optical techniques like refractometry and reflectometry [Pawliszyn2005] can be used in gas analysis, indeed the potential use of refractometry in the field

of natural gas analysis was explored in the first part of the work by Rahmouni et al. [Rahmouni2003a]. An interesting overview of the use of fiber optic sensor arrays for vapor sensing application was reported by Aernecke and Walt in 2009 [Aernecke2009].

#### 2.4.7 PELLISTORS

---

Pellistors are based on the catalytic (flameless) combustion of a target gas. Heat produced by combustion is then transduced into an electrical signal. Since they measure the heat produced by a combustion, they can be classified as calorimetric sensors. In general a thermoresistive transduction principles is the most commonly used. The operating principle of pellistors is based on an oxidizing metal (catalyst) dispersed on a porous wide surface area of a ceramic substrate which provides a number of reaction sites where molecular bonds are broken or formed. Combustible gases coming into contact with the catalytic metal are oxidized (burned), releasing an energy that changes the electrical resistance of the thermoresistive bead. Due to the presence of an oxidation reaction, the sensors are designed typically to operate in environments in the presence of air, for this reason they are not suitable for the selected application.

#### 2.4.8 THERMAL CONDUCTIVITY SENSORS

---

Sensors which operate based on thermal processes have already been described in previous sensors such as the detectors in IR systems or the pellistors. In these sensors the thermal process provides information of the measured gas in combination with other processes, the combustion in the case of pellistors, and the absorption of IR radiation in IR systems.

There are sensors which rely only on a thermal transduction process as the main sensing process. This thermal transduction is based only on a heat transfer process, there is no reaction and they can be considered as chemically passive. The different thermal conductivity of different gases produces a different response in the thermal conductivity sensors (TCS). TCS have a low sensitivity and are usually used to detect changes in gas composition in the per cent range. Two examples are considered in this section, the thermal conductivity detector (TCD) which is commonly used as a detector in GC; generic thermal conductivity microsensors which are commercially available (often found in combination with other sensors in multisensor devices presented in section 2.3.3).

The thermal conductivity detector (TCD) is a detector commonly used in GC. This detector senses changes in the thermal conductivity of the column effluent and compares it to a reference flow of carrier gas. Since most compounds have a thermal conductivity much less than that of the common carrier gases of helium or hydrogen, when an analyte elutes from the column the effluent thermal conductivity is reduced, and a detectable signal is produced. The TCD is probably the first and the mostly widely used detector for GC in general gas analysis and in environmental testing

[Scott1998]. The use of thermal conductivity measurement for gas analysis dates back to the last century [Daynes1933]. Although the TCD is not as sensitive as solute property detectors such as the flame ionization detector (FID) [Scott1998], it continues to be popular in recent years in some GC applications owing to its simplicity and robustness. TCDs are concentration sensitive devices which are suitable for high gas concentrations (typically above 0.1%) while GC detectors of higher sensitivities are mainly ionization detectors which are mass sensitive. As the detector size is reduced, the detector volume decreases, but the gas concentration is not greatly affected. Thus TCDs are at a large advantage in a miniature system compared to other types of GC detectors [Jerman1981, Chen2000, Wu2002, Sun2011]. The first TCDs consisted of a thin metallic wire or a thermistor bead. Using the photolithography technique and chemical or physical deposition process developed for fabricating microelectronics, TCDs which are several orders of magnitude smaller than conventional hot-wire or thermistor-bead TCDs have been developed and are commercially available. These miniature TCDs generally involve a thin film of heating element deposited on the floor or suspended in the middle of a microchannel etched on a silicon wafer [Jerman1981, Chen2000, Wu2002, Sun2011]. Several thermal conductivity cell configurations are possible, as depicted in Figure 2.14.

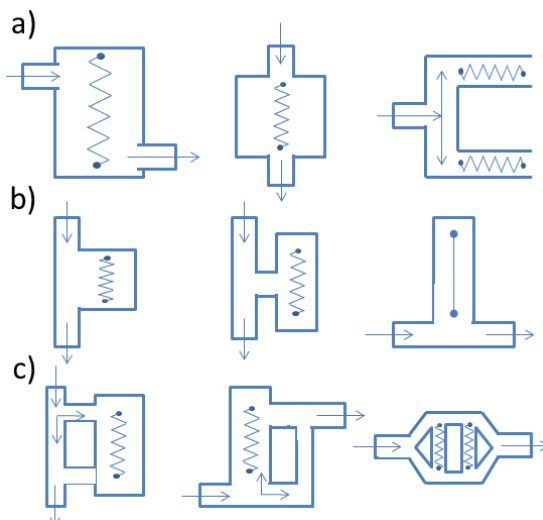


**Figure 2.14 Different configurations thermal conductivity cells a) flow-through b) diffusion c) semi-diffusion. From [Sevcik1976]**

The main heat transfer process in micro TCDs is commonly conduction through the gas volume. However, it has been suggested that convection should be taken into account for high accuracy estimations [Chen2000]. The device reported by Puente et al. [Puente2005] which was presented in section 2.3.3.8 has clear analogies to a TCD, including the presence of a fluidic microchannel, but without the analyte separation provided by the chromatographic column.

Other general purpose thermal conductivity sensors are commercially available, and are used for diverse applications including binary gas mixture analysis and vacuum sensors (pirani gauges). As a main difference to TCDs, these devices typically do not include an integrated fluidic channel or measurement cell. Companies such as Microsens (Switzerland), Xensor Integration (Netherlands) or Durham Instruments (Canada) commercialize thermal conductivity microsensors based on MEMS technology. Application of this type of sensors has been commonly limited to the analysis of binary gas mixtures though patents have suggested the use of similar configurations for the analysis of other gas mixtures [Goeldner1990, Grunewald2004] however, this type of sensors is frequently combined with other types in multisensor systems for natural gas analysis presented in section 2.3.3. Among these, research works by Rahmouni et al. [Rahmouni2003a, Rahmouni2003b]; Loubar et al. [Loubar2007], Wild et al. [Wild2001] and Kastner [Kastner2005] outstand as the most interesting approaches (refer to section 2.3.3).

The previous research expertise in design of thermoelectric MEMS sensors in the research group for optical sensing [Calaza2003b] provided a good basis for the study of this type of sensors as suitable thermal sensors. A photograph of a MEMS thermoelectric sensor is shown in Figure 2.15.

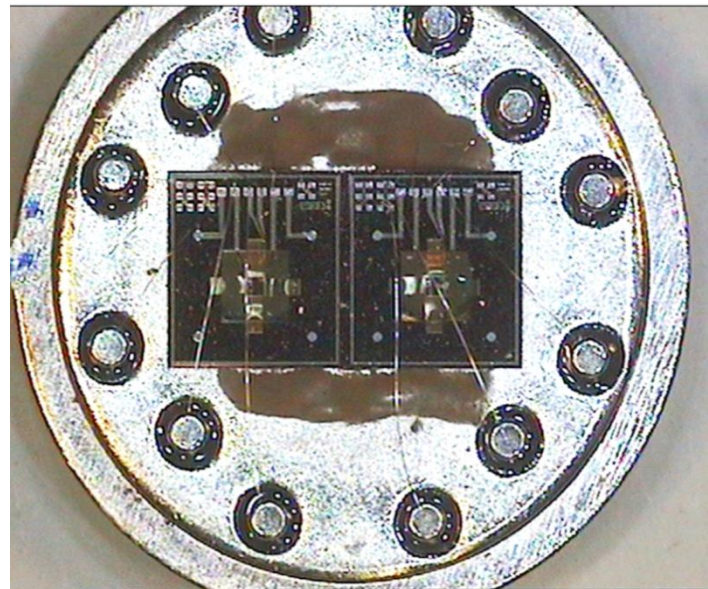


**Figure 2.15 A photograph of an encapsulated device featuring two MEMS thermoelectric sensors**

#### **2.4.9 METAL-OXIDE SEMICONDUCTOR SENSORS**

---

A metal-oxide semiconductor (MOX) sensor is a resistive device which relies on a metal-oxide as a gas sensitive material; their detection principle is complex and is based on reduction or oxidation reactions that take place in the metal-oxide surface when it is heated at high temperatures

[Wetchakun2011], typically between 100°C and 300°C, but sometimes even higher temperatures which are achieved with the use of a heater integrated in the sensor device. The reactions at the metal oxide surface change the conductivity of the sensing layer, which can be electrically read in order to obtain a signal proportional to the concentration of the target gas. The most popular metal-oxide used in the tin-oxide ( $\text{SnO}_2$ ). The resistance change in  $\text{SnO}_2$  due to the absorption of gas in its surface was demonstrated in 1953, and Taguchi and Seiyama reported in 1960 the first MOS structures for gas sensing [Moseley1997] hence the usual terminology of Taguchi gas sensors (TGS) for this kind of devices. Due to the intervention of oxygen in the sensing and recovery processes in these sensors, they are not suitable for the application.

#### 2.4.10 VELOCITY OF SOUND SENSORS

These type of sensors have found widespread use in ultrasonic flow metering devices, thanks to this it is a well known and reliable technology in industrial environments. It has been also proposed for the analysis of binary gas mixtures [Vyas2006] and interesting possibilities for the analysis of ternary mixtures were proposed in the 1990s [Zipser1995] which seem yet to be explored in depth. Velocity of sound metering has found application in the natural gas metering field as previously described in section 2.3. Some of the proposed instruments for natural gas analysis have used this technology as was shown in table 2.2 [Pannemann2001, Jaeschke2002]. Measurement setups up to date are bulky, with instrument volumes in the range of several dm<sup>3</sup>, however the recent developments in miniature acoustic transducers and high availability stimulated by the mobile phone industry can provide an improved basis for this technological approach. The technique has a low sensitivity, so it mainly adequate for gas concentration measurements in the per cent range.

#### 2.4.11 MICROFLUIDIC OSCILLATOR SENSORS

The sensing principle of microfluidic oscillators is closely related to that of velocity of sound sensors. The resonating frequency of a microfluidic oscillator is mainly determined by the speed of sound in the given fluid, that is molecular weight and adiabatic index of the gas (closely related to gas viscosity). For this reason both technologies are closely related. This technology is quite common in the analysis of fluids in the field of biosensors as a measurement of fluid density and viscosity [Lucklum2011], but the same concepts may be applied to the measurement of gases [Zipser2000]. The approach shows however low sensitivity and selectivity, what has restricted its use to the measurement of binary gas mixtures [Zipser2000] in the per cent range of compositions.

#### 2.4.12 DIELECTRIC PERMITTIVITY SENSORS

---

Another physical property which is characteristic of gases and varies with composition is the dielectric (or electric) permittivity either relative  $\epsilon_r$  or absolute  $\epsilon$ . This intrinsic property has a significant variation in particular for each of the natural gas main components [Schmidt2003], this circumstance was used by Jaeschke [Jaeschke2002] for the development of a high accuracy natural gas analyzer based on dielectric permittivity measurements as already summarized in section 2.3. Applications to other gas mixtures have not been found. However, the initial work by Jaeschke [Jaeschke2002] seems to have motivated significant interest in the dielectric permittivity of natural gas components [Schmidt2003] and its calculation and correlations for mixtures [Harvey2005]. The time response of this technological approach is not clear from the available information, but it seems an interesting approach for industrial process control applications. However the fabrication of the sensor itself appears as a technically demanding task.

### 2.5 COMPARISON OF CONSIDERED TECHNOLOGIES AND DISCUSSION

---

The presented gas sensing technologies can be compared according to a large number of criteria. In this work, and taking into account the particular application considered, seven different criteria have been selected and evaluated for each candidate technology. These are the cost; the suitability of integration in a MEMS device; its response time; the possibility of using the sensor as an in-pipe probe; the time stability of the sensor signal during long operating periods; the possibility of operating the sensor in an anoxic environment, and the sensor setup complexity in the sense of number of parts it is composed of, size, and the precision needed for their allocation, etc...

A ranking of the suitability of each technology for the presented application was elaborated and is shown in the last column of table 2.3. This rank position takes into account the global evaluation for the different criteria. According to this criteria, the thermal sensors technology was selected as a candidate technology for the proposed compact smart sensor for natural gas analysis.

**TABLE 2.3 GAS SENSING TECHNOLOGY EVALUATION FOR NG ANALYSIS USING MEMS SENSORS**

	Cost	MEMS fabrication	Response time	In-pipe measurement	Time stability	Operative Without oxygen	Setup complexity	rank
<b>PY</b>	A	A	C	B	D	A	A	6
<b>QMB</b>	B	C	A	A	A	A	A	2
<b>EC</b>	B	D	C	A	B	D	B	8
<b>PA</b>	B	B	A	A	A	A	B	3
<b>NDIR</b>	B	B	A	C	A	A	C	5
<b>PEL</b>	A	B	B	C	C	E	D	11
<b>FO</b>	C	C	A	A	A	A	C	4
<b>TS</b>	B	A	B	A	A	A	A	1
<b>MOX</b>	B	A	C	B	D	E	A	10
<b>VS</b>	C	C	A	D	A	A	C	7
<b>MO</b>	B	C	A	C	A	A	B	8
<b>DP</b>	D	D	B	D	C	A	C	9

A: optimal B: good C: average D: below average E: bad (may rule out the technology for the considered application)

Technology abbreviations: **MOX**: metal oxide sensors; **TS**: thermal sensors; **FO**: fiber optic sensors; **NDIR**: infra-red sensors; **PA**: photoacoustic sensors; **EC**: electrochemical sensor; **QMB**: quartz microbalance sensors (uncoated); **PY**: conducting polymer sensors; **VS**: velocity of sound sensors; **MO**: microfluidic oscillators; **DP**: dielectric permittivity sensors

## 3. OBJECTIVES

---

**T**wo sets of objectives sprout from the initial task planning of this PhD thesis. A first set of objectives is related to the conceptual design of a smart chemical sensor, directly related to the initial funding by the NEPSSI project aimed to the development of a compact (portable) gas sensor array instrument with integrated intelligent signal processing.

The **design of an optimal smart chemical sensor architecture**, was thus a first objective.

The design of the instrument was chosen to be based on standards and in particular IEEE-1451.2 as the underlying architecture. Additionally, the quality metrics standard BS-7986 was selected for the self-determination of measurement quality.

The novel **combination of the highly complementary IEEE-1451.2 and BS-7986 smart sensor standards** posed many challenges in the design and programming of the prototype smart sensor. This objective is covered in chapter 6.

A second set of application-related objectives is related to the selected application, namely natural gas analysis. Currently, available instrumentation is characterized in general by high acquisition and/or maintenance costs, bulkiness and often slow time response, as thoroughly reviewed in section 2.3. The aim was to try to **solve the natural gas quality analysis problem by using a lower cost approach taking advantage of MEMS technology, smart sensor features, and embedded intelligent signal processing**.

The first application-related objective was **selecting a suitable gas sensing technology**, for which a study of available technologies was considered. After that the simulation and test of the selected technology was needed, related research forms the body of chapter 4, together with a preliminary analysis of the sensor response to natural gas compositions. After that first **sensor evaluation**, the next objective was the selection of a **suitable signal processing approach** which had to allow the estimation of natural properties from the sensor readings. After this technological selection of sensor and signal processing, a practical demonstration of the sensor application was needed, together with an **estimation of uncertainty sources** and **expected metrological limits** of the technological approach. These three objectives are addressed in chapter 5.

As a final objective, the demonstration of both the application related and smart-sensor related was intended in a **working smart-sensor prototype**, and its validation with experimental measurements. This final objective is covered in chapter 6.

## 4. STUDY OF A NOVEL APPROACH: A MICROMACHINED THERMOELECTRIC GAS SENSOR FOR NATURAL GAS ANALYSIS

---

4.1. Introduction.....	58
4.2. Sensor fabrication and operating principle.....	59
4.3. Sensor characterization.....	62
4.4. Thermal conductivity of gas mixtures .....	63
4.5. Physical model .....	66
4.6. Model results and validation.....	68
4.6.1. Laboratory testbench and validation results.....	69
4.6.2. IR imaging and discussion.....	73
4.7. Estimation of the sensor sensitivity.....	73
4.8. Chapter conclusions.....	77

## 4.1 INTRODUCTION

Section 2.3 provided a discussion about the importance and the state of the art of natural gas quality metering. The three main groups of existing techniques were presented, the combustion calorimeters, the PGC and the correlative methods. Insight in the latter category showed that these correlative methods are basically implemented in multisensor devices. An hypotheses was drawn that the present instrumentation could be improved, at least in some aspects, by the use of a MEMS approach. An ideal situation can be devised, in which a single microsensor would be located inside a natural gas pipe as a probe, and transmit the gas properties in real-time. This chapter covers the first step of the research, where a candidate MEMS technology was studied and simulated to evaluate its suitability for the application of natural gas analysis.

Section 2.4 has discussed on different considered gas sensing technologies for implementation in a low cost smart sensor for natural gas analysis. Among these the thermal sensors stood out as a particularly interesting option as show in the comparison table 2.15. For this reason, and given the previous experience of this research group in the field of thermoelectric MEMS sensors [Calaza2003b], a microfabricated hotplate device was selected, simulated, fabricated and validated using experimental measurements.

In this case, the micromachined hotplate is heated at a temperature above ambient, establishing a heat transfer between the hotplate and the heat-sinking region across a measured gas, as will be further described in section 4.2. The sensor response provides an indirect measurement of the thermal conductivity of the surrounding gas. In this point the sensing mechanism is analogous to that of thermal conductivity sensors presented in section 2.4.8, which are typically used for the analysis of binary gas mixtures. However, the results of the presented analysis supported the possibility of using advanced signal processing techniques to analyze natural gas typically consisting of more than two components.

Related relevant previous works were discussed in section 2.3.3, including the measurement of natural gas properties using discreet common (not micromechanized) thermal conductivity sensors by Rahmouni et al. [Rahmouni2003a, Rahmouni2003b] suggesting that multisensor analysis could be an option for fast measurements with moderate accuracy (around 1%). The technique was able to resolve three components of natural gas. Another related work is the TCD-like approach reported by Puente et al. [Puente2005] already mentioned in section 2.3.3.8 for methane number evaluation of natural gas, but some features, mainly time response and resolution, were not optimum for fast and accurate gas analysis (as would probably be the case with most

micromechanized TCDs [Wu2002]). From these works [Puente2005, Wu2002, Pollack1993] the need of accurate simulation tools for the design of this kind of MEMS sensors becomes evident.

The chapter is organized as follows; it first covers the description of the thermoelectric device. Technology and operating principle are presented in section 4.2. A preliminar characterization of the sensing element, the thermopile, is reported in section 4.3. The thermal conductivity model for gas mixtures is described in section 4.4. A model of the device itself is needed for simulation. Section 4.5 presents the finite element model of the device which was used. The obtained simulation results are compared against experimental measurements in section 4.6. Using some of this measurements, the sensitivity of the real and simulated device was estimated and compared using experimental design and response surface methods in section 4.7. Last of all, the chapter conclusions are drawn in section 4.8.

## 4.2 SENSOR FABRICATION AND OPERATION PRINCIPLE

---

The sensor measures the differential temperature increase between the hot spot in a micromachined membrane and the silicon rim. The temperature of the hot spot is risen by an integrated resistive heater. Similar sensor configurations have been reported for infrared sensing [Calaza2003] or microcalorimetry [Minakov2006],

The device studied in this work has been fabricated with CMOS compatible micromachining processes, leading to many advantages, namely the possibility to integrate electronic signal acquisition and conditioning in the same chip, an enhancement of sensing properties, as well as achieving low power consumption.

At the beginning of the device fabrication process, a 300  $\mu\text{m}$  thick silicon wafer is heavily doped with boron to define the thermal spreader area. After that, the oxide-nitride sandwich layers are deposited (100 nm SiO<sub>2</sub>, 300 nm Si<sub>3</sub>N<sub>4</sub> and 50 nm SiO<sub>2</sub>). On top of that, a polysilicon resistor is defined on the membrane by deposition of a 480 nm thick layer and posterior etching to pattern the stripes. Electrical isolation of the resistor is accomplished by deposition of a 500 nm oxide layer. Following that, 500 nm aluminum thermocouple stripes and electrical contacts are patterned. Then, a last layer of passivation (silicon oxide-nitride layer) is deposited. Finally, an anisotropic wet etching process is performed to eliminate the silicon from the backside and thus defining the supporting membrane (the high level boron doping of the silicon island prevents it to be removed). A top view of the final device can be seen in Fig. 4.1.

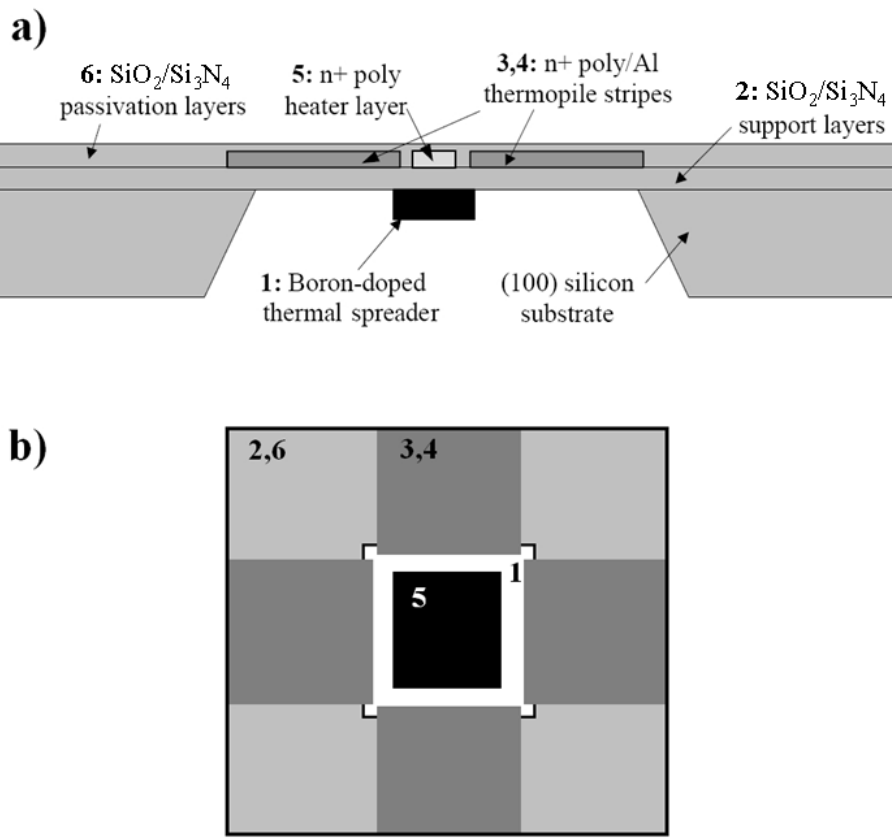


**Figure 4.1 Schematic (a) cross-sectional and (b) top views of the device. 1, silicon thermal spreader; 2,  $\text{SiO}_2/\text{Si}_3\text{N}_4$  support layer; 3,4, n+poly/Al thermopile stripes; 5, polysilicon heater layer; 6,  $\text{SiO}_2/\text{Si}_3\text{N}_4$  passivation layer.**

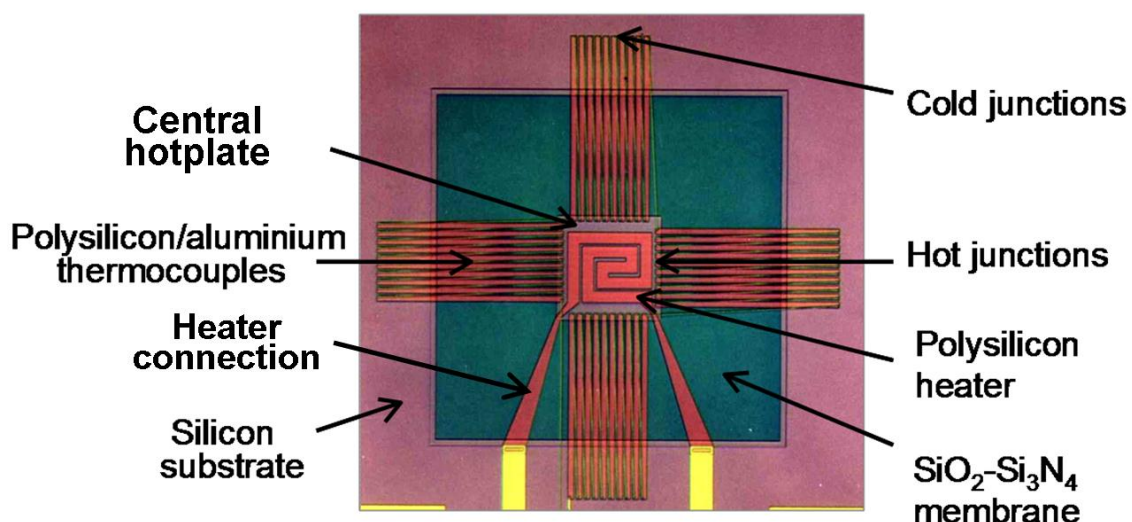


**Figure 4.2 Photograph of the active part of the sensor (Top view)**

The sensor structure consists of a thin membrane defined on a silicon chip, as seen in Fig. 4.2. The membrane is a  $1500 \mu\text{m} \times 1500 \mu\text{m}$  multilayer sandwich structure of  $\text{SiO}_2/\text{Si}_3\text{N}_4$  which sustains the thermocouple stripes extending from the silicon rim (where their cold junctions stand) to a hotplate in the center of the membrane (where the hot junctions lay). The device has 10 thermocouples per side, for a total of 40. A polysilicon heater is located in the hotplate to heat up the hot junctions at a desired temperature and a boron-doped silicon island is located right below as a thermal spreader for better temperature homogeneity across the hotplate. Heater dimensions are  $366 \times 310 \mu\text{m}^2$  and the thermal spreader is  $450 \times 450 \mu\text{m}^2$ . The backside of the die is attached to a metal casing (TO-8) using a high thermal conductivity epoxy adhesive. The metal casing acts as a heat sink to keep the substrate (and thus rim) temperature approximately constant. The TO-8 casing presents a drilled hole in the area right below the membrane, which improves gas exchange with the surrounding atmosphere.

The materials chosen to make the thermocouples are of key importance since they greatly determine the sensor performance. In fact a compromise arises between a high Seebeck thermoelectric effect and the goodness of the structure's thermal behaviour [Salleras2005, Baltes1998], in terms of thermal conductance and overall thermal noise. The chosen materials were aluminum and n-doped polysilicon. In Table 1 the values of thermal conductivity of different device materials are shown. These were the values used in the simulations.

**TABLE 1. THERMAL CONDUCTIVITY OF DIFFERENT MATERIALS**

Material	Thermal conductivity (W/m K)
Silicon	150
$\text{Si}_3\text{N}_4$ <sup>a</sup>	12
$\text{SiO}_2$	1.4
Aluminum	180
Poly-n+	30

The thermal conductivity used for  $\text{Si}_3\text{N}_4$  is an equivalent value between doped and undoped LPCVD nitride, with conductivity values of 2.4 [Sabate2005b] and 24 W/m K respectively. Regarding aluminum, its thermal conductivity value was obtained from the literature [Paul1993], providing a smaller value than the bulk aluminum ( $k_{\text{Al,bulk}} \sim 235 \text{ W/m K}$ ).

The measurement principle consists of heating up the hotplate by applying a voltage at the heater, thus producing a temperature distribution across the device geometry. The heat generated flows through the surrounding gas, as well as through the membrane. Hence the temperature reached at the centre of the membrane will depend on the thermal conductivity of said surrounding gas, as it happens in GC TCDs, but without the presence of a specifically designed fluidic channel. The sensor stationary signal output is related to the thermal conductivity of the gas. The thermal isolation of

the membrane and the high thermal conductivity of the silicon bulk are of great importance in order to enhance the temperature difference between hot and cold junctions. The use of a thermopile to measure the temperature instead of measuring the heater resistance, as done in most TCDs, allows for better resolution and for a differential measurement that partially rejects changes in room temperature.

### 4.3 SENSOR CHARACTERIZATION

Calibration of the sensor consisted in finding the Seebeck coefficient of the thermocouples and thus knowing the effective curve  $V_{out}(\Delta T)$  of the thermopile sensor.

To perform this calibration, the heater temperature dependence had to be found out, in order to provide a reference to calibrate the thermopile. The resistance versus temperature was recorded using a climatic chamber in the range from 25°C to 80 °C. A linear variation of the resistance was assumed, as in Eq. 4.1, resulting in a value for the temperature coefficient,  $TCR$ , of  $8.5 \times 10^{-4} \text{ K}^{-1}$  and a value for the resistance,  $R_0$ , of  $981 \Omega$ , being  $T_0=0 \text{ }^{\circ}\text{C}$ .

$$R = R_0 [1 + TCR(T - T_0)] \quad (4.1)$$

A resistor placed in the substrate rim is also calibrated in this way, so it can be used to monitor slight changes in substrate temperature, where the cold junctions are placed.

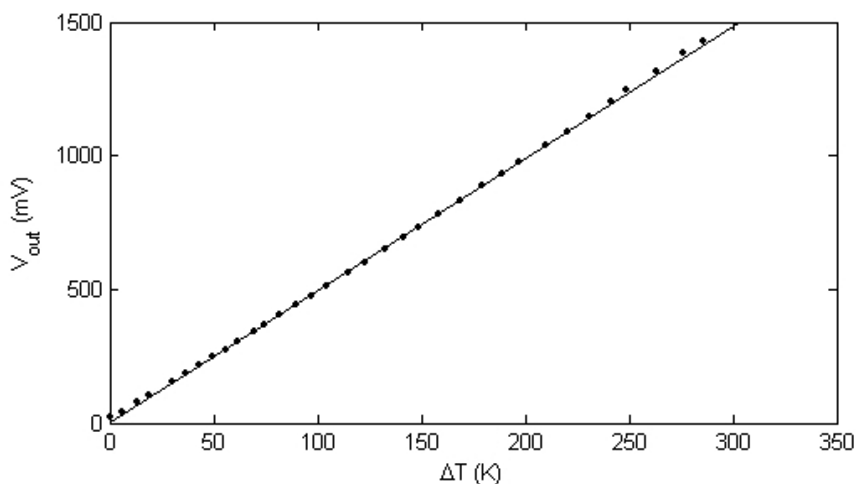


**Figure 4.3 Plot of the thermopile output versus calculated temperature difference (using the heater resistance calibrated thermal coefficient). There is only a slight non-linearity.**

Dependency of the thermopile signal versus the power applied to the heater was obtained by applying different voltages ( $V_h$ ) to it; its resistance was also recorded. Given this, the signal output versus temperature difference between hot and cold junctions could be plotted. Here, it is assumed that the resistance is just due to the central heater and the heater legs can be disregarded. Figure 4.3 shows this voltage signal versus temperature difference. The Seebeck coefficient of the thermocouples can be obtained from the slope.

Assuming a constant Seebeck coefficient, the result is of  $124 \mu\text{V/K}$ . The apparently linear behaviour of the sensor output with temperature can lead to misinterpretation: the Seebeck coefficient seems constant. Nevertheless, it is well-known [Arx1997] that the Seebeck coefficient is temperature dependent and, therefore, this value can only be reliable for small values of  $\Delta T$ . The reason for the apparent linearity in the graph is that due to inhomogeneity in the membrane temperature distribution, the increase in  $\alpha$  is compensated by the fact that the hot junctions of the thermopile are slightly below the temperature of the heater. Moreover, this temperature difference increases with temperature, appearing as an effective reduction of the sensor output. Both effects subtly compensate, resulting in an apparent, and misleading, linearity.

#### 4.4 THERMAL CONDUCTIVITY OF GAS MIXTURES

---

The sensor is expected to work immersed in a gas mixture and its behaviour will be modulated by the thermal conductivity of said gas. To perform a predictive simulation a sufficiently accurate model for the thermal conductivity of a gas mixture is fundamental.

Natural gas is a complex mixture of hydrocarbons and other minor components. In this case, it is modelled as a mixture of the main components: methane, ethane, nitrogen and carbon dioxide. Their thermal conductivities against temperature are shown in Figure 4. 4.

It is worth noting that thermal conductivity of a gas mixture is not a linear function of thermal conductivities of its components. An exact resolution for a mixture of more than two gases is yet not yet known, though many models have been proposed essentially based on empirical measurements, most of which can be reduced to some form of the Wassiljewa equation 4.2 [Poling2001],

$$k_m = \sum_{i=1}^n \frac{x_i k_i}{\sum_{j=1}^n x_j A_{ij}} \quad (4.2)$$

where  $k_m$  is the thermal conductivity of the mixture,  $k_i$  the thermal conductivity of component  $i$ ,  $x_i$  the concentration of component  $i$ , and  $A_{ij}$  some function to be specified.

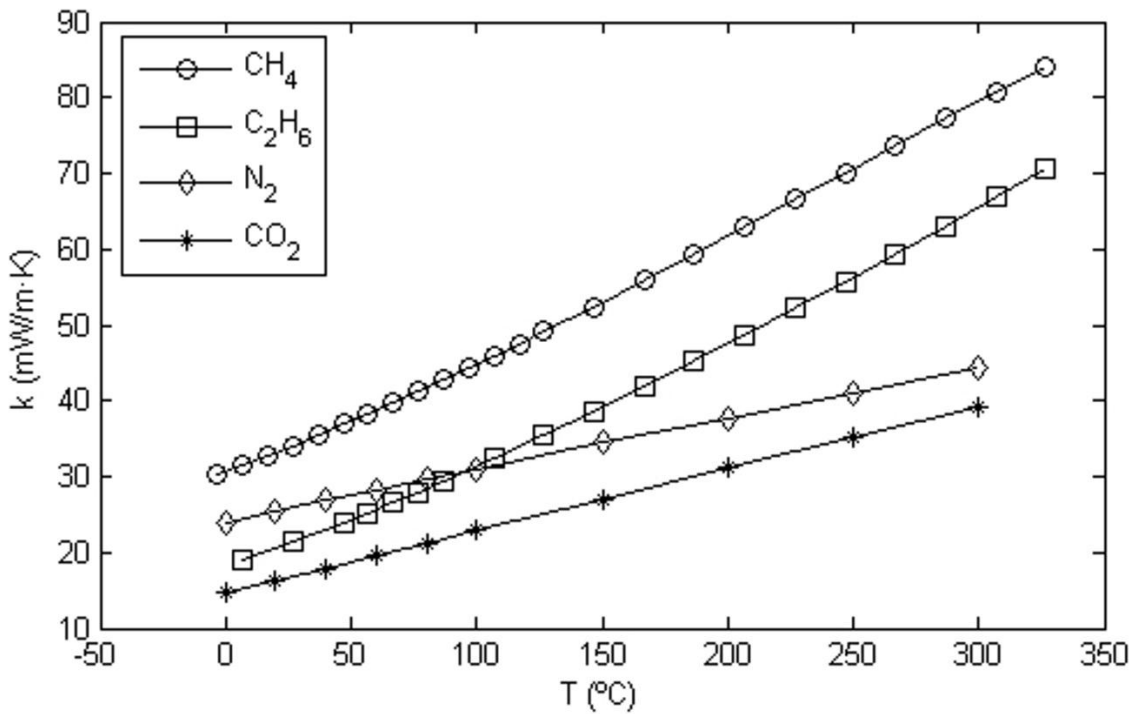


**Figure 4.4 Temperature dependence of the gas thermal conductivities of the natural gas main components. Notice slight non-linearity for the hydrocarbons. From [Younglove1987, Uribe1990]**

Model 4.2 was used, along with the Mason and Saxena proposal [Poling2001] for calculating  $A_{ij}$ ,

$$A_{ij} = \frac{\varepsilon \left[ 1 + \left( \frac{k_{tr,i}}{k_{tr,j}} \right)^{1/2} \left( \frac{M_i}{M_j} \right)^{1/4} \right]^2}{\left[ 8 \left( 1 + \frac{M_i}{M_j} \right) \right]^{1/2}} \quad (4.3)$$

where  $M_i$  is the molecular weight of component  $i$ , a value of 1.065 is used for  $\varepsilon$  and  $k_{tr}$  is the coefficient of frozen conductivity ( $A_{ii}$  is assumed to be unity). These coefficients account for the monatomic value of thermal conductivity (when no rotational degrees of freedom are considered) and their relations appearing in Eq. 4.3 can be computed using Eq. 4.4,

$$\frac{k_{tr,i}}{k_{tr,j}} = \frac{\Gamma_j}{\Gamma_i} \frac{\left[ e^{(0.0464T_r)} - e^{(-0.2412T_r)} \right]}{\left[ e^{(0.0464T_r)} - e^{(-0.2412T_r)} \right]} \quad (4.4)$$

where  $T_r$  is the reduced temperature ( $T_r = T/T_c$ ) and the values of  $\Gamma$  are calculated using Eq. 4.5,

$$\Gamma = 210 \left( \frac{T_c M^3}{P_c^4} \right)^{1/6} \quad (4.5)$$

where  $T_c$  and  $P_c$  are the critical temperature and pressure, respectively.

To check the convenience of this chosen model, the values of the thermal conductivity at 20 and 70 °C of several common natural gases [Rahmouni2003a] were compared with the model's prediction.

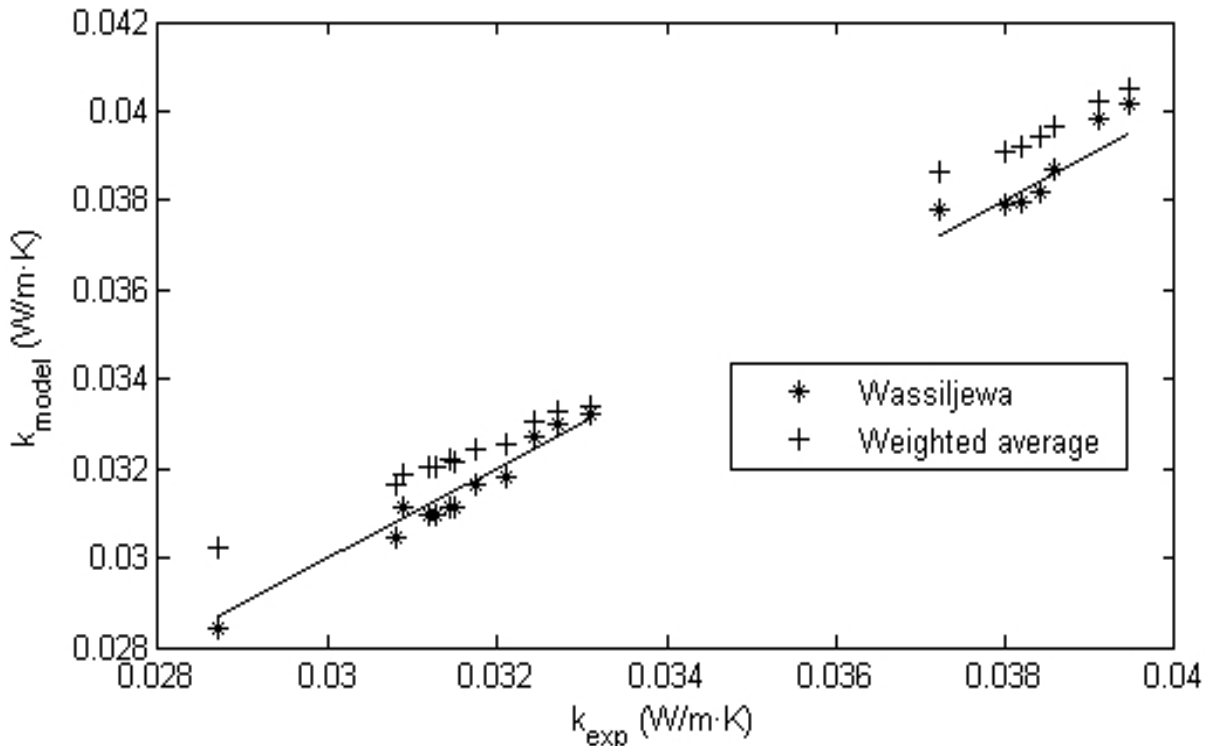


**Figure 4.5 Comparison of the Wassiljewa model with the weighted average model for calculating the thermal conductivity of a gas mixture. Solid line shows the expected perfect match First group of values corresponds to the calculations at 20 °C while the second ones are at 70 °C. Experimental values from [Rahmouni2003a] were used.**

The Wassiljewa equation (4.2) provides a better fitting than a simple weighted average as shown in Figure 4.5. Nevertheless, some gases show larger deviation than others. At 70 °C, the two points with larger thermal conductivity have a larger error than the rest. These points correspond to a higher relative concentration of one of the components of the gas mixture (methane).

## 4.5 PHYSICAL MODEL

To simulate the operation of the device, a finite element method (FEM) model was developed using ANSYS® (v10.0). The model consisted of a silicon volume, a gas volume, and the 2D membrane areas (as temperature gradients perpendicular to the membrane can be neglected). In Figure. 4.6, the constructed solid model can be seen.

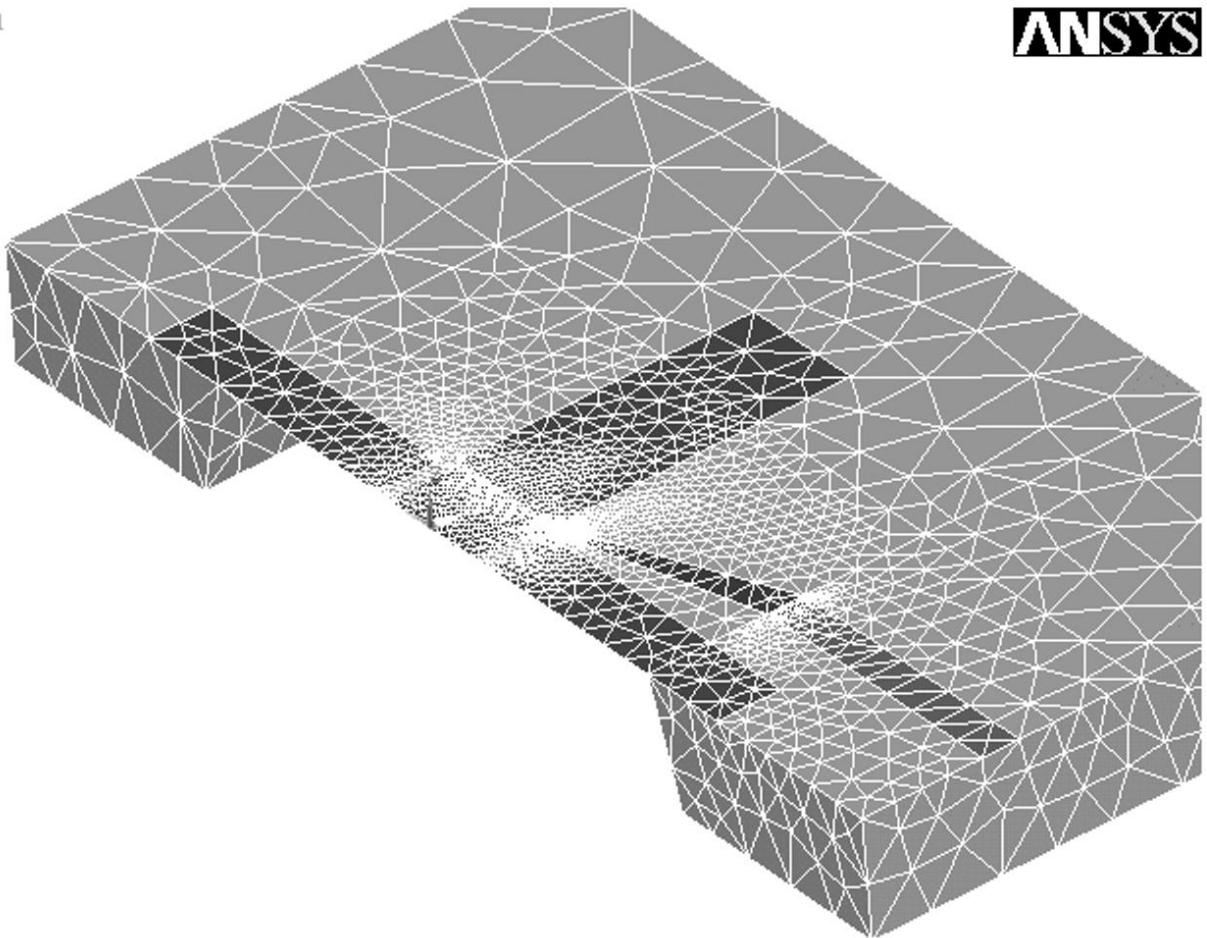


**Figure 4.6 Geometrical view of the model. (For clarity, the gas volumes have been suppressed).**

A half-symmetry model was considered to take advantage of the symmetries present in the device and boundary conditions. In order to preserve this symmetry, the heater shape was approximated with a half symmetrical shape; compare Figures. 4.12 and 4.2. In addition, boundary conditions are set so as to maintain the bottom of the silicon volume (the attaching point to the metal heat sink casing) at room temperature, and also to keep the lateral areas in adiabatic conditions. The dimensions of the surrounding gas volume were taken to allow the free distribution of the heat flux

to reach the substrate heat sink through the gas. The heat generated at the heater was calculated taking into account its different polysilicon track widths, with heat dissipation being inversely proportional to these.

The properties of each different area in the multilayered membrane were calculated by averaging the properties of each layer across the entire thickness. In the regions containing the thermocouples, a second averaging was performed taking into account the proportion of area corresponding to each material. The effective thermal conductivity can then be calculated as in Eq. 4.6,

$$k_{eq} = \frac{\sum_i k_i h_i A_i}{\sum_i h_i A_i} \quad (4.6)$$

where  $k_i$ ,  $h_i$  and  $A_i$  are the thermal conductivity, thickness and area of each material, respectively.

The model included conduction and radiation, but not convection. The Rayleigh number was calculated using Eq. 4.7 to check if the system was getting near the critical temperature above which convection might have become significant [Zhong2005].

$$R_A = \frac{\rho^2 \cdot g \cdot \gamma \cdot L^3 \cdot \Delta T \cdot c_p}{\mu \cdot k} \quad (4.7)$$

where  $\rho$  is the fluid density,  $g$  the gravity,  $\gamma$  the volumetric coefficient of expansion,  $L$  a characteristic length,  $\Delta T$  the temperature difference reached,  $c_p$  the fluid's specific heat,  $\mu$  its dynamic viscosity and  $k$  the thermal conductivity. By using a worst-case estimation of each of these variables, a Rayleigh number of 120 is obtained. The values above which convection is significant vary depending on the system, but the threshold is at some thousands [Amiroudine2001], so it was assumed that convection could be neglected.

A stationary temperature distribution calculated with this model beside an IR image of the sensor can be seen in Fig. 4.12 for comparison and model evaluation.

## 4.6 MODEL RESULTS AND VALIDATION

Two sets of simulations are presented, one using several synthetic natural gases and calculating the dependency of  $k(T)$  using the Wassiljewa model and the data shown in Fig. 5, and a second set of simulations in air using tabulated  $k(T)$  [Stephan1985].

**TABLE 2. COMPOSITION OF THE SIMULATED GASES**

CH <sub>4</sub> (%)	C <sub>2</sub> H <sub>6</sub> (%)	N <sub>2</sub> (%)	CO <sub>2</sub> (%)
100.00	0.00	0.00	0.00
84.58	8.11	6.09	1.22
81.75	8.11	8.92	1.22
80.80	11.89	6.09	1.22
77.97	11.89	8.92	1.22
84.02	8.11	6.09	1.78
81.19	8.11	8.92	1.78
80.24	11.89	6.09	1.78
77.41	11.89	8.92	1.78
82.50	10.00	7.50	0.00
79.50	10.00	7.50	3.00
91.00	0.00	7.50	1.50
71.00	20.00	7.50	1.50
88.50	10.00	0.00	1.50
73.50	10.00	15.00	1.50
81.00	10.00	7.50	1.50
100.00	0.00	0.00	0.00
97.70	2.30	0.00	0.00
87.44	9.38	3.18	0.00
95.24	2.70	2.06	0.00
93.22	4.60	1.08	1.10

Table 2 shows the considered natural gases based on the composition variation ranges found in Europe [Rahmouni2003a], while Fig. 4.7 shows their thermal conductivity versus temperature when Eq. 4.2 is used. For the natural gases, 7 different powers were dissipated at the heater, by applying a heater voltage of 3 to 9 volts (1 V increments).

To allow comparison with the IR images the device was also simulated in air, applying 60 mW to the heater, corresponding to a heater voltage of 8.7 V.

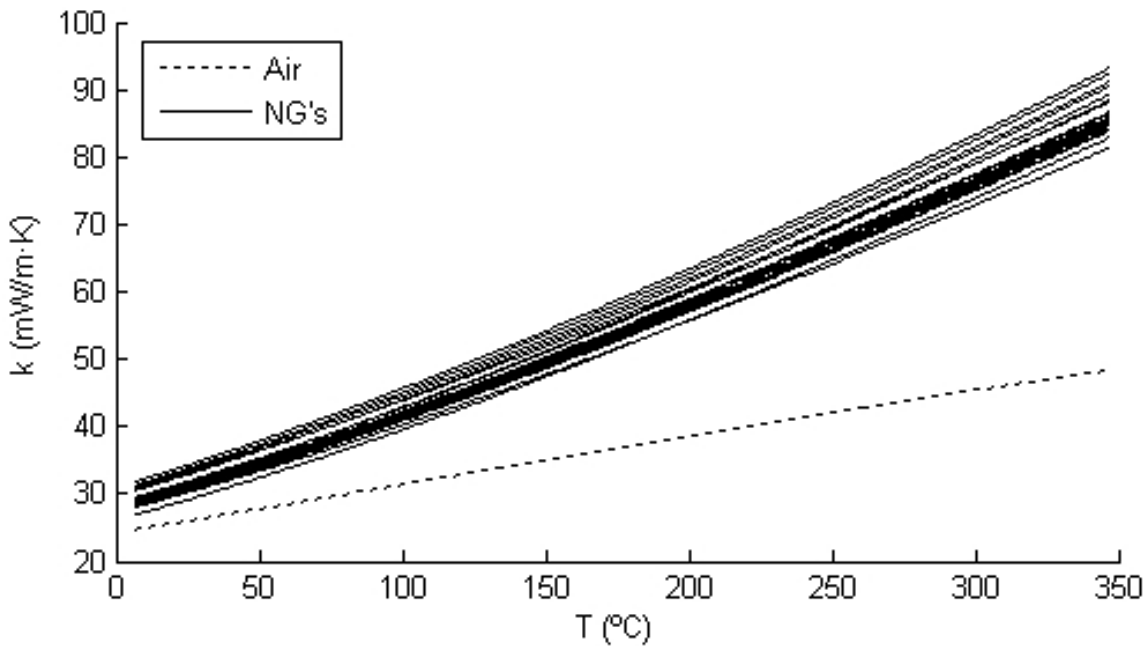


**Figure 4.7 Temperature dependence of the thermal conductivity of the gases considered, according to Wassiljewa equation (2). Air is shown to provide a magnitude comparison. Notice how identification of the  $k(T)$  curves does require very fine thermal conductivity measurements. Values for air were collected from [Stephan1985]**

#### 4.6.1 LABORATORY TESTBENCH AND VALIDATION RESULTS

---

A gas mixing station was specifically configured to output controlled mixtures of four of the natural gas main components: ethane, methane, carbon dioxide and nitrogen. Static atmospheres of the synthetic natural gases were supplied to a sensor chamber where measurements were acquired. A schematic of the gas station setup is shown in Figure 4.8 and a hardware connection setup is shown in Figure 4.9. The gas measurement station was programmed using Labview 8.0, and was designed as completely configurable for easy exchange of MFC and measurement gases. A diagram of the Labview program is shown in Figure 4.10.

The gas was supplied at room temperature and atmospheric pressure. The expected variations of the ambient temperature and pressure in the laboratory were expected to have limited influence on the sensor output and were intently considered as experimental variance, due to the small variations in laboratory conditions, and the expect ambient temperature rejection provided by the differential thermopile measurements, this temperature noise rejection assumptions were afterwards proved to be slightly overoptimistic (see chapter 5, and section 5.3.2).

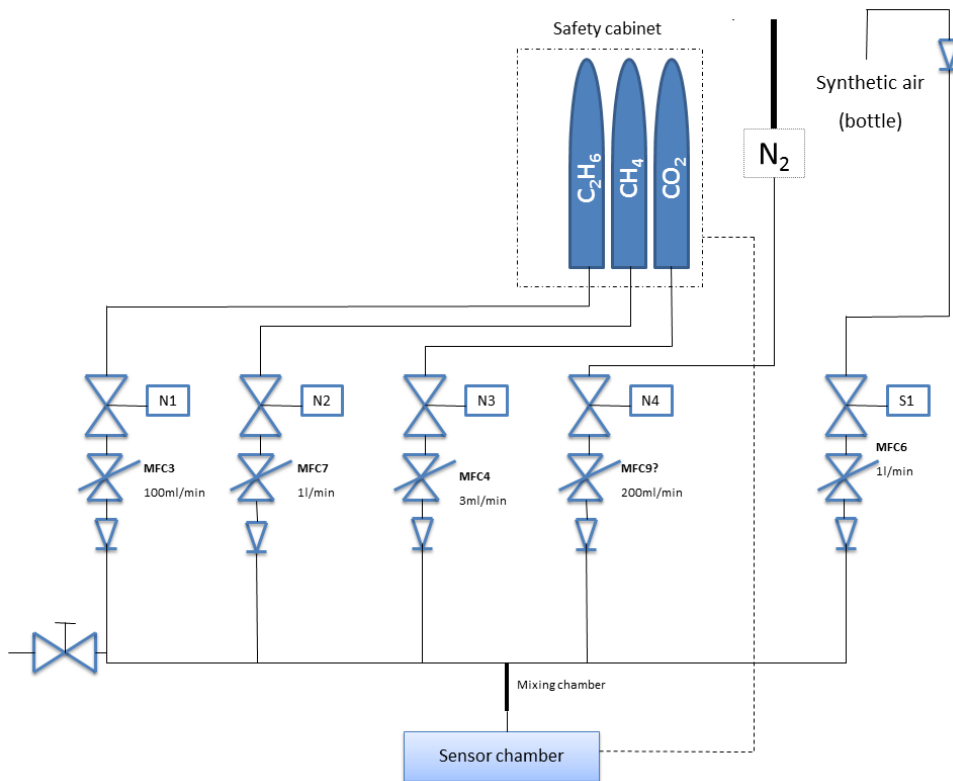


**Figure 4.8 Fludic schematic of the configurable gas station**

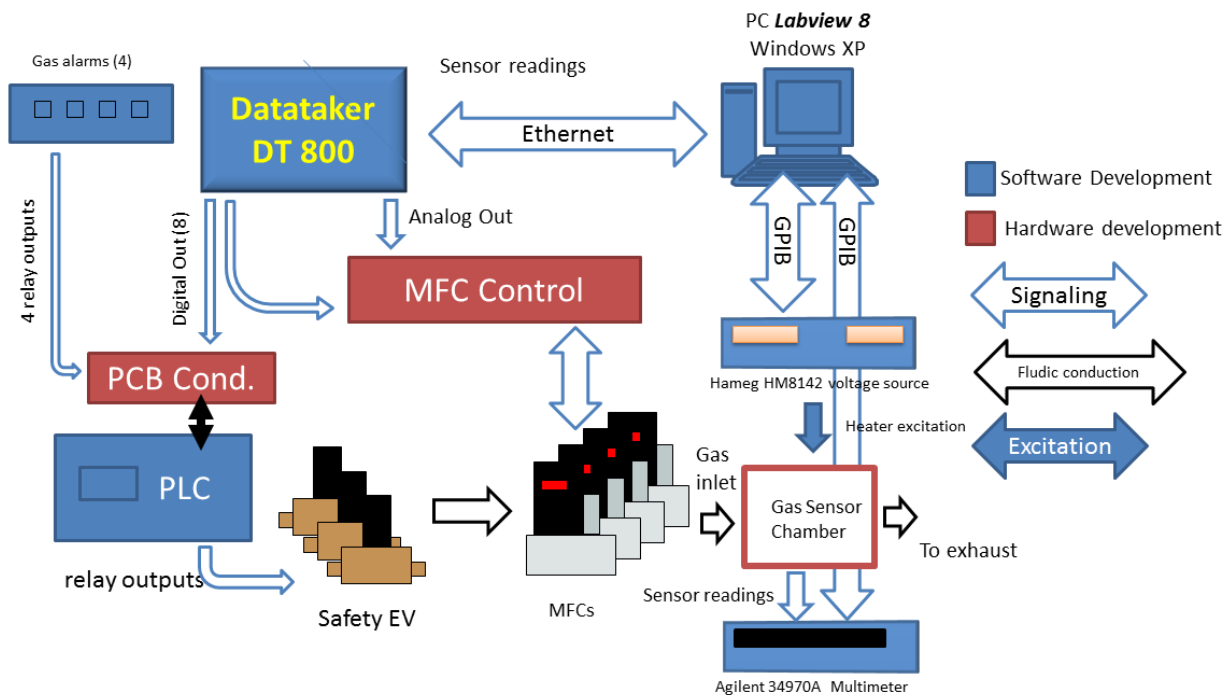


**Figure 4.9 Hardware connection diagram of the configurable gas station.**

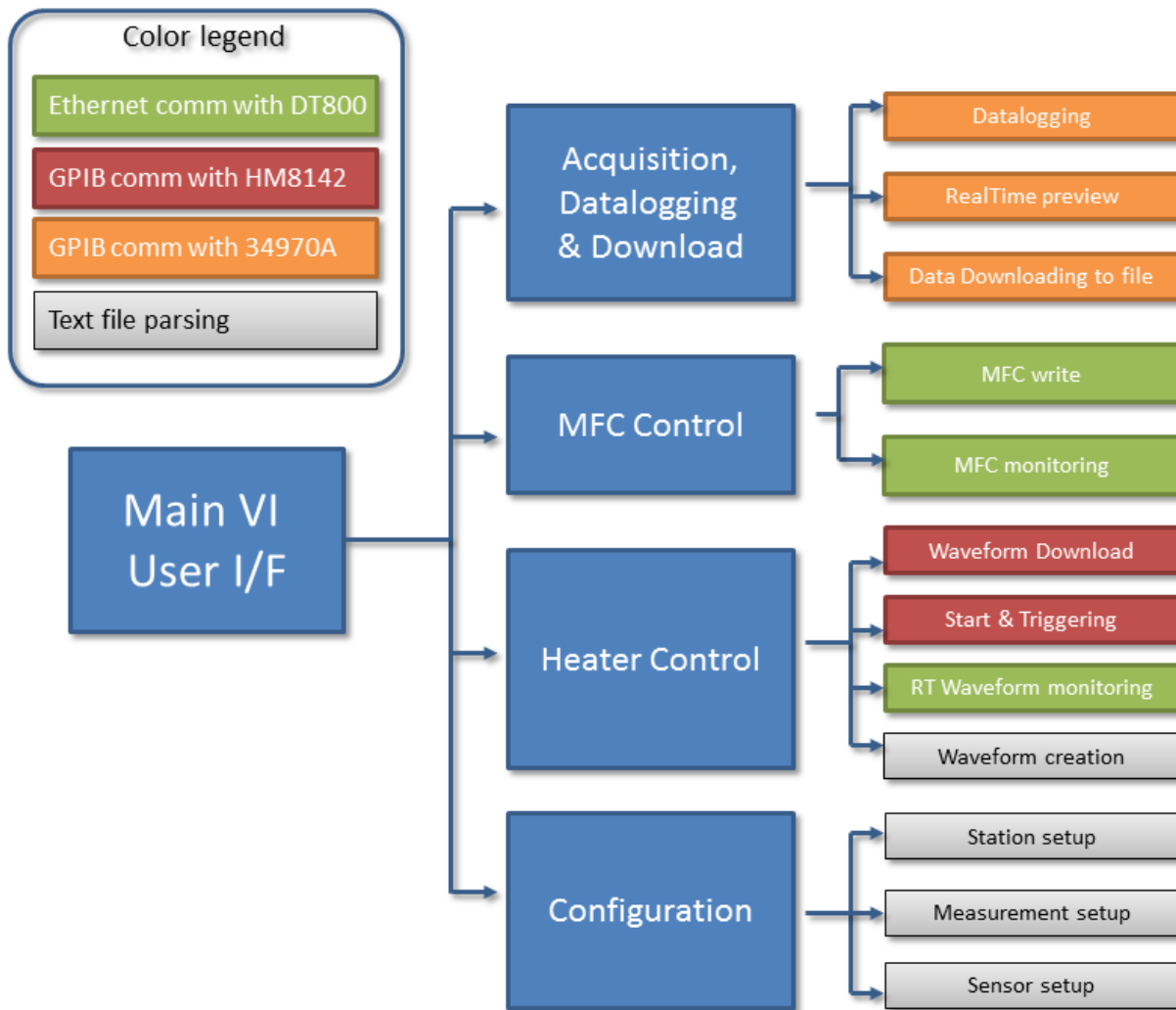


**Figure 4.10 Summarized software blocks of the configurable gas station control program implemented in Labview 8.0**

Uncertainties in the gas mixture volumetric composition were calculated and estimated as absolute concentration uncertainties (95% confidence interval) of 0.06% in CO<sub>2</sub>, 0.16% in C<sub>2</sub>H<sub>6</sub>, 0.26% in N<sub>2</sub>, and 0.40% in CH<sub>4</sub> (Calculation of these uncertainties is explained in section A.3). A 34970A Agilent multimeter sampling at 25 Hz was used to measure the voltage output of the sensor. An HM8142 programmable waveform generator (Hameg Instruments, Germany) was used to supply the power steps, with a specified accuracy in the voltage output of 0.2% of the setting.

A measurement procedure was performed so as to cancel the influence of the gas flow rate, by generating a stable flow of 500 ml/min across the system during a period of time sufficient to ensure a stationary concentration inside the sensor chamber (approx. 15 min), after this period all

flows were simultaneously stopped, and the sensor was operated in a static atmosphere of known concentration.

Figure 4.11 compares the results of the simulations with the acquired experimental data. The temperature dependency of  $\alpha$  was taken from the literature [Arx1997]. In this last reference, the temperature ranges from 100K to 400K. For higher temperature values, a linear extrapolation was applied. Figure 4.11 shows there is a good agreement by using  $\alpha$  with a temperature dependency. In this case, the maximum error was approximately 1.5%. As our technology is different than that published in Ref. [Arx1997], values of  $\alpha_0$  and  $\alpha'$  were obtained in order to reduce the maximum error. With values of  $\alpha_0$  of 122  $\mu\text{V}/\text{K}$  (a value nearer to our measured value than that from literature) and  $\alpha'$  of 77.2  $\mu\text{V}/\text{K}^2$ , the maximum error was 1.5%, while using the values in Ref. [Arx1997] the error rose to 4.5%. As can be seen from the literature [Bouchich2002], these two coefficients are dependent on the polysilicon doping level.

By removing the reduced number of points providing the largest errors, the maximum error would be drastically reduced. Such an action could be plausible because these points correspond to those providing higher errors in the thermal conductivity gas model at 70°C (see Fig. 4.5). These points correspond, more specifically, to the almost pure methane gas composition.

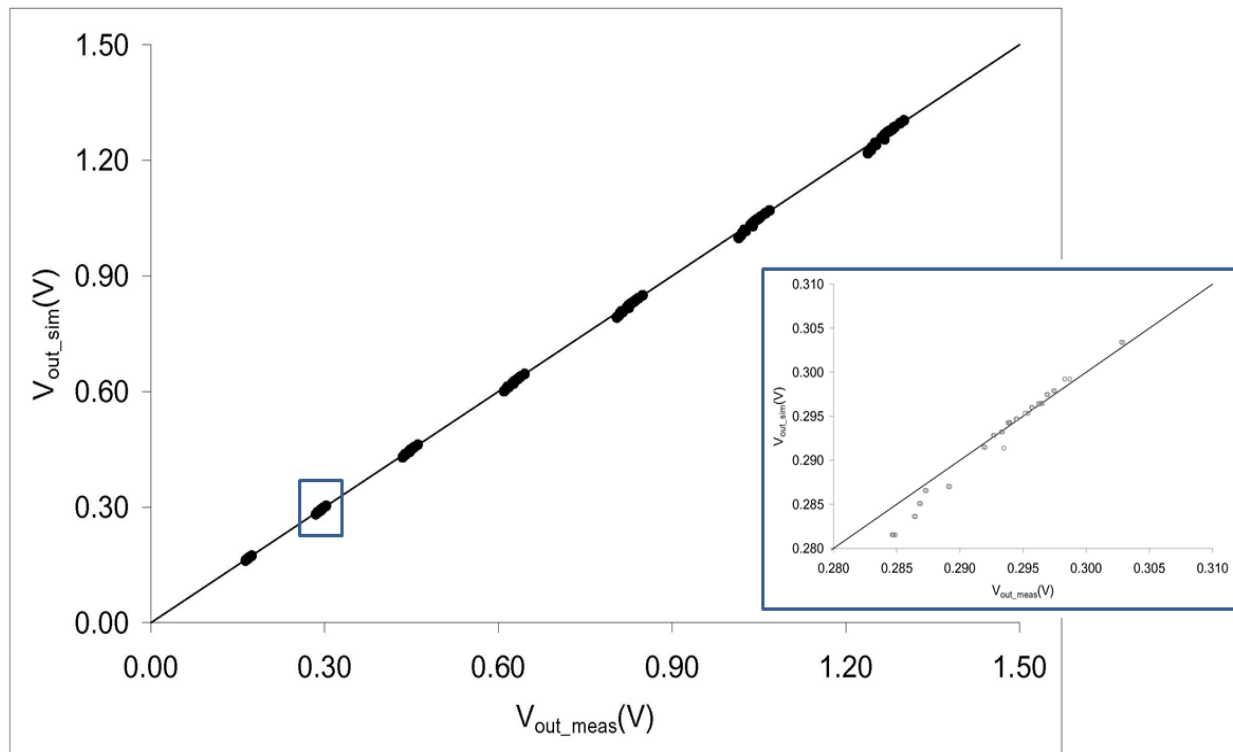


**Figure 4.11** Comparison between measured responses and simulated ones; Insert shows a detailed view for one of the power steps (with  $V_h=4\text{V}$ ).

#### 4.6.2 IR IMAGING AND DISCUSSION

Measurements in air were taken to allow an IR camera to record the radiometry map of the sensor in air. A ThermoVision™ A40M IR camera from FLIR SYSTEMS (Wilsonville, Oregon, USA) was used and a 34401 Agilent multimeter was used for the electrical measurements.

Figure 4.12 (see next page) shows the IR image when dissipating 59.50 mW. Expected emissivity differences between thermocouple and membrane areas are shown as discontinuous temperature fields; dissipation occurring at the heater legs is also clear and in good qualitative agreement with the simulation. It is in this legs area that the maximum temperatures occur, as a result of increased resistance and thus dissipation, due to the heater track narrowing. On the other hand the images also confirm that the silicon rim shows no significant temperature increase with respect to ambient. While no emissivity correction has been performed, a good qualitative agreement is clear.

#### 4.7 ESTIMATION OF THE SENSOR SENSITIVITY

In order to establish the sensor response to the composition of natural gas, 10 experimental points were selected which set up a cubic experimental design in a reduced region, as shown in Table 4.3.

**TABLE 4.3. EXPERIMENTAL POINTS USED FOR THE SENSITIVITY ESTIMATION<sup>\*</sup>.**  
**(Composition expressed in volume fraction)**

	[CH <sub>4</sub> ]	[C <sub>2</sub> H <sub>6</sub> ]	[N <sub>2</sub> ]	[CO <sub>2</sub> ]
<b>1</b>	0.8458	0.0811	0.0609	0.0122
<b>2</b>	0.8175	0.0811	0.0892	0.0122
<b>3</b>	0.8080	0.1189	0.0609	0.0122
<b>4</b>	0.7797	0.1189	0.0892	0.0122
<b>5</b>	0.8402	0.0811	0.0609	0.0178
<b>6</b>	0.8119	0.0811	0.0892	0.0178
<b>7</b>	0.8024	0.1189	0.0609	0.0178
<b>8</b>	0.7741	0.1189	0.0892	0.0178
<b>9</b>	0.8100	0.1000	0.0750	0.0150

\*The concentration points for [C<sub>2</sub>H<sub>6</sub>] [N<sub>2</sub>] [CO<sub>2</sub>] define a cubic experimental design

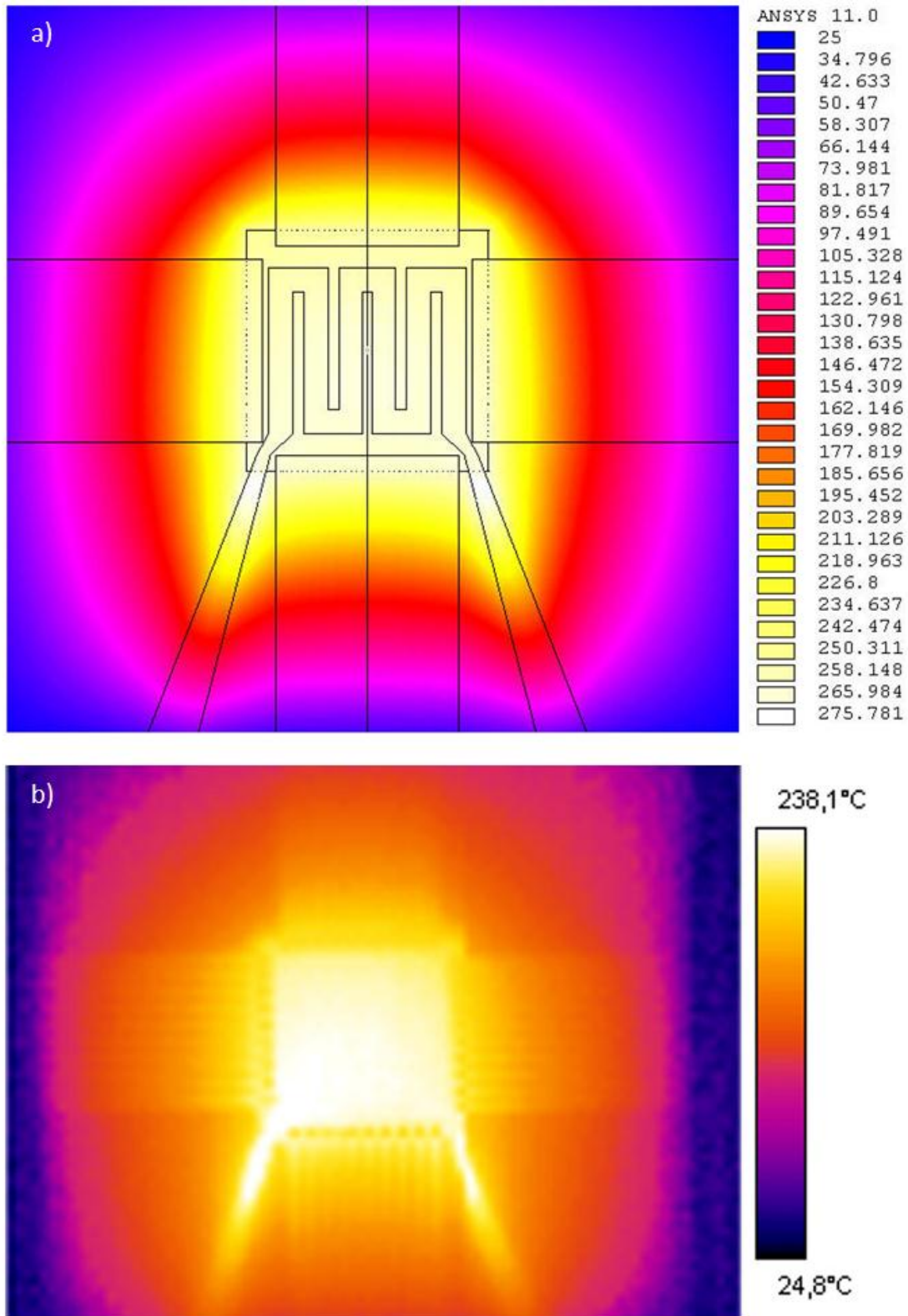


Figure 4.12 Simulated (a) and recorded (b) temperature map of the device operation with air and 59.50 mW of dissipation.

There was a strong reason for reducing the experimental domain considered. Preliminary analysis of the experimental sensor response showed that the dependency with the inputs has a mild non-linear contribution, with significative terms being higher in order than quadratic, meaning that a complex model and a large amount of experimental data should be committed to perform an accurate full-domain sensitivity analysis. In this chapter the preliminary analysis of the device sensitivity is presented and for this purpose a simpler, more easily interpretable linear model, which nicely fitted the reduced experimental domain, was used.

The chosen linear model is that of Eq. 4.8.

$$\hat{y} = b_1 + b_2[CO_2] + b_3[C_2H_6] + b_4[N_2] \quad (4.8)$$

In this model,  $b_1$  is a bias term in the sensor response, while  $b_2$ ,  $b_3$  and  $b_4$  are the sensitivities to carbon dioxide, ethane, and nitrogen concentrations. The output is expressed in the unit of V, and so are the coefficients  $b_i$ , while concentrations are expressed as molar fractions.

The 4 component mixture has 3 degrees of freedom, so methane concentration was not considered explicitly in the model, though it could of course be calculated using the equation for the mixture

$$[CH_4] + [CO_2] + [C_2H_6] + [N_2] = 1 \quad (4.9)$$

Least-squares multi-linear response surface models for heater voltages of 3 V, 5 V, 7 V and 9 V were computed using the simulated and experimental response data, rendering the results shown in Fig. 4.13.

In order to reduce the constant term in the model, for a more comprehensive interpretation, the average of the experimental sensor output within each heater voltage was subtracted from both the experimental and the simulated points; in consequence the constant term  $b_1$  in the experimental data model (Eq. 4.9) was zero. This is not so in the simulated data due to an effect which is later discussed.

Figure 4.13 shows that a good qualitative agreement is reached with the simulations, though the sensitivities to ethane and nitrogen are overestimated by about 10% while the sensitivity to Carbon dioxide is underestimated by around 20%. These effects are mainly due to the inaccuracy in the thermal conductivity calculations using the Wassiljewa equation (4.2). It has been observed that typical errors in the thermal conductivity estimations using Eq. 4.3 are in the 1% range (see Fig.

4.5). This is a bad specification since a close look at Fig. 4.7 shows that the composition information we are looking for in the full range case (see Table 4.2) involves a total variation range of thermal conductivity of about 10%. In the case of the reduced range described in Table 4.3, the total thermal conductivity excursion is yet halved, thus 5% variations are involved and our SNR is then as poor as 5. Thus, the Wassiljewa equation introduces an effective 20% of noise in the reduced range case.

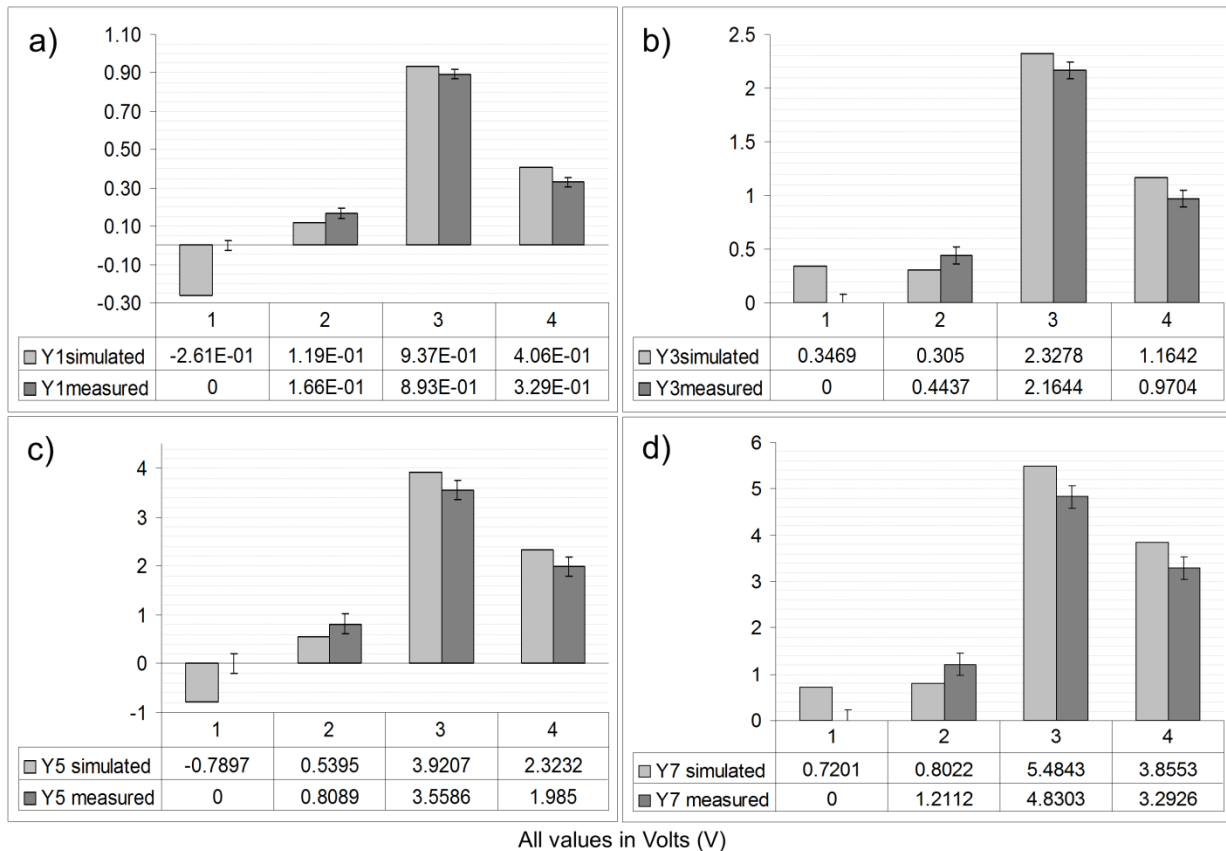


**Figure 4.13 Fitted coefficients of the simulated and measured sensor response (approximated as a hyperplane) for the sensor working at a)  $V_h = 3V$ , b)  $V_h = 5V$ , c)  $V_h = 7V$ , d)  $V_h = 9V$ . Coefficients 1, 2, 3 and 4 account for the constant term ( $b_1$ ), sensitivity to CO<sub>2</sub> ( $b_2$ ), sensitivity to C<sub>2</sub>H<sub>6</sub> ( $b_3$ ), and sensitivity to N<sub>2</sub> ( $b_4$ ) respectively. Qualitative and even a significant quantitative agreement can be observed. Deviations are attributed to TC biasing due to the Wassiljewa equation.**

With this consideration in mind, the results in Fig. 4.13 shall be regarded as considerably better than could be initially expected.

The bar graphs in Fig. 4.13 show that the sensor's relative sensitivity to each of the 3 gases changes with the heater voltage. A way of interpreting this is that the thermoelectric sensor behaves as a different sensor (in terms of selectivity and sensitivity) for each heater voltage; thus we are

obtaining a multivariate signal containing more information than in the single univariate sensor case. This additional information can allow independent quantification of each of the gases with an appropriate multivariate data analysis as shown in chapter 5.

In the current model setup, sensitivity to nitrogen is higher at higher heater voltages relative to ethane sensitivity, while relative sensitivity to carbon dioxide varies little across the heater voltages. Note that sensitivities are significantly above experimental error, even for the case of carbon dioxide where the concentration variation range was only 0.56% in volume.

Finally in regard to the apparent offset in the simulated responses, which appears as a non-negligible  $b_1$  term in the models, it has been attributed to differences in the power applied to the device in the experiments and simulations, mainly due to the uncertainty in the HM8142 voltage source.

## 4.8 CHAPTER CONCLUSIONS

---

This chapter presented a preliminary study of a selected micromachined thermoelectric device as a natural gas sensor. FEM modelling allowed in-depth exploration and understanding of the main sensing mechanisms in the device. Simulation was compared and validated with a set of experimental data, showing a very good agreement between them. The sensor performance at detecting small variations in the gas thermal conductivity was explored using surface response methods and a cubic experimental design. The results of this analysis showed that the device has high sensitivity to composition changes, allowing small changes of the main natural gas components to be detected.

Experimental results as well as simulations confirmed that sensor excitation at different heater voltages provides additional information of the mixture due to changes in the relative sensitivity of the sensor to each gas. The next step is to use this information to provide a quantification of the natural gas main components, or other properties depending on composition. Sensitivity of the sensor to the composition of other gas mixtures may be qualitatively explored using simulation with the reported model, and expected sensitivity values can be approximated. However, there is a serious limitation in the predictive ability of the models which arises from the own limitations of the Wassiljewa model (Eq. 4.2). A more accurate estimation of the thermal conductivity of gas mixtures would be needed in order to cast quantitative predictions of the thermoelectric sensor response.

The next chapter describes the use of multivariate calibration techniques for the real-time monitoring of natural gas composition and properties.

---

## 5. MICROMACHINED THERMOELECTRIC GAS SENSOR FOR NATURAL GAS ANALYSIS: CALIBRATION

---

5.1. Introduction.....	79
5.2. Multivariate calibration: methodology.....	80
5.2.1. Simulation setup.....	80
5.2.2. Experimental setup.....	81
5.2.3. Signal processing.....	85
5.2.4. Uncertainty analysis.....	86
5.2.5. Validation.....	88
5.2.6. Performance limits estimation.....	89
5.3. Multivariate calibration results and discussion.....	90
5.3.1. Calibration and validation results.....	90
5.3.2. Uncertainty analysis results.....	94
5.3.3. Performance limits estimation results.....	97
5.4. Chapter conclusions.....	100

## 5.1 INTRODUCTION

---

In the previous chapter, a candidate microsensor was studied and characterized using experimental measurements and finite element modelling (FEM) simulations, in order to determine its potential for fast, low-cost natural gas analysis. Though the sensor consisted of a commonly used thermal sensor structure [Herwaarden1988, Semancik2001, Calaza2003b], a variable excitation mode of the sensor heater allowed obtaining measures which are related (indirectly) to the thermal conductivity as a function of temperature,  $k(T)$ . In particular the chapter showed the different behaviour of the sensor when excited at different heater temperatures, showing changes in the sensitivity to different components of natural gas. The previously presented results corresponded to a reduced variation of the natural gas components, to mitigate the non-linearity degree present in the full-domain problem.

Extracting this complex information from the sensor measurements is a demanding task in the signal processing stage due to its high sensitivity to undesired interferences (ambient temperature, pressure, and noise in the heater excitation voltage), the small changes in  $k(T)$  to be detected, and the presence of non-linearities in the sensor response.

The data analysis procedure brings the presented approach to close relation to other techniques of analytical chemistry such as spectrometry (infrared, mass or nuclear magnetic resonance among others), where chemical substances are identified by their spectral patterns. In this case, the proposed approach can be regarded as a kind of thermal spectrometry of the gas sample.

The choice of the proposed sensor is expected to provide a high stability and reliability in exchange for a low sensitivity as typically occurs with other thermal conductivity sensors (see 2.4.8). This is not a strong drawback, since measuring natural gas properties does not require a very high sensor sensitivity (variations are expected in the % range), but very high sensor stability is desirable.

Three main objectives of this thesis are addressed in this chapter. In first place, the sensor suitability for prediction of natural gas properties is demonstrated with the use of a multivariate calibration. Second, the various uncertainty sources affecting (or potentially affecting) the sensor performance are described and quantified. Third, with the aid of simulation results obtained from the available models described in Chapter 4 as well as experiments, the expected metrological limits of this new sensing approach are estimated.

To the best of our knowledge this is the first work reporting the assessment of properties and composition of a multi-component (of more than 2 components) gas mixture using only a single thermal microsensor.

The chapter is organized as follows. Section 5.2 presents the methodology of the analysis including signal processing, validation, uncertainty analysis and performance limits estimation as well as the

experimental and simulation setups. Some details of the uncertainty analysis were left out and are available as supplementary material in appendix A. The results and discussion section (section 5.3) is divided into three sections covering the results of the three objectives of the work: the first section provides the quantitative results for the predictions of the PLS models, the second section provides the results of the the uncertainty analysis, and the third section provides the results of the estimation of the metrological limits, results are also discussed along section 5.3. Closing the chapter, some conclusions are drawn in section 5.4.

## 5.2 MULTIVARIATE CALIBRATION: METHODOLOGY

This chapter makes use of two sets of data, a set of experimental results obtained in laboratory conditions, and an additional set of computer finite element modelling (FEM) simulation results which is based in the models presented in chapter 4. The first set is used for the main discussion and performance analysis, while the second set is used to complement the knowledge of the sensor operation, performance, and metrological limits. For both measurement sets, the sensor output is processed using Partial Least Squares (PLS) [Geladi1986], and a PLS regression model is computed in order to predict natural gas properties from the sensor data in real-time (see section 5.2.3 for details). In order to perform a detailed uncertainty analysis, a Monte Carlo analysis was set up, with synthetic noise addition to the experimental data.

A description of the simulation and experimental setups is provided next in sections 5.2.1 and 5.2.2, as well as the signal processing and PLS model validation methods (section 5.2.3). Additionally, the uncertainty and performance limits analysis are introduced (5.2.4, 5.2.6), which aimed to bound the expected performance of the sensing principle as well as providing some quantitative insights in the sensor operation and its uncertainty sources, the validation approach is also introduced in section 5.2.5. More details on the uncertainty analysis has been placed in Appendix A to keep the conciseness and continuity in the description of the main work.

It must be noted that no direct measurement was available for three of the predicted properties: normal density, Superior Heating Value and Wobbe index. In these cases, calculations were based in the ISO6976 [ISO1995] standard which provides guidelines to calculate them from a known composition. This standard is widely known and used in natural gas industrial metering.

### 5.2.1 Simulation setup

Simulated measurements required the construction of two different simulation instances as described in chapter 4. The first one was a FEM model of the sensor device which reproduces the sensor thermal response to the electrical stimulation of the heater (See section 4.6). The FEM modeled device reaches a steady-state temperature distribution which is dependent on the

surrounding gas. For the purpose of these simulations, the gas is strictly defined by the thermal conductivity as a function of temperature,  $k(T)$ . A second simulation instance was needed, a formula which correlates the composition of a synthetic natural gas mixture with a calculated  $k(T)$  curve (see section 4.5). In this way the concentrations of individual natural gas main components (see experimental setup 5.2.2) can conveniently become the input of the simulations. This was not a straightforward calculation since only approximate solutions are available to the problem of calculating the  $k(T)$  curve of a gas mixture. A common approach is the use of the equation of Wassiljewa [Poling2001], as described in section 4.5.

In effect, disagreement between experimental and simulation data can easily reach 5%. This has been considered to be a systematic error, which usually appears as a bias between simulation and experimental results. Despite this bias, both results rely on the same underlying sensing mechanisms. PLS modelling greatly rejects the systematic error, extracting only the underlying information. For this reason, the PLS model using simulated data recovers the same performance as the PLS model for experimental data, when the expected amount of experimental noise is added. Moreover, both PLS models are expected to degrade almost identically with the addition of noise. These results have encouraged the study of the performance limits of the system by using simulated data. More details on the simulation setup can be found in the previous chapter.

### 5.2.2 EXPERIMENTAL SETUP

---

In order to determine the properties of natural gas, previous works [Wild2001,Rahmouni2003b] made use of the assumption that natural gas can be approximated with a three or four pseudo-component mixture, with an acceptable loss of accuracy in the properties estimation. Following this approach, a gas mixing station was specifically configured to deliver controlled mixtures of four of the natural gas main components: methane, ethane, nitrogen and carbon dioxide. The setup is essentially the same used in the work presented in chapter 4 and already described in section 4.6.1. Again, it was expected that results with this four component mixture could be extended to other generic compositions. For this second work, the measurement cycle was slightly shortened as described below.

A total 500 ml<sup>1</sup>/min flow of the synthetic natural gas was supplied to a sensor chamber. After 11 minutes the concentration inside the chamber was stable (as explained in section A.3), and the flow was stopped to perform a measurement of the sensor response in static gas conditions. The gas was supplied at room temperature and atmospheric pressure. Expected accuracy of the volumetric gas composition, with the gas mixing setup, were absolute concentration uncertainties (95%

---

<sup>1</sup> Referenced to IUPAC standard conditions

confidence interval) of 0.06% in CO<sub>2</sub>, 0.16% in C<sub>2</sub>H<sub>6</sub>, 0.26% in N<sub>2</sub>, and 0.40% in CH<sub>4</sub> (Calculation of these uncertainties is explained in section A.3).

It is important to note that derived magnitudes and properties calculations were referenced to standard conditions of the natural gas. This is particularly relevant when calculating the SHV, normal density and Wobbe index from ISO6976 [ISO1995], since these values were used as calibration data for the prediction models obtained from the sensor measurements.

A 34970A multimeter (Agilent technologies, CA, US) sampling at 25 Hz was used to measure the voltage output of the sensor. An HM8142 programmable waveform generator (Hameg Instruments, Germany) was used to supply the voltage waveform, with a specified uncertainty in the voltage output of 0.2% of the setting. However the truly relevant specification to evaluate the consistency of calibrations across different measurement runs is the voltage setpoint repeatability instead of total setpoint uncertainty. No repeatability data was provided by the manufacturer, so it was experimentally measured and estimated at 1.2mV (daily repeatability), and basically independent of the voltage setpoint (0.004% of full scale). This results in a considerably lower noise specification and proved to be in good agreement with the measurement results.

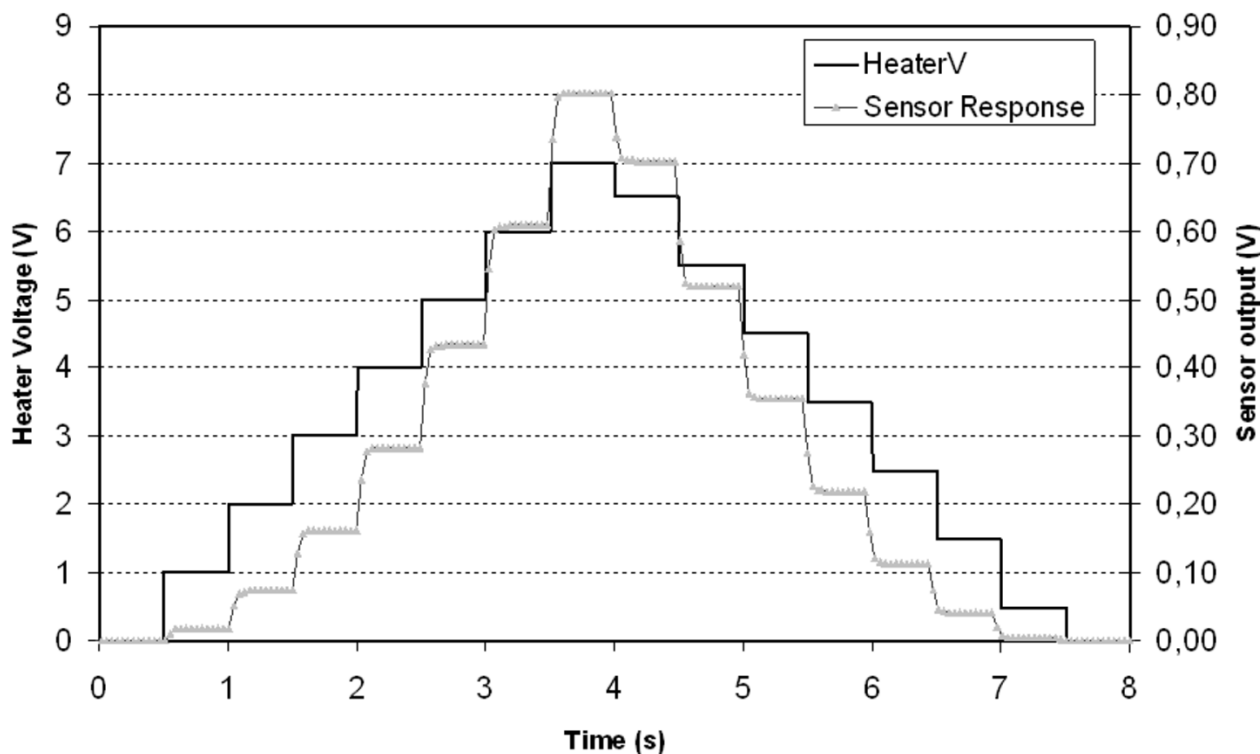


**Figure 5.1 Heater and sensor output voltage waveforms. Heater voltage waveform, with overlapped sample sensor response for pure methane. Line 'HeaterV' (in black) is read in the left axis. Line 'Sensor response' (in grey) is read in the right axis.**

The stimulation of the sensor heater was done by programming the HM8142 with a voltage steps train. The excitation waveform is shown in Figure 5.1, together with an example sensor response to pure methane. Heater voltage levels span from 0.5V to 7V in 0.5V steps, with a step duration of 500ms, as shown in Figure 5.1. The power consumption during excitation is in average of 25mW. The complete excitation cycle takes 7 seconds. Note how the sensor output is stable after approximately 150ms (T90 around 100ms), which implies that the excitation time may be easily reduced to 3 seconds. Sensor output is usually comprised in the 0-1V range under normal working conditions. At the limit condition of  $V_{Heater} = 7V$  a maximum temperature of the device of approximately 200°C is expected under normal operating conditions (immersed in methane), this temperature is safely below the three critical temperatures which are:

1. the auto-ignition temperature of methane at 595°C;
2. the Al-Si alloying temperature, starting at 400°C;
3. Typical Aluminum annealing temperatures, which can be as low as 300°C.

In case the sensor is operated in air, temperature rises considerably to values of about 300°C, making it advisable to operate the sensor only when immersed in natural gas. Even so, operation in air during short times does not negatively affect the sensor performance.

The synthetic natural gas mixtures used for calibration and validation are described in Table 5.1 (next page). In order to define the measuring points, experimental design, data from literature [Rahmouni2003a] and analysis certificates kindly provided by ENAGAS LNG regasification plant in Barcelona were considered. Points 2 to 16 define of Table 5.1 a cubic centered experimental design, each point was duplicated, and pure methane was measured 4 times, since it was the point with a higher set point precision. Measurements 35 to 38 are approximations of real natural gas compositions from Holland, Norway, Russia and Algeria [Rahmouni2003a]. Composition is expressed in %. Superior Heating Value, Wobbe Index and normal density (SHV, W, d respectively) are indicated. Row FS shows the full scale variation for each of the properties.

Pure methane (99.995 % purity) was added as an additional measurement point for convenience, as it is a high precision point with lower cost compared to gravimetric mixtures.

**TABLE 5.1 EXPERIMENTAL POINTS USED IN THE CALIBRATION AND VALIDATION SETS**

Calibration set							
n	[CH <sub>4</sub> ] (%)	[C <sub>2</sub> H <sub>6</sub> ] (%)	[N <sub>2</sub> ] (%)	[CO <sub>2</sub> ] (%)	SHV (MJ·m <sup>-3</sup> )	W (MJ·m <sup>-3</sup> )	d (MJ·m <sup>-3</sup> )
<b>1</b>	100.0	0.0	0.0	0,0	39.831	53.469	0.717
<b>2</b>	84.7	8.0	6.1	1.22	39.357	49.538	0.816
<b>3</b>	81.8	8.1	8.9	1.22	38.234	47.678	0.831
<b>4</b>	80.8	11.8	6.1	1.22	40.496	50.229	0.840
<b>5</b>	78.0	11.9	8.9	1.22	39.371	48.398	0.856
<b>6</b>	84.0	8.1	6.1	1.78	39.139	49.039	0.824
<b>7</b>	81.2	8.1	8.9	1.78	38.012	47.198	0.839
<b>8</b>	81.4	12.0	6.2	0.42	40.827	50.901	0.832
<b>9</b>	77.4	11.9	8.9	1.78	39.152	47.931	0.863
<b>10</b>	82.6	10.0	7.5	0.0	39.865	50.040	0.821
<b>11</b>	79.6	10.0	7.5	2.99	38.687	47.486	0.858
<b>12</b>	91.1	0.0	7.4	1.50	36.272	46.822	0.776
<b>13</b>	71.1	19.9	7.5	1.50	42.262	50.579	0.903
<b>14</b>	88.5	10.1	0.0	1.50	42.263	53.743	0.800
<b>15</b>	73.6	10.0	14.91	1.50	36.305	44.029	0.879
<b>16</b>	81.0	10.0	7.5	1.50	39.274	48.740	0.839
<b>17</b>	100.0	0.0	0.0	0.0	39.831	53.469	0.717
<b>18</b>	100.0	0.0	0.0	0.0	39.831	53.469	0.717
<b>19</b>	73.6	10.0	14.92	1.50	36.300	44.021	0.879
<b>20</b>	100.0	0.0	0.0	0.0	39.831	53.469	0.717
Validation set							
n	[CH <sub>4</sub> ] (%)	[C <sub>2</sub> H <sub>6</sub> ] (%)	[N <sub>2</sub> ] (%)	[CO <sub>2</sub> ] (%)	SHV (MJ·m <sup>-3</sup> )	W (MJ·m <sup>-3</sup> )	d (MJ·m <sup>-3</sup> )
<b>21</b>	84.7	8.1	6.1	1.22	39.365	49.548	0.816
<b>22</b>	81.8	8.1	8.9	1.22	38.238	47.682	0.831
<b>23</b>	80.8	11.9	6.1	1.22	40.502	50.236	0.840
<b>24</b>	78.0	11.9	8.9	1.22	39.377	48.407	0.856
<b>25</b>	84.0	8.1	6.1	1.78	39.144	49.045	0.824
<b>26</b>	81.2	8.1	8.9	1.78	38.017	47.203	0.839
<b>27</b>	80.3	11.9	6.1	1.78	40.281	49.750	0.848
<b>28</b>	77.4	11.9	8.9	1.78	39.154	47.934	0.863
<b>29</b>	82.6	10.0	7.5	0.0	39.865	50.041	0.821
<b>30</b>	79.6	10.0	7.5	3.00	38.688	47.488	0.858
<b>31</b>	91.1	0.0	74	1.50	36.274	46.824	0.776
<b>32</b>	71.1	19.9	7.5	1.50	42.267	50.583	0.903
<b>33</b>	88.5	10.0	0.0	1.50	42.264	53.742	0.800
<b>34</b>	81.1	10.0	7.5	1.50	39.276	48.745	0.839
<b>35</b>	81.8	8.1	8.9	1.22	38.238	47.682	0.831
<b>36</b>	87.5	9.3	3.2	0.00	41.392	52.842	0.793
<b>37</b>	95.3	2.7	2.1	0.00	39.825	52.450	0.745
<b>38</b>	93.2	4.6	1.1	1.09	40.337	52.406	0.766
<b>FS</b>	28.9	19.9	14.92	3	5.995	9.722	0.186

### 5.2.3 SIGNAL PROCESSING

Rahmouni et al. (see chapter 2, section 2.3.3.10), measured the actual values of the thermal conductivity of the natural gas mixtures using appropriate instrumentation [Rahmouni2003a], and suggested a graphical resolution method, providing interesting results. In this work however, the estimation of the thermal conductivity at a particular temperature is avoided, as it can introduce additional errors. The microsensor output is a value which directly contains information of a portion of the  $k(T)$  curve ranging from the maximum temperature to roughly room temperature corresponding to the first excitation step. For this reason, techniques from the chemometrics field, that are suitable for extracting the chemical information even in poor signal conditions (in this case, noise and high correlation among sensor steps) were chosen. Among the full set of techniques, for reasons of improved flexibility, scalability and applicability, Partial Least Squares (PLS) [Geladi1986] was selected.

PLS regression was performed on the experimental and simulated data. The reported results were obtained with a data pre-processing consisting of extracting the stationary part of the sensor response for every voltage step (four measurements of the flat region were averaged) and mean centering the data, since autoscaling the signal proved to be counterproductive for the PLS predictive ability.

Measurements were used to build PLS prediction models for seven properties, four of them the individual gas concentrations of CH<sub>4</sub>, C<sub>2</sub>H<sub>6</sub>, CO<sub>2</sub> and N<sub>2</sub>, and three relevant properties namely: the normal density (*d*), the Wobbe index (*W*) and the Superior Heating Value (*SHV*) of the gas mixture. As previously mentioned, ISO6976 [ISO1995] was used to derive the three properties *d*, *W* and *SHV* of the gas from its composition.

For clarity, and in order to discuss the effect of the uncertainty sources, it is convenient to recall two basic equations of multivariate linear regression, which basically correspond to the operation (or prediction) phase and the calibration (or training) phase.

In first place the inverse linear regression:

$$y_{pred} = \mathbf{x}^T \cdot \mathbf{b} \quad (5.1)$$

where  $y_{pred}$  is the predicted value of a property of interest, in this case either ***W***, ***d***, or ***SHV***.  $\mathbf{x}$  is the input vector of measurements  $\{x_1, x_2, \dots, x_{14}\}$  formed by each stationary sensor output voltage as a response to each of the 14 heater voltage steps, and  $\mathbf{b}$  is the regression vector, a set of regression coefficients obtained by the PLS calibration (or modelling) procedure.

Equation (5.1) is normally calculated in real-time when the system is operating in the normal operation mode. The PLS model is effectively vector  $\mathbf{b}$ , which can be expressed as

$$\mathbf{b} = f_{PLS}(\mathbf{X}_{cal}, \mathbf{Y}_{cal}) \cdot \mathbf{Y}_{cal} \quad (5.2)$$

Where  $\mathbf{X}_{cal}$  is the array of experimental measurements, formed by each sensor output vector  $\{x^{i_1}, x^{i_2}, \dots, x^{i_{14}}\}$  for each of the 20 calibration points  $i = \{1, 2, \dots, 20\}$  as in equation (5.3) (see also table 1);

$$\mathbf{X} = \begin{pmatrix} x_1^1 & x_2^1 & \dots & \dots & x_{14}^1 \\ x_1^2 & x_2^2 & \dots & \dots & x_{14}^2 \\ \vdots & \vdots & & & \vdots \\ \vdots & \vdots & & & \vdots \\ x_1^{20} & x_2^{20} & \dots & \dots & x_{14}^{20} \end{pmatrix} \quad (5.3)$$

and  $\mathbf{Y}_{cal}$  the corresponding values (for each observation  $i$ ) of the properties of interest we want to model in the present case the properties are modeled individually, so  $\mathbf{Y}$  becomes a column vector,  $\mathbf{y}$ ; its values  $y_i$  can be retrieved from table 1, being each column the  $\mathbf{y}$  for each of the seven PLS models calculated. Function  $f_{PLS}$  represents the calibration procedure and is a function of the experimental calibration measurements,  $\mathbf{X}_{cal}$  and its corresponding values of the properties to be predicted,  $\mathbf{y}_{cal}$ .

Note that equation (5.2) is computed once in the calibration mode of the system, before going into operation mode. A system might not enter again in the calibration mode, unless a recalibration procedure is performed.

#### 5.2.4 UNCERTAINTY ANALYSIS

A detailed analysis of sources of uncertainty and the propagation to predictions was performed for a full understanding of the system limitations and weak points and as a necessary step for the performance limits estimation which was another main objective of the thesis. The different uncertainty sources are presented in this section and it is indicated whether they have an effect in the operation mode or the calibration mode. After that, the expected magnitudes for the different uncertainty contributions are presented as subsections. Results for uncertainty propagation and its influence on the performance of the system are provided and discussed in the results and discussion section.

Considering the operation phase (equation (5.1)) the total error in the prediction stage has two independent contributions: the uncertainty due to the new measurements  $\mathbf{\epsilon}_x$  and the uncertainty due to the calibration  $\mathbf{\epsilon}_b$ , as in equation (5.4).

$$\mathbf{\epsilon}_{y_{pred}} = \sqrt{(\mathbf{\epsilon}_x \cdot \mathbf{b})^2 + (\mathbf{x} \cdot \mathbf{\epsilon}_b)^2} \quad (5.4)$$

Factors contributing to noise in the sensor measurement vector  $\mathbf{x}$  can be listed in the first place those affecting *sensor measuring point reproducibility* (see appendix A), which are

- Heater voltage reproducibility,
- Ambient temperature,
- Sensor intrinsic noise,
- Voltage acquisition noise,
- Aging, sensor degradation.

A second group of factors affecting the noise in  $\mathbf{x}$  can be described as uncertainty sources affecting *gas mixture thermal conductivity*, which are

- Ambient temperature (again, but considering its effect on the gas, not on the sensor),
- Gas pressure (which is affected by ambient pressure in the presented setup),

During operation mode, the regression vector  $\mathbf{b}$  is constant,  $\mathbf{\epsilon}_b$  is a fixed contribution to the prediction uncertainty, and the prediction cannot get any better than  $\mathbf{x} \cdot \mathbf{\epsilon}_b$ .

Equation (5.5) shows the propagation of uncertainties in the  $\mathbf{X}_{cal}$  matrix of calibration measurements and the  $\mathbf{y}_{cal}$  property calibration values vector to the regression vector  $\mathbf{b}$  in an explicit way.

$$\varepsilon_b = \sqrt{\left( \frac{\partial \mathbf{b}}{\partial \mathbf{X}_{cal}} \cdot \mathbf{\epsilon}_x \right)^2 + \left( \frac{\partial \mathbf{b}}{\partial \mathbf{y}_{cal}} \cdot \mathbf{\epsilon}_y \right)^2} \quad (5.5)$$

It shall be noted that uncertainty in  $\mathbf{b}$  ( $\mathbf{\epsilon}_b$ ) has a direct contribution from uncertainty in  $\mathbf{y}_{cal}$  ( $\mathbf{\epsilon}_y$ ), the vector of calibration values for the predicted property. Uncertainty sources affecting  $\mathbf{X}_{cal}$  (the full calibration measurements set) and  $\mathbf{x}_{cal}$  (a single measurement), are basically identical as detailed in the operation mode. Uncertainty sources affecting  $\mathbf{y}_{cal}$  have diverse origins and correspond to those uncertainty sources affecting the *effective gas mixture composition*, namely:

- Mass Flow Controller (MFC) uncertainty,
- Uncertainty about the completeness of the gas replacement inside the sensor chamber (gas exchange dynamics), and
- Possible leaks or contamination of gases.

These uncertainty sources are discussed in detail in appendix A (section A.3).

Note that a different grouping of error sources as differential and common mode error sources is provided in 3.6. This grouping is convenient when considering the addition of synthetic noise over simulated data to discuss the performance limits of the system.

### 5.2.5 VALIDATION

---

The Prediction error of the PLS models and other figures of merit were estimated using a test set validation with hold-out. Two datasets, of 20 calibration points and 18 validation points were used. Calibration and validation datasets are displayed in Table 5.1.

For the simulation data, the same concentration points in Table 5.1 were simulated. This allows for a better matched comparison with experimental results. Larger simulation datasets were also used for extended interpretation of the sensor response modeling, and also to estimate the influence of the presence of propane in the natural gas mixture.

The number of latent variables to build the prediction models was selected by inspecting the residual validation variance, which has been calculated using equation (5.6)

$$R_{\text{var}}^{\text{val}} = \frac{\sum_{i=1}^n (y_{\text{val}}(\mathbf{X}) - \hat{y}_{\text{val}}(\mathbf{X}))^2}{v} \quad (5.6)$$

Where  $y$  is the measured experimental point,  $\hat{y}$  is the predicted PLS model output for a given  $X$ , and  $v$  is the number of degrees of freedom calculated as the number of points  $n$  minus the PLS model parameters or latent variables (LV)  $p$ . Inspection of the normalized residual variance for the obtained PLS prediction models, provides a simple and consistent criterion to select the number of latent variables for each PLS model, by choosing the number of LVs which minimizes the residual variance in the validation set.

In order to evaluate the performance of the system, a number of figures of merit for the different measured variables will be presented, in particular:

- The absolute concentration error (in %) for each of the synthetic natural gas components.
- The relative error (relative to expected true value) in the normal density, Superior Heating Value and Wobbe index.

These figures of merit were calculated for the experimental and the simulation data, for comparison.

It was expected that for simulations, in absence of experimental noise, residual variance would decrease monotonically when the number of latent variables was increased. The residual variance for SHV was calculated for experimental and simulated data in order to compare the effect of the experimental uncertainties.

### 5.2.6 PERFORMANCE LIMITS ESTIMATION

---

An expected SHV prediction performance for different experimental situations has been estimated by adding synthetic noise to the simulation results. Even though the performance limits estimation was centered in the study of the SHV prediction, an analogous discussion can be drawn for the other prediction models.

In order to characterize different amounts of added synthetic noise, a *differential error factor* was introduced which simulated possible experimental situations. To understand this characterization it was convenient to split the X-block uncertainties into two categories:

- Common mode error sources which included ambient temperature and pressure variations. These affect simultaneously (and with high correlation) all the steps of the sensor output waveform.
- Differential error sources which included heater voltage noise, voltage acquisition noise and the sensor intrinsic noise (thermal noise). These affect independently (in an uncorrelated way) each of the components of the sensor output vector (each component consisting in the response to a different heater voltage).

The *differential error factor* is defined as a proportionality factor which has been applied to the differential noise sources to display its influence in SHV prediction. Results are plotted and discussed in section 4.3.

## 5.3 Multivariate calibration results and discussion

### 5.3.1 CALIBRATION AND VALIDATION RESULTS

As described in the materials and methods section, seven PLS models were computed using the experimental data. The normalized residual variance of each PLS model is shown in Figure 5.2; the number of latent variables for each PLS model was selected according to these results.

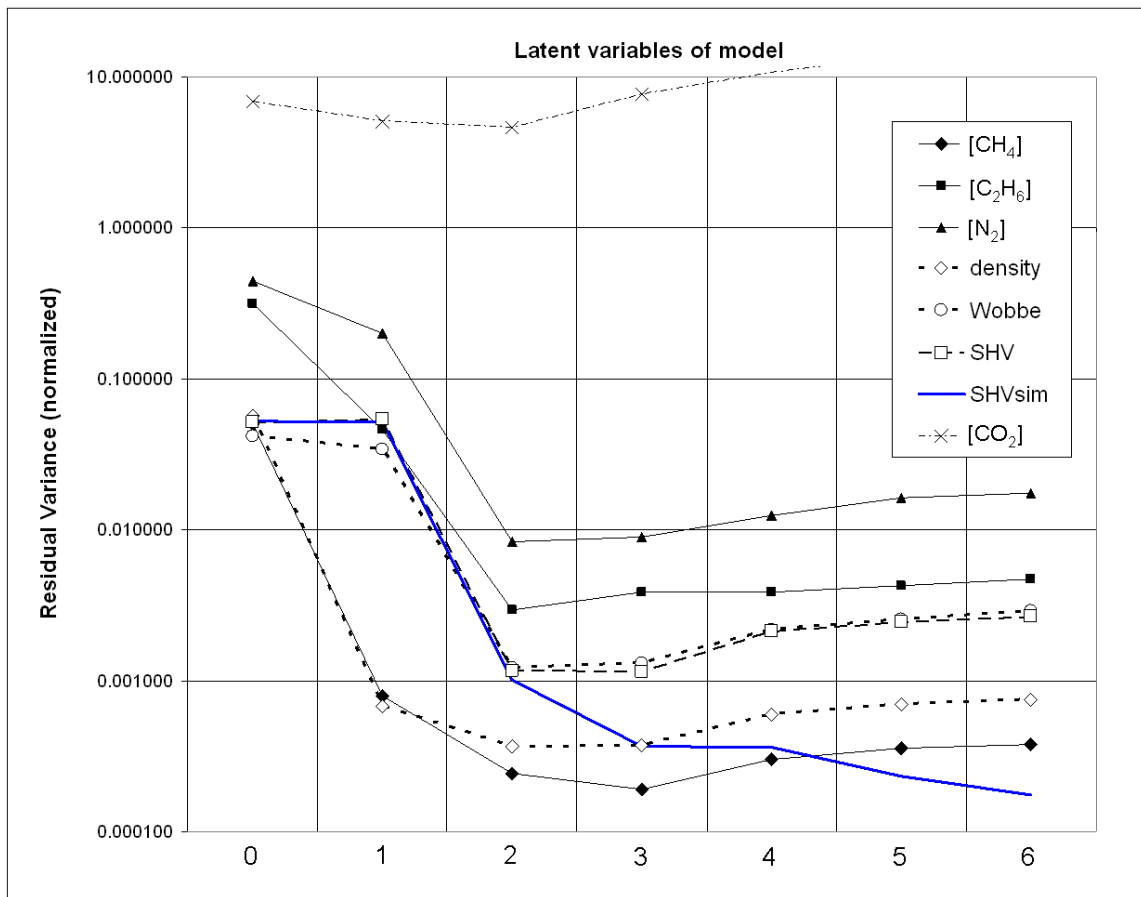


**Figure 5.2 Residual variance of the PLS models.** Normalized residual variance of the predictions of the 7 PLS models as a function of the number of LVs. Variances increase monotonically beyond PC 6, noise dominates. Validation results are shown. Solid line with no markers corresponds to simulation results for SHV prediction. Note that the 0 LV model corresponds to a single constant prediction value, the calibration measurements mean for that property.

It can be seen that five of the PLS models perform best considering two LVs, and two of them improve slightly when considering a third LV.

Residual variance values were normalized to the squared full-scale range of the predicted properties, this normalization allows PLS model performances to be compared in the same graph. Curves in Figure 5.2 provide information about which properties are best predicted with the PLS models. The graph is in concordance with the figures of merit in Table 5.2, which is discussed below, for instance in that methane and normal density predictions are the best performing ones.

An additional bold solid line is displayed which corresponds to simulated data. This solid line gives information about expected PLS model performance in theoretical absence of experimental uncertainty.

Residual variance for the carbon dioxide reveals the low quality of the PLS model fit, reflecting mainly experimental uncertainty.

One relevant effect can be pointed out from the simulation results shown in Figure 5.2 (solid line). The performed measurements correspond to a four component mix (it has three effective degrees of freedom). However, more than three LVs provide improved calibration PLS models according to simulation results. The reason for this is that the regression problem is slightly non-linear, and higher LVs contribute to linearize the input and output spaces. This non-linearity was hinted in previous simulation results and is masked in the experimental measurements by noise. In accordance with this argument, none of the PLS models for any property showed a performance improvement when considering more than three LVs.

Figure 5.3 shows the performance of the PLS models for the concentration of three individual components, and for normal density, Wobbe index and Superior Heating Value. Calibration points are indicated in grey and test set validation points in black. It can be observed that prediction of methane is accurate, nitrogen and ethane can be predicted with slightly impaired accuracy, but prediction of carbon dioxide was not effectively possible. The reason for this is that variation of CO<sub>2</sub> in the different mixtures is small compared to the other gases, and also its thermal conductivity as a function of temperature curve is highly correlated to that of nitrogen. A clear relation can be drawn with results in Figure 5.2 showing that two latent variables hold most of the information for almost all PLS models, instead of the *a priori* expectation of three (the number of degrees of freedom in the gas mixture). Information about CO<sub>2</sub> concentration apparently lied under the noise level for this experimental setup. Prediction of the carbon dioxide concentration is a problem commonly tackled in instruments based on correlative methods by use of NDIR measurements (see section 2.3). This option was discarded in this work to keep the advantages of the single microsensor approach.

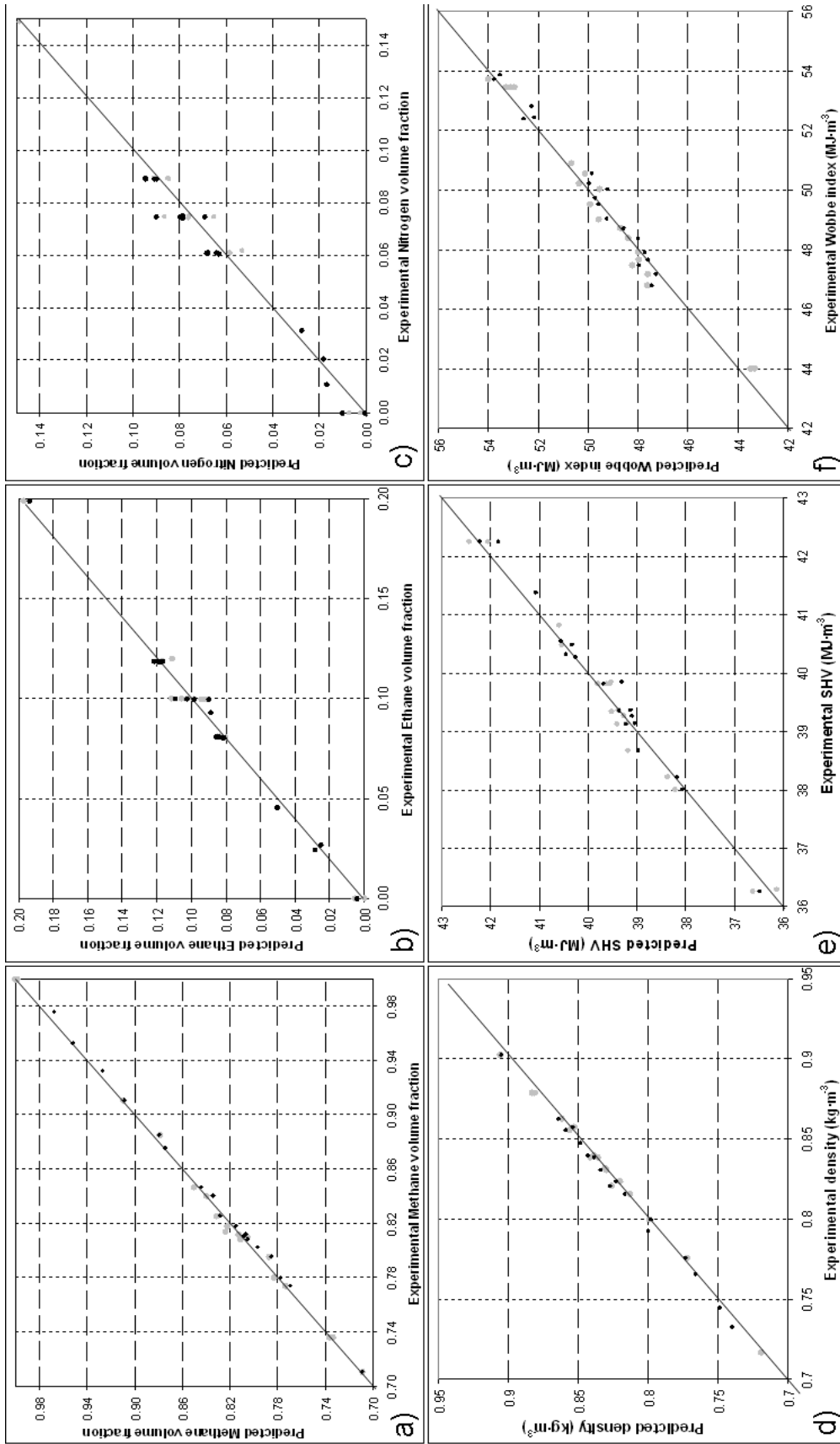


**Figure 5.3 Performance of the PLS models.** a,b,c) Performance plot of the  $\text{CH}_4$  (a),  $\text{C}_2\text{H}_6$  (b) and  $\text{N}_2$  (c) normal volume fraction prediction models, 3, 2 and 2 LVs were used respectively. d) Performance plot for the normal density PLS model. e) Performance plot for the Superior Heating Value PLS model. f) Performance plot of the Wobbe index PLS model. All plots show calibration points in grey and validation points in black. Straight lines are not fits; they depict the ideal performance line (unity slope line).

For the other three properties of interest, normal density, Superior Heating Value and Wobbe index, results show good prediction performance of the PLS models, particularly in the case of normal density. Figures of merit of all the PLS models are summarized in Table 5.2.

Table 5.2 features simulation results which can be used for comparison. The number of latent variables used is indicated in each case.

Results show that under laboratory experimental conditions it was possible to attain a remarkable accuracy in most predictions except in the case of carbon dioxide as detailed in Table 5.2. The sensor performed best at predicting methane concentration, with a 0.60% absolute error in concentration, and assessing gas normal density with a 0.82% relative error. It is of particular relevance that SHV can be determined within a relative error of 1% (all values estimated at the 95% confidence interval).

TABLE 5.2 FIGURES OF MERIT OF THE PLS CALIBRATION

Property	Experimental (2-3LV)		Sim. 3LV		Sim. 6LV	
	Abs. Error	R	Abs. Error	R	Abs. Error	R
[CH <sub>4</sub> ]	0.60% (3 LV)	0.9990	0.25%	0.9998	0.12%	0.9999
[C <sub>2</sub> H <sub>6</sub> ]	1.0% (2 LV)	0.9950	0.57%	0.9990	0.41%	0.9990
[CO <sub>2</sub> ]	1.3%(2 LV)	0.5660	1.1%	0.8350	0.58%	0.9470
[N <sub>2</sub> ]	0.90% (2 LV)	0.9900	0.73%	0.9940	0.22%	0.9995
Rel. Error		R	Rel. Error	R	Rel. Error	R
<i>d</i>	0.82% (2 LV)	0.9970	0.54%	0.9990	0.30%	0.9999
<i>SHV</i>	1.0% (3 LV)	0.9920	0.68%	0.9970	0.43%	0.9990
<i>W</i>	1.5% (2 LV)	0.9860	1.0%	0.9980	0.72%	0.9970

Simulation results provide an approximation of expected performances in theoretical absence of experimental uncertainty. It should be noted that results indicate that in order to predict carbon dioxide concentration with some accuracy, a six LV PLS model would be needed.

Nevertheless, simulation results in Table 5.2 have to be considered with prudence as the underlying FEM modelling equations and correlations rely on the equation of Wassiljewa to correlate the thermal conductivity to the composition of the gas mixture (see section 4.4); this equation is empirical and approximate. For this reason, as more LVs are considered, the reliability of the simulations (and derived calibration PLS models) may drop.

Considering propane, another important component of natural gas, an exploratory analysis was performed using simulations in order to check its influence on the metrological performance of the sensor. A slightly impaired performance was found in moderate accuracy PLS models (three LVs), an increased non-linearity in the sensor readings, made it difficult to get below the 1% uncertainty threshold in the SHV prediction. Given the same experimental setup and number of calibration points, the presence of typical levels of propane would be expected to degrade by about a 30% the prediction performances in Table 5.2. By means of an increase in the number of calibration points, or an improvement in the differential experimental uncertainties (more precise excitation and/or sensor reading) the system may revert to the stated performances.

### 5.3.2 UNCERTAINTY ANALYSIS RESULTS

A detailed uncertainty analysis has been performed as described in 5.2.4 and appendix A. Quantitative results of the sensitivity of the sensor to every uncertainty source, at every voltage step of the sensor excitation are provided in Table 5.3. This table presents detailed results, which fully characterize the sensitivity of the sensors to the different uncertainty sources, it can be seen that this sensitivity is dependent on the heater voltage step considered. In fact, the sensor is acting as 14 different but highly correlated sensors, with different sensitivities to noise.

Among the noise sources, ambient temperature variations dominate, though for the lower voltage steps, other contributions become comparable. Table 5.3 presents the temperature induced uncertainty for a 0.2°C variation, which is the typical temperature oscillation inside the measurement chamber for a 24h period of time. For this reason, results in table 5.2 hold in general for daily recalibrations of the system.

Table 5.3 is basically a summary of the experimental uncertainties. It is interesting to note that the influence of the ambient pressure appears to be negligible compared with the ambient temperature, voltmeter and heater noise. This is an important result which simplifies the conception of a real measurement device, as no special pressure regulation or compensation would be needed in first instance.

**TABLE 5.3 EFFECT OF RELEVANT UNCERTAINTY SOURCES ON THE SENSOR OUTPUT VECTOR.**

Heater Voltage (V)→	1	2	3	4	5	6	7	6.5	5.5	4.5	3.5	2.5	1.5	0.5
<b>Uncertainty sources affecting sensor measuring point repeatability</b>														
Thermal noise ( $\mu\text{V}$ )	0.10	0.10	0.11	0.11	0.11	0.12	0.12	0.12	0.11	0.11	0.10	0.10	0.10	0.10
Voltmeter noise ( $\mu\text{V}$ )	7.8	10.1	13.8	18.8	25.0	32.2	40.2	36.1	28.5	21.7	16.1	11.7	8.7	7.8
T noise in $V_{\text{out}}$	See below													
$V_{\text{heater}}$ noise in $V_{\text{out}}$ ( $\mu\text{V}$ )	11	21	31	40	50	58	65	62	54	45	36	26	16	6
<b>Uncertainty sources affecting gas mixture thermal conductivity</b>														
P noise in $V_{\text{out}}$ (25mbar) ( $\mu\text{V}$ )	0.5	1.5	1.5	2.0	4.5	6.0	5.0	6.0	8.0	4.5	5.0	3.5	2.5	1.0
T noise in $V_{\text{out}}$ (0.2°C) ( $\mu\text{V}$ )	-7	-26	-55	-91	-133	-168	-210	-188	-153	-110	-70	-38	-15	-2

Results in table 5.3 were analytically estimated using known specifications for the sensor and acquisition equipment, and deriving the thermal conductivity dependence to pressure and temperature from available data for methane in the National Institute of Standards and Technology (NIST, Gaithersburg, MD, USA) [NIST2011] database (more information in available in appendix A). Differential noise sources in table 5.3 (thermal noise, voltmeter noise and heater voltage noise) contribute in an uncorrelated way to each voltage step while common mode ones contribute in a highly correlated way, results in the next section highlight the importance of this. Note that differential noise may be reduced by increasing signal integration times.

Uncertainty related to the calibration process, uncertainty in the values of the properties (y block) and more broadly the combined influence of the uncertainty sources in the predictions is displayed in Table 5. 4.

**TABLE 5.4 TOTALIZED CONTRIBUTION OF THE UNCERTAINTY SOURCES TO THE PREDICTION ERROR.**

<b>Uncertainty source</b>	Amb. Temp. variation (0.2°C)	Amb. Pressure variation (25mbar)	V acquisition noise	Heater V noise	Thermal noise	b model (calibration error)	Expected prediction error (relative)
<b>Density (kg·m<sup>-3</sup>)</b>	6.4x10 <sup>-4</sup>	6.2x10 <sup>-6</sup>	1.5x10 <sup>-4</sup>	2.5x10 <sup>-4</sup>	5.3x10 <sup>-7</sup>	6.2x10 <sup>-3</sup>	6.2x10 <sup>-3</sup> (0.76 %)
<b>SHV (MJ·m<sup>-3</sup>)</b>	-5.8x10 <sup>-2</sup>	-8.2x10 <sup>-3</sup>	2.7x10 <sup>-2</sup>	4.8x10 <sup>-2</sup>	1.1x10 <sup>-4</sup>	5.3x10 <sup>-1</sup>	5.4x10 <sup>-1</sup> (1.4%)
<b>W (MJ·m<sup>-3</sup>)</b>	-1.1x10 <sup>-1</sup>	-9.5x10 <sup>-3</sup>	2.4x10 <sup>-2</sup>	4.35x10 <sup>-2</sup>	1.0x10 <sup>-4</sup>	1.10	1.12 (2.4%)
<b>[CH<sub>4</sub>]</b>	-7.0x10 <sup>-4</sup>	-5.9x10 <sup>-4</sup>	2.3x10 <sup>-3</sup>	4.5x10 <sup>-3</sup>	1.3x10 <sup>-5</sup>	0.75x10 <sup>-2</sup>	0.76%
<b>[C<sub>2</sub>H<sub>6</sub>]</b>	-1.8x10 <sup>-4</sup>	-1.10x10 <sup>-4</sup>	4.7x10 <sup>-4</sup>	8.3x10 <sup>-4</sup>	1.9x10 <sup>-6</sup>	1.0x10 <sup>-2</sup>	1.0%
<b>[CO<sub>2</sub>]</b>	4.8x10 <sup>-5</sup>	-2.6x10 <sup>-6</sup>	2.1x10 <sup>-5</sup>	3.6x10 <sup>-5</sup>	7.7x10 <sup>-8</sup>	1.28x10 <sup>-2</sup>	1.3%
<b>[N<sub>2</sub>]</b>	1.3x10 <sup>-3</sup>	1.25x10 <sup>-4</sup>	3.4x10 <sup>-4</sup>	6.2x10 <sup>-4</sup>	1.4x10 <sup>-6</sup>	0.9x10 <sup>-2</sup>	1.1%

NOTE: Results estimated with Monte Carlo analysis and adding synthetic Gaussian noise to the experimental measurements. PLS model (b) uncertainty is the calibration uncertainty  $\varepsilon_b$ , which is affected by  $\varepsilon_x$  and  $\varepsilon_y$  uncertainties.

The contribution to prediction error of each different uncertainty source is detailed in Table 5.4, note that operation mode is considered. Estimated values for each of the contributions building up  $\epsilon_x$  are provided, and also the PLS model uncertainty  $\epsilon_b$  values are listed. The PLS model uncertainty  $\epsilon_b$  corresponds to the uncertainty strictly related to the calibration process. Estimation of  $\epsilon_b$  was done by including all uncertainty sources, including gas concentration uncertainty  $\epsilon_y$  in a Monte Carlo analysis.

The obtained values compare well with the experimental results and validation, though are slightly overestimated in the case of Superior Heating Value and Wobbe index. Table 5.4 shows that error due to the PLS model  $\epsilon_b$  (the calibration uncertainty) dominates the prediction error. This is not at all surprising, since the calibration uncertainty is in fact affected by the combined influence of all the uncertainty sources. So despite  $\epsilon_b$  dominates, reducing  $\epsilon_b$  is essentially a problem of reducing other important uncertainty sources. According to results in Table 5.4, thermal noise in the sensor and ambient pressure variations have very little influence in prediction. However, it is important to note that, leaving  $\epsilon_b$  aside, there is a non-negligible contribution from several other uncertainty sources.

This result is in agreement with the performance limits estimation in next section, and in particular with Figure 5.4. However, the apparent overestimation of the uncertainty in  $y_{cal}$  was probably making this uncertainty source more prominent than others. Next section provides more insight in the relative influence of the uncertainty sources.

### **5.3.3 PERFORMANCE LIMITS ESTIMATION RESULTS**

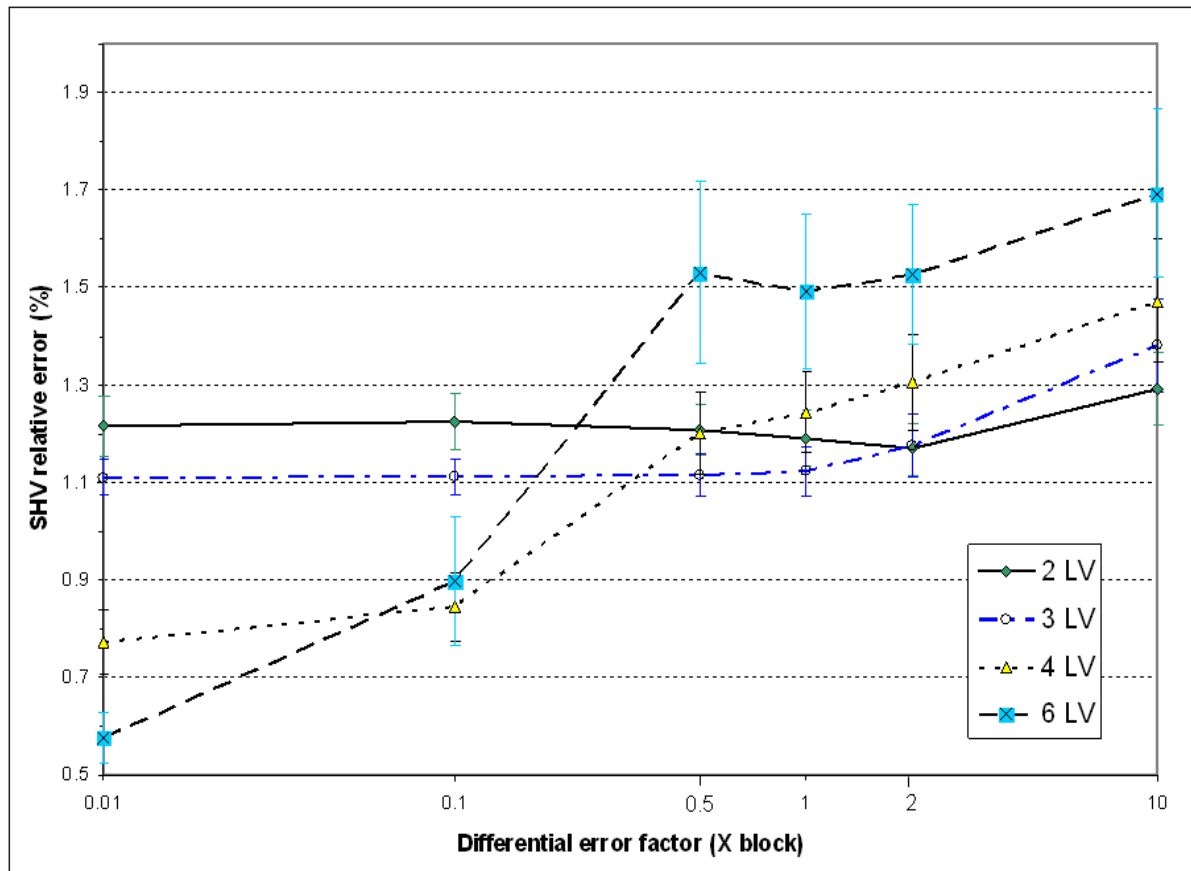
---

Figure 5.4 shows the relative error in SHV prediction as a function of the *differential error factor*, for different PLS models corresponding to 2, 3, 4 and 6 latent variables.

Results in Figure 5.4 are in good agreement with experimental results in Figure 5.2 as SHV prediction performance does not significantly improve for PLS models of more than two latent variables. Also relative error values are in close agreement with experimental results for a *differential error factor* of one which corresponds to the estimated real experimental noise situation.

As expected, PLS modeling appeared considerably robust to uncertainty sources. Despite this, getting below the 1% error seems to require a considerable effort in experimental uncertainty reduction. Even in this case the performed simulation analysis suggested that an error around 0.5% is the best performance the present technological approach can render even with a costly two order of magnitude reduction of the differential error sources. This two order of magnitude reduction is

an approximate limit already estimated according to results in Table 5.3, as would bring heater voltage and voltage reading errors down to the level of the sensor intrinsic thermal noise. However, a significant increase in integration times (of a factor ten and above) may improve this estimation. Also a significant increase in the number of calibration points (of a factor three and above) may enable improved PLS modeling with a higher number of LVs and thus reducing  $\epsilon_b$ . Nonetheless, if the experimental uncertainties ( $\epsilon_x$ ) are not reduced at the same time, only a mild improvement shall be expected since  $\epsilon_x$  would quickly dominate over  $\epsilon_b$  in the predictions.



**Figure 5.5 Estimated SHV relative prediction error under different noise conditions. Relative error in SHV prediction as a function of different levels of added synthetic Gaussian noise characterized by a differential error factor. Different curves correspond to 2, 3, 4 and 6 latent variable PLS models. Relative error is expressed at the 95% ( $2\sigma$ ) confidence interval. Error bars expressed at the 68% ( $1\sigma$ ) confidence interval for clarity. Values estimated with 200 Monte Carlo runs.**

Regarding common mode uncertainties (pressure and temperature), simulations suggested that PLS modeling performed very well at rejecting them when they are large enough to sensibly influence the relative error figures. In particular an increase of common mode noise variation by a factor of ten did not affect the prediction in a statistically significant way. Interestingly, in this latter case the optimal PLS model became a three LV model. The presence of this third latent variable hinted that the PLS model was able to reject the very high common mode error source by capturing its influence in this third latent variable.

Uncertainties in the Y block were due to inexact knowledge of the true gas mixture composition. They can be regarded as common mode uncertainties as they affect in a correlated way all the values of the sensor output vector. Simulation analysis hints that an uncertainty reduction in the Y block ( $\epsilon_y$ ) by a factor of ten or uncertainty increase by a factor of two did not affect prediction performance significantly after recalculation of the PLS model. This result complemented the interpretation of Table 5.4, by revealing that the PLS model uncertainty (see Table 5.4) was due to several uncertainty contributions other than  $\epsilon_y$  as already suggested in 4.2. The presence of these uncertainty contributions were preventing the computation of more accurate PLS models, and strongly influenced the prediction error.

Results in Tables 5.2 and 5.4 offer an in-depth view of the system limitations. Pressure dependence appears negligible when typical ambient pressure variations are considered. Ambient temperature, heater voltage excitation and sensor voltage reading come as the next error sources in importance. The two differential error sources (heater voltage excitation and voltage reading) were not well rejected by the PLS modelling.

These results suggests that combined action on the relevant uncertainty sources should be taken in order to improve the system performance, for instance by introducing temperature compensation, by improving heater repeatability and sensor voltage acquisition, as well as increasing the calibration gas composition accuracy, these improvements were implemented in a working prototype as described in chapter 6.

## 5.4 CHAPTER CONCLUSIONS

As a general trend, the development in micro gas-sensors has lately focused on the quest for higher sensitivity and improving detection limits [Hierlemann2007], while sensors based on thermal sensing have an intrinsically lower sensitivity. In the present application, a very high sensitivity is not needed, since the concentrations to determine are in the percent range. However, measuring the different gas properties with reliability and accuracy is of critical importance. In exchange for the lower sensitivity, an intrinsically stable and reliable sensing mechanism has been presented. Improved reliability is expected due to the absence of chemical interaction in the transduction process, a known cause of sensor drift and aging [Hierlemann2007, Marco1998, Artursson2000, Matsumiya2003].

It has been shown that the presented thermoelectric microsensor device, in combination with PLS regression, is able to predict different properties of natural gas with high accuracy. As a consequence, the reported single sensor approach opens a perspective for low-cost natural gas analyzers, ultimately enabling affordable energy consumption meters, with a dramatic cost reduction with respect to current technologies.

The presented results reporting the accuracy of properties determination were complemented with an in-depth analysis of uncertainties, for a complete understanding of the system limitations and possible improvements. It was determined that experimental uncertainties flaw the system performance, and improvements shall be obtained by reducing two differential error sources: heater voltage generation repeatability and voltmeter acquisition accuracy. Also, temperature compensation seems advisable in order not to deteriorate the system performance in field conditions, though simulation results hint that the system performance decrease would be limited due to the noise rejection capabilities of the PLS algorithm.

In third place, simulation results with the addition of synthetic noise were used to estimate the performance limits of this approach for the determination of SHV of natural gas. Results showed that accuracies below 0.6% seem to be extremely hard to reach and can be regarded as an intrinsic limit of this technological approach. However, exploration of the effect of an increase in the number of calibration samples is needed to confirm or revise this system limitation. Also the use of an alternative excitation of the sensor heater with other techniques [Vergara2007,Amrani1998] may positively affect these limits.

Regarding other sensor specifications, a remarkable analysis time of eight seconds has been presented, but shorter analysis times were possible by optimizing the sensor excitation and/or geometry, and a low power consumption of 25 mW is achieved.

## 6. SMART CHEMICAL SENSOR DESIGN: THE NATURAL GAS ANALYZER PROTOTYPE

---

6.1. Introduction.....	102
6.2. Description of the electronic instrumentation.....	103
6.2.1. Sensor excitation.....	105
6.2.2. Sensor reading.....	107
6.2.3. Combined implementation of IEEE-1451 and BS-7986 standards.....	109
6.2.4. Communications.....	113
6.2.5. PC data-logging software.....	114
6.3. Signal processing.....	115
6.3.1. Signal pre-processing and temperature correction.....	116
6.3.2. PLS regression.....	118
6.3.3. Fault detection.....	119
6.3.3.1. Univariate fault detection.....	119
6.3.3.2. Multivariate fault detection.....	123
6.3.4. Training and operation modes.....	123
6.4. Experimental.....	124
6.4.1. Sensor chamber and sampling.....	124
6.4.2. Design of experiments.....	125
6.4.3. Validation measurements.....	126
6.5. Test results.....	127
6.6. Chapter conclusions.....	130

## 6.1 INTRODUCTION

Chapters 1 and 2 provided insight in the state of the art of smart chemical sensors and natural gas analysis instrumentation. Chapters 4 and 5 have shown the measurement fundamentals of a micromachined thermoelectric gas sensors aimed for natural gas analysis. In this chapter, the implementation of the selected sensor approach in a prototype smart chemical sensor is described and discussed.

When the design of a new instrument was first considered, it was very important to take note of the requirements of the particular field of natural gas analysis. Stability and resilience to a wide variety of environmental conditions is a must, and the possibility of operational status self-assessment would definitely be desirable. The lack of robustness and the need of frequent recalibrations are common problems in current natural gas analysers based in PGC, implying burdensome maintenance costs. Calibration, maintenance and expert operation costs build up a considerable yearly bill, which adds up to high initial installation and acquisition costs.

Keeping this in mind, the design of the smart prototype instrument was aimed for high reliability, enhanced by the advantages of implementing the IEEE-1451 and BS-7986 smart sensor standards. An effort was made to combine the enhanced network interfacing and sensor replacement provided by IEEE-1451, with the standard operational self-assessment and data quality metrics provided by BS-7986, these two standards are highly complementary in its definitions, though none of the two were originally designed to work in combination. A possible way of combining them is herein presented.

Besides the smart sensor features, a high reliability of the instrument is pursued, by taking advantage of intrinsically highly stable sensor operating principle (due to the absence of chemical interaction with the sample) and a robust data analysis and signal processing approach which exploits the presence of high analytical redundancy in the sensor data for sensor fault diagnostics and potential (future) sensor correction according to BS-7986.

The concept of the combination of these two standards was already suggested by Karatzas et al. [Karatzas2007]. A comparison with this previous proposal is provided in section 6.2.3.

Other additional design goals included a compact design, low power consumption and low installation, operation and maintenance costs. In particular it was expected that calibration frequency shall be several times lower than current instruments (PGC) as a consequence of the aforementioned sensor robustness and stability. A short analysis time of less than five seconds was pursued, for improved sampling and measurement accuracy with respect to other instruments with analysis times of several minutes (see section 2.3).

The chapter is organized as follows, the electronic design is described in section 6.2, including a system overview, consideration on the implementations of standards, sensor excitation and readout electronics and communications. The last part of the section includes a description of the PC software acting as a host processor for the STIM (NCAP). Section 6.3 describes the signal processing and pre-processing of the sensor data while section 6.4 focuses on the experimental aspects of the measurement setup. Section 6.5 presents the results of the work, mainly focusing on the performance of the prototype in measuring superior heating value ( $H_S$ ) of the gas. Section 6.6 draws the conclusions of the chapter.

## 6.2 DESCRIPTION OF THE ELECTRONIC INSTRUMENTATION

---

The presented device incorporates a number of innovative features, due to the use of a new sensor technology as well as the implementation of advanced standards for smart instrumentation, namely IEEE-1451.2 and BS-7986. Table 6.1 shows a summary of the initially pursued specifications.

In order to implement the necessary firmware for standards implementation, sensor excitation and reading, and signal processing, a MSP430F1612 (Texas Instruments inc., USA) microcontroller is used. The device has six digital ports, two timers and an SPI port (used for the IEEE-1451.2 interface) together with 55 Kb of Flash memory and 5 Kb of RAM. These characteristics provided plenty of I/O and processing power offering good design flexibility. Moreover the MSP430 family are affordable low power consumption microcontrollers. An external high-end analog-to-digital converter is used, the AD7711, to ensure a high quality signal acquisition due to its 24 bit maximum performance. Previous uncertainty analysis for the implemented sensor indicated that signal acquisition and excitation stages shall be designed very carefully to reduce its noise contribution (see uncertainty analysis in section 5.3.2). Figure 6.1 shows a general block diagram of the device.

The device is externally commanded using the IEEE-1451.2 interface (see section 4.4). External requests via the Transducer Independent Interface (TII as defined in IEEE-1451.2) are processed by the MSP430F1612 microcontroller. The microcontroller also manages the sensor excitation block with the eight digital lines of I/O port P2. Two identical sensors are available in the same TO-8 encapsulation, providing instant sensor replacement if needed. The sensor signal is filtered and taken to the AD7711 analog-to-digital converter which communicates with the microcontroller using a dedicated serial interface. The microcontroller is in charge of keeping the digital readings in memory and providing them with quality metrics codes according to BS-7986. The SHT-75 (Sensirion AG, Switzerland) temperature sensor is directly read by the microcontroller using another specific serial communication bus (termed the sensibus). Microcontroller programming,

and system debugging is performed through the available JTAG interface. The relevant blocks are explained in more detail below.

**TABLE 6.1 PURSUED NATURAL GAS ANALYZER STIM PROTOTYPE SPECIFICATIONS**

<b>Measured Properties</b>	$H_s$ ( $W$ , $\rho$ , $[CH_4]$ , $[C_2H_6]$ , $[N_2]$ , $[C_3H_8]$ , others) <sup>1</sup>
<b>Ranges of operation</b>	$H_{s(25/0)}$ : 34 – 49 MJ/m <sup>3</sup> $W$ : 43 – 61 MJ/m <sup>3</sup> $d$ : 0.52 – 0.75 Kg/m <sup>3</sup> $[N_2]$ : 0 – 11%* $[CO_2]$ : 0 – 3.5% $[CH_4]$ : 65 – 100 % $[C_2H_6]$ : 0 – 22 % $[C_3H_8]$ : 0 – 3.5%
<b>Communications:</b>	IEEE-1451.2 interface (with smart sensor features)
<b>Fault detection:</b>	BS-7986 coded fault detection
<b>Accuracy:</b>	$H_s < 1.3\%$ (SNR of sensor readings > 60dB)
<b>Noise rejection:</b>	<i>Heater noise in <math>V_{out}</math>:</i> < 40 $\mu$ V for all steps <i>Voltage reading noise:</i> < 40 $\mu$ V for all steps
<b>Size of prototype PCB:</b>	10 cm x 10 cm
<b>Power consumption:</b>	14-24V - 60 mA max. (0.85 W)
<b>Calibration stability:</b>	>2 months
<b>Analysis time:</b>	<5s

<sup>1</sup> Other properties shall be measured by adapting the calibration

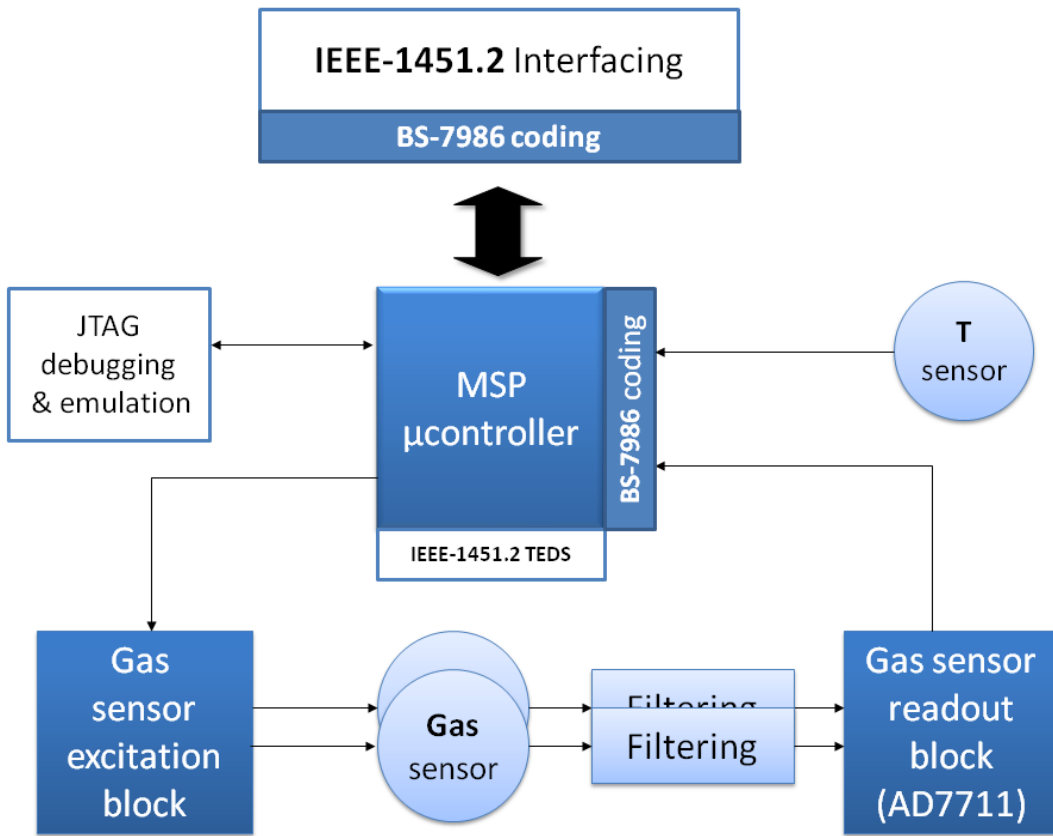


**Figure 6.1 prototype STIM System overview showing IEEE-1451.2 and BS-7986 features**

### 6.2.1 SENSOR EXCITATION

The stability of the sensor excitation has a high impact in the quality of the measurements as was previously discussed in chapter 5, section 5.3.2. For this reason a highly repeatable voltage steps generator was specifically designed for the sensor excitation. The adopted approach was also aimed for simplicity and avoiding high costs. Its schematic design can be seen in Fig 6.2

The simple but highly stable voltage divider consisted of four low temperature coefficient resistors (10 ppm/ $^{\circ}\text{C}$ ) which can be biased at different voltages by selecting different paralleled resistors with an analog micro switch. This resistors are in turn biased by a high precision and low TC (9 ppm/ $^{\circ}\text{C}$ ) ADR03 (Analog Devices Inc, USA) voltage reference. One to four 1k $\Omega$  resistors can be paralleled to provide a biasing of the voltage divider of between 2.307 V and 1.875 V, 1k $\Omega$  values were conveniently selected to provide some loading for the voltage reference ensuring a minimum

current flow in the range of  $100\mu\text{A}$ , safely away from possible leakage currents in the multiplexer, or biasing currents at the opamp, but avoiding unnecessary power consumption

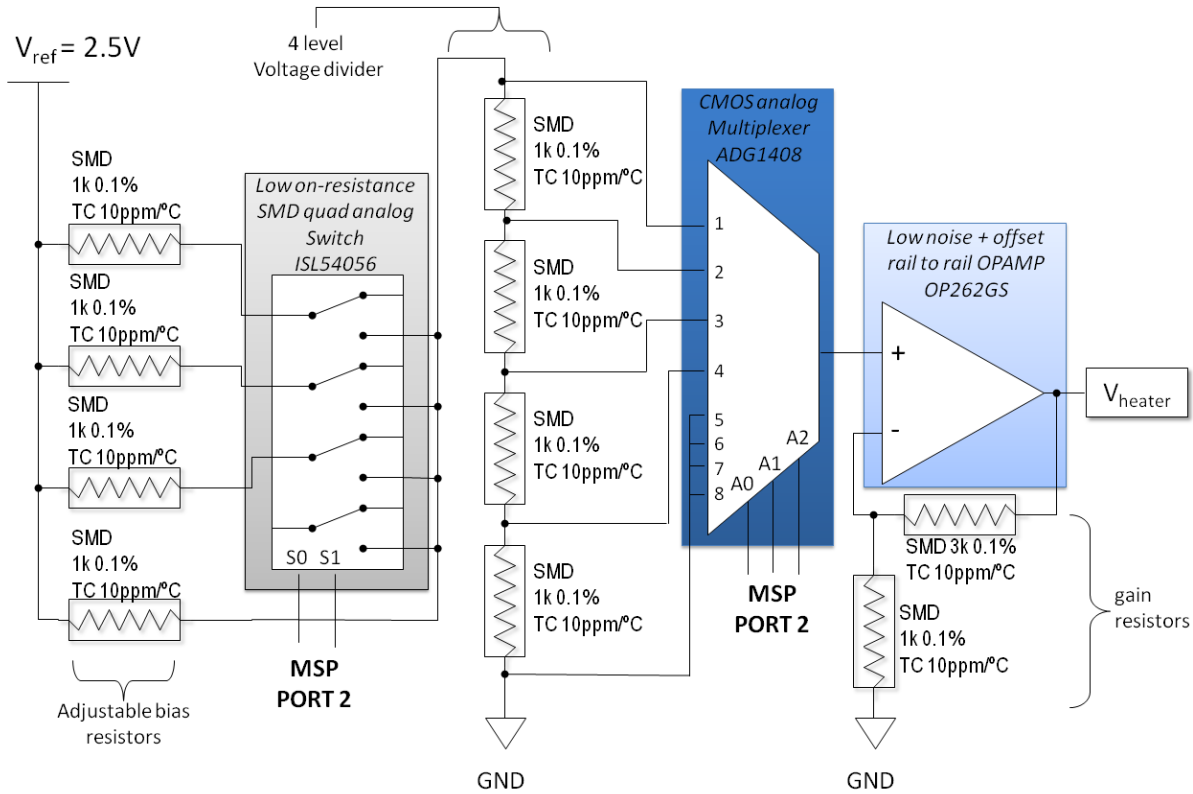


**Figure 6.2 High repeatability heater excitation block**

This simple resistor bridge approach provides an accuracy matching that of expensive top-class digital-to-analog (DAC) converters such as the AD760 (buffered) DAC or the AD5791 (considering effect of added buffer), both from Analog Devices Inc. (USA) ,and the DAC1220 (considering effect of added buffer) from Texas Instruments Inc. (USA). A low noise operational amplifier connected as a non-inverting voltage amplifier of gain 4 provides current buffering, isolation and the necessary voltage range for sensor heater excitation. The multiplexer and amplifier section are duplicated to allow partially independent heater (the variable voltage divider biasing is shared) stimulation for the two available sensors in the prototype. The full excitation waveform consists of 16 increasing voltage steps. The design is ratiometric, in that all resistors have the same temperature coefficient and thus temperature induced variations of the reference voltage are rejected by design. With this design an experimentally estimated voltage repeatability of 20 ppm or  $\pm 90 \mu\text{V}$  (highest voltage step) to 50 ppm or  $\pm 10 \mu\text{V}$  (lowest voltage step) is achieved. Temperature coefficients can be defined independently for each voltage step and have been estimated in the range of 50-5 ppm/ $^{\circ}\text{C}$ .

### 6.2.2 SENSOR READING

---

Another crucial factor in the accurate estimation of gas properties is the accuracy of the sensor output voltage readings, as was indicated by the uncertainty analysis provided in chapter 5, section 5.3.2. Section 5.3.2 provided a quantified estimation of the influence of noise in the voltage readout in the system performance which showed that if heater excitation could be significantly improved, voltage acquisition would quickly kick in as the dominant error source.

To try to improve the sensor acquisition, a high-resolution (24bit) and high-end analog-to-digital converter was selected for signal conversion, together with a 4-pole Butterworth low-pass filter with 37 Hz cutoff frequency which was implemented with two cascaded Sallen-key cells. This filter was aimed to reject all noise coming from the digital signals and mains power supply, the settling time of the filter is very close to the settling time of the sensor hotplate.

The analog-to-digital converter (ADC) is a high precision sigma-delta converter sampling at 39Khz (for a 10MHz external clock), it features an internal programmable gain amplifier (PGA) which has been set at a gain of 1 and also a programmable digital filter (a rolling average filter) which was set at a cutoff frequency of 13.1 Hz to maximize noise rejection. The choice of this internal filter implies a 50Hz sample data rate by design (refer to AD7711 datasheet); this is the data rate out of the AD7711 output interface after internal processing while the input sampling frequency is of 39 KHz (though the internal sigma-delta modulator runs at 19.5 KHz).

The two available gas sensors in each device are filtered separately and can be converted separately using the two available internally multiplexed ADC analog inputs. The difference between output data rate (50 Hz) and cutoff frequency (13.1 Hz) implies that if our signal of interest lies below the cutoff frequency (which is the case as we are measuring a stationary signal), the microcontroller is receiving “oversampled” data in a factor of four, for this reason four A/D reads are averaged (for each stationary sensor step) to supply a more stable value to the transducer channel. The effect of the cascaded filters present in the design is discussed in the signal pre-processing and temperature correction section 6.3.1.

A summary of the sensor acquisition performance is shown in Table 6.2. The analysed data were obtained using the on-board data acquisition routines managing the AD7711, and processed offline from a datalog file generated by the NCAP-PC software (refer to 6.2.5). Table 6.2 shows the ripple in the sensor output signal after filtering and conversion, the mean output voltage, the relative ripple as a ratio of the ripple to the mean voltage, and SNR estimation.

**TABLE 6.2 SENSOR OUTPUT RIPPLE AT THE 95% CONFIDENCE INTERVAL FOR EACH COMPONENT OF THE OUTPUT VECTOR\***

	Ripple ( $\mu$ V)	Mean (V)	Rel. Ripple (ppm)	SNR (dB)
$x_1$	40	0.08	500	50
$x_2$	4	0.09	37	74
$x_3$	4	0.10	35	75
$x_4$	4	0.11	33	76
$x_5$	5	0.30	17	82
$x_6$	5	0.37	14	83
$x_7$	6	0.40	14	82
$x_8$	6	0.42	15	83
$x_9$	8	0.65	12	83
$x_{10}$	10	0.79	12	83
$x_{11}$	10	0.845	12	83
$x_{12}$	12	0.89	14	82
$x_{13}$	12	1.08	11	83
$x_{14}$	14	1.30	10	83
$x_{15}$	15	1.38	11	83
$x_{16}$	17	1.44	12	83

\* expressed as absolute ripple (in  $\mu$ V), as ripple relative to the mean sensor output (in ppm) and as a signal to noise ratio (in dBs) considering as signal the maximum variation of each sensor output component  $x_s$  when exposing the sensor to the different calibration gas mixtures.

SNR has been calculated by considering the signal of interest to be the peak to peak amplitude change in the sensor output as a result of the different calibration gas mixtures considered. This amplitude is many times lower (factors ranging from 50-200) than the amplitude of the sensor output change induced by the heater excitation, (used for the relative ripple calculation as explained next). In the case of ripple and relative ripple in the sensor output, calculations were performed for a static measurement where surrounding gas is kept unchanged. Relative ripple is calculated as a ratio between the heater induced DC sensor voltage level and the sensor output voltage ripple. Ripple and noise levels are remarkably low. Apparently when the heater voltage is lowest for the first component of the sensor output  $x_1$  noise is more prominent, possibly due to digital crosstalk in the signal path from the integrated switch (ISL54056) which is filtered in the other steps due to the presence of higher impedances along the signal path. This effect boosts the ripple significantly. However, the ripple still lays 50dBs below the maximum signal. The figures show that the pursued initial minimal noise rejection by design has been amply fulfilled, and in all cases exceeded but for step number 1 (See Table 6.1). These figures represent almost a factor four improvement with respect to the laboratory excitation and acquisition setup reported in sections 5.2.2 and 5.3.2 (see table 5.3).

### 6.2.3 COMBINED IMPLEMENTATION OF IEEE-1451.2 AND BS-7986 STANDARDS

---

A combination of IEEE-1451 and BS-7986 two standards was already proposed by Karatzas et al. in 2006 [Karatzas2007], as a means of rationalizing and optimizing the design of smart sensors. Figure 1 from [Karatzas2007] summarizes the authors' proposal of a smart sensor combining IEEE-1451 and BS-7986. The herein presented implementation is conceptually consistent with this previous one, with some particularities:

- All sensor inputs lie at the same level (there is no distinction between primary mesurand and environmental mesurand, because the Sensirion temperature sensor measurements are processed indistinctly from the thermoelectric sensor readings)
- VV, VVstatus, VU and VUstatus is transmitted for every sensor measurement (in fact for every point of the sensor output vector).
- The different systems blocks are formally included in a IEEE-1451.2 fully compliant system structure. This includes the BS-7986 quality metrics, which are added complementing IEEE-1451.2 and bypassing the simpler quality self-assessment features of IEEE-1451.2.

These particularities arise in one hand from the specific needs of chemical multisensor instruments, and on the other hand from a system design strategy aimed to maximize compliance with IEE-1451, and specifically IEEE-1451.2. The system mainframe is provided by the IEEE-1451.2 which is only slightly *tweaked* to fit BS-7986 in it.

Figure 6.3 shows a block diagram of the firmware (what is referred in [Karatzas2007] as software) structure of the instrument, and has been conveniently set up to allow comparison of the presented with the previous proposal by Karatzas et al.

Sensors 3 and 4 (Transducer channels 5 to 8) are not shown explicitly. These correspond to combined modes of reading sensors 1 and 2. These optional modes are left out of discussion in this work as they do not provide additional relevant insight in the proposal.

Several analogous blocks can be spotted when comparing Figure 1 in [Karatzas2007] and Fig. 6.3, the left side of the diagram is structured to emphasise the parallelism among both systems, a block description and comparison follows.

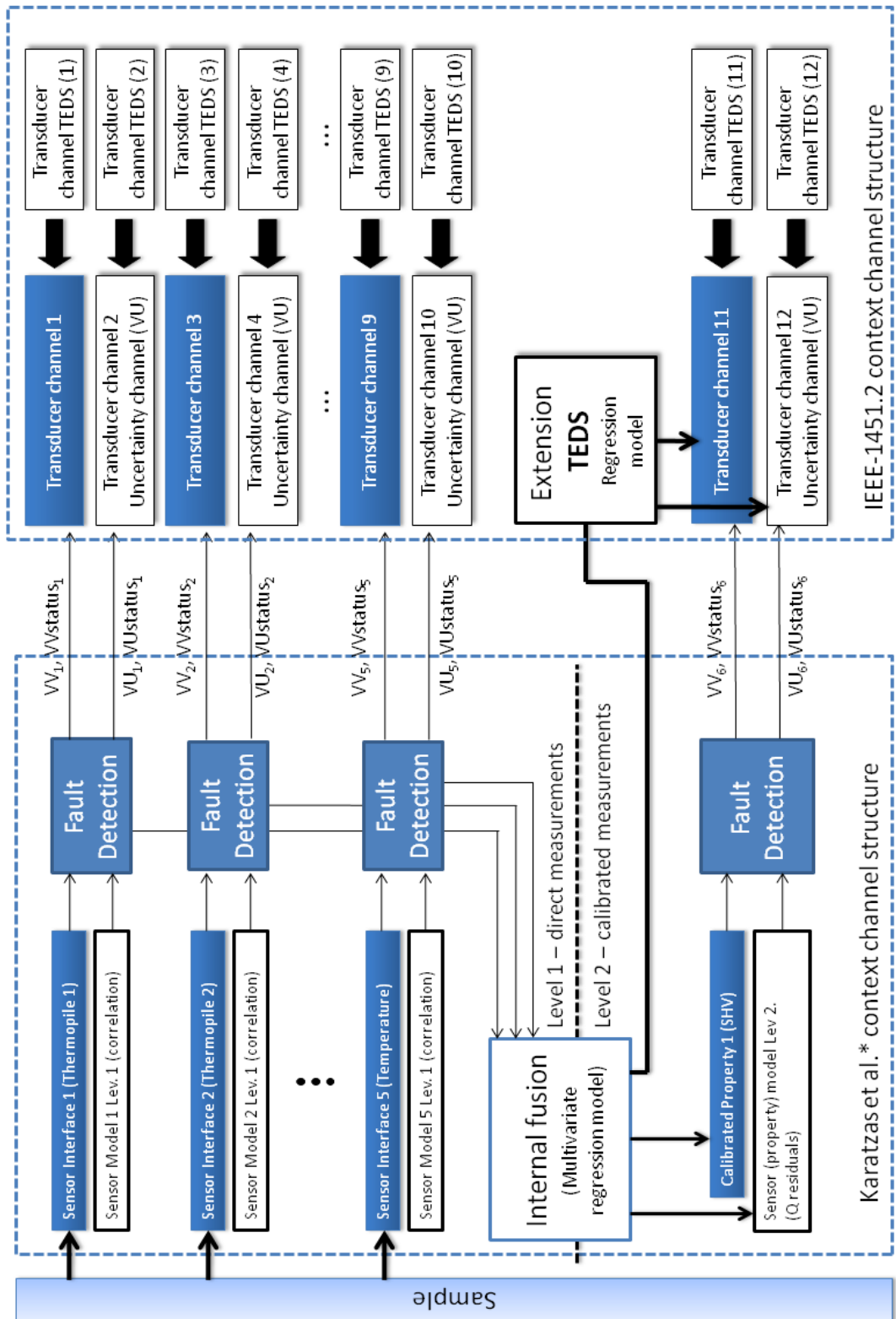


Figure 6.3. IEEE-1451.2 and BS-7986 context diagram, comparison with [Karatzas2007] is provided

**Sensor interface** block: every sensor presents a firmware interface which is in charge of communicating with the sensing element hardware, obtaining measurements on demand and performing basic signal processing (and eventually unit conversion) as appropriate.

Previous paragraphs on sensor excitation (6.2.1) and sensor reading (6.2.2) have already given detailed insight in the sensor interface for the thermopile sensors, other examples can be found in the selected smart sensor examples [Bissi2007] see 1.5.1 and [Pardo2006] 1.5.2. The sensor interface model defined in [Karatzas2007] includes also the storage and delivery of sensor element identification information, these functionalities are entirely defined by the IEEE-1451.2 functions and TEDS, so they were placed conceptually in another block inside the IEEE-1451.2 structure block.

**Sensor model** block: in [Karatzas2007] the *Sensor Model Provider* (SMP) block is in charge of providing a theoretical sensor model for a specific sensor or range of similar sensors. In effect it stores a given model data and communicates it to requesting instances. The Sensor model here presents a similar approach, the block is in charge of storing and providing a computed statistical model based on a buffer of historical data to the fault detection block. This is the first of two levels of fault detection mechanisms present in the system:

- A univariate model computed in “real-time” with statistics from a short historical measurement buffer (in this case 10 samples), which constitutes the correlation model in level one, taking advantage in this case of *time domain constraints* following the terminology in section 1.4.3 .
- A multivariate model computed with a large set of historical data (the training set) based in the Q residual statistics of the PLS model, which constitutes the multivariate model in level 2, note that once the model is computed offline, the model prediction and its residuals are computed in real time, the presence of unusually high values for this statistic is an indication of a faulty sensor reading [Wise1996, Padilla2007, Yoon2001], this mechanism is based on *analytical redundancy* according to terminology in 1.4.3.

A discussion of these models and how they are used to detect sensor faults is described under the *Fault detection* section (6.3.3).

**Fault detection** block: The Fault detection block performs the detection of faulty data in the basis of the model provided by the sensor model, quality metrics codes are assigned according to BS-7986. The fault detection block also would also perform sensor readings correction as proposed in [Karatzas2007], indicating the correction using BS-7986 codes. Moreover, this block is also in charge of estimating the uncertainty values considering the information made available to it by the sensor readings, sensor TEDS and the statistical sensor model. Compliant to the BS-7986 standard, the uncertainty value denotes the error band of the associated data value at a 95% level of

confidence and is represented in the same units and with the same precision as the data value. Insight on the specific algorithms for fault detection and sensor correction is provided in section 6.3.3.

**Internal fusion** block: Keeping the terminology in [Karatzas2007], the block in charge of combining several sensors into one output has been termed the internal fusion block. In this case it is specifically a multivariate regression model calculated using a PLS algorithm (see sections 6.3.2 and previous description in 5.2.3 for details). The multivariate regression projects a vector of input measurements obtained from the thermoelectric and temperature sensors in presence of a sample, into a scalar value of a predicted property (or quality) of interest, which in this case is superior heating value in MJ/m<sup>3</sup>. Similar regression models can be analogously obtained for several other properties of interest such as Wobbe Index, density, or individual component concentration (see chapter 5, sections 5.2.3 and 5.3.1). Despite the thermoelectric sensor is physically a single sensor and considered as such in the block diagram, it provides a vector output and from a computational point of view it is treated as an array of sensors. For this reason internal fusion not only combines the output of two physically different sensors (thermoelectric and temperature) but also combines the different readings of the thermoelectric sensor (which build up the output vector).

The internal Fusion block makes use of regression model data (coefficients) stored in extension TEDS as a channel calibration. Unfortunately, the current version of IEEE-1451.2 only allows the calibration of a channel with extension TEDS placed outside the STIM (see Table 31 in the IEEE-1451.2 standard [IEEE1997]). This means that the NCAP requesting data must have previously read and stored the custom calibration TEDS, and shall apply it to the sensor channel readings at the moment of the readout. This rather strange impossibility to perform channel correction with custom TEDS inside the STIM, has been corrected in newer revisions of the IEEE-1451 standard, and in particular IEEE-1451.0 (see table 49 in the IEEE-1451.0 standard [IEEE2007]).

The **right side** of the diagram in Fig. 6.3 shows the system structure regarding the IEEE-1451.2 context, once data is pre-processed, quality indicators added and uncertainty calculated, the values enter the IEEE-1451.2 context using standard transducer channels, these channels are complemented with identification information in the transducer channel TEDS. A more detailed description of the blocks is provided below:

**Transducer channels:** The IEEE-1451.2 building blocks are the transducer channels, these are instances normally associated to sensor or actuators which interact with external phenomena. However a transducer channel may also contain data regarding to internal processes or simply indirectly related to external measurements. This is the case the for Transducer channels 2, 4, 6, 8, 10, 11 and 12. Transducer channel 11 is a combination of measurements from other channels (in the current setup transducer channels 1 and 9) to obtain a calibrated property, the other channels (2, 4, 6, 8, 10 and 12) are VU channels which provide a way of accessing the uncertainty estimation

calculated in the fault detection block. These channels are not physical sensors, but *virtual sensors* according to the IEEE-1451.2 terminology. The VU channels are updated after each trigger of the corresponding sensor channel; in this way VV and VU are updated simultaneously, when a trigger for the VV channel is executed. Channel readings are provided to the TII interface upon issue of a transducer channel data read command by the NCAP. Channel readings are updated upon issue of a channel trigger command by the NCAP.

**Transducer channel TEDS:** A transducer channel is formally defined by a number of parameters and specifications, which are defined according to the IEEE-1451.2 standard in the channel TEDS (see table 30 in ref [IEEE1997]). In addition to the technical parameters in the channel TEDS, identification information is allocated in the Channel Identification TEDS. There is also specific calibration information allocated in the Calibration TEDS., and associated to it the Calibration identification TEDS provide descriptive information. In the presented implementation the general format of the calibration TEDS is not convenient, so the PLS regression info has been placed in an extension TEDS. **Extension TEDS** can allocate additional parameters or calibration information associated with the channels, as required by the STIM manufacturer. In Fig. 6.3 the Transducer channel TEDS block conceptually represents all these TEDS associated to a channel, not only the Channel TEDS.

**System Meta TEDS** block: Global information common to all sensor channels is stored in the Meta TEDS, which contain parameter values and options. These are also complemented with a Meta-identification TEDS for system-level identification information.

#### 6.2.4 COMMUNICATIONS

---

The STIM module communicates to a master device termed the NCAP (as defined in IEEE-1451.2 [IEEE1997]). Figure 1.4 already showed the placement of the NCAP device in the IEEE-1451.2 context. The NCAP issues request commands using the Transducer Independent Interface, which is a specific interface defined in IEEE-1451.2. Function codes and frame formats are defined in detailed in the standard [IEEE1997]. The presented work makes use of a desktop PC acting as the NCAP. The TII has been programmed in a FTDI FT2232H Hi-Speed Dual USB UART/FIFO Integrated Circuit which is controlled using a USB port of the desktop PC.

The TII interface has been implemented using the MSP microcontroller digital ports and voltage level conversion ICs (SN74LVC1T45 and SN74LVC4245A), which are needed to convert the 3.3V digital ports of the MSP to the 5V level specified for the TII. Figure 1.7 showed the TII interface signals. The specific electronic implementation in the prototype is shown in Figure 6.4.

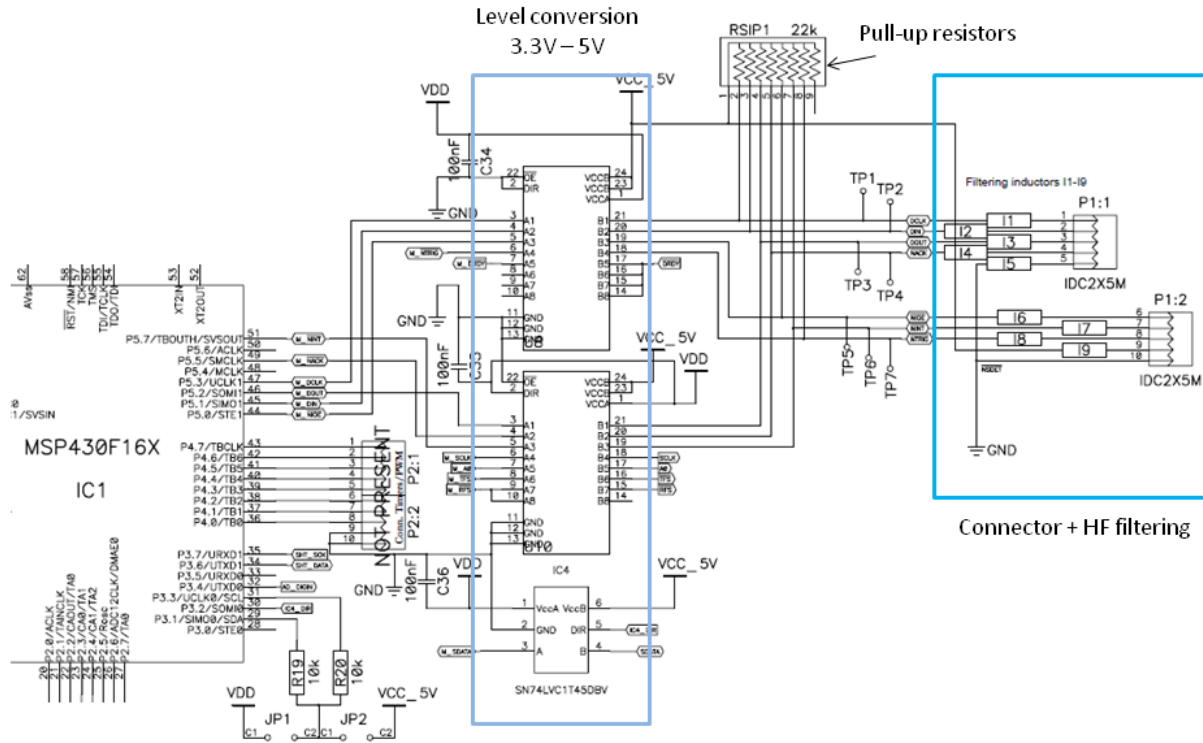


**Figure 6.4. Electronic schematic showing the TII connection to the MSP1430F1612 Microcontroller. A voltage level conversion is needed.**

### 6.2.5 PC DATA-LOGGING SOFTWARE

In order to allow the acquisition, storage, processing and presentation of the prototype measurements, a data-logging application was programmed in Delphi 2007 (CodeGear, USA) for windows. The application controls the FTDI device and data transfer with the STIM. The application is able to issue all the IEEE-1451.2 functions and to interpret the received data according to the standard definitions. The program takes advantage of the IEEE-1451.2 features and provides the following main features:

- Self-configuration for adequately reading the STIM sensor channels
- On-screen visualization of all the STIM TEDS
- On-screen summary and detection of the STIM channels
- Programmable data-logging routine enabling long-term measurement runs with configurable sampling rate.

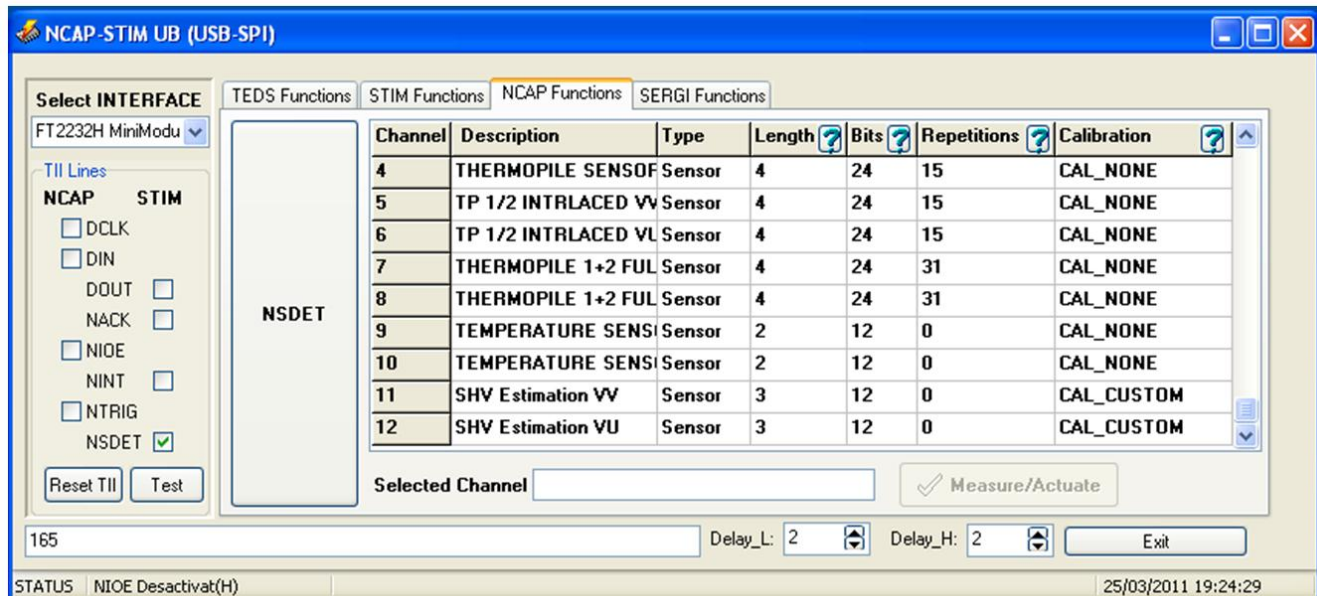


**Figure 6.5 Screenshot of the NCAP-PC software. The channel auto-detection window is shown.**

A screenshot of the NCAP program window showing the STIM transducer channels auto detection is shown in Fig. 6.5.

The program stores data from one of the thermoelectric sensors which is selected at the automatic data-logging setup window. Transducer channel 9 corresponding to temperature is also stored.

### 6.3 SIGNAL PROCESSING

The experimental and results sections make reference to two different datasets, calibration and validation data which have been used separately to calculate and validate the multivariate model of the sensor response. Results based on these two datasets correspond to a first stage of the system development which is the training or calibration phase. This phase is based on offline data processing.

After the instrument is calibrated, the instrument shall enter the operation phase. The operation phase relies on real-time data processing (see section 5.2.3). As a consequence, these two phases present differences in regards to signal processing which will be described next.

Sections 6.3.1 and 6.3.2 provide a description of the signal pre-processing and multivariate modelling performed in the training phase, while section 6.3.3 presents the fault detection which is performed in the operation phase, and section 6.3.4 summarizes the differences between signal processing in the calibration phase and signal processing in the operation phase. Offline signal analysis was performed in MATLAB (r) using the PLS toolbox by Eigenvector research inc (Wenatchee, WA, USA).

### 6.3.1 SIGNAL PRE-PROCESSING AND TEMPERATURE CORRECTION

---

Signal pre-processing includes two main items, on one hand several cascaded filters rejecting the noise, and on the other hand a linear temperature compensation which has been implemented. Filters consist of:

Filters affecting the original signal previous to digital conversion:

- The sensor thermal mass itself acts as a first order low pass filter with cut frequency of 8 Hz
- The analog butterworth filter of 37Hz cut frequency (see 4.2)

After digital conversion the signal is filtered again with digital filters:

- A rolling average filter is applied by the AD7711 ADC with cut frequency of 13.1Hz (notch at 50Hz). This is performed internally by the ADC.
- Four readings of the AD7711 are averaged in the microcontroller (firmware programmed) to obtain the stationary output value which is passed through as the channel reading.
- Logged data is median filtered (using a window of three measurements) before the offline data processing which consists in calculating the PLS model of the sensor response to the properties of interest.

The combined frequency response of the filters results in a -3dB cutoff frequency of 5Hz and an attenuation at 50Hz of 120 dB.

On the other hand, influence of temperature was pointed out as the most important uncertainty source in chapter 5, section 5.3.2. The presence of a temperature sensor in the prototype is used to perform a linear temperature compensation in order to reject first order effects of temperature in the sensor output, the applied correction is shown in equation 6.1.

$$\chi_{(i,s)} = x_{(i,s)} + \gamma_s (T_i - T_0) \quad (6.1)$$

Where  $\chi_{(i,s)}$  is the temperature corrected sensor response for experiment  $i$  and sensor output component  $s$  in V;  $x_{(i,s)}$  is the raw sensor measurement for experiment  $i$  and sensor output component  $s$  in V;  $\gamma_s$  is the calculated coefficient for the temperature correction of readings corresponding to heater step  $s$  (calculated with a least-squares linear regression) in V/ $^{\circ}$ C;  $T_i$  is the measured temperature in experiment  $i$  in  $^{\circ}$ C and  $T_0$  is the average reference laboratory temperature of 25 $^{\circ}$ C.

Coefficients ( $\gamma_s$ ) were calculated from one of the calibration experiments (experiment 7), this experiment was selected because of its large temperature oscillations along its duration. The same correction coefficients calculated from experiment 7 were applied to all calibration and validation data. Figure 6.6 shows the evolution of the sensor signal, temperature, and corrected sensor signal for the highest excitation voltage step, for a period of roughly 70 hours (25k samples at 10s sampling period). The composition inside the sensor chamber changed slowly during the experiment due to small leakage, thus the sensor response was expected to slowly increase.

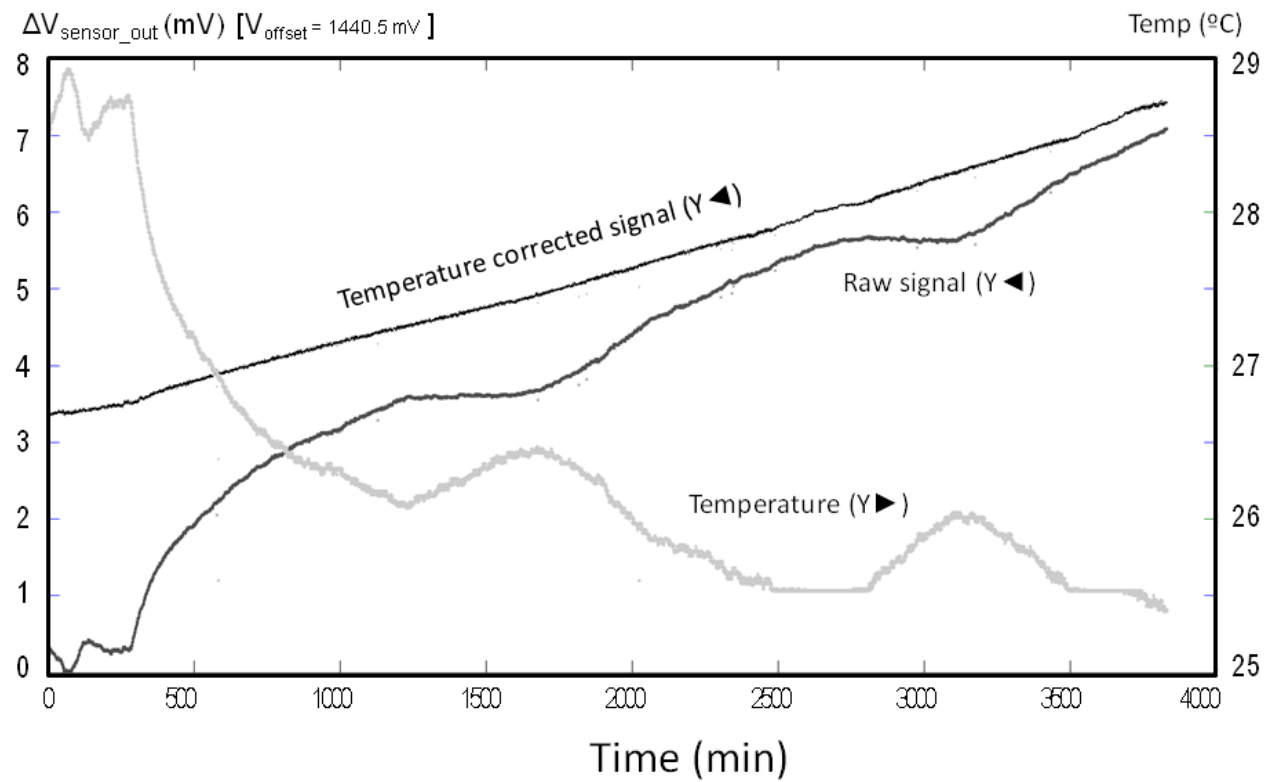


**Figure 6.6** Experiment 7 signal plots corresponding to: the raw sensor signal for the highest heater excitation voltage (Raw signal, in black); the temperature sensor signal (Temperature, in light grey); and the temperature corrected and median filtered sensor signal (Temperature corrected signal, in dark grey).

Figure 6.6 shows a clear correlation between the sensor response and chamber temperature measured by the SHT75 temperature sensor. A similar graph can be drawn for each of the other 15 voltage steps. Figure 6.6 shows also a steadily increasing drift which is due to the mentioned slow change in the gas composition inside the measurement chamber. The linear temperature correction is performing very well in rejecting temperature effects at the sensor output.

Also, spurious communications and acquisition errors which can be spotted along the curves for the temperature and raw sensor signals in light grey and black are effectively rejected by the median filter, as showed by the corrected sensor signal in dark grey. A short initial transient can be seen at the very left end of the graph which corresponds to a system warm-up time of around 30 minutes. The data points corresponding to this transient were removed from the analysis datasets.

### 6.3.2 PLS REGRESSION

PLS regression was briefly presented in chapter 5, section 5.2.3. It is an extensively used multivariate regression technique, which has found wide application in the analytical chemistry field. Excellent PLS theory papers and tutorials are available by Geladi and Kowalski, and Svante Wold et al.[Geladi1986, Wold2001]. The approach in the presented prototype implementation is almost identical to the description in 5.2.3, with the difference that the temperature sensor readings were added to the experimental  $\mathbf{x}$  vector.

PLS provides excellent noise rejection for the highly correlated sensor measurements. In the presented work the same PLS approach is taken, though there has been an effort to try to minimize the error sources already pointed out in chapter 5 (5.3.2), as it? has been described in section 6.2. The PLS regression model was computed to predict the superior heating value (SHV) of natural gas. Special care was taken in the validation and performance analysis, which are described in section 6.4.3 and 6.5.

For the PLS analysis, the corrected datasets were mean-centered. The temperature sensor was also included in the PLS analysis, but the signal was amplified by a factor 1000 to match the range of the sensor response to that the average output of the thermoelectric sensor. This signal boost enabled a better interpretation of the loadings of the PLS model.

### 6.3.3 FAULT DETECTION

---

Fault detection is a task which is performed online during the operation phase, as opposed to the offline measurement filtering in the calibration stage, involving mainly offline signal processing and identification of the best measurement sets for use in the calibration (refer to 6.3.1 and 6.3.4).

Fault detection in the instrument is performed at two levels. Section 6.2.3 briefly presented the implemented ones. From a design point of view the STIM can take advantage of the three possible fault detection approaches (as classified in section 1.4.3), there is a second identical thermoelectric sensor to take advantage of *hardware redundancy* detection, the highly correlated sensor output vector can allow *analytical redundancy* fault detection, and the knowledge of signal *time and frequency domain constraints* can also be used for fault detection. Of these approaches, two were implemented in this version of the prototype, a univariate fault detection approach based on the “historical” trend of the signal for each of the sensors which serves as a basic detection based on *time domain constraints*. The second level fault detection is a multivariate approach based in PLS model diagnostics which exploits the *analytical redundancy* of the sensor readings.

---

#### 6.3.3.1 UNIVARIATE FAULT DETECTION

---

Each of the components of the sensor output vector can be considered separately as a single virtual sensor. A range of ‘normal variations’ of the signal may be defined by examination of the calibration measurements and additional knowledge of the system operating conditions. Additionally, virtual sensor signals are usually low-pass and consequently highly correlated with previous sampling times. A sliding window approach can be used to compute the correlation for every virtual sensor. Any indication of correlation degradation is a clear indication of the presence of sensor faults.

One simple (and algorithmically lightweight) way to estimate the “normality” of a signal variation is to use correlation of the incoming sensor measurement with a window of previous measurements. In this case ten measurements were used and a ‘normality’ window was set consisting on a high and a low threshold, which allows a measurement to be labelled as suspiciously abnormal if its correlation value falls outside it. Figure 6.7 shows an example of error detection using univariate correlation. Despite in this case the detection has been applied to spurious errors, the approach is also valid for other more critical faults. In particular the approach can easily detect an insensitive sensor (value stuck, correlation increases above the maximum threshold) or an excessively noisy sensor (correlation decreases below threshold). In any case, this level one univariate fault detection is backed up by a level two multivariate fault detection.

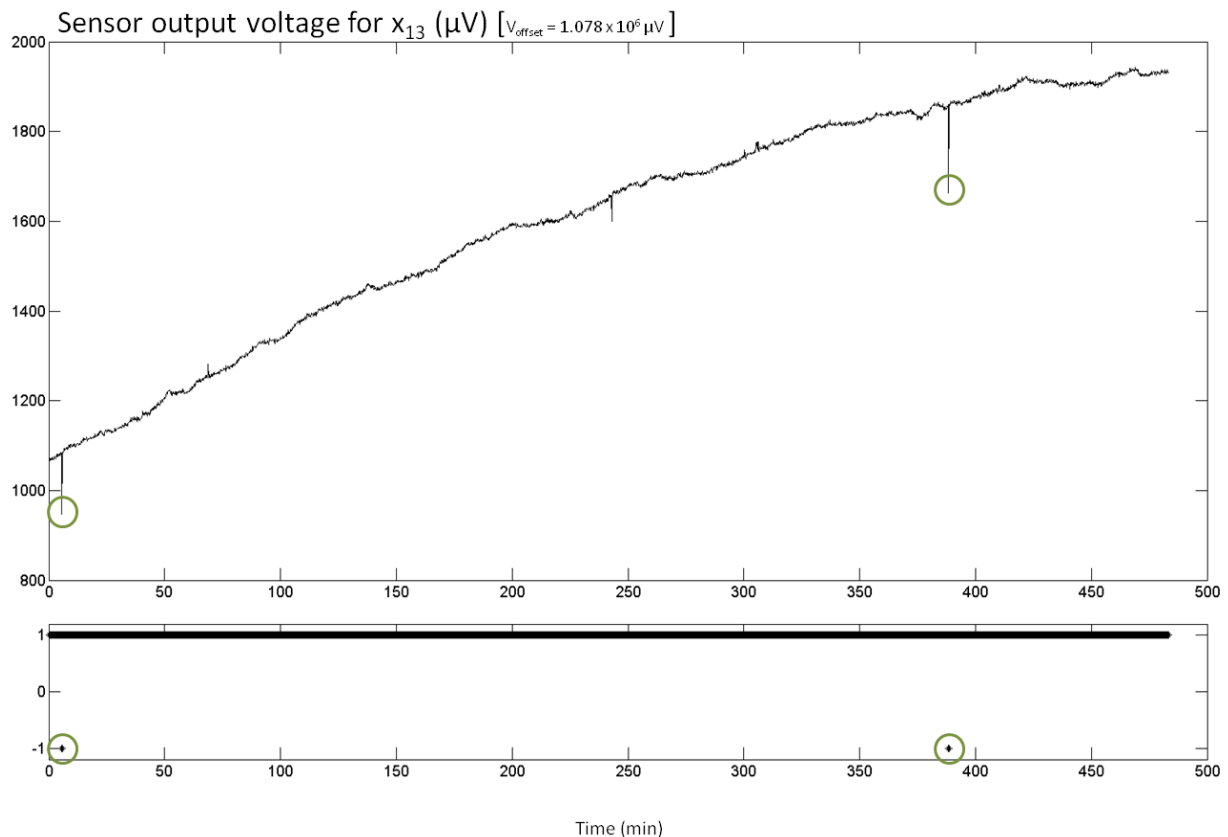


**Figure 6.7** Univariate fault detection based in the correlation of the sensor output (component  $x_{13}$ ). Lower plot indicates suspicious data as -1 and correct data as 1. Note that the correlation threshold is set to a low sensitivity setting so only large faults are detected (indicated with grey circles).

The suspicious measurement is marked by using the BS-7986 codes (see tables 2-5 of the BS-7986 standard document) [BSI2005], the VVstatus byte is assigned an UNCERTAIN quality value for the first time, if the sensor becomes stuck into a single value, it is assigned a BAD VVstatus value is assigned after a pre-set number of UNCERTAIN values. Sensitivity of the status assignments can be adjusted, in the case shown in figure 8, only measurements which are clearly outside normality are marked, other suspicious points can be observed in the curve, but they lie below the correlation upper threshold that has been set. Figure 6.8 shows a block diagram of the fault detection and BS-7986 VVstatus codes assignment.

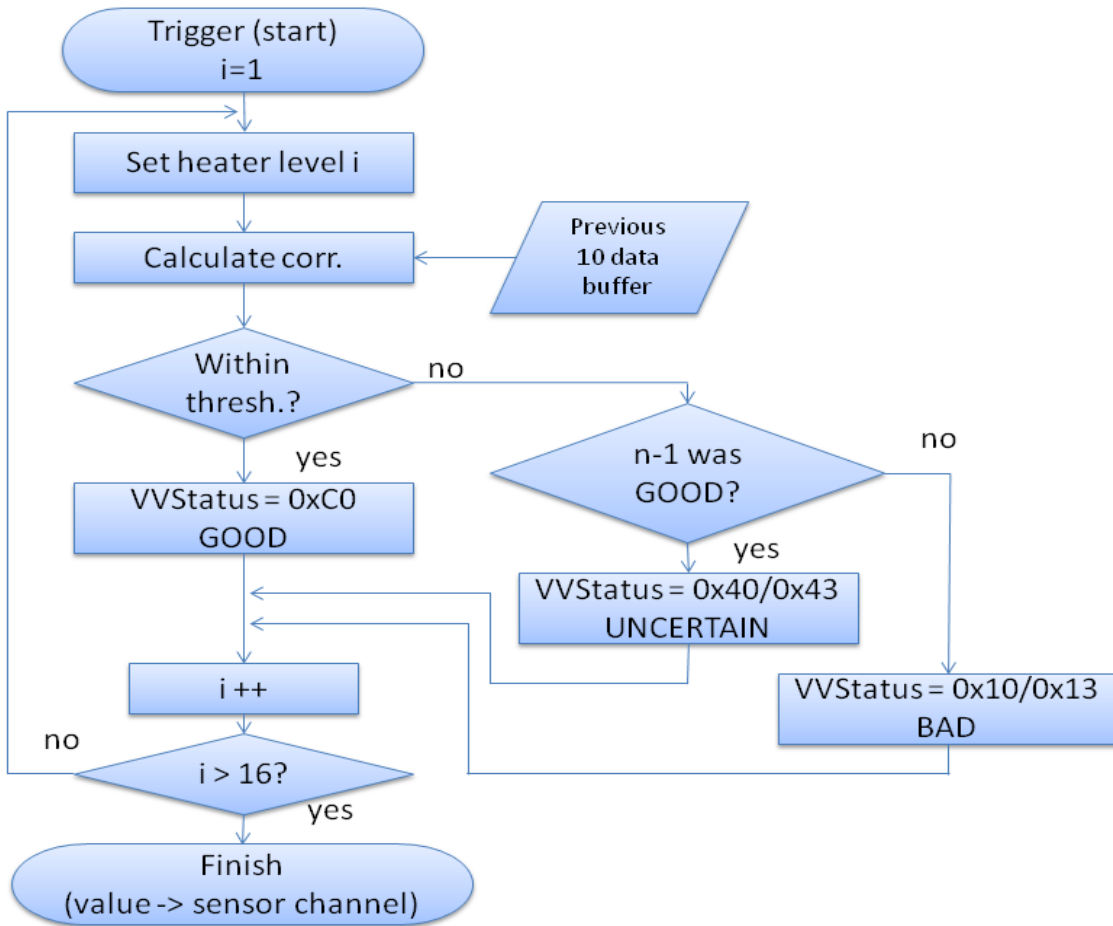


**Figure 6.8.** Flowchart of the univariate fault detection showing BS-7986 VVstatus code assignments. The process is repeated for the 16 voltage steps forming a measurement vector. The within threshold decision block covers two aspects, in first place the mentioned correlation limits and in second place a range detection of the value. Allowable ranges need to be previously estimated during calibration and stored in the TIM TEDS.

The UNCERTAIN 0x4x and BAD 0x1x include specific coding in its four LSB to indicate if the value is below limits, above limits, or constant (see table 3 in [BSI2005]). This univariate fault detection implementation is a first simple approach to illustrate the capabilities and procedure for quality self-assessment using BS-7986 and IEEE-1451.2. Different algorithmic approaches may be implemented so long as the microcontroller can assume its workload.

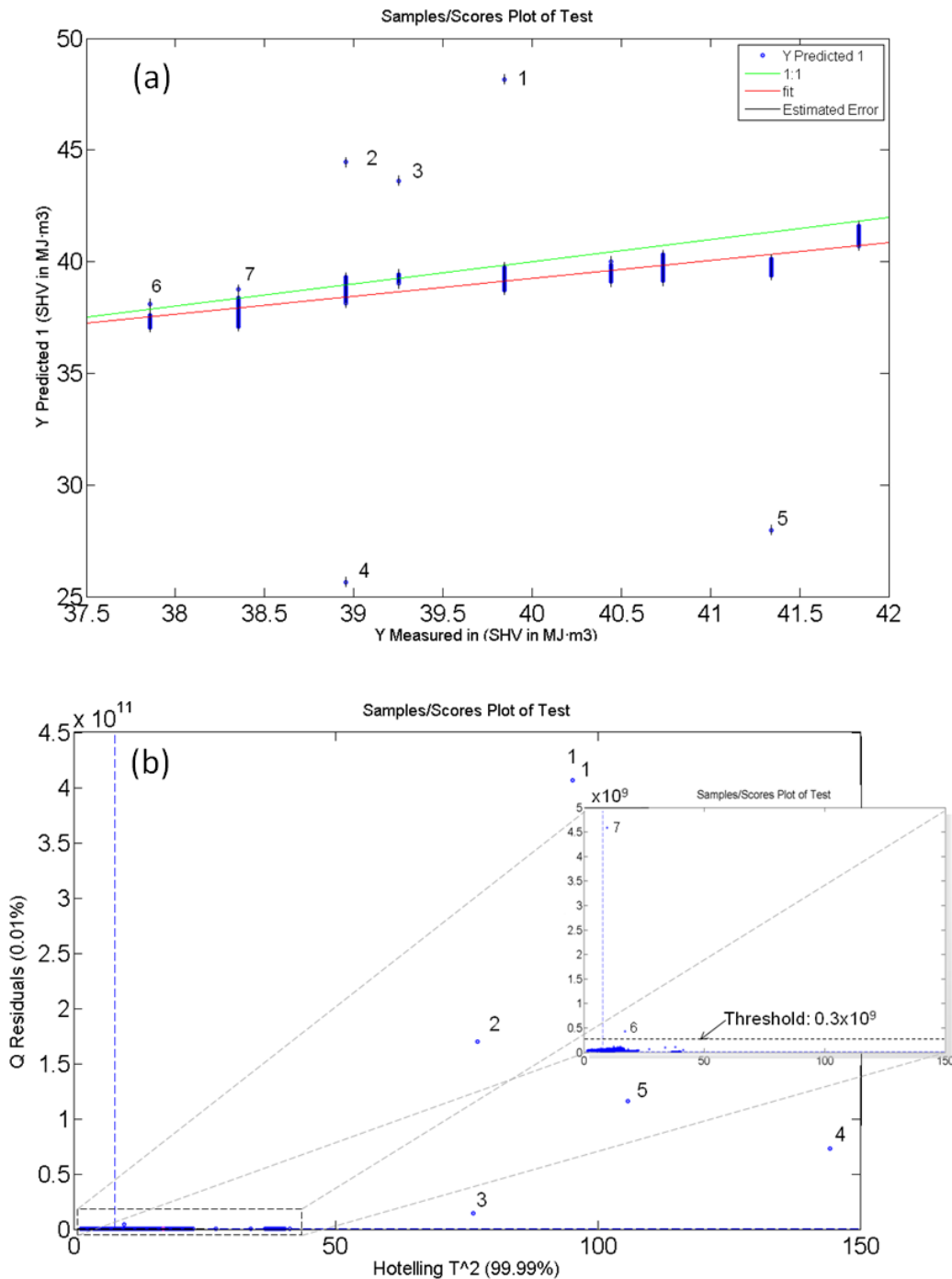


**Figure 6.9** Plot (a) shows the prediction results (in MJ/m<sup>3</sup>) for the validation data, including 7 faulty measurements indicated 1-7. Plot (b) shows the Q-residuals of the faulty data versus the T<sup>2</sup> Hotelling faults are also indicated 1-7. A zoom in is displayed to show the position of faults 6 and 7. Faulty data is clearly separable from normal data by setting a threshold for the Q-residual value.

### 6.3.3.2 MULTIVARIATE FAULT DETECTION

---

The use of PLS model diagnostics such as Q-residuals for fault detection was proposed by Wise et al. [Wise1996] and the concept has found application in many examples, for instance implementations by Padilla et al. [Padilla2007] and Yoon and MacGregor [Yoon2001]. In the present application the Q-residuals statistic provided a convenient method to detect faults in the sensor signals. Figure 6.9 shows an example of Q-residuals calculation for a single experiment, for the purpose of fault detection, raw signals with no median filtering were used.

A valid measurement threshold can easily be defined as shown the zoomed plot b) where valid measurements and faulty ones appear as clearly separable in two extremely separated groups. Thresholds in Q-residuals and T<sub>2</sub> should be high enough to avoid frequent false alarms but low enough to be sensitive. Since normal operation is the expected state, the operation mode is an extremely unbalanced condition. Setting the limits to the typical 0.05 or 0.01 risk will lead to an unacceptable number of false alarms due to the multiple testing condition. For this reason, it is usual procedure to apply a correction factor to the risk factor and decide the final limits on the basis of costs considerations taking into account the cost of false alarms and the cost of fault miss-detection.

Faulty measurements exceed the Q-residual values of calibration and validation measurements clearly (up to several orders of magnitude), making fault detection straightforward as shown in Fig. 12, in this case. Those measurements determined as bad are indicated in the prediction (a) and Q-residuals (b) plots with numerals 1-7. Note how even errors 6 and 7 with relatively low impact in the SHV prediction error, are easily detected by the Q-residuals statistic. Abnormal values are assigned an UNCERTAIN VVstatus or BAD VVstatus depending on the Q-residual value. The threshold for the Q-residuals has been set at the a middle point between the lowest Q-residual for a faulty measurement (6) and all the group of measurements considered non-faulty.

### 6.3.4 TRAINING AND OPERATION MODES

---

The two modes of the instrument can be differentiated by a number of characteristics in regards to signal processing, namely:

Training mode:

The highest quality measurements are needed to build the PLS model Offline signal processing can be performed (additional median-3 filtering)

- Faults can be discarded visually

- BS7986 quality codes are not used
- Experiments are designed, samples presented to the instrument are controlled.

Operation mode:

- Signal processing is performed in real-time
- Real-time fault detection and measurement quality assessment is performed
- BS7986 quality codes are used (by a high level user application)
- Samples presented to the instrument are unknown.

## 6.4 EXPERIMENTAL

---

### 6.4.1 SENSOR CHAMBER AND SAMPLING

---

A specifically designed sensor chamber was designed to be integrated in the prototype. The chamber was designed as a small cylindrical cavity with an open top in order to present the sample gas to the thermoelectric sensor in the PCB board. Chamber volume was kept low (less than 9 ml) to ensure quick gas exchange, but large enough to grant a distance between the sensor and the chamber walls to avoid thermal coupling, a known problem in thermoelectric micro-devices [Fonollosa2009a]. The main chamber cavity is a cylinder of 31mm of diameter and 8mm of height, a 13 mm of diameter and 20.5 mm long conduction exits the main cavity in its centre, inside a standard half inch parallel gas connection. A photograph showing the chamber mounted in the prototype (the STIM) can be seen in Fig. 6.10.

Once the chamber is closed, it clamps the PCB board between its two pieces. Screws pass the PCB through available holes. Tightness is provided by an elastomeric Viton toroidal seal. A good tightness was achieved inside the chamber, with no observable pressure loss in the range of a few hours.

Gas samples were presented to the sensor by refilling the chamber with each gravimetrically prepared calibration gas mixture. The gas was supplied through the ½" connection. After the chamber refilling operation, a precisely known gas concentration was obtained inside the sensor chamber.

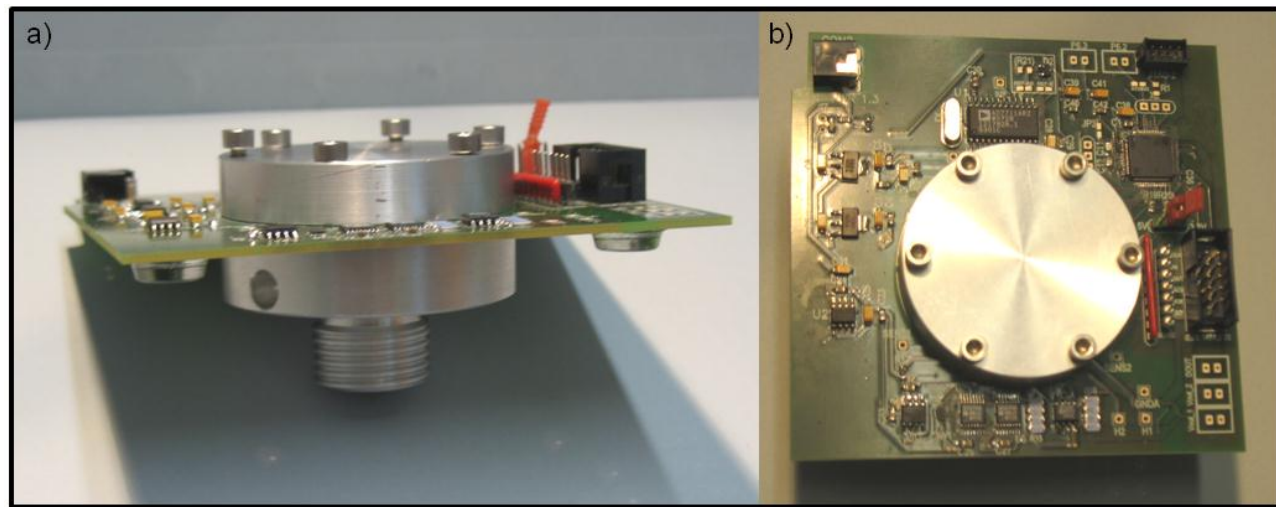


**Figure 6.10** Sideways (a) and top view (b) of the fabricated prototype. Size of the board is 95x90 (mm).

#### 6.4.2 DESIGN OF EXPERIMENTS

Each sample presented to the sensor consisted of a gravimetrically prepared mixture of gases of accurately known composition. Four of the natural gas main components: Ethane, Propane, Carbon Dioxide and Nitrogen were varied in the variation range of interest as shown in Table 6.3. The use of gravimetric mixtures (see table 6.4) allows a significant reduction of the uncertainty in the property values used for calibration, the  $y_{cal}$  vector (see 5.2.3), during the calibration of the system. The molar fraction uncertainties reported by Linde (Munich, Germany), are displayed also in Table 6.4.

TABLE 6.3 VARIATION RANGES CONSIDERED FOR THE NATURAL GAS COMPOSITION					
	C <sub>2</sub> H <sub>6</sub>	C <sub>3</sub> H <sub>8</sub>	C <sub>4</sub> H <sub>10</sub>	CO <sub>2</sub>	N <sub>2</sub>
Min	0%	0%	0%	0%	0%
Max	10%	5%	1%	3%	10% 71% 100%

Butane, as a minor constituent of natural gas, was added in a fixed amount of 0.35% (0.2% n-butane; 0.15% i-butane) to all mixtures, for added fidelity to real gas compositions. Methane is added as balance gas. A cubic experimental design for the four main components, with an added central point was used. The cubic design is expected to capture linear dependencies of the sensor response to the different components. This means that a moderate accuracy can be expected since

previous studies suggest the presence of some moderate non-linearity of the sensor response to different gas concentrations as described in chapters 4 and 5, however considering the cost of adding measurement points to the experiment, the presented design was considered to lie in a good compromise between cost and expected accuracy. The resulting nine gravimetric mixtures used in the experimental design are presented in Table 6.4.

**TABLE 6.4 EXPERIMENTAL POINTS USED FOR CALIBRATION AND VALIDATION. METHANE ADDED AS A BALANCE GAS**

Bottle number	C <sub>3</sub> H <sub>8</sub> %	C <sub>2</sub> H <sub>6</sub> %	N <sub>2</sub> %	CO <sub>2</sub> %	I- C <sub>4</sub> H <sub>10</sub> %	N- C <sub>4</sub> H <sub>10</sub> %	CH <sub>4</sub> %
1	3.18±0.03	5.06±0.05	5.11±0.05	1.54±0.02	0.148±0.003	0.198±0.004	85.15
2	0	5.02±0.05	5.02±0.05	1.54±0.02	0.148±0.003	0.198±0.004	88.15
3	1.50±0.02	10.1±0.1	4.93±0.05	1.59±0.02	0.149±0.003	0.197±0.004	81.65
4	1.49±0.02	0	5.00±0.05	1.56±0.02	0.149±0.003	0.197±0.004	91.65
5	1.48±0.02	5.05±0.05	10.0±0.1	1.64±0.02	0.148±0.003	0.198±0.004	81.65
6	1.57±0.02	5.04±0.05	0	1.57±0.02	0.147±0.003	0.198±0.004	91.65
7	1.56±0.02	5.00±0.05	5.06±0.05	3.03±0.03	0.147±0.003	0.197±0.004	85.15
8	1.54±0.02	5.08±0.05	4.93±0.05	0	0.150±0.003	0.201±0.004	88.15
9	1.48±0.02	4.98±0.05	4.82±0.05	1.50±0.02	0.148±0.003	0.198±0.004	86.65

#### 6.4.3 VALIDATION AND MEASUREMENTS

Two independent series of measurements were made for calibration and validation. The measurements were taken in a randomized order in both series. The first measurement set was used for calibration of the regression model. The second set was used only as a test set for validation. Each measurement consisted of several hours of continuous sampling of the sensor response in presence of a sample gas as described in 6.4.1. A summary of the measurement dates and duration is shown in table 6.5. Note that validation measurements were performed 2-3 months after the calibration ones. This time span was considered to allow the evaluation of the system stability, and compliance with the pursued requirements (see table 6.1).

Temperature correction factors (see 5.1) were calculated from measurement X and were applied to all other measurements, including the validation set.

**TABLE 6.5 SUMMARY OF THE PERFORMED MEASUREMENT RUNS**

<b>Bottle number</b>	<b>Date</b>	<b>Bottle number</b>	<b>Date</b>
<i>Calibration</i>		<i>Validation</i>	
<b>4</b>	6/30/2010	<b>5</b>	9/8/2010
<b>2</b>	7/1/2010	<b>6</b>	9/13/2010
<b>9</b>	7/2/2010	<b>1</b>	9/14/2010
<b>3</b>	7/5/2010	<b>9</b>	9/16/2010
<b>1</b>	7/6/2010	<b>2</b>	9/17/2010
<b>6</b>	7/8/2010	<b>4</b>	9/21/2010
<b>8</b>	7/9/2010	<b>7</b>	10/19/2010
<b>5</b>	7/13/2010	<b>3</b>	10/19/2010
<b>7</b>	7/16/2010	<b>8</b>	10/20/2010

## 6.5 TEST RESULTS

---

After software and communications debugging, the PC was correctly set up as an NCAP and it communicated correctly with the prototype STIM, measurements were acquired according to the procedure described in previous sections, the sensor readings incorporated the corresponding BS-7986 quality code, with detection and report of sensor failures (which were simulated by turning the heater voltage off).

Once the calibration and validation datasets were acquired, the PLS regression was computed. The optimal number of latent variables (LVs) for the PLS model was determined from the calibration set, with internal cross-validation. The selected number was five, which also provided the best prediction results for the validation set. This is not a surprising result since it was already known that for sensor responses not including variations of propane and without temperature in the data analysis the optimal number was three LVs (see chapter 5, section 5.3.1), addition of these two new parameters has apparently influenced the number of optimal LVs by increasing it in two. The explained Y variance as a function of the number of latent variables is shown in Fig. 6.9 a).

Only considering calibration data it would seem that modelling with over three LVs would imply an over fitting of the calibration data since 99.99 and 97.20 of the total variance of the X and Y blocks respectively are captured by three LVs. However, this is not so since the small variance captured by higher LVs allows to fine tune the predictions as confirmed by the predictions with validation data. Figure 6.9 b) shows the loadings plots for the five LVs of the PLS model, it must be noted that despite the temperature has been partially compensated in the pre-processing stage there is still a great influence of it in the regression model as shown by the loading of variable 17 (temperature sensor). Loadings in LV two (b) show a main influence of the sensor responses corresponding to the

higher heater voltages ( $k$  at high temperatures), all sensor responses (except temperature) contribute with the same sign, this might be interpreted as a overall offset in the  $k(T)$  curve. Loadings in LV three (c) show a main influence of the middle steps, with opposite sign influence of the higher ones, it can be seen as a variable estimating of the curvature of  $k(T)$  at high temperatures. Loadings in LV4 and LV5 (d,e) seem to try to capture specific shapes in the  $k(T)$  curve, with an apparently special importance of the contribution of sensor responses number 13 and 14. It might be possible that the shape of the  $k(T)$  curve around the temperatures of the heater in steps 13 and 14 is in some way characteristic of the different gas mixtures. A larger calibration dataset or additional heater steps and sensor readings between steps 13 and 14 might be a way to confirm this *a priori* interesting effect. According to simulation results obtained in previous research (see chapters 4 and 5), steps 13 and 14 should correspond to average heater temperatures of around 260°C and 300°C.

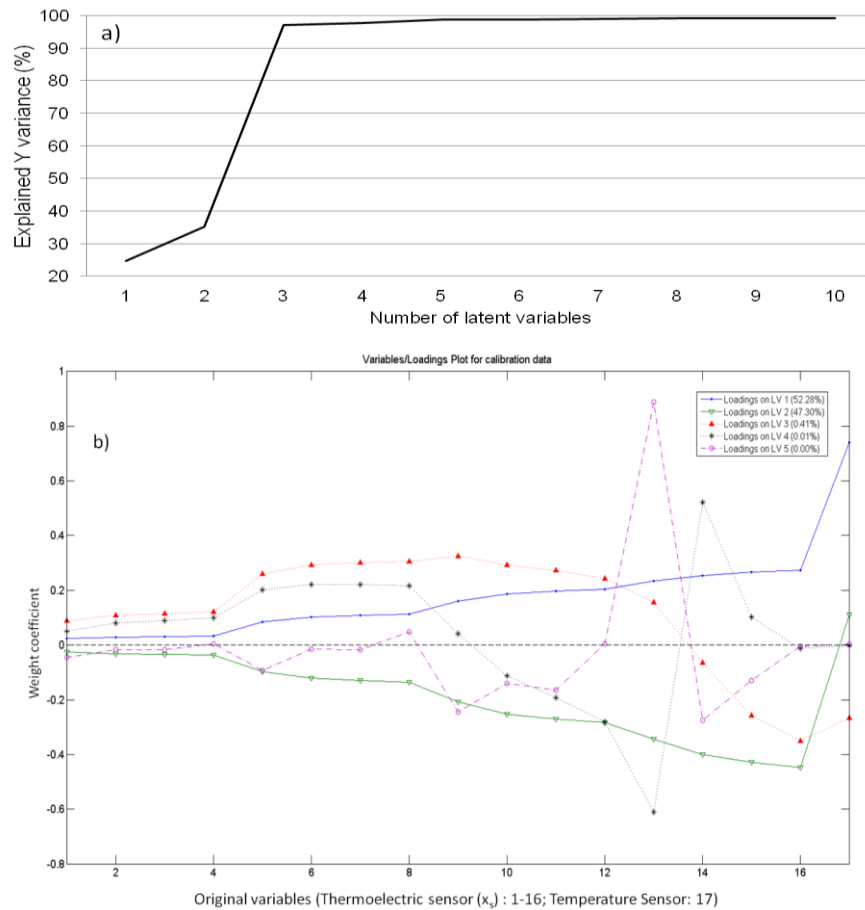


**Figure 6.9 Overview of the PLS model latent variables. Graph a) shows the explained variance as a function of the number of latent variables. Graph b) shows the loadings plot for LVs 1 to 5.**

**Variables in 1 to 16 in the X axis correspond to the sensor output for the 16 different heater voltages in increasing order. Variable 17 is the temperature sensor reading.**

The SHV value prediction performance plot is shown in Fig. 6.10. The unity slope line would correspond to a perfect prediction.

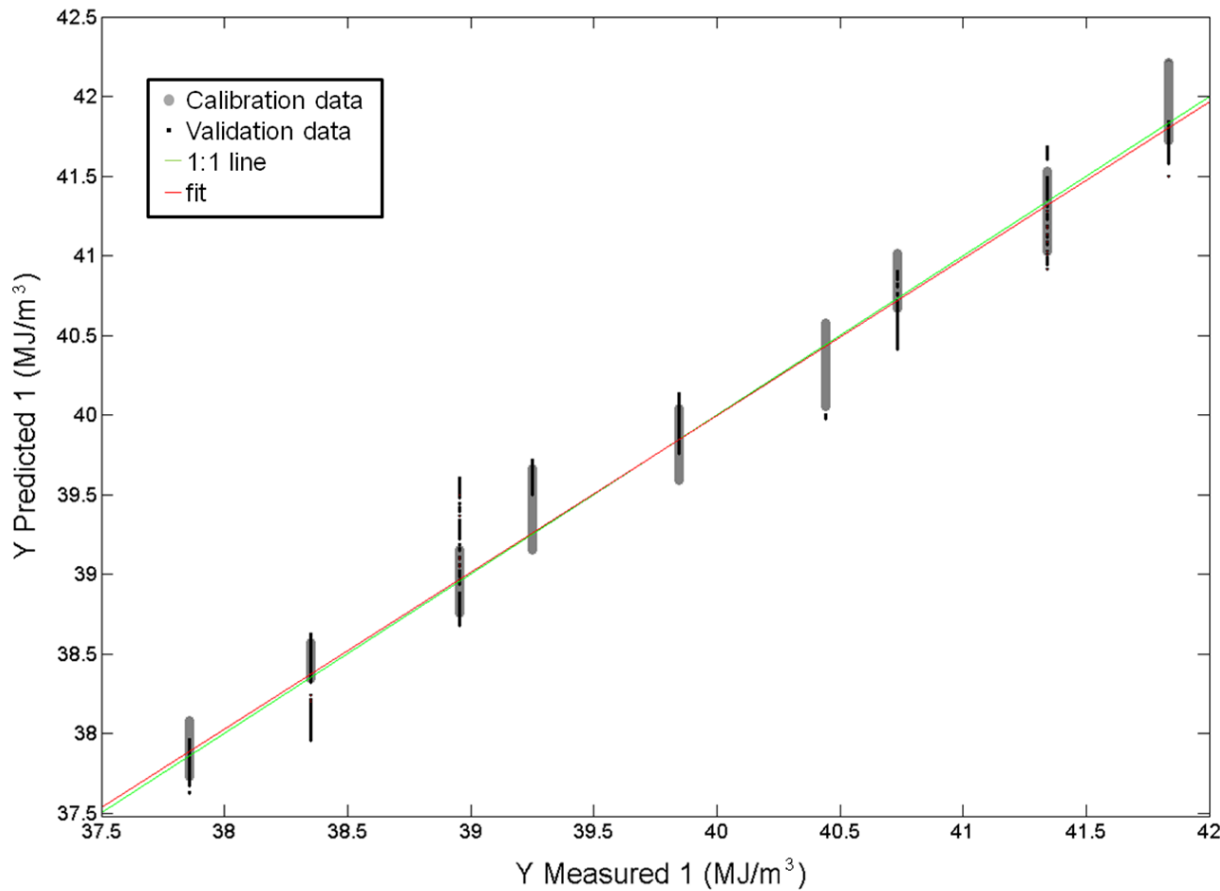


**Figure 6.10 Performance plot of the PLS model for prediction of the SHV. Validation data is predicted within 1.1% relative error.**

Validation data residuals were used to calculate the relative error of the prediction which was rated at 1.1% (95% confidence interval). This means the system is within intended initial specifications in Table 6.1, and is also in good agreement with expected accuracies reported in previous estimations reported in chapter 5, section 5.3.3. The usage of a more realistic set of calibration mixtures including propane was initially expected to impair the prediction model performance. The 30% degradation of the SHV prediction performance (suggested in section 5.3.1) seems to have been compensated to a great extent the factor four uncertainty reduction (in average) in data acquisition and heater excitation due to careful hardware design, as well as reduction of the uncertainty in  $y_{cal}$  due to the use of gravimetric mixtures. The biasing in some groups of measurements presented in Fig. 6.10 may be due to some lack of repeatability in the sampling

procedure or also non-linearity of the sensor response to gas composition changes. However, the use of validation data collected 2-3 months after calibration confirms that the sensor stability exceeds the pursued specification of a minimum of two month validity of the calibrations. Measurements suggest a high reliability and stability along larger time periods which should be confirmed with further long-term measurements.

## 6.6 CHAPTER CONCLUSIONS

A prototype of a natural gas smart instrument was described. Advanced instrument data structures were designed according to the IEEE-1451.2 standard, including TEDS information and TII communications, which enable hot-plugging and replacement, self-identification to a networks, and remote operation among other features. Additional features from the BS-7968 standard have been included to report self-assessed measurement quality codes and fault detection which shall be used by higher instances (NCAP) for system diagnostics and maintenance or service requests. It has been shown that both standards are essentially compatible and complementary in a practical implementation of a real instrument despite they were designed independently from one another. The implementation has been compared to the proposal by Karatzas et al. [Karatzas2007], which had the ambitious aim to address the totality of the intelligent sensor goals.

Advanced fault detection features were implemented using two different approaches, one based on a univariate sensor evaluation based on correlation with historical data, and a second one based on the Q-residuals of the multivariate regression model which takes advantage of the analytical redundancy of the highly correlated sensor output.

Moreover, The smart instrument confirmed the expected results for the novel microsensor approach reported in chapters 4 and 5, and even exceeded the expected performance by obtaining a remarkable 1.1% of the measurement relative error in SHV prediction with a reduced number of calibration samples (nine) in a very compact and potentially low cost prototype. A new generation of low-cost, medium accuracy natural gas analyzer instruments can be envisioned from the presented work. This kind of devices may open new perspectives in domestic and industrial energy metering of natural gas.

## 7. CONCLUSIONS

---

The presented original research work has covered two primary aspects. In first place a number of design concepts were presented in order to build an optimal smart chemical sensor. These concepts relied on proposed standards IEEE-1451.2 and BS-7986 which were introduced in chapter 1. The basic functionality and structure of both standards has been described, and an architecture for their combined implementation has been proposed in an application example as shown in chapter 6.

The smart sensor implementation in Chapter 6 illustrated extensive smart sensor features as a result of combined standards implementation. In particular the sensor implemented:

- Multi-level fault detection and data quality and operational status self-assessment. Communication of quality codes in standard format (BS-7986)
- Self-identification to a network.
- Hot-plugging provided by the TII interface (IEEE-1451.2)
- Enhanced sensor replacement provided by the TEDS (IEEE-1451.2), which contain information of the available transducers, data formats and units, as well as calibration information.
- High immunity to spurious errors due to the high redundancy in the sensor readings.

Future work could include the extensive test of fault detection algorithms and the implementation of real-time fault correction, taking advantage of the high sensor redundancy. Also, the compliance to the new IEEE-1451.2 standard should be ensured, and harmonized with the IEEE-1451.0. This would allow the self-calibration of the system without NCAP intervention. The proposed implementation of smart sensor concepts has been applied to a demanding industrial application, the natural gas analysis.

In second place, the natural gas analysis application offered the opportunity of improving some features of the state-of-the-art instrumentation by using MEMS technology. Chapter 4 showed a preliminary study of the suitability of a MTGS for natural gas analysis, with promising results. FEM simulation proved extremely useful for studying the behaviour of MTGS sensors operated in the proposed variable heating excitation mode.

The initial study hinted that the sensor would be suitable for natural gas analysis application, this expectations were later confirmed by multivariate calibration results as has been shown in chapter 5. It was demonstrated that natural gas properties can be estimated from the MTGS measurements with high accuracy, and in particular achieving an accuracy of 1% in the prediction of SHV. Other properties were also predicted with remarkable accuracy, such as 0.8% for density estimation, or 1.5% for Wobbe index estimation. Moreover, an in-depth uncertainty analysis was performed which allowed the determination of the expected performance limits of the technology.

These limits show that the technology is not suitable for the highest accuracy applications, with a prediction performance limits for SHV prediction of around 0.5%.

Chapter 6 further confirmed the expected performance results in a working smart sensor prototype. Experimental measurements in chapter 6 confirmed the outstanding stability of the sensor which resulted in the validity of a same calibration throughout several months, as measurements taken three months after initial calibration showed no significant degradation in the sensor performance.

Future work on the sensor may cover a stability study over longer periods of time, the optimisation of the heater excitation waveforms, and the design of faster devices based on the same sensing principle, by optimising and reducing the device geometry.

Overall, the proposed new instrument surpasses the specifications of available natural gas analysers in the aspects of size, power consumption, analysis speed and potentially cost.

Last but not least, the proposed MEMS approach can be applied to the real-time analysis of many other gas mixtures with a limited number of components in the per-cent range such as: biogas, human breath capnometry, protective atmospheres in food industry, air-gas proportion for burner control, analysis of exhaust gases, or even gross in-situ analysis of extra-terrestrial atmospheres.

## REFERENCES

---

---

[Abdlerahman2000] M. Abdelrahman, F.J. Kandasamy, Methodology for the fusion of redundant sensors, Proceedings of the American Control Conference, 2000, 4, 2922-2926

[Adhikari2004] B. Adhikari, M. Majumdar, Polymers in sensor applications, Progress in Polymer Science, 2004, 29, 699-766

[Aernecke2009] M.J. Aernecke, D. Walt, Optical-fiber arrays for vapor sensing, Sensors and Actuators B: Chemical, 2009, 142, 464-469, doi: 10.1016/j.snb.2009.06.054

[Alexandrov2002] Y.I. Alexandrov, Estimation of the uncertainty for an isothermal precision gas calorimeters, Thermochimica Acta, 2002, 382, 55-64, doi: 10.1016/S0040-6031(01)00736-5

[Amiroudine2001] S. Amiroudine, P. Bontoux, P. Larroude, B. Gilly, B. Zappoli, Direct numerical simulation of instabilities in a two-dimensional near-critical fluid layer heated from below, J. Fluid Mechanics, 2001, 442, 119-140

[Amrani1998] M. E. H. Amrani, R. M. Dowdeswell, P. A. Payne, K. C. Persaud, Pseudo-random binary sequence interrogation technique for gas sensors, Sensors and Actuators B: Chemical, 47(1-3) (1998) 118-124

[Arora2010] A. Arora, G. Simone, G. B. Salieb-Beugelaar, J. T. Kim, A. Manz, Latest Developments in Micro Total Analysis Systems, Analytical Chemistry, 2010, 82, 4830-4847, doi: 10.1021/ac100969k

[Artursson2000] T. Artursson, T. Eklov, I. Lundstrom, P. Martensson, M. Sjostrom, M. Holmberg, Drift correction for gas sensors using multivariate methods, Journal of chemometrics, 2000, 14, 711-723

[Arx1997] M. von Arx, O. Paul, H. Baltes, Test structures to measure the seebeck coefficient of CMOS IC polysilicon, IEEE Trans. Semicond. Manufact. 1997, 10, 201-208

[ASTM1958] ASTM Standards on Gaseous Fuels, September 1958.

[Bahadori2007] A. Bahadori, S. Mokhatab, B.F.Towler, Rapidly Estimating Natural Gas Compressibility Factor, Journal of Natural Gas Chemistry, 2007, 16, 349-353

[Bai2007] Hua Bai and Gaoquan Shi, Gas Sensors Based on Conducting Polymers, *sensors*, 2007, 7, 267-307.

[Baltes1998] H. Baltes, O. Paul, O. Brand, Micromachined thermally based CMOS microsensors, *Proc. of the IEEE*, 1998, 86, 1660-1678

[Batista2012] E.A. Batista, L. Gonda, A.C.R. Silva, S.R. Rossi, M.C. Pereira, A. A. de Carvalho, C.E. Cugnasca, HW/SW for an intelligent transducer network based on IEEE 1451 standard, *Computer Standards & Interfaces*, 2012, 34, 1-13

[Barberree2002] D. Barberree, The next generation of thermocouples for the turbine engine industry, *Proceedings of the International Instrumentation Symposium*, 2002, 48, 419-29.

[Barberree2003] D. Barberree, Dynamically self-validating contact temperature sensors, *AIP Conference Proceedings*, 2003, 684, 1097-102

[Ruzsanyi2005] V. Ruzsanyi, J. I. Baumbach, S. Sielemann, P. Litterst, M. Westhoff, L. Freitag, Detection of human metabolites using multi-capillary columns coupled to ion mobility spectrometers, *Journal of Chromatography A*, 2005, 1084, 1-2, 145-151, doi: 10.1016/j.chroma.2005.01.055

[Bissi2007] L. Bissi, , P. Placidi, A. Scorzoni, I. Elmi, S. Zampolli, Environmental monitoring system compliant with the IEEE 1451 standard and featuring a simplified transducer interface, *Sensors and Actuators A: Physical*, 2007, 137, 175-184, doi: 10.1016/j.sna.2007.02.004

[Bouchich2002] M. Bouthchich, K. Ziouche, P. Godts, D. Leclercq, Characterization of phosphorus and boron heavily doped LPCVD polysilicon films in the temperature range 293-373 K, *IEEE Electron Device Letters*, 2002, 23, 139-141

[Brown2004] A.S. Brown, M.J.T. Milton, C.J. Cowper, G.D. Squire, W. Bremser, R.W. Branch, Analysis of natural gas by gas chromatography: Reduction of correlated uncertainties by normalisation, *Journal of Chromatography A*, 2004, 1040, 215-225, doi: 10.1016/j.chroma.2004.04.007

[BSI2005] British Standard, BS-7986:2005, Data Quality Metrics For Industrial Measurement And Control Systems. Specification, BSI group, 2005.

[Calaza2003a] C. Calaza, E. Meca, S. Marco, M. Moreno, J. Samitier, L. Fonseca, I. Gracia, C. Cane, Assessment of the final metrological characteristics of a MOEMS-based NDIR spectrometer through system modeling and data processing, *IEEE Sensors Journal*, 2003, 2, 587-594

[Calaza2003b] C. Calaza, Design, modeling, fabrication and test of MOEMS for optical gas detection, PhD Thesis, Universitat de Barcelona, Dept. Electrònica, 2003.

[Calvo2011] D. Calvo, N. Tort, J.P. Salvador, M.P. Marco, F. Centi, S. Marco, Preliminary study for simultaneous detection and quantification of androgenic anabolic steroids using ELISA and pattern recognition techniques, *Analyst*, 2011, 136, 4045-4052, doi: 10.1039/c1an15114b

[Castro2002] A. de Castro, T. Riesgo, E. de la Torre, Y. Torroja, J. Uceda, Custom hardware IEEE 1451.2 implementation for smart transducers, *IEEE 2002 28th Annual Conference of the Industrial Electronics Society (IECON'02)*, 2002, 4, 2752-2757, doi: 10.1109/IECON.2002.1182830

[Chang2000] S. Chang, H. Muramatsu, C. Nakamura, J. Miyake, The principle and applications of piezoelectric crystal sensors, *Materials science and engineering*, 2000, 12, 111-123.

[Chen2000] K. Chen, Y. Wu, Thermal analysis and simulation of the microchannel flow in miniature thermal conductivity detectors, *Sensors and actuators A: physical*, 2000, 79, 211-218

[Cheng2005] H. Cheng, H. Qin, A design of IEEE 1451.2 compliant smart sensor based on the Nios soft-core processor, *IEEE International Conference on Vehicular Electronics and Safety*, 2005, 193-198, doi: 10.1109/ICVES.2005.1563640

[Chou2000] J. Chou, Hazardous gas monitors: A practical guide to selection, operation and applications, McGraw-Hill and SciTech Publishing, 2000

[Clarke1996] D.W. Clarke, P.M.A Fraher, Model-based validation of a DOx sensor, *Control Engineering Practice*, 1996, 4, 1313-1320, doi: 10.1016/0967-0661(96)00139-6

[Clifford1983] P. K. Clifford, D. T. Tuma, Characteristics of semiconductor gas sensors I. Steady state response, *Sensors and actuators*, 1983, 3, 233-254

[Comini2009] E. Comini, C. Baratto, G. Faglia, M. Ferroni, A. Vomiero, G. Sberveglieri, Quasi-one dimensional metal oxide semiconductors: Preparation, characterization and application as chemical sensors, *Progress in Materials Science*, 2009, 54, 1-67, doi: 10.1016/j.pmatsci.2008.06.003

[Conway2000] P. Conway, D. Heffernan, B. O'Mara, P. Burton, T. Miao, IEEE 1451.2: An interpretation and example implementation, *Proceedings of the 17th IEEE Instrumentation and Measurement Technology Conference*, 2000. (IMTC 2000), 2000, 2, 535-540, doi: 10.1109/IMTC.2000.848795

[Cozzani2007] E. Cozzani, C. Summonte, L. Belsito, G.C. Cardinali, A. Roncaglia, Design study of micromachined thermal emitters for NDIR gas sensing in the 9-12  $\mu\text{m}$  wavelength range, 2007 IEEE Sensors (conference proceedings), 2007, 181-184

[Cremoncini2000] A. Cremoncini, F. DiFrancesco, B. Lazzerini, F. Marcelloni, T. Martin, S.A. McCoy, L. Sensi, G. Tselenitis, Electronic noses using intelligent processing techniques, Proc. of the 7<sup>th</sup> Internation symposium on olfaction and electronic nose (ISOEN2000), 2000, UK, 69-70

[Davis1984] W. R. Davis, Hot-Wire Method for the Measurement of the Thermal Conductivity of Refractory Materials, in K. D. Maglić, A. Cezairliyan, V. Peletsky, (Eds.) Compendium of Thermophysical Property Measurement Methods, Vol. 1 Survey of Measurement Techniques, New York, London, Plenum Press, 1984, 161

[Daynes1933] H.A. Daynes, Gas Analysis by Measurement of Thermal Conductivity, Cambridge Univ. Press, Cambridge, Great Britain, 1933, 1-302

[Depari2007] A.Depari, P. Ferrari, A. Flammini, D. Marioli, A. Taroni, A VHDL Model of a IEEE1451.2 Smart Sensor: Characterization and Applications, IEEE Sensors Journal, 2007, 7, 619-626, doi: 10.1109/JSEN.2007.894900

[Diaz2002] J.A. Diaz, A.E.M. Vargas, F.C. Diaz, J.P. Squire, V. Jacobson, G. McCaskill, H. Rohrs, R. Chhatwal, Test of a miniature double-focusing mass spectrometer for real-time plasma monitoring, TrAC, Trends Anal. Chem., 2002, 21, 515-525, doi: 10.1016/S0165-9936(02)00705-7

[Ding2007] H. Ding, Bo Zhang, Y. Ding, B. Tao, On a novel low-cost web-based power sensor via the Internet, Sensors and Actuators A: Physical, 2007, 136, 456-466, doi: 10.1016/j.sna.2006.11.036

[Doyle2004] P. Doyle, D. Heffernan, D. Duma, A time-triggered transducer network based on an enhanced IEEE 1451 model, Microprocessors and Microsystems, 2004, 28, 1-12, doi: 10.1016/S0141-9331(03)00088-7

[Economides2009] M.J. Economides, D.A. Wood, The state of natural gas, Journal of Natural Gas Science and Engineering, 2009, 1, 1-13, doi: 10.1016/j.jngse.2009.03.005

[Fanget2011] S. Fanget, S. Hentz, P. Puget, J. Arcamone, M. Matheron, E. Colinet, P. Andreucci, L. Duraffourg, Ed. Myers, M.L. Roukes, Gas sensors based on gravimetric detection—A review, Sensors and Actuators B, 2011, 160, 804- 821, doi: 10.1016/j.snb.2011.08.066

[Feng2007] Z. Feng, Q. Wang, K. Shida, A review of self-validating sensor technology, *Sensor review*, 2007, 1, 48-56, doi: 10.1108/02602280710723488

[Feng2009] Z. Feng, Q. Wang, K. Shida, Design and Implementation of a Self-Validating Pressure Sensor, *IEEE sensors journal*, 2009, 9, 207-218, doi: 10.1109/JSEN.2008.2011949

[Fonollosa2008] J. Fonollosa, R. Rubio, S. Hartwig, S. Marco, J. Santander, L. Fonseca, J. Wöllensteiner, M. Moreno, Design and fabrication of silicon-based mid infrared multi-lenses for gas sensing applications, *Sensors and actuators B: Chemical*, 2008, 132, 498-507

[Fonollosa2009a] J. Fonollosa, M. Carmona, J. Santander, L. Fonseca, M. Moreno, S. Marco, Limits to the integration of filters and lenses on thermoelectric IR detectors by flip-chip techniques, *Sensors and Actuators A: Physical*, 2009, 149, 65-73, doi: 10.1016/j.sna.2008.10.008

[Fonollosa2009b] J. Fonollosa, B. Halford, L. Fonseca, J. Santander, S. Udina, M. Moreno, J. Hildenbrand, J. Wöllensteiner, S. Marco, Ethylene optical spectrometer for apple ripening monitoring in controlled atmosphere store-houses, *Sensors and Actuators B: Chemical*, 2009, 136, 546-554, doi: 10.1016/j.snb.2008.12.015

[Fonollosa2009c] J. Fonollosa, Development of a compact NDIR spectrometer based on MOEMS components for fruit ripening monitoring, PhD thesis, Universitat de Barcelona, Dept. Electrònica, 2009. Available online at: [http://205.209.45.207/Hantale/WEB.nsf/Anexos/ECB36CA619F8DDB48725766A004C6C0D/\\$FILE/Tesi\\_jfonollosa\\_fina15.PDF](http://205.209.45.207/Hantale/WEB.nsf/Anexos/ECB36CA619F8DDB48725766A004C6C0D/$FILE/Tesi_jfonollosa_fina15.PDF)

[Frank1982] I.E. Frank, B.R. Kowalski, Chemometrics, *Analytical Chemistry*, 1982, 54, 232R-243R, doi: 10.1021/ac00242a023

[Frey2007] U. Frey, M. Graf, S. Taschini, K.U. Kirstein, A. Hierlemann, A digital CMOS architecture for a micro-hotplate array. *IEEE J. Solid-State Circuits*, 2007, 42, 441-450

[Frey2011] C.M. Frey, F. Luxenburger, S. Droege, V. Mackoviak, B. Mizaikoff, Near-Infrared Hollow Waveguide Gas Sensors, *Applied spectroscopy*, 2011, 65, 1269-1274, doi: 10.1366/11-06286

[Friend1989] D.G. Friend, J.F. Ely, H. Ingham, Thermophysical properties of Methane, *J. Phys. Chem. Ref Data*, 1989, 18, 583-638

[Frolik2001] J. Frolik, M. Abdelrahman, A confidence-based approach to the self-validation, fusion and reconstruction of quasi-redundant sensor data, IEEE Transactions on Instrumentation and Measurement, 2001, 50, 6, 1761-1769.

[Gardner1994] J. W. Gardner, T. C. Pearce, S. Friel, A multisensor system for beer flavour monitoring using an array of conducting polymers and predictive classifiers, Sensors and Actuators B: Chemical, 1994, 18, 240-243, doi: 10.1016/0925-4005(94)87089-6

[Geladi1986] P. Geladi, B. Kowalski, Partial Least Squares Regression: A tutorial, Analytica Chimica Acta, 1986, 185, 1-17

[Girerd2000] C. Girerd, S. Gardien, J. Burch, S. Katsanevas, J. Marteau, Ethernet network-based DAQ and smart sensors for the OPERA long-baseline neutrino experiment, IEEE Nuclear Science Symposium Conference Record, 2000, 2, 12/111-12/115, doi: 10.1109/NSSMIC.2000.949950

[Goeldner1990] H.D. Goeldner, B. Horn, T. Liedtke, W.R. Marx, W. Schaefer, Measuring component concentration in a gas blend, patent application number: US4902138A1

[Gopel1992] W. Göpel, J. Hesse, J.N. Zemel, Sensors. A comprehensive survey. Weinheim: VCH (Germany), 1992, 3, 8.

[Grunewald2004] A.U. Grunewald, Method and device for determining the gas concentrations in a gas mixture, patent number: US6688159B1

[Guadarrama2000] A. Guadarrama, M.L. Rodriguez, C. Sanz, J.L. Rios, J.A. Saja, electronic nose based on conducting polymers for the quality control of olive oil aroma. Discriminating quality, variety of olive and geographic origin, Proc. Of the 7<sup>th</sup> international symposium on olfaction and electronic nose (ISOEN2000), 2000, UK, 125-126

[Gutierrez2010] R. Gutierrez-Osuna, A. Hierlemann, Adaptive microsensor systems, Annual review of analytical chemistry, 2010, 3, 255-276, doi: 10.1146/annurev.anchem.111808.073620

[Heberle2000] I. Heberle, A. Liebminger, U. Weimar, W. Göpel, Optimised sensor arrays with chromatographic preseparation: characterisation of alcoholic beverages, Sensors and Actuators B, 2000, 68, 53-57, doi: 10.1016/S0925-4005(00)00461-5

[Herwaarden1988] A. V. van Herwaarden, A. W. Sarro, Performance of integrated thermopile vacuum sensors, Journal of Physics E, 1988, 21, 1162-1167

[Henry1993] M.P. Henry, D.W. Clarke, The self-validating sensor: rationale, definitions and examples, *Control Engineering Practice*, 1993, 1, 585-610, doi: 10.1016/0967-0661(93)91382-7

[Hierlemann2007] A. Hierlemann, R. Gutierrez-Osuna, Higher order chemical sensing, *Chemical Reviews*, 2007, 108, 563-613, doi: 10.1021/cr068116m

[Hinshaw2006] J.V. Hinshaw, The Thermal Conductivity Detector, LCGC North America (online magazine article), 2006, <http://chromatographyonline.findpharma.com/lcgc/Column%3A+GC+Connections/The-Thermal-Conductivity-Detector/ArticleStandard/Article/detail/283449>, (Last accessed March 2008).

[Hulanicki1991] A. Hulanicki, G. Stanislaw, F. Ingman, Chemical sensors definition and classification, *Pure & App. Chemistry*, 1991, 63, 1247-1250.

[Hulme2004] J.P. Hulme, P.R. Fielden, N.J. Goddard, Fabrication of a spectrophotometric absorbance flow cell using injection-molded plastic, *Analytical Chemistry*, 2004, 76, 238-243, doi: 10.1021/ac034755a

[Hyde1960] C.G. Hyde, M.W. Jones, *Gas Calorimetry*, 2nd Edition, Ernest Benn Ltd., UK, 1960.

[IEA2009] International Energy Agency (IEA), IEA scoreboard 2009 – 35 key energy trends over 35 years, IEA publications, France, 2009

[IEA2010] International Energy Agency (IEA), 2010 Key World Energy Statistics, IEA publications, France, 2010, 60

[IEEE1997] IEEE 1451.2 standard, IEEE Standard for a Smart Transducer Interface for Sensors and Actuators - Transducer to Microprocessor Communication Protocols and Transducer Electronic Data Sheet (TEDS) Formats, USA, 1997, doi: 10.1109/IEEEESTD.1998.88285

[IEEE1999] IEEE 1451.1 standard, Smart Transducer Interface for Sensors and actuators – Network Capable Application Processor (NCAP) Information Model, USA, 1999, doi: 10.1109/IEEEESTD.2000.91313

[IEEE2003] IEEE 1451.3 standard, IEEE Standard for a Smart Transducer Interface for Sensors and Actuators-Digital Communication and Transducer Electronic Data Sheet (TEDS) Formats for Distributed Multidrop Systems, USA, 2003, doi: 10.1109/IEEEESTD.2004.94443

[IEEE2004] IEEE 1451.4 standard, IEEE Standard for a Smart Transducer Interface for Sensors and Actuators - Mixed-Mode Communication Protocols and Transducer Electronic Data Sheet (TEDS) Formats, USA, 2004, doi: 10.1109/IEEESTD.2004.95745

[IEEE2007] IEEE 1451.0 standard, IEEE Standard for a Smart Transducer Interface for Sensors and Actuators - Common Functions, Communication Protocols, and Transducer Electronic Data Sheet (TEDS) Formats, USA, 2007, doi: 10.1109/IEEESTD.2007.4338161

[IEEE20072] IEEE1451.5 standard, IEEE Standard for a Smart Transducer Interface for Sensors and Actuators Wireless Communication Protocols and Transducer Electronic Data Sheet (TEDS) Formats, USA, 2007, doi: 10.1109/IEEESTD.2007.4346346

[ISO1995] ISO6976:1995 standard, Natural gas -- Calculation of calorific values, density, relative density and Wobbe index from composition, Internartional Organitzation for Standardization, Switzerland, 1995

[Janata2003] J. Janata, Electrochemical microsensors, Proc. of the IEEE, 2003, 91, 864-869

[Jerman1981] J.H. Jerman, A miniature thin-film thermal conductivity detector for an integrated gas chromatograph, PhD thesis, Stanford University, Stanford, CA, 1981

[Jurs2000] P. C. Jurs, G. A. Bakken, H. E. McClelland, Computational Methods for the Analysis of Chemical Sensor Array Data from Volatile Analytes, Chemical reviews, 2000, 100, 2649-2678

[Karatzas2007] D. Karatzas, A. Chorti, N.M. White, C.J. Harris, Teaching old sensors new tricks: archetypes of intelligence, IEEE Sensors Journal, 2007, 7, 868-881.

[Kastner2002] J. Kastner, P. Schley, Novel optical techniques for process analysis of natural gas quality, 3<sup>rd</sup> Conference on optical analysis technology, 2002, Germany

[Kastner2005] J. Kastner, Online gas quality measurement technique based on optical and thermal gas properties, 2-day technical conference: Natural gas quality, energy measurement, and interchangeability, 2005, USA, (available online: [http://www.elster-instromet.fr/downloads/FLO\\_DM\\_gas\\_lab\\_Q1\\_TR\\_UK\\_2005\\_12.pdf](http://www.elster-instromet.fr/downloads/FLO_DM_gas_lab_Q1_TR_UK_2005_12.pdf))

[Kakuta2003] M. Kakuta, D.A. Jayawickrama, A.M. Wolters, A. Manz, J.V. Sweedler, Micromixer-based time-resolved NMR: Applications to ubiquitin protein conformation, Analytical Chemistry, 2003, 75, 956-960, doi: 10.1021/ac026076q

[Kim2005] J.S. Kim, S.O. Sohn, J.S. Huh, Fabrication and sensing behavior of PVF2 coated-polyaniline sensor for volatile organic compounds. *Sens. Actuators B*, 2005, 108, 409-413

[King 1964] W.H. King, *J. Anal. Chem.* 36 1964 1735.

[Kolesov1979] V.P. Kolesov, Bomb combustion of gaseous compounds in oxygen, in: S. Sunner, M. Måansson (Eds.), *Experimental Chemical Thermodynamics*, Vol. 1: Combustion Calorimetry, Pergamon Press, 1979, Oxford, 1–16 (Chapter 13)

[Kularatna2008] N. Kularatna, B.H. Sudantha, An environmental air pollution monitoring system based on the IEEE 1451 standard for low cost requirements, *IEEE sensors journal*, 2008, 8, 415-422, doi: 10.1109/JSEN.2008.917477

[Kumar2011] A. Kumar, I.P. Singh, S.K. Sud, Energy Efficient and Low-Cost Indoor Environment Monitoring System Based on the IEEE 1451 Standard, *IEEE Sensors Journal*, 2011, 11, 2598 – 2610, doi: 10.1109/JSEN.2011.2148171

[Lange2008] U. Lange, N. V. Roznyatovskaya, V. M. Mirsky, Conducting polymers in chemical sensors and arrays, *Analytica Chimica Acta*, 2008, 614, 1–26, doi: 10.1016/j.aca.2008.02.068

[Lee1998] K. Lee, An Overview of the IEEE 1451 – A family of proposed smart transducer interface standards, *Proc. Sensors Expo*, 1998, 159-167.

[Lee2005] K. Lee, E.Y. Song, Object-oriented application framework for IEEE-1451.1 standard, *IEEE Transactions on Instrumentation and measurement*, 2005, 54, 1527-1533.

[Lee2006] K. Lee, E.Y. Song, A Wireless Environmental Monitoring System Based on the IEEE 1451.1 Standards, 2006 *Instrumentation and measurement technology conference (IMTC2006)*, Sorrento, Italy, 2006.

[Lee2009] F. Lee, G. Zhou, H. Yu, F.S. Chau, A MEMS-based resonant-scanning lamellar grating Fourier transform, *Sensors and actuators A: Physical*, 2009, 149, 221-228

[Leung2007] A. Leung, P. M. Shankar, R. Mutharasan, A review of fiber-optic biosensors, *Sensors and Actuators B*, 2007, 125, 688-703, doi: 10.1016/j.snb.2007.03.010

[Lewis1989] E.A. Lewis, R.M. Hart, H. Greenfield, Design and testing of a new isothermal flow gas calorimeter: the Hart Field-deployable natural gas energy meter, *thermochimica acta*, 1989, 154, 167-185

[Lonergan1996] M. C. Lonergan, E. J. Severin, B. J. Doleman, S. A. Beaber, R. H. Grubbs, N. S. Lewis, 1. Array-based vapor sensing using chemically sensitive carbon black polymer resistors, *Chemistry of Materials*, 1996, 8, 2298-2312

[Liu2001] R.P. Liu, M.J. Fuent, M.P. Henry, M.D. Duta, A neural network to correct mass flow errors caused by two-phase flow in a digital coriolis mass flowmeter, *Flow Measurement and Instrumentation*, 2001, 12, 53-63

[Loubar2007] K. Loubar, C. Rahmouni, O. Le Corre, M. Tazerout, A combustionless determination method for combustion properties of natural gases, *Fuel*, 2007, 86, 2535-2544, doi: 10.1016/j.fuel.2007.02.024

[Makhoukhi2005] N. Makhoukhi, E. Pere, R. Creff, C. Pouchan, Determination of the composition of a mixture of gases by infrared analysis and chemometric methods, *Journal of Molecular Structure*, 2005, 744-747, doi: 10.1016/j.molstruc.2005.01.021

[Marco1998] S. Marco, A. Ortega, A. Pardo, J. Samitier, Gas identification with tin oxide sensor array and self-organizing maps: adaptive correction of sensor drifts, *IEEE Transactions on Instrumentation and Measurement*, 1998, 47, 316-321

[Matsumiya2003] M. Matsumiya, W. Shin, F. Qiu, N. Izu, I. Matsubara, N. Murayama, Poisoning of platinum thin film catalyst by hexamethyldisiloxane (HMDS) for thermoelectric hydrogen gas sensor, *Sensors and Actuators, B: Chemical*, B, 2003, 96, 516-522

[Moseley1997] P. Moseley, solid state gas sensors, *Meas. Sci. Technol.*, 1997, 8, 223-237.

[Malenshek2009] M. Malenshek, D.B. Olsen, Methane number testing of alternative gaseous fuels, *Fuel*, 2009, 88, 650-656, doi: 10.1016/j.fuel.2008.08.020

[Minakov2006] A. Minakov, J. Morikawa, T. Hashimoto, H. Huth, C. Schick, Temperature distribution in a thin-film chip utilized for advanced nanocalorimetry, *Meas. Sci. Technol.*, 2006, 17, 199-207

[Nagaraju1998] M. Nagaraju, T. P. Kumar, Networked electronic energy meters with power quality analysis, *Power Quality'98*, 1998, 45-57, doi: 10.1109/PQ.1998.710336

[Nagle1998] H. Nagle, R. Gutierrez-osuna, S. Schiffman, The how and why of electronic noses, *IEEE spectrum*, 1998, 22-34.

[NIST2011] National Institute of Standards and Technology (NIST), Chemical web book, <http://webbook.nist.gov/chemistry/fluid>, last accessed April 2012.

[Noda2005] M. Noda, Uncooled thermal infrared sensors: Recent status in microbolometers and their sensing materials, Sensor letters, 2005, 3, 194-205

[Ohira2008] S. Ohira, K. Toda, Micro gas analyzers for environmental and medical applications, Analytica Chimica Acta , 2008, 619, 143–156, doi: 10.1016/j.aca.2008.05.010

[OMG2003] Object Management Group (OMG). Smart Transducers Interface (v1.0), 2003. Available at <http://www.omg.org> (acronym SMART), last accessed April 2012.

[Padilla2007] M. Padilla, A. Perera, I. Montoliu, A. Chaudry, K. Persaud, S. Marco, Poisoning fault diagnosis in chemical gas sensor arrays using multivariate statistical signal processing and structured residuals generation, IEEE International Symposium on Intelligent Signal Processing (WISP 2007), 2007, 1-6.

[Padilla2010] M. Padilla, Improving the robustness of artificial olfaction systems by multivariate signal processing, PhD thesis, Universitat de Barcelona, Dept. Electronica, 2010.

[Paiserb2008] P. Paiserb, M. rekas, Solid-state potentiometric gas sensors—current status and future trends, J. Solid State Electrochem. ,2009, 13, 3–25

[Palucka2000] T. Palucka, Catalytic bead and infrared techniques for the detection of combustible gases, Rimbach publishing, Industrial hygiene news, January 2000

[Pan2004] T. Pan, R.T. Kelly, M.C. Asplund, A.T. Woolley, Fabrication of calcium fluoride capillary electrophoresis microdevices for on-chip infrared detection, Journal of chromatography A, 2004, 1027, 231-235, doi: 10.1016/S0021-9673(03)01300-1

[Pannemann2001] H.J. Pannemann, C.W. Koreman, A. Kroon, H. Horstink, M. Jaeschke, J.A. Schouten, J.P.J. Michels, A fast energy measurement system suitable for process control and off-shore metering application, Proc. 2001 international gas research conference, 2001, The Netherlands.

[Pardo2006] A. Pardo, L. Cámera, J. Cabré, A. Perera, X. Cano, S. Marco, J. Bosch, Gas measurement systems based on IEEE1451.2 standard, Sensors and Actuators B: Chemical, 2006, 116, 11-16, doi: 10.1016/j.snb.2006.03.012

[Paul1993] O. Paul, H. Baltes, Thermal conductivity of CMOS materials for the optimization of microsensors, J. Micromech. Microeng. 1993, 3, 110-112

[Pawliszyn2005] J. Pawliszyn, R.E. Hummel, OPTICAL SPECTROSCOPY | Refractometry and Reflectometry, Encyclopedia of Analytical Science (Second Edition), 2005, 452-461, doi: 10.1016/B0-12-369397-7/00434-9

[Persaud1996] K.C. Persaud, S.M. Khaffaf, J.S. Payne, Sensor array techniques for mimicking the mammalian olfactory system, Sensors and actuators B, 1996, 35, 267-273

[Petru2010] P. Petru, B. Mircea, Hardware implementation of a PIC18F448 based TIM for IEEE1451.2 compliant actuator control, 9th International Symposium on Electronics and Telecommunications (ISETC), 2010, 119-122, doi: 10.1109/IETC.2010.5679304

[Poling2001] B. E. Poling, J. M. Prausnitz, J. P. O'Connell, The Properties of Gases and Liquids, 5th editions, McGraw-Hill, New York, 2001, 10.1-10.70.

[Pollack1993] G. Pollak-Diener, E. Obermeier, Heat-conduction microsensor based on silicon technology for the analysis of two- and three-component gas mixtures, Sens. Actuators B Chemical, 1993, 13, 345-347

[Qin1997] S. J. Qin., H. Yue, R. Dunia, Self-validating inferential sensors with application to air emission monitoring, Industrial and Engineering Chemistry Research, 1997, 36, 1675-85.

[Rahmouni2003a] C. Rahmouni, M. Tazerout, O. Le Corre, Determination of the combustion properties of natural gases by pseudo-constituents, Fuel, 2003, 82, 1399-1409

[Rahmouni2003b] C. Rahmouni, O. Le Corre, M. Tazerout, Online determination of natural gas properties, C. R. Mecanique, 2003, 331, 545-550

[Ramos1986] L.S. Ramos, K.R. Beebe, W.P. Carey, E. Sanchez, B.C. Erickson, B.E. Wilson, L.W. Wangen, B.R. Kowalski, Chemometrics, Analytical Chemistry, 1986, 58, 294R-315R

[Ramos2004] H.M.G. Ramos, J.M.D. Pereira, V. Viegas, O. Postolache, P.M.B.S. Girao, A virtual instrument to test smart transducer interface modules (STIMs), IEEE Trans. Instrum. Meas, 2004, 53, 1232-1239, doi: 10.1109/TIM.2004.831183

[Rancourt1996] J.D. Rancourt, Optical thin films: User handbook, SPIE, 1996.

[RMG7111] RMG Meßtechnik GmbH, Measuring device for Calorific Value, Wobbe Index and Standard Density – WOM 2000 S, Publication 7111-E, Germany

[RMG7121] RMG Meßtechnik GmbH, Superior Calorific Value, Standard Density and Wobbe Index Measuring Device - EMC 500, Publication 7121-E, 2005, Germany

[Rubio2006] R. Rubio, J. Santander, J. Fonollosa, L. Fonseca, I. Gracia, C. Cane, M. Moreno, S. Marco, Exploration of the metrological performance of a gas detector based on an array of unspecific infrared filters, Sensors and actuators B: Chemical, 2006, 116, 183-191

[Rubio2007] R. Rubio, Nueva arquitectura para un nuevo analizador compacto de gases basado en una matriz de microsensores de infrarrojo no específicos, , PhD thesis, Universitat de Barcelona, Dept. Electronica, 2007.

[Sabate2005] N. Sabate, R. Rubio, C. Calaza, J. Santander, L. Fonseca, I. Gracia, C. Cane, M. Moreno, S. Marco, Mirror electrostatic actuation of a medium-infrared tunable Fabry-Perot interferometer based on a surface micromachining process, Sensors and actuators A: Physical, 2006, 123-124, 584-589

[Sabate2005b] N. Sabate, J. Santander, I. Gràcia, L. Fonseca, E. Figueras, E. Cabruja, C. Cane, Characterization of thermal conductivity in thin film multilayered membranes, Thin Solid Films, 2005, 484, 328-333

[Salleras2005] M. Salleras, J. Palacín, M. Moreno, L. Fonseca, J. Samitier, S. Marco, A methodology to extract dynamic compact thermal models under time-varying boundary conditions: application to a thermopile based IR sensor, Microsystem Technol., 2005, 12, 21-29

[Semancik2001] S. Semancik, R. E. Cavicchi, M. C. Wheeler, J. E. Tiffany, G. E. Poirier, R. M. Walton, J. S. Suehle, B. Panchapakesan, D. L DeVoe, Microhotplate platforms for chemical sensor research, Sensors and Actuators B: Chemical, 2001, 77, 579-591

[Sevcik1976] Jiri Sevcik, Detectors in gas chromatography, Journal of chromatography library, 1976, 4, Chapter 2.

[Sillon2002] N. Sillon, R. Baptist, Micromachined mass spectrometer, Sensors and actuators B-Chemical, 2002, 83, 129-137, doi: 10.1016/S0925-4005(01)01070-X

[Schilz2000] J. Schilz, Applications of thermoelectric infrared sensors (Thermopiles): gas detection by infrared absorption; NDIR, thermophysical minima, Perkin Elmer optoelectronics, 2000 [Scott1998] R.P.W. Scott, Introduction to Analytical Gas Chromatography, 2<sup>nd</sup> ed., Marcel Dekker, New York, 1998, 55-105

[Schmidt2003] J. W. Schmidt, M. R. Moldover, Dielectric Permittivity of Eight Gases Measured with Cross Capacitors, International journal of thermophysics, 2003, 24, 375-403, doi: 10.1023/A:1022963720063

[Song2005] G. Song, A. Song, W. Huang, Distributed measurement system based on networked smart sensors with standardized interfaces, Sensors and Actuators A: Physical, 2005, 120, 147-153, doi: 10.1016/j.sna.2004.11.011  
[Song2008] E.Y Song, K. Lee, Understanding IEEE 1451-Networked smart transducer interface standard - What is a smart transducer?, IEEE Instrumentation & measurement magazine, 2008, 11, 11-17.

[Song2008b] E.Y. Song, K. Lee, Sensor Network based on IEEE 1451.0 and IEEE p1451.2-RS232, IEEE Instrumentation and measurement technology conference, 2008 (IMTC 2008), 2008, 1728-1733, doi: 10.1109/IMTC.2008.4547323

[Stepanenko2006] A. Stepanenko, K. Lee, R. Kochan, V. Kochan, A. Sachenko, Development of a minimal IEEE 1451.1 model for microcontroller implementation, IEEE Sensors Appl. Symp., 2006, Houston, USA,

[Stephan1985] K. Stephan, A. Laecke, The thermal conductivity of fluid air, J. Phys. Chem. Ref. Data, 1985, 14, 227-234

[Stewart1997] G. Stewart, W. Jin, B. Culshaw, Prospects for fibre-optic evanescent-field gas sensors using absorption in the near-infrared, Sensors and Actuators B, 1997, 38, 42-47, doi: 10.1016/S0925-4005(97)80169-4

[Strathmann2001] S. Strathmann, Sample conditioning for multi-sensor systems dissertation. Fakultät für Chemie und Pharmazie, Eberhard-Karls-Universität. Thesis. Tübingen (Germany), 2001.

[Stufkens1975] J.S. Stufkens, H.J. Bogaard, Rapid method for the determination of the composition of natural gas by gas chromatography, Analytical Chemistry, 1975, 47, 383-386, doi: 10.1021/ac60353a060

[Sun2011] J. Sun, D. Cui, X. Chen, L. Zhang, H. Cai, H. Li, Design, modeling, microfabrication and characterization of novel micro thermal conductivity detector, Sensors and Actuators B, 2011, 160, 936- 941, doi: 10.1016/j.snb.2011.09.006

[Suslick2004] K. S. Suslick, N. A. Rakow, A. Sen, Colorimetric sensor arrays for molecular recognition, Tetrahedron, 2004, 60, 11133-11138, doi: 10.1016/j.tet.2004.09.007

[Tao2011] C. Tao, X. Li, J. Yanga, Y. Shib, Optical fiber sensing element based on luminescence quenching of silica nanowires modified with cryptophane-A for the detection of methane, Sensors and Actuators B, 2011, 156, 553- 558, doi: 10.1016/j.snb.2011.01.067

[Tai2012] H. Tai, D. Li, C. Wang, Q. Ding, C. Wang, S. Liu, Design and characterization of a smart turbidity transducer for distributed measurement system, Sensors and Actuators A: Physical, 2012, 1-8, doi: 10.1016/j.sna.2011.11.028

[Tao2005] B. Tao, H. Ding, Y.L. Xiong, Design and implementation of an embedded IP sensor for distributed networking sensing, Sensors and Actuators A: Physical, 2005, 119, 567-575, doi: 10.1016/j.sna.2004.10.011

[Tardy2004] P. Tardy, J.R. Coulon, C. Lucat, F. Menil, Dynamic thermal conductivity sensor for gas detection, Sensors and Actuators B: Chemical, 2004, 98, 63–68, doi: 10.1016/j.snb.2003.09.019

[Taymanov2011] R. Taymanov, K. Sapozhnikova, I. Druzhinin, Sensor devices with metrological self-check, Sensors and Transducers, 2011, 10, 30-45

[Tsang2010] K.M. Tsang, W.L. Chan, Data validation of intelligent sensor using predictive filters and fuzzy logic, Sensors and Actuators A, 2010, 159, 149–156, doi: 10.1016/j.sna.2010.03.013

[Tuantranont2011] A. Tuantranont, A. Wisitsora-at, P. Sritongkham, K. Jaruwongrungsee, A review of monolithic multichannel quartz crystal microbalance: A review, Analytica Chimica Acta, 2011, 687, 114–128, doi: 10.1016/j.aca.2010.12.022

[Ulbig2001] P. Ulbig, D. Hoburg, Determination of the calorific value of natural gas by different methods, thermochimica acta, 2002, 382, 27-35

[Uribe1990] F. J. Uribe, Thermal Conductivity of Nine Polyatomic Gases at Low Density, J. Phys. Chem. Ref. Data, 1990, 19, 1123-1136

[Vergara2007] A. Vergara, E. Llobet, J. Brezmes, P. Ivanov, C. Cané, I. Gràcia, X. Vilanova, X. Correig, Quantitative gas mixture analysis using temperature-modulated micro-hotplate gas sensors: Selection and validation of the optimal modulating frequencies, Sensors and Actuators B: Chemical, 2007, 123, 1002-1016

[Viegas2005] V. Viegas, J.M. Dias Pereira, and P.M.B. Silva Girão, Using a commercial framework to implement and enhance the IEEE 1451.1 Standard, Proc. Instrumentation and measurement technology conference 2005, 2005, Ottawa, Canada,

[Viegas2007] V. Viegas, J.M. Dias Pereira, P.M.B. Silva Girão, .NET Framework and Web Services: A Profit Combination to Implement and Enhance the IEEE 1451.1 Standard, IEEE Transactions on instrumentation and measurement, 2007, 56, 2739-2747, doi: 10.1109/TIM.2007.908136

[Viegas2008] V. Viegas, .M. Dias Pereira, P.M.B. Silva Girão, A brief tutorial on the IEEE 1451.1 standard, IEEE instrumentation & measurement magazine, 2008, 11, 38-46, doi: 10.1109/MIM.2008.4483732

[Vilkner2004] T. Vilkner, D. Janasek, A. Manz, Micro Total Analysis Systems. Recent Developments, Analytical Chemistry, 2004, 76, 3373-3386, doi: 10.1021/ac040063q

[Vyas2006] J.C. Vyas, V.R. Katti, S.K. Gupta, J.V. Yakhmi, A non-invasive ultrasonic gas sensor for binary gas mixtures, Sensors and Actuators B, 2006, 115, 28-32, doi: 10.1016/j.snb.2005.08.016

[Wall2003] R.W. Wall, A. Ekpruke, Developing an IEEE 1451.2 compliant sensor for real-time distributed measurement and control in an autonomous log skidder, The 29th Annual Conference of the IEEE Industrial Electronics Society 2003 (IECON'03), 2003, 3, 2482-2487, doi: 10.1109/IECON.2003.1280635

[Wang2004] S. Wang, Y. Chen, Sensor validation and reconstruction for building central chilling systems based on principal component analysis, Energy Conversion and Management, 2004, 45, 673-695

[Wang2005] Y. Wang, M. Nishikawa, R. Maeda, M. Fukunaga, K. Watanabe, A smart thermal environment monitor based on IEEE 1451.2 standard for global networking, IEEE Transactions on instrumentation and measurement, 2005, 54, 1321-1326, doi: 10.1109/TIM.2004.839767

[Warrior1997] J. Warrior, The IEEE P1451.1 Object Model Network Independent Interfaces for Sensors and Actuators, Proc. Sensors Expo, 1997, 1-14

[Wei2005] J. Wei, N. Zhang, N. Wang, D. Lenhert, M. Neilsen, M. Mizuno, Use of the “smart transducer” concept and IEEE 1451 standards in system integration for precision agriculture, Computers and Electronics in Agriculture, 2005, 48, 245-255, doi: 10.1016/j.compag.2005.04.006

[Wetchakun2011] K.Wetchakun, T. Samerjai, N. Tamaekong, C. Liewhiran, C. Siriwong, V. Kruefu, A. isitsoraat, A. Tuantranont, S. Phanichphant, Semiconducting metal oxides as sensors for environmentally hazardous gases, Sensors and Actuators B: Chemical, 2010, doi:10.1016/j.snb.2011.08.032 (In press)

[White1942] J. White, Long optical paths of large aperture, Journal of the optical society of America, 1942, 32, 4

[Wild2001] K. R. Wild, D. L. Ehrich, Energy metering technologies, Proc. of 2001 International gas research conference, 2001, Amsterdam, The Netherlands.

[Wise1996] B.M. Wise, N.B. Gallagher, The process chemometrics approach to process monitoring and fault detection, Journal of Process Control, 1996, 6, 329-348

[Wold2001] S. Wold, M. Sjöström, L. Eriksson, PLS-regression: a basic tool of chemometrics, *Chemometrics and Intelligent Laboratory Systems*, 2001, 58, 109–130

[Wobschall2002] D. Wobschall, An implementation of IEEE 1451 NCAP for internet access of serial port-based sensors, 2<sup>nd</sup> ISA/IEEE Sensors for Industry Conference, 2002, 157-160.

[Wobschall2004] D. Wobschall, W. S. Poh, A smart RTD temperature sensor with a prototype IEEE 1451.2 internet interface, *Proceedings the ISA/IEEE Sensors for Industry Conference*, 2004, 183-186, doi: 10.1109/SFICON.2004.1287157

[Wobschall2009] D. Wobschall, A. Stepanenko, I. Maykiv, R. Kochan, A. Sachenko, V. Kochan, A multi-port serial NCAP using the IEEE 1451 smart transducer standard, *IEEE Sensors Applications Symposium, 2009 (SAS 2009)*, 2009, 293 – 297, doi: 10.1109/SAS.2009.4801818

[Wu2002] Y.E. Wu, K. Chen, C.W. Chen, K.H. Hsu, Fabrication and characterization of thermal conductivity detectors (TCDs) of different flow channel and heater designs, *Sens. Actuators A*, 2002, 100, 37-45

[Xu2006] J. Xu, B. You, Q Li, Implementation of an IEEE 1451 Smart Quartz Tuning fork Temperature Transducer for Real-time Distributed Measurement and Control System, *The Sixth World Congress on Intelligent Control and Automation, 2006 (WCICA 2006)*, 2006, 2, 5411-5416, doi: 10.1109/WCICA.2006.1714105

[Younglove1987] B. A. Younglove, J. F. Ely, Thermophysical Properties of Fluids. II. Methane, ethane, propane, isobutane and normal butane, *J. Phys. Chem. Ref. Data*, 1987, 16, 577-798.

[Yoon2001] S. Yoon, J.F. MacGregor, Fault diagnosis with multivariate statistical models part I: using steady state fault signatures, *Journal of Process Control*, 2001, 11, 387-400, doi: 10.1016/S0959-1524(00)00008-1

[Zdankiewicz1997] E. M. Zdankiewicz, Gas detection in theory and in practice, *Sensors*, 1997, 20-38

[Zeisel1999] D. Zeisel. H. Menzi, L. Ullrich, A precise and robust quartz sensor based on tuning fork technology for (SF<sub>6</sub>) - gas density control, *Sensors and actuators A: Physical*, 2000, 80, 233-236.

[Zhaochun2009] L. Zhaochun, C. Yuzhu, H. Jin, Design of Smart Temperature Sensor Based on IEEE1451.2 Standard, *International Forum on Information Technology and Applications*, 2009 (IFITA '09), 2009, 3, 312-314, doi: 10.1109/IFITA.2009.331

[Zhang2001a] J. Zhang, Y. Yan, A self-validating differential pressure flow sensor, IEEE Instrumentation and Measurement Technology Conference, 2001, 5, 21-23

[Zhang2001b] J. Zhang, Y. Yan, A wavelet-based approach to abrupt fault detection and diagnosis of sensors, IEEE Transactions on Instrumentation and Measurement, 2001, 50, 5, 1389-1396

[Zhong2005] J.-Q. Zhong, J. Zhang, Thermal convection with a freely moving top boundary, Phys. Fluids, 2005, 17, 115105.1-115105.12

[Zipser1995] L. Zipser, F. Wächter, Acoustic sensor for ternary gas analysis, Acoustic sensor for ternary gas analysis, Sensors and Actuators: B. Chemical, 1995, 26, 195-198, doi: 10.1016/0925-4005(94)01585-6

[Zipser2000] L Zipser, F Wächter, H Franke, Acoustic gas sensors using airborne sound properties, Sensors and Actuators B: Chemical, 2000, 68, 162-167, doi: 10.1016/S0925-4005(00)00478-0

# APPENDIX A. UNCERTAINTY ANALYSIS

## A.1 UNCERTAINTY SOURCES AFFECTING SENSOR REPEATABILITY<sup>1</sup>

The different uncertainty sources in this category group those strictly related to the sensor operation point. To clarify, if we consider an ideal case where the sensor is surrounded by a gas volume of constant thermal conductivity  $k$  (regardless of ambient conditions), all non-repeatability of the measurements would be generated by this group of uncertainties. Uncertainty in the voltage readout has also been included in this section.

Heater voltage reproducibility has a very strong influence in the sensor performance, as the temperature difference of hot and cold junctions depends in first approximation as the square of the heater voltage as is shown in equation (A1)

$$\Delta T = R_{th}(T) \cdot P_h \cong R_{th} \cdot \frac{V_h^2}{R_h(V_h)} \quad (\text{A1})$$

Where  $\Delta T$  is the temperature difference between hot and cold junctions of the thermopile, to which the sensor output is proportional, as shown in equation (1),  $R_{th}$  is the thermal resistance to the ambient (dissipation),  $P_h$  is the power applied to the heater element,  $R_h$  is the resistance of the heater element, and  $V_h$  is the voltage applied to the heater element. Dependence of  $R_{th}$  with temperature (and voltage) is not an effect related to the sensor operation point and only for the purpose of this discussion it will be considered a constant. Despite this assumption, it can be noted in advance that its contribution is in this case masked by the magnitude of the other terms  $V_h^2$  and  $R_h(V_h)$ .

To estimate the uncertainty in  $\Delta T$  due to noise in  $V_h$  lets first consider equations (A2) and (A3)

$$\epsilon_{\Delta T}(V_h) = \frac{d\Delta T}{dV_h} \cong R_{th} \cdot \frac{2V_h}{R_h(V_h)} \cdot dV_h - \frac{1}{R_h(V_h)^2} \cdot \frac{dR_h}{dV_h} \cdot dV_h \quad (\text{A2})$$

---

<sup>1</sup> X block

$$\frac{dR_h}{dV} = \frac{dR_h}{dT} \cdot \frac{dT}{dV_h} = TCR \cdot \frac{d\Delta T}{dV_h} \quad (A3)$$

Derivatives on  $T$  and  $\Delta T$  are identical, as one of the reference temperatures is considered to be fixed (the cold junction).  $TCR$  is the temperature coefficient of the resistor. Inserting the expression in equation (A3) into equation (A2), and also considering the output voltage equation (4.1), Propagation of the heater voltage noise to the sensor output  $\mathcal{E}_{V_o}$  can be obtained as in equation (A4).

$$\mathcal{E}_{V_o}(V_h) = \frac{dV_o}{dV_h} = n \cdot S \cdot \mathcal{E}_{\Delta T}(V_h) = n \cdot S \cdot \frac{d\Delta T}{dV_h} \cdot \mathcal{E}_{V_h} \cong \frac{2 \cdot n \cdot S \cdot R_{th} \cdot V_h}{R_h + R_h(V_h) \cdot R_{th} \cdot TCR} \cdot \mathcal{E}_{V_h} \quad (A4)$$

Equation (A4) shows a main dependency in  $V_h$  in the numerator, and there is an additional dependency in the resistance heater term which can be determined considering a typical linear variation of  $R_h$  with temperature as in equation (A5).

$$R_h(T) \cong R_h^0 \cdot [1 + TCR \cdot (T - T_0)] \quad (A5)$$

Note that equation (A5) is an approximation since  $R_h(T)$  is slightly non-linear, particularly at high temperatures however, the linear approximation holds for a large temperature range [48].

Equations (A4) and (A5) provide an interesting insight into how the heater voltage uncertainty propagates to the output voltage. However, In order to determine the effective sensitivity of the sensor output voltage to the heater voltage noise the derivative  $dV_o/dV_h$  was estimated empirically from performed measurements. In particular, for noise calculations a sensitivity value has been calculated for each heater voltage step and approximated as a constant value for small variations around that heater voltage. This was a more convenient approach rather than estimating the individual contributions expressed in (A4) given the available data.

Effects of ambient temperature changes in the voltage output, can be described by equation (A6).

$$\mathcal{E}_{V_o}(T_a) = \frac{dV_o}{dT_a} = n \cdot S \cdot \mathcal{E}_{\Delta T}(T_a) = n \cdot S \cdot \frac{d\Delta T}{dT_a} \cdot \mathcal{E}_T; \quad (A6)$$

Where  $T_a$  is the ambient temperature and  $V_o$  is the output voltage. Variable  $\mathcal{E}_T$  is the ambient temperature change, which in the presented measurement setup is considered as a very low frequency noise, in the 10-<sup>4</sup>Hz range.

Estimation of  $dV_o/dT_a$  was performed using two different approaches; the first one was estimating an upper boundary for the derivative  $dR_{th}/dT_a$ . The second one was exploration with FEM simulation results. Both results were rather consistent and allowed a rough estimation of  $\mathcal{E}_{V_o}(Ta)$ . These two approaches are discussed in section A.2 as they do not refer to changes in the sensor operation itself.

In the actual context of this work, *sensor degradation* (aging) will be neglected, since no observable degradation occurred in the considered time frame.

As for the sensor intrinsic noise, only thermal noise has to be considered for thermoelectric sensors [48]. The thermal noise voltage,  $V_N$ , of a thermopile is given by the expression (A7)

$$V_N = \sqrt{4kTR_{el}\Delta f} \quad (\text{A7})$$

With  $k$  denoting the Boltzmann constant,  $R_{el}$  the electrical resistance and  $\Delta f$  the bandwidth of the measurement. Using the values:  $T=293\text{K}$ ,  $R=12\text{k}\Omega$  and  $\Delta f= 12.5\text{ Hz}$ , in equation (A7) results in,

$$V_N = 49.25\text{nV}.$$

The result is the standard deviation  $\sigma$  for the thermopile output due to thermal noise, so for the 95% confidence interval we shall consider  $2\sigma \approx 0.1\mu\text{V}$ .

Acquisition uncertainty from the Agilent voltmeter is according to specifications: 0.0035% of reading plus  $50\text{\textmu V}$  for a 10V full scale selection.

## A.2 UNCERTAINTY SOURCES AFFECTING GAS MIXTURE THERMAL CONDUCTIVITY<sup>2</sup>

---

The  $k(T)$  curve for four main natural gas components is shown in Figure 4.4. As pointed before, for a given operation point of the sensor and gas mixture, two parameters may affect the thermal conductivity at each point of the gas volume: the ambient temperature, and the pressure of the gas mix. These are herein considered as the uncertainty sources affecting the gas mixture thermal conductivity.

As the sensors works in isobaric conditions, we shall for now consider only the temperature dependence of  $k$ , with the explicit notation  $k(T)$ . The gas volume exhibits a temperature gradient as depicted by Figure A1(TD). The thermal conductivity  $k(T)$  of a given gas mixture is determined at each point by  $T(x,y,z)$ . Heat dissipation by conduction occurs according to Fourier's law,

$$\vec{q} = -k(T)\nabla T \quad (\text{A8})$$

---

<sup>2</sup> X block

Where  $\vec{q}$  is the heat flux per unit area,  $k$  is the thermal conductivity, and  $\nabla T$  is the temperature gradient. In the steady state,  $\vec{q}$  is a constant for each point in the space, and is determined by the power dissipated at the sensor heater. The gas surrounding the sensor determines  $k(T)$ , and thus the Temperature distribution in the system. See Fig. A1.

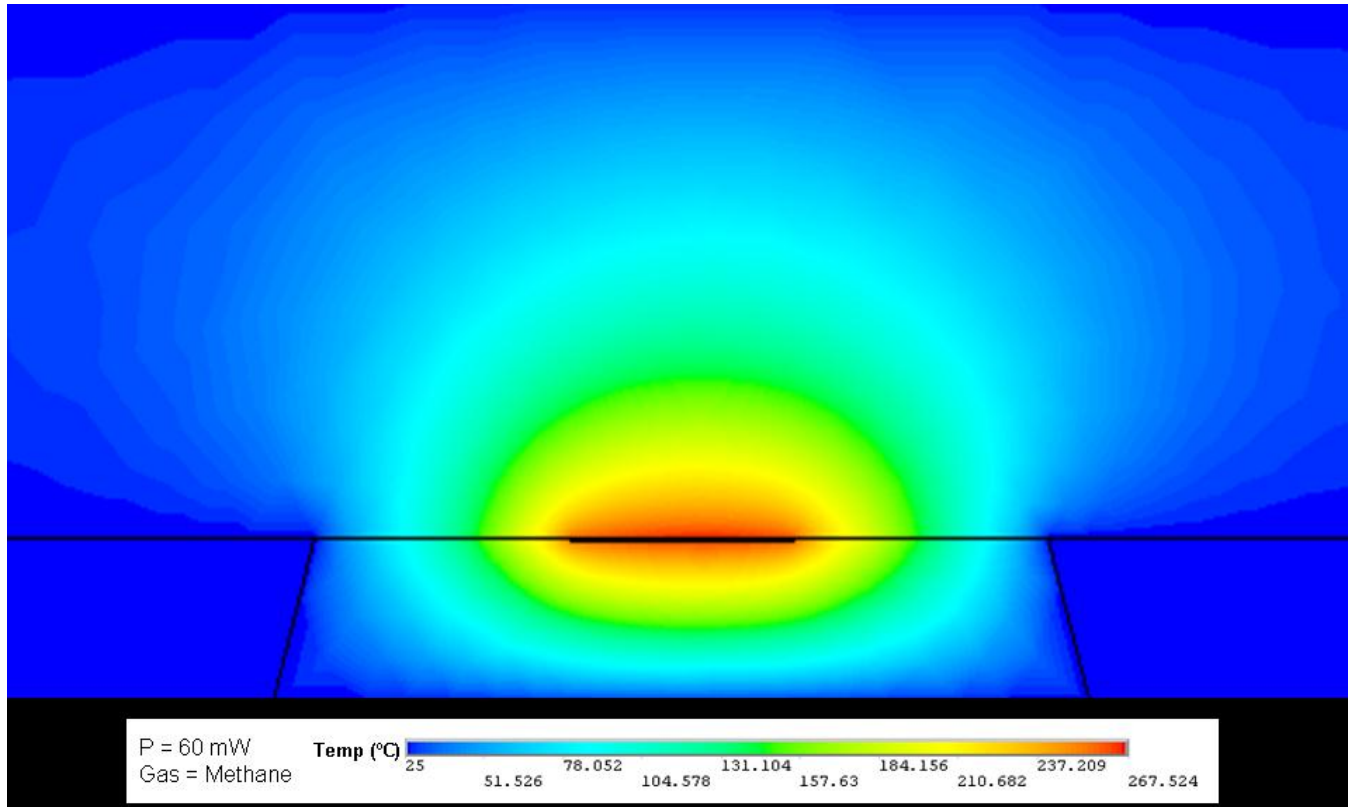


**Figure A.1 Cross-section of the simulated temperature distribution across the gas volume.** Graph has been obtained with ANSYS. Membrane width is 1500  $\mu\text{m}$ . It can be seen that about 1 mm above the hotplate there is almost no temperature change. The sensor measurement seems to be mainly affected by 1mm $^3$  of gas surrounding the hotplate.

Integration of  $\vec{q}$  flowing through the gas volume results in  $Q$ , the total heat flow, and  $\Delta T/Q$  is the total thermal resistance  $R_{th}$ .

Ambient temperature influence at the sensor output was described by equation (A6). In the previous section, reference to two estimation methods for the estimation of  $dV_o/dT_a$  was made. These two methods are described next.

Regarding the first method, it is assumed that the main contribution to the  $dV_o/dT_a$  derivative in equation (A6) is the term depending on the thermal conductivity of the gas  $dR_{th}/dT_a$ , an upper boundary for this derivative was calculated assuming that all the gas volume is isothermally set at temperature  $T_h$ , which is the maximum temperature occurring in any point of the gas volume in a real situation. Note that, curves of  $k(T)$  for natural gas mixtures are slightly curved upwards (see Figure 4.7) which means that variations of  $k$  with small temperature changes  $dk/dT$  are stronger at higher temperatures. For these reason assuming

that the whole gas volume is set at  $T_h$  renders an overestimation of  $dR_{th}/dT_a$  and  $dk/dT$ , which can be used to estimate an upper boundary for  $\mathcal{E}_{V_o}(Ta)$  (see equation A6), and greatly simplifies the calculations, as represented by equation (A9).

Once thermalization at  $T_h$  is assumed,  $k$  at  $T_h$ , or  $k(T_h)$ , is estimated from FEM simulations for two different ambient temperatures  $T_a$  resulting in two different  $k(T_h)$ . Then a difference between the two values  $\Delta k(T_h)$  is calculated by using currently accepted correlations for  $k(T)$  [Friend1989] and available online at the NIST webbook [NIST2011]. After that, a sensitivity  $\Delta V_o/\Delta k(T_h)$  is easily estimated from experimental data considering measurements of two different gas mixtures of (approximately) known  $k$  at the same measurement conditions. This procedure allows determination of inequation (A10).

$$\Delta k(T_h) > \int_{T_a}^{T_h} \frac{k(T)}{dT} dT \quad | \quad T_h > T_a \quad (A9)$$

$$\mathcal{E}_{V_o}(T_a) < \frac{\Delta V_o}{\Delta k(T_h)} \cdot \frac{\Delta k(T_h)}{\Delta T_a}; \quad (A10)$$

And this is the first estimation method providing an upper boundary for uncertainty  $\mathcal{E}_{V_o}(Ta)$ .

Despite errors in the available values for  $k$  due to the calculation method as discussed in section 4.4, it is considered that that represents mainly a bias in the experimentally determined  $k(T_h)$ , and so determination of  $\Delta k(T_h)$  is considered to be flaws by considerably smaller errors.

On the other hand, equation (A6) can be developed into equation A(11), by taking the derivative of (A1)

$$\mathcal{E}_{V_o}(T_a) = n \cdot S \cdot \mathcal{E}_T \left( \frac{dR_{th}}{dT_a} \cdot \frac{V^2}{R_h(T_h)} - \frac{R_{th}}{R_h(T_h)^2} \cdot TCR \right) \quad (A11)$$

Where  $T_h$  is the temperature at the heater, which in practice will be approximated by  $\Delta T + T_a$ .

Equation (A11) shows the influence of two terms, one resulting from variation of the thermal resistance of the dissipation path  $dR_{th}/dT_a$  and the other one due to the variation of the heater resistance with temperature  $dR_h/dT_a = TCR$ . It must be noted that inequation (A10) holds assuming that the first term dominates over the second one, or at least that influence of this second term is never as great as to invalidate the calculated upper boundary. This assumption is backed up by simulation results, hinting an overestimation of  $\mathcal{E}_{V_o}(Ta)$  in a factor of 2 for low temperatures, and of 1.5 for high ones.

The influence of ambient pressure has been estimated using the currently accepted correlations for thermal conductivity [49] and available online at the NIST webpage [44]. It is apparent from these

correlations that thermal conductivity sensitivity to expectable ambient pressure variations is orders of magnitude lower than to ambient temperature variations. The extremely small variations of thermal conductivity due to pressure changes in the 25 mbar range make the estimation of  $dV_o/dP_a$  sensible to the uncertainty in the values of thermal conductivity. Values provided in Table 3 for P noise in  $V_{out}$  have to be regarded as order of magnitude approximations, and the apparent anomalous behavior of the noise contribution is an artifact introduced by uncertainty in (and truncation of) the values of thermal conductivity used. For the purpose of this work, this noise source was neglected.

Laboratory variations of pressure and temperature have been measured and statistically evaluated for daily and monthly expected temperature variations. Values of 1°C and 3°C have been measured as conservative daily and monthly variations inside the laboratory. However, the large thermal mass and the partial tightness of the measurement chamber produce daily temperature variation smoothing to about 0.2 °C, this second value has been used in adding noise to simulation results, and provide a clear consistency with experimental observations. Typical pressure variations of 25 mbar have been considered. These values are used in the estimation of uncertainties provided in the results section.

### A.3 UNCERTAINTY SOURCES AFFECTING GAS MIXTURE COMPOSITION<sup>3</sup>

---

Uncertainty in the real composition of the measured gas has a critical effect in the calibration of all predicted values, since the composition is used to calculate all values using ISO6976 [ISO1995]. Precise determination of the composition of the mixture is in direct relation with the quality of the dataset used for calibration and test. Three different uncertainty sources can contribute to this effect, the first one is leaks or gas source contamination, which in results presented in chapters 4 and 5 relying on short measurements was determined to be negligible as the fluidic system was checked for leaks and it was assumed that gas bottles complied with the supplier's specifications. However results for static measurements presented in chapter 6, showed a slow drift over long times, which suggested the presence of a small leakage process. For this reason data analysis of results in chapter 6 relied on the first hours of the measurement.

The second uncertainty source is transient in the gas exchange dynamics inside the sensor chamber. The gas exchanging time was estimated analytically and confirmed empirically. A full (99.9%) replacement time  $t_{99.9}$  of around 5 min was estimated. Measurements presented in chapter 5 were performed with a conservative 11 min of gas exchange time in order to minimize the composition uncertainty due to gas exchanging dynamics.

---

<sup>3</sup> Y block

The third uncertainty source is the uncertainty in the MFC setpoints, which was estimated using uncertainty propagation and based on the manufacturer's specifications.

The concentration of component  $i$  can be expressed as a function of gas flows when the steady state is reached as:

$$x_i = \frac{f_i}{\sum_{j=1}^n f_j} \quad (\text{A12})$$

Where  $f_i$  is the flow rate of component  $i$  (in standard ml/min).

Uncertainty in each of the  $f_i$  flows is basically independent, thus uncertainty in the concentration can be expressed as:

$$dx_i = \sqrt{\frac{\partial x_i}{\partial f_1}^2 + \frac{\partial x_i}{\partial f_2}^2 + \dots + \frac{\partial x_i}{\partial f_n}^2} \quad (\text{A13})$$

Two different equations shall (A14) and (A15) be used for the partial derivatives by deriving equation (A12):

$$\frac{\partial x_i}{\partial f_i} = \frac{df_i}{\sum_{j=1}^n f_j} - \frac{f_i \cdot df_i}{\left(\sum_{j=1}^n f_j\right)^2} \quad (\text{A14})$$

Where the manufacturer uncertainty specification will be used as  $df_i$ . Proceeding similarly for  $j \neq i$  we obtain:

$$\frac{\partial x_i}{\partial f_{j \neq i}} = -\frac{f_i \cdot df_i}{\left(\sum_{j=1}^n f_j\right)^2} \quad (\text{A15})$$

Applying equations (A14) and (A15) to equation (A13) allows computation of uncertainties for each of the components in the synthetic natural gas mixture. Numerical results were already provided in the experimental setup section. However, these results rely completely on a datasheet manufacturer's specification and have not been empirically determined. Using this datasheet specification may have led to overestimation of the effective uncertainty, since it is common that in order to ensure that the MFC instruments lie within datasheet specification, their effective uncertainty is sensibly lower. This is a

possible explanation for the differences found in simulated and experimental SHV and W prediction error as reported in Table 5.4.

## APPENDIX B. LIST OF PUBLICATIONS

---

In chronological order, journal papers in black, conferences in grey, patent applications in blue, book chapters in brown:

1. Jose Bosch, **Sergi Udina**, Antonio Pardo, Xavier Cano, Santigao Marco, Electronic nose based on IEEE1451 standard, XXI Conference on Design of Circuits and Integrated Systems (DCIS 2006), 2006, Barcelona, Spain (Oral presentation)
2. R. Rubio, S. Udina, J. Santander, L. Fonseca, I. Gràcia, C. Cané, M. Moreno, and S. Marco, "Non-selective NDIR array for gas detection," presented at Eurosensors XX, Göteborg, Sweden, 2006 (Poster presentation)
3. Guillem Carles, **Sergi Udina**, Marc Salleras, Joaquín Santander, Luis. Fonseca, Santiago Marco, A micromachined thermoelectric sensor for natural gas analysis: Thermal model and experimental results, Proc. 13<sup>th</sup> International conference on Thermal, Mechanical and Multi-physics Simulation and Experiments in Microelectronics and Microsystems (Eurosime 2007), 2007, London, UK (Oral presentation)
4. Rafael Rubio, Joaquín Santander, Luis Fonseca, Neus Sabaté, Isabel Gràcia, Carles. Cané, **Sergi Udina**, Santiago Marco, Non-selective NDIR array for gas detection, Sensors and Actuators B: Chemical, 2007, 127, 69-73

5. **Sergi Udina**, Manuel Carmona, Guillem Carles, Joaquín Santander, Luis Fonseca, Santiago Marco, A micromachined thermoelectric sensor for natural gas analysis: Thermal model and experimental results, Sensors and Actuators B: chemical, 2008, 134, 551-558
6. **Sergi Udina**, Antonio Pardo, Santiago Marco, Joaquín Santander, Luis Fonseca, Thermoelectric MEMS Sensors for Natural Gas Analysis, Proc. IEEE sensors 2008 conference, 2008, Lecce, Italy. (Oral presentation)
7. **Sergi Udina** and Santiago Marco, Método y sistema para la determinación del poder calorífico de un gas combustible constituido por más de dos componentes, PCT Patent application: WO2009/106661 A1
8. Jordi Fonollosa, Bernard Halford, Luis Fonseca, Joaquín Santander, **Sergi Udina**, Mauricio Moreno, Jürgen Hildenbrand, Jürgen Wöllensteine, Santiago Marco, Ethylene optical spectrometer for apple ripening monitoring in controlled atmosphere store-houses, Sensors and Actuators B: Chemical, 2009, 546–554.
9. L. Fonseca, R. Rubio, J. Santander, N. Sabaté, P. Ivanov, E. Figueras, I. Gracia, C. Cané, **S.Udina**, M. Moreno, S. Marco, Qualitative and quantitative substance discrimination using a CMOS compatible non selective NDIR microarray, Proc. 12<sup>th</sup> International meeting on Chemical Sensors, 2008, Columbus, USA (Oral presentation)
10. L. Fonseca, R. Rubio, J. Santander, C. Calaza, N. Sabaté, P. Ivanov, E. Figueras, I. Gràcia, C. Cané, **S. Udina**, M. Moreno, S. Marco, Qualitative and quantitative substance discrimination using a CMOS compatible non-specific NDIR microarray, Sensors and Actuators B: Chemical, 2009, 141, 396-403

11. **Sergi Udina** and Santiago Marco, Método y sistema para la determinación del flujo energético de un gas combustible constituido por más de dos componentes, PCT Patent application: WO2011/012758 A2
12. Manuel Carmona, Carlos Calaza, **Sergi Udina**, Modeling of micromachined thermoelectric gas sensors, Book chapter to be published in "Chemical Sensors: Simulation and Modeling".
13. **Sergi Udina**, Manuel Carmona, Antonio Pardo, Carlos Calaza, Joaquín Santader, Luis Fonseca, Santiago Marco, A micromachined thermoelectric sensor for natural gas analysis: Multivariate calibration results, Sensors and Actuators B: Chemical, In Press, Corrected Proof, Available online 1 March 2012
14. **Sergi Udina**, Jose Bosch, Carlos Calaza, Antonio Pardo, Santiago Marco, A MEMS compact natural gas analyzer implementing IEEE-1451.2 and BS-7986 smart sensor standards, 2012 International Meeting on Chemical Sensors, to be held May 2012, Nüremberg, Germany.  
(Poster presentation)

---

## APPENDIX C. RESUM EN CATALÀ

---

# ÍNDEX

## C1 INTRODUCCIÓ

C1.1 Introducció als sensors intel·ligents.....	4
C1.2 Sensors químics.....	5
C1.3 Estàndards de sensors intel·ligents.....	6
C1.4 Perspectives per als sensors sensors intel·ligents .....	7

## C2 APLICACIÓ: CONTROL DE QUALITAT DEL GAS NATURAL

C2.1 La importància del gas natural i el seu control de qualitat.....	8
C2.2 Instruments i tècniques per al control de qualitat del gas natural.....	9
C2.3 Selecció d'una tecnologia de sensat.....	11

## C3 OBJECTIUS

C7 Objectius.....	12
-------------------	----

## C4 ESTUDI D'UN MICROSENSOR TERMOELÈTRIC PER ANÀLISI DEL GAS NATURAL

C4.1 Descripció del sensor .....	13
C4.2 Simulació.....	14
C4.3 Resultats i validació de la simulació .....	16

## C5 CALIBRACIÓ MULTIVARIANT

C5.1 Mètode.....	17
C5.2 Resultats.....	19

C5.3 Estimació de límits en la precisió del sensor.....	21
---	----

---

## C6 DISSENY DE SENSORS QUÍMICS INTEL·LIGENTS: EL PROTOTIP D'ANALITZADOR DE GAS NATURAL

---

C6.1 Disseny de l'Instrumentació electrònica .....	22
C6.2 Implementació combinada de IEEE-1451.2 i BS-7986.....	23
C6.3 Comunicacions.....	25
C6.4 Experimental.....	26

---

## C7 CONCLUSIONS

---

C7 Conclusions.....	29
---------------------	----

# C1 INTRODUCCIÓ

## C1.1 INTRODUCCIÓ ALS SENSORS INTEL·LIGENTS

Les noves tecnologies de micromecanitzat i nous desenvolupaments en tecnologia electrònica i microelectrònica han portat a una nova generació de sensors típicament denominats *sensors intel·ligents*. Aquest terme és però d'utilització ambigua a la literatura [KoFung1982, IEEE1997, Song2008, Henry1993, Karatzas2007] ja que pot referència a diferents funcionalitats avançades d'un sensor. En general s'accepta que un sensor intel·ligent és bàsicament un sensor que fa "quelcom més" que un sensor tradicional. Aquest "quelcom més" es pot descriure en general com algun dels casos de la figura 1.1.

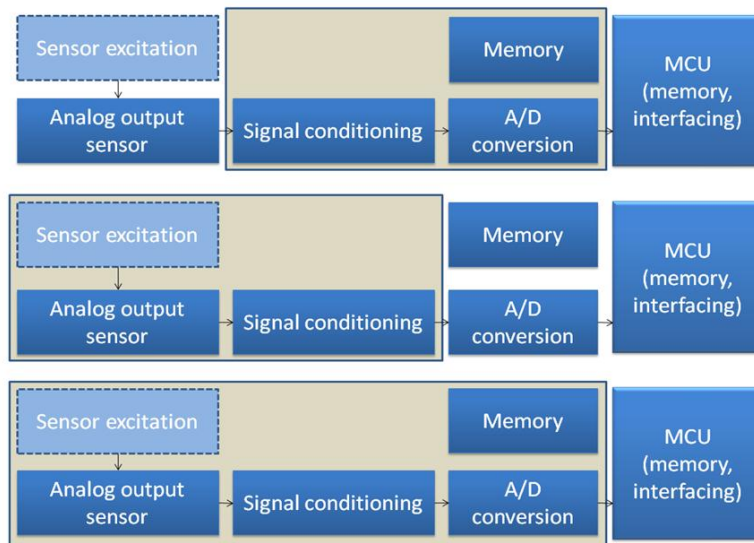


**Figura 1.1 Possibilitats d'integració en un sensor intel·ligent**

Existeixen diverses implementacions comercials de sensors intel·ligents, però hi ha una gran dispersió en l'ús de xarxes i interfícies que sovint implica esforços recurrents en el disseny d'aquests sensors.

Per tal de millorar aquesta situació s'han anat difonent diferents estàndards que prenenen simplificar i donar unitat i coherència al disseny de sensors intel·ligent. Dos dels més interessants son la família d'estàndards IEEE-1451 i el BS-7986 [IEEE1997, Song2008, BSI2005]. Aquests dos estàndards cobreixen aspectes ben diferents del disseny de sensors intel·ligents com es descriu en la secció C1.3.

Els sensors químics mereixen una especial consideració dins els sensors intel·ligents, degut a un nombre de particularitats que es descriuen a continuació.

## C1.2 SENSORS QUÍMICS

Un sensor químic és un sensor que transforma informació química en una senyal analíticament útil. Aquesta senyal útil pot originar-se per una reacció química de l'analit o per una propietat física del sistema mesurat [Hulanicki1991].

En general es distingeixen dues parts en un sensor químic, la part receptora del sensor que interacciona directament amb l'analit, i la part transductora que transforma aquesta interacció en la senyal [Hulanicki1991]. Els transductor en sí mateix no proporciona selectivitat. La part receptora del sensor es pot basar en diferents principis, donant lloc a diferents tipus de sensors químics tal com es pot apreciar a la figura 1.2.

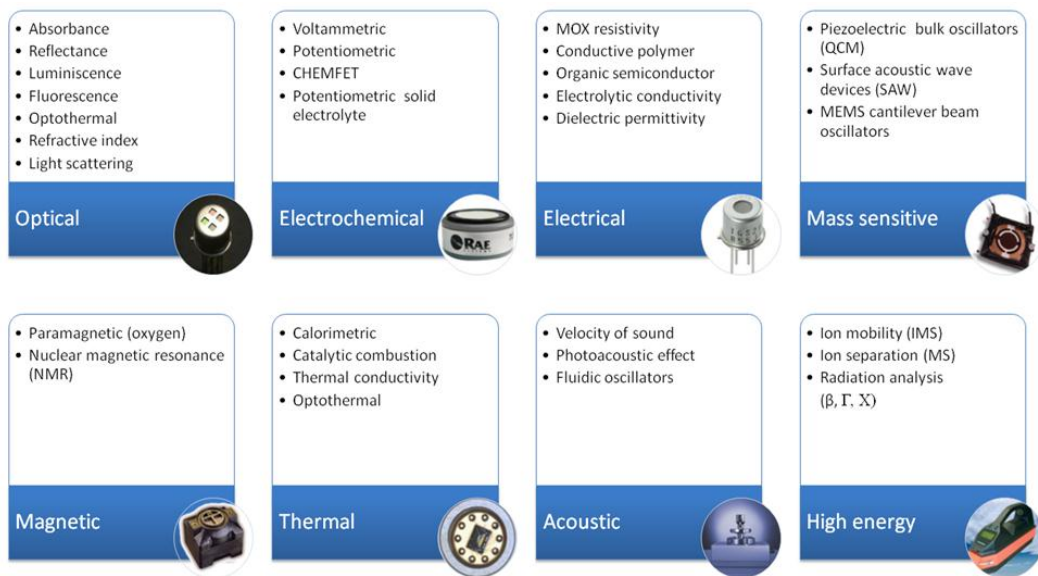


**Figura 1.2 Una possible classificació per als sensors químics**

Els sensors químics son sovint sensibles a una gran quantitat de factors interferents, fet que fa que les tècniques basades en un sol sensor selectiu per mesurar un analit d'interés com ara a [Janata1989, Janata2001, Gopel1991, Hierlemann2007], tal com es fa en altres camps de la instrumentació siguin en alguns casos poc adequades. Aquesta particularitat del camp del sensat químic va motivar una línia de recerca cap a les matrius de sensors inespecífics, els nassos electrònics que conceptualment van iniciar-se al 1982 amb el treball de Persaud et al.

[Persaud1982]. Aquestes característiques complexes dels sensors químics els fan candidats particularment interessants per al disseny de sensors intel·ligents.

### C1.3 ESTÀNDARDS DE SENSORS INTEL·LIGENTS

Els sensors intel·ligents poden implementar diverses característiques avançades com ja s'ha comentat prèviament. L'orígen dels estàndards de sensors intel·ligents cal buscar-lo en la recerca d'evitar esforços recurrents en el disseny de sensors intel·ligents. Per aquest propòsit, l'IEEE i el NIST varen editar la família d'estàndards IEEE-1451. La figura 1.2 presenta un resum dels diferents estàndards de la família, la seva data d'edició, el tipus d'interfície que defineix i el seu estat actual.

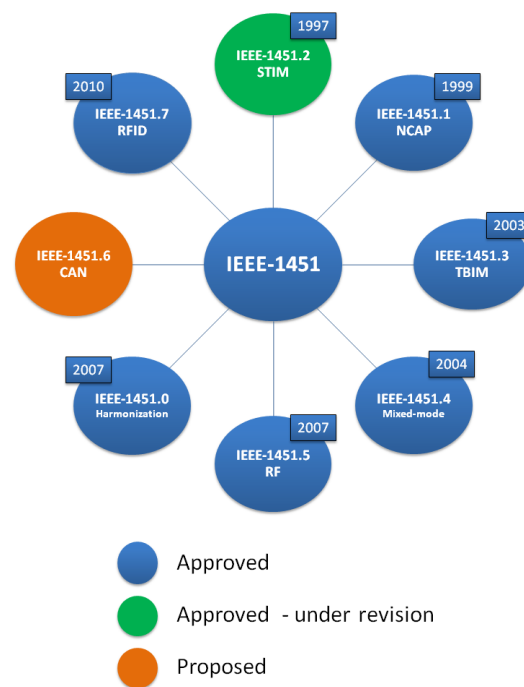


**Figura 1.3 Família d'estàndards IEEE-1451**

En aquesta família d'estàndards es defineix una partició entre un mòdul transductor anomenat STIM o TIM (Smart Transducer Interface Module) i el mòdul encarregat de l'execució d'aplicacions i de les comunicacions a xarxa d'alt nivell, el NCAP (Network Capable Application Processor).

La definició inicial del IEEE-1451.2 es referia a la connexió punt a punt cablejada entre un STIM i el NCAP. Posteriorment es van anar definir diferents formes de comunicació entre STIM i NCAP. La figura 1.4 mostra un diagrama de blocs del contexte definit per IEEE-1451.2.

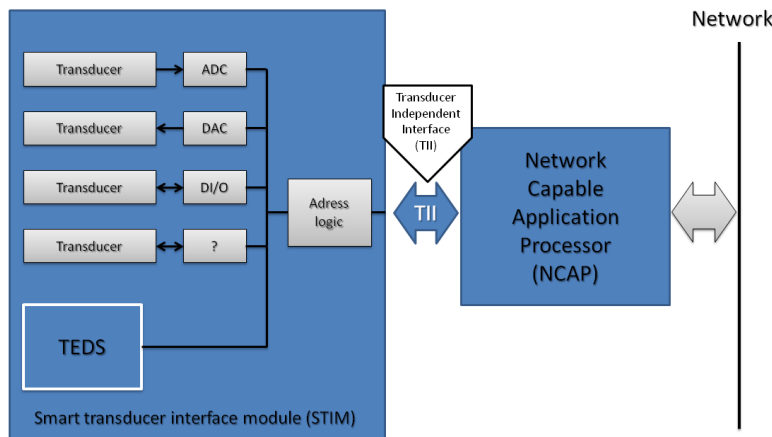


**Figura 1.4 Diagrama de blocs del contexte definit per IEEE-1451.2**

Per altra part, el British Standards Institute (BSI) va recollir els conceptes de sensors autovalidants (SEVA) proposats per Henry i Clarke el 1993 [Henry 1993] en format de standard [BSI2005] per a la seva aplicació generic a la autoavaluació dels sensors en quant a estat operacional i qualitat de les seves mesures. Aquesta mètrica de la qualitat del sensor pretén facilitar el manteniment del sensor, habilitar en formats estàndar la autocorrecció de mesures i minimitzar la possibilitat d'errades en el control de processos. Aqueta autoavaluació principalment en dos variables principals:

- El Valor validat (VV) que es la quantitat d'interés be mesurada o be estimada mitjançant correcció d'errors, i
- La incerteza validada (VU) que és una estimació de l'error present en el valor validat.

Ambdos valors s'acompanyen sempre d'un byte de status que proporciona informació sobre el mètode de generació de VV i VU, així com possibles errades en el sistema.

## C1.4 PERSPECTIVES PER ALS SENSORS INTEL·LIGENTS

La ambigüitat en el terme *sensor intel·ligent* fa que sigui difícil de dir si el terme tindrà èxit en la denominació de les futures generacions de sensors. En el context actual l'ús precís d'aquest terme es troba fortament lligat a l'ús de estàndards, i particularment al IEEE-1451. És possible que tal com ha passat amb el terme SEVA, altres terminologies s'acabin emprant per a descriure més específicament perquè el sensor és intel·ligent.

Més enllà de consideracions semàntiques, el camí a recórrer en la millora de les tecnologies de sensat és enorme. L'explotació de la redundància hardware i de correlacions en sistemes multisensor que conformen redundàncies analítiques ofereixen enormes possibilitats de futur que asseguraran l'interés de la comunitat de recerca en intstrumentació.

És difícil imaginar un futur no els busos de camp industrials siguin substituïts per interfícies IEEE-1451. És probable que el IEEE-1451 trobi paulatinament aplicacions i mercats, probablement en les xarxes de sensors més modernes in en particular en les definicions IEEE-1451.5 i 1451.7 per a comunicacions sense fils. Tot i així l'experiencia fins a la data en els mercats industrials indica que aquest serà un procés lent i que només assolirà una autèntica difusió si alguna gran companyia del camp de la instrumentació aposte per ella.

En la meva opinió, és possible que SEVA tingui una evolució diferent. A pesar de que la recerca ha emprat SEVA escadusserament, aquest tipus d'estratègia és altament compatible i independent de les diferents interfícies. El cost d'implementació també és menor el que fa que sigui possible que SEVA trobi aplicació amplia en els camps, per exemple, mèdics i de seguretat.

## C2 APLICACIÓ: CONTROL DE QUALITAT DEL GAS NATURAL

### C2.1 LA IMPORTANCIA DEL GAS NATURAL I EL SEU CONTROL DE QUALITAT

El gas natural és actualment la tercera font d'energia en importància [IEA2009]. L'alta disponibilitat de fuels fòssils, i una indústria d'explotació madura en fan una font d'energia comercialment atractiva. Tanmateix, les propietats del gas natural poden variar fortament en funció del seu orígen, fet que fa que calgui mesurar acuradament les seves propietats en diferents aplicacions com ara durant les transaccions comercials del gas, el seu emmagatzemament, i en el control de processos, motors, cremadors i combustió en general. En aquestes aplicacions la mesura del poder calorífic, densitat, factor de compressibilitat, index de Wobbe o nombre de metà entre d'altres, és necessària. A continuació es descriuen breument dues d'aquestes propietats d'interès:

**Poder calorífic:** És una mesura del contingut energètic del gas. En concret la quantitat de calor despesa per la combustió d'un volum unitari ( $m^3$  estàndard en unitats del SI). El poder calorífic té un rang de variació típic d'entre 33 i 44 MJ/ $m^3$  [IEA2010].

**Index de Wobbe:** És un indicador de la intercanviabilitat d'un gas amb altre en màquines operades a gas. Es calcula com el quotient entre poder calorífic superior i l'arrel quadrada de la densitat relativa del gas. Per a gas natural té un rang de variació típic d'entre 39 a 56 MJ/m<sup>3</sup>.

La taula C2.1 recull variacions típiques del poder calorífic del gas natural per a diferents països segons la agència internacional de l'energia [IEA2010].

TAULA C2.1. VALORS TÍPICS DEL PODER CALORÍFIC PER A DIFERENTS PAISOS [IEA2010]	
COUNTRY	CALORIFIC VALUE (MJ/m <sup>3</sup> )
United States	38.267
Russian federation	37.578
Canada	38.320
Iran	39.356
Norway	39.720
China	38.931
Qatar	41.400
Algeria	42.000
Netherlands	33.339
Indonesia	40.600

## C2.2 INSTRUMENTS I TÈCNIQUES PER AL CONTROL DE QUALITAT DEL GAS NATURAL

Diverses tècniques i instruments han estat proposats per a la mesura del poder calorífic del gas natural, que és la propietat més important per al control de qualitat del gas [Ulbig2001]. Podem distingir tres grans generacions d'instruments. En primer lloc els primers instruments en ser emprats van ser els calorímetres de combustió [Ulbig2001], en segon lloc els cromatògrafs de gasos de procés [Stufkens1975] que substituiren en bona mesura els calorímetres de combustió, i finalment una última generació recent d'instruments més ràpids i de més baix cost que s'ha anat progressivament introduint a la indústria i que podem denominar instruments basats en mètodes correlatius [Schley2001].

Són de particular relevància per aquesta tesi les característiques dels cromatògrafs de procés i dels citats mètodes correlatius. La Figura C2.1 mostra un esquema del principi de funcionament d'un cromatògraf de procés.

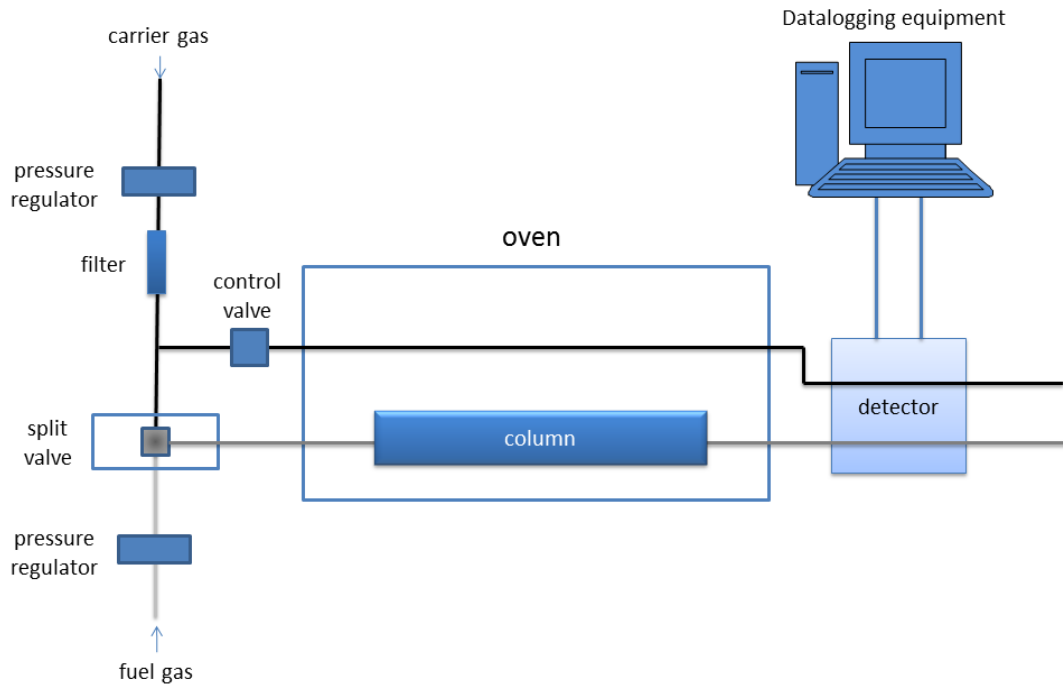


**Figura C2.1 Principi de funcionament d'un cromatògraf de procés**

Actualment els cromatògrafs de procés són la tecnologia més freqüent i establerta en l'anàlisi del gas natural, tot i que el seu elevat cost de manteniment i la necessitat d'operaris qualificats així com un alt cost d'adquisició van motivar l'aparició de nous mètodes.

Els mètodes correlatius prenenen donar resposta a les limitacions de la cromatografia de procés. Aquests es basen en la mesura d'un nombre de magnituds físiques que després son correlacionades amb la composició i propietats del gas [Schley2001]. La tria d'aquestes propietats mesurades ha estat ben diversa en les diferents propostes existents, donant lloc a un bon nombre de dispositius tal com recull la taula C2.2. En aquesta taula s'hi pot una revisió de diferents instruments basats en mètodes correlatius, i hi apareixen les característiques principals dels mateixos. Alguns d'ells només han estat prototips de laboratori metre que d'altres es comercialitzen actualment amb relatiu èxit. Cal dir que per ara la substitució dels cromatògrafs de procés per instruments basats en mètodes correlatius sembla llunyana degut sobretot a l'alt conservadurisme del sector.

TAULA C2.2 REVISIÓ DE MÉTODES CORRELATIUS I ALTERNATIUS PER ANÀLISI DE GAS NATURAL

Nº	DEVICE	DEVELOPED BY	INPUTS	OUTPUTS	UNCERTAINTY $\Delta H_s(\%)$	STATUS	RESP. TIME
1	<b><math>\epsilon</math> method</b>	Rurhgas AG / Gasunie	$\epsilon, V_s, X_{CO_2}, P, T$	$H_s, H_b, W, \rho_n, X_{CO_2}$	0.2	Lab prototype	-
2	<b>IR Spectrometer</b>	FlowComp	$A_{IR}(CH), A_{IR}(CO_2), P, T$	$H_s, H_b, W, \rho_n, X_{CO_2}$	0.2	Lab prototype	-
3	<b>2VOS-meter</b>	Gasunie/Instromet	$V_s(HP), V_s(LP), A_{IR}(CO_2), T, P$	$H_s, H_b, W, \rho_n, X_{CO_2}$	0.3	Available	4 s
4	<b>WOM 2000</b>	RMG	$C_p, Th, \eta, P, T$	$H_s, H_b, W, \rho_n$	1.0	Relegated	28s
5	<b>EMC 500</b>	RMG	$C_p, Th, \eta, P, T, A_{IR}(CO_2)$	$H_s, H_b, W, \rho_n, X_{CO_2}$	0.5	Available	<60 s
6	<b>GasPT / GasPT2</b>	Advantica	$V_s, Th(T1), Th(T2), T, P$	$H_s, H_b, W, \rho_n, MN$	0.5	Available	(2 s) 50 s
7	<b>Gas-lab Q1</b>	Ruhrgas AG, FlowComp	$Th, A_{IR}(CH), A_{IR}(CO_2), T, P$	$H_s, H_b, W, \rho_n, X_{CO_2}, MN$	0.4	Available	15 s
8	<b>MN microsensor</b>	Ikerlan	$Th$	$MN$	-	Lab prototype	30 min
9	<b>ANGus</b>	Itron	$Th, A_{IR}(CO_2), T, P$	$H_s, H_b, W, \rho_n, X_{CO_2}, MN, SG$	1.0	Available	2 min
10	<b>Laboratory setup</b>	CRPE research centre (Rahmouni et al.)	$Th(T1), Th(T2), T$	$H_b, W, AFR$	1.0	Lab prototype	-
11	<b>Laboratory setup</b>	CRPE research centre (Loubar et al.)	$Th(T1), Th(T2), V_s, X_{CO_2}, T$	$H_s, W, AFR$	0.5	Lab prototype	-

$\epsilon$ : relative permittivity;  $A_{IR}$ : infrared absorption;  $V_s$ : velocity of sound;  $C_p$ : heat capacity;  $Th$ : Thermal conductivity;  $\eta$ : viscosity;  $x$ : molar fraction;  $H_s$ : superior calorific value;  $H_b$ : inferior calorific value;  $W$ : Wobbe index;  $\rho_n$ : normal density;  $MN$ : Methane number;  $SG$ : Specific gravity;  $AFR$ : Air-fuel ratio;  $T$ : Temperature;  $P$ : Pressure

## C2.3 SELECCIÓ D'UNA TECNOLOGIA DE SENSAT

Un cop evaluats els diferents mètodes existents per a l'anàlisi del gas natural, s'estudia la idoneitat de les diferents tecnologies de sensat de gasos per al disseny d'un prototip intel·ligent d'analityador de gas natural. Es valoren diferents criteris per a la selecció de la tecnologia, que es troben recollits a la taula C2.3, però concretament es prioritza la estabilitat de la tecnologia sensora en el temps, que permet minimitzar la necessitat de calibracions, la rapidesa de l'anàlisi, que permet una precisió efectiva major en la monitorització de propietats i el seu us en control de processos crítics, i una estructura compacta i de baix cost que permeti l'elaboració de sondes de relatiu baix cost que puguin operar en línia amb la canalització de gas. Aques aspectes es troba en bona part lligat a la utilització de tecnologia de microsistemes (MEMS).

TAULA C2.3 AVALUACIÓ DE TECNOLOGIES DE SENSORS DE GASOS PER A L'ANÀLISI DE GAS NATURAL

Cost	MEMS fabrication		Response time	In-pipe measurement	Time stability	Operative		Setup complexity	rank
						Without oxygen	A		
PY	A	A	C	B	D	A	A	A	6
QMB	B	C	A	A	A	A	A	A	2
EC	B	D	C	A	B	D	B	B	8
PA	B	B	A	A	A	A	B	B	3
NDIR	B	B	A	C	A	A	C	C	5
PEL	A	B	B	C	C	E	D	D	11
FO	C	C	A	A	A	A	C	C	4
TS	B	A	B	A	A	A	A	A	①
MOX	B	A	C	B	D	E	A	A	10
VS	C	C	A	D	A	A	C	C	7
MO	B	C	A	C	A	A	B	B	8
DP	D	D	B	D	C	A	C	C	9

A: optimal B: good C: average D: below average E: bad (may rule out the technology for the considered application)

Technology abbreviations: **MOX**: metal oxide sensors; **TS**: thermal sensors; **FO**: fiber optic sensors; **NDIR**: infra-red sensors; **PA**: photoacoustic sensors; **EC**: electrochemical sensor; **QMB**: quartz microbalance sensors (uncoated); **PY**: conducting polymer sensors; **VS**: velocity of sound sensors; **MO**: microfluidic oscillators; **DP**: dielectric permittivity sensors

## C3 OBJECTIUS

Aquesta tesi té dues línies bàsiques de recerca que conformen els objectius. El primer conjunt d'objectius està relacionat amb el disseny de sensors intel·ligents.

- El disseny d'un sensor químic intel·ligent amb una estructura de dades òptima, que permeti servir de disseny de referència per a futures implementacions de sensors químics intel·ligents.
- En línia amb el primer, la combinació dels estàndards IEEE-1451.2 i BS-7986 en un mateix sensor, que permeti al sensor disposar de totes les característiques avançades ofertes per aquests estàndards, com ara l'autoavaluació de l'estat operacional i la qualitat de les

mesures, la autoidentificació del sensor a una xarxa, l'emmagatzematge de paràmetres de calibració i identificació en el propi sensor i la millora en el manteniment del sensor, així com demostrar la possibilitat d'implementar tasques avançades de detecció i correcció de mesures.

Un segon conjunt d'objectius sorgeix de la tria de l'aplicació concreta de l'anàlisi del gas natural:

- La implementació d'un prototip compacte, basat en tecnologia MEMS que ofereix bones prestacions d'anàlisi a baix cost.
- La selecció d'una tecnologia sensora adient, estable i ràpida per a la mesura.
- La selecció d'un processat de dades adient per al sensor.
- La determinació dels límits en la precisió del sensor i el processat de dades emprat.
- La implementació d'un prototipus operatiu d'analitzador que demostri l'aplicabilitat dels conceptes desenvolupats.

---

## C4 ESTUDI D'UN MICROSENSOR TERMOELÈTRIC PER ANÀLISI DEL GAS NATURAL

---

### C4.1 DESCRIPCIÓ DEL SENSOR

---

D'acord amb el treball previ realitzat en la selecció de la tecnologia sensora, es decideix seleccionar un sensor termoelèctric per a la mesura del gas. Aquest tipus de sensor es basa en una configuració de tipus *plataforma tèrmicament aillada* comuna en sensors d'infrarroig [Calaza2003a] o bé en microcalorimetria[Minakov2006]. En aquest tipus de sensors trobem una part central tèrmicament aillada per una fina membrana de nitru de silici que conté un calefactor i les unions calentes dels termoparells com es pot apreciar a la figura C4.1

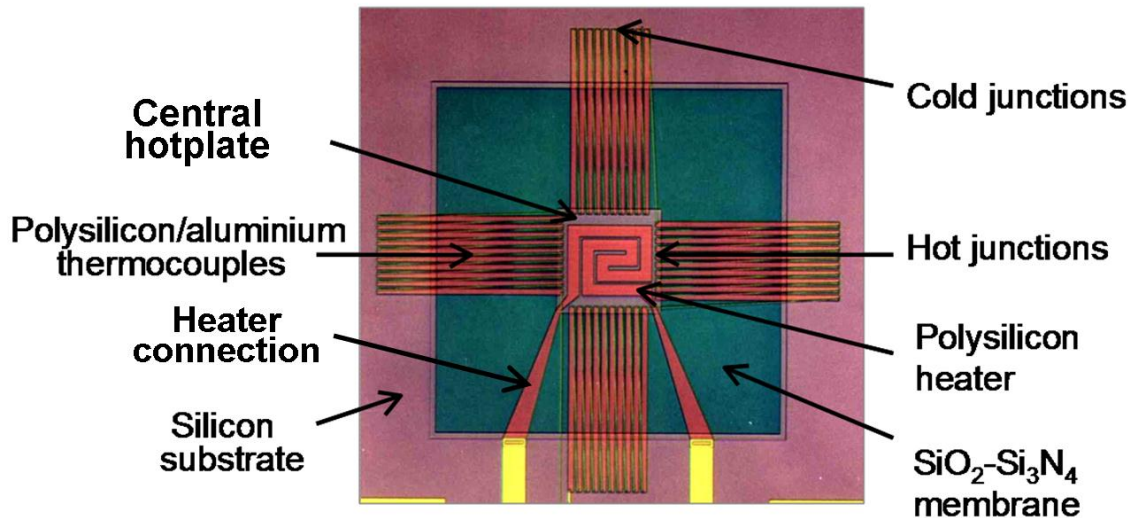


**Figura C4.1 Fotografia de la part activa del sensor termoelèctric (vista superior)**

La membrana de nitrur (que apareix en verd) té una extensió de 1,5 mm x 1,5 mm. La plataforma central on es trova el calefactor té una mida de 0,45 x 0,45 mm. El dispositiu presenta 10 termoparells a cada costat del quadrat que conforma la plataforma central. Les unions fredes dels termoparells reposen sobre el cos principal de silici, que actua com a pou de calor per mantenir les unions a temperatura ambient. D'aquesta manera la sortida en tensió del sensor proporcionada pels termoparells és funció de la diferència de temperatura entre unions fredes i unions calentes, donant una bona mesura de la temperatura de la plataforma calefactada central.

## C4.2 SIMULACIÓ

Per tal d'estudiar inicialment la idoneitat del sensor, es realitza una simulació per elements finits del comportament esperat del mateix. Per aquestes simulacions es realitza un model físic del dispositiu, que es pot veure a la figura C4.2 i un model matemàtic, una correlació entre la composició del gas natural (que es la nostra variable d'entrada a la simulació) i la conductivitat tèrmica en funció de la temperatura del gas natural corresponent a aquella composició.

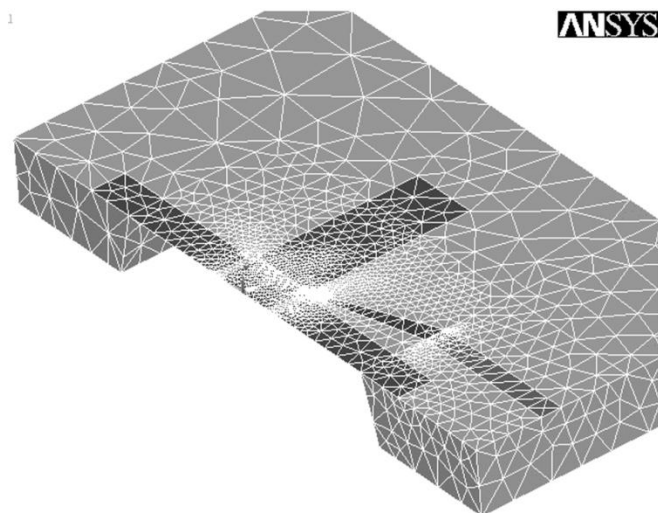


**Figura C4.2 Vista geomètrica del model d'elements finits (FEM). El volum de gas s'ha suprimit per major claredat.**

Aquesta correlació entre la composició del gas i la seva conductivitat tèrmica no és trivial, ja que no hi ha una equació exacta per al seu càlcul, i s'han emprat les correlacions de l'equació de Wassiljewa per obtenir els valors [Poling2001]. En general la dependència de la conductivitat tèrmica amb la temperatura per a cada component principal del gas natural és diferent, com es pot veure a la figura C4.3. Aquest principi és el que es pretén emprar per a poder analitzar el gas natural amb aquest únic microsensor com s'explica més endavant. Les simulacions consisteixen en excitar el calefactor del sensor a diferents potències i veure com canvia la resposta del sensor per a cada potència i per a cada composició diferent del gas natural. Es calculen set graons diferents corresponents a entre 3 i 9 volts de tensió del calefactor.

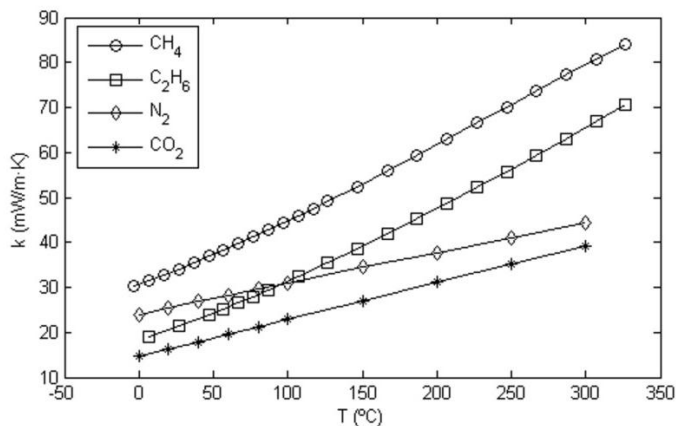


**Figura C4.3 Dependència de la conductivitat tèrmica amb la temperatura per a quatre components principals del gas natural.**

### C4.3 RESULTATS I VALIDACIÓ DE LA SIMULACIÓ

Es van realitzar simulacions amb dos conjunts de dades diferents, en primer lloc simulacions en aire emprant valors tabulats de conductivitat tèrmica  $k(T)$ [Stephan1985] i en segon lloc 21 composicions diferents de gasos naturals simulats. Posteriorment es realitzen mesures experimentals per tal de validar els resultats d'aquestes simulacions. Per a fer-ho es dissenya una estació de mesura de gasos que permet sintetitzar mesclades de gasos naturals de diferents composicions com es veu a la figura C4.4.

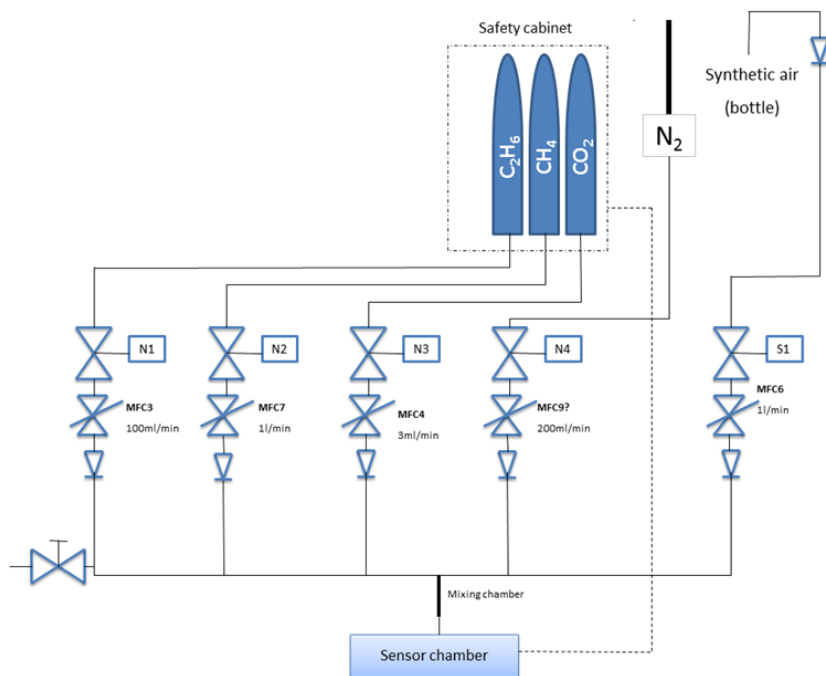


**Figura C4.4 Esquema fluïdic de la estació de síntesi de gasos naturals.**

Un cop fetes les mesures es comparen els resultats experimentals amb els de simulació, obtenint un acord bo, tal com es pot veure a la figura C4.5. El bon acord en els resultats fonamenta l'estudi preliminar de la sensibilitat del sensor respecte canvis en la composició del gas natural que es fa posteriorment. Els resultats d'aquest estudi preliminar encoratgen la investigació de mètodes multivariants de calibració per tal d'extreure la informació sobre les propietats del gas mesurat de la resposta del sensor. Aquesta qüestió es discuteix en l'apartat següent.

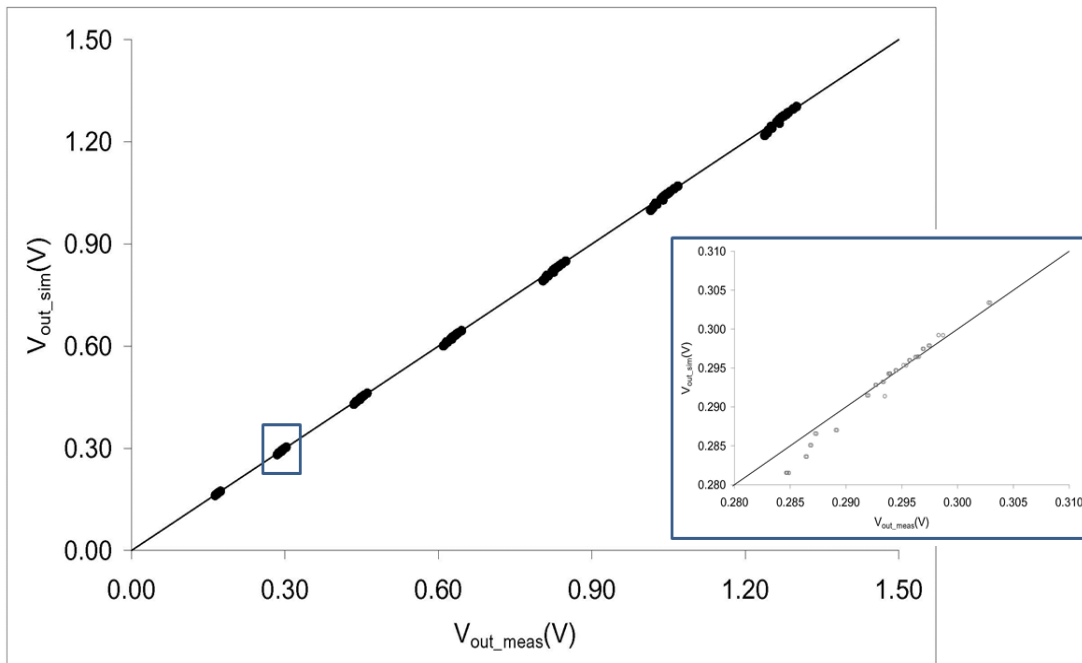


Figura C4.5 Comparació entre els resultats experimentals i simulacions. El detall mostra una ampliació d'un dels graons de potència corresponent a 4V de tensió de calefactor.

## C5 CALIBRACIÓ MULTIVARIANT

### C5.1 MÈTODE

En l'anàlisi presentat es van emprar dos conjunts de dades, un conjunt de resultats experimentals obtinguts en condicions de laboratori, i un conjunt complementari de dades obtingudes mitjançant els models de simulació. Les dades experimentals es van emprar per estimar la precisió de les estimacions del sensor, i les dades simulades es van emprar per a una millor estimació dels límits esperats en la precisió del sensor.

En quant als experiments, el sensor es va excitar amb una font de tensió programable HM8142 (Hameg instruments, Alemanya) s'empra per generar un tren de tensions que s'apliquen al calefactor del sensor per obtenir una lectura proporcional a les diferents temperatures, tal com es pot veure a la figura 5.1.

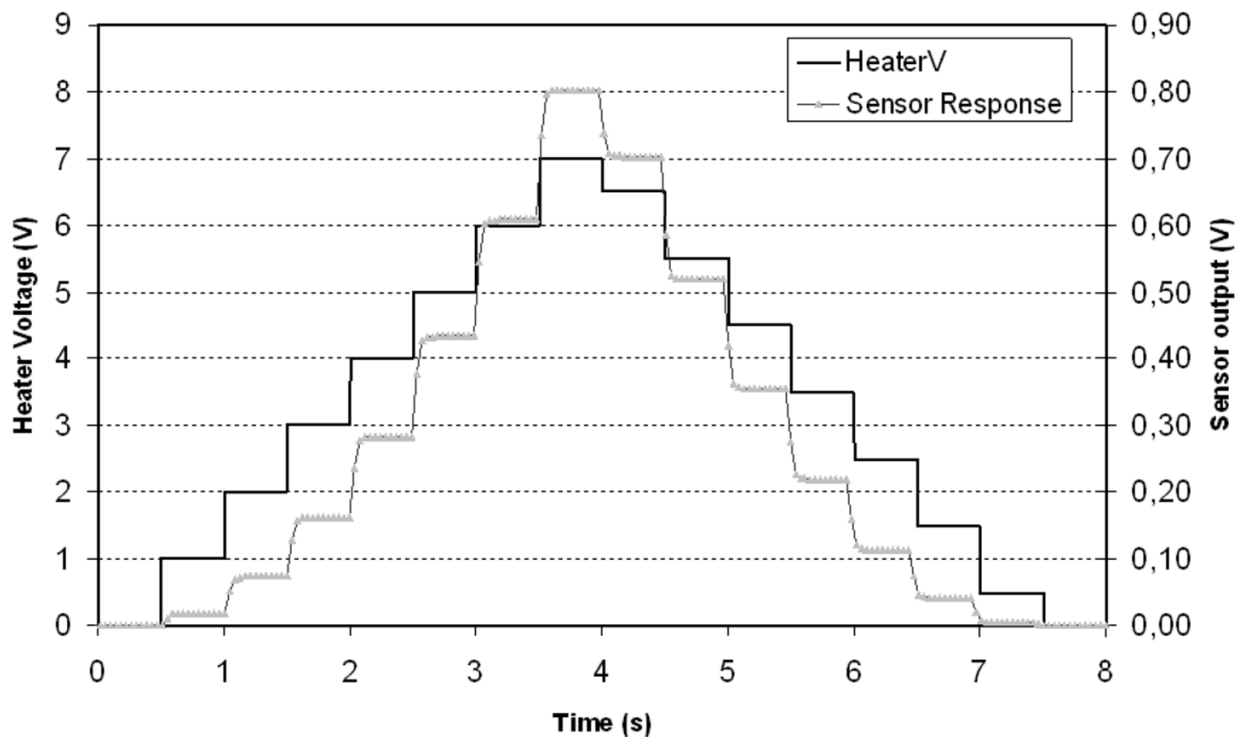


**Figura C5.1 Gràfica de la tensió d'excitació del calefactor i la tensió de sortida del sensor. La línia negra es llegeix a l'eix de l'esquerra mentre que la línia gris es llegeix a l'eix de la dreta.**

El conjunt de punts emprat per calibració i validació es mostren a la taula 5.1 (veure cos de la tesi). En total hi ha 20 punts per a calibració i 18 punts per a validació. Es treballa amb dos conjunts separats (hold out) per maximitzar la fiabilitat de la validació.

Per tal de calibrar el sensor es va optar d'acord amb els resultats mostrats en l'apartat C4, per un mètode de calibració multivariant. D'entre els diferents mètodes disponibles, es tria el Partial Least Squares (PLS) [Geladi1986] per raons d'escalabilitat, aplicabilitat i pel seu bon comportament en senyals altament correlades.

A més dels resultats de la precisió obtinguda per la calibració, calculada amb el conjunt de validació corresponent al conjunt de dades experimental, es realitza un estudi dels límits de precisió assolibles. Per aquest estudi s'empren dades simulades, amb l'addició de soroll sintètic estimat de les diferents fonts d'error presents al sistema.

## C5.2 RESULTATS

La gràfica C5.2 mostra els resultats de les prediccions calculades emprant la calibració obtinguda amb PLS contra els resultats esperats, per a sis diferents propietats del gas natural. A la gràfica s'hi mostren els conjunts experimentals de calibració i validació. Les propietats calculades son la concentració de Metà, d'Età i de Nitrògen i per altra banda la densitat, l'índex de Wobbe i el poder calorífic superior. També s'intenta calibrar la concentració de Diòxid de carboni però sense èxit, aparentment la informació corresponent a aquest component que es troba en concentració relativament baixa, rau per sota del nivell de soroll del nostre sistema.

Per a les propietats que si que es poden predir adequadament, la precisió és força bona, i particularment destacable el 1% de la lectura assolit en la determinació del poder calorífic del gas natural, o el 0,8% de la lectura per a la densitat. La taula C5.1 mostra un resum dels resultats.

TAULA C5.2 FIGURES DE MÈRIT DE LA CALIBRACIÓ PLS						
Property	Experimental (2-3LV)		Sim. 3LV		Sim. 6LV	
	Abs. Error	R	Abs. Error	R	Abs. Error	R
[CH <sub>4</sub> ]	0.60% (3 LV)	0.9990	0.25%	0.9998	0.12%	0.9999
[C <sub>2</sub> H <sub>6</sub> ]	1.0% (2 LV)	0.9950	0.57%	0.9990	0.41%	0.9990
[CO <sub>2</sub> ]	1.3%(2 LV)	0.5660	1.1%	0.8350	0.58%	0.9470
[N <sub>2</sub> ]	0.90% (2 LV)	0.9900	0.73%	0.9940	0.22%	0.9995
Rel. Error		R	Rel. Error	R	Rel. Error	R
<i>d</i>	0.82% (2 LV)	0.9970	0.54%	0.9990	0.30%	0.9999
<i>SHV</i>	1.0% (3 LV)	0.9920	0.68%	0.9970	0.43%	0.9990
<i>W</i>	1.5% (2 LV)	0.9860	1.0%	0.9980	0.72%	0.9970

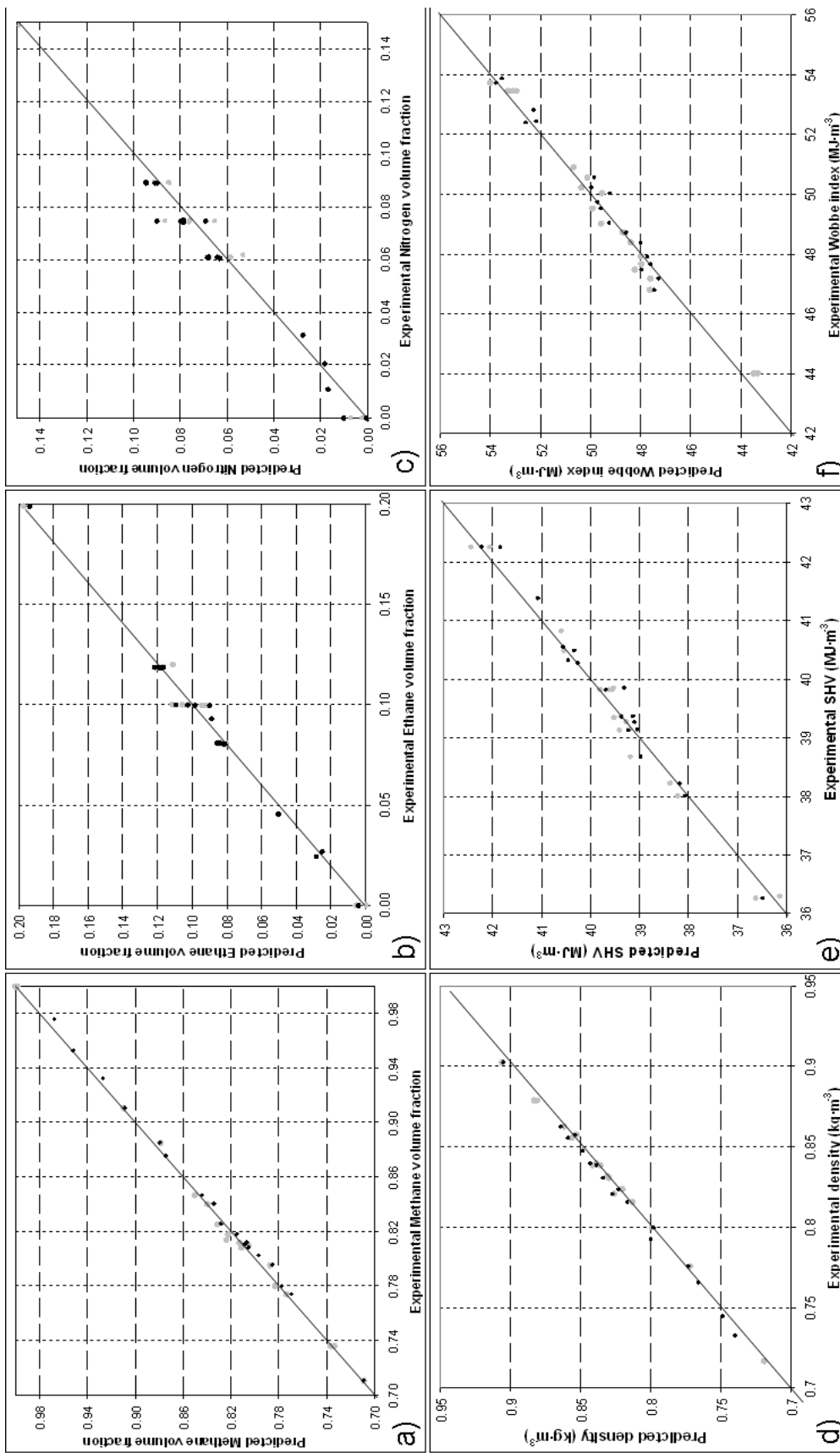


**Figura C5.2 Precisió de les calibracions obtingudes amb PLS.** Les gràfiques a), b) i c) mostren els valors estimats per la calibració contra els valors reals estimats de les concentracions de Metà, Età i Nitrogen respectivament. Les gràfiques d), e) i f) mostren els valors estimats per la calibració contra els valors reals estimats de la densitat, el poder calorífic superior i l'índex de Wobbe. Les línies sòlides mostren la calibració ideal, el pendent unitari.

### C5.3 ESTIMACIÓ DE LIMITS EN LA PRECISIÓ DEL SENSOR

Mitjançant l'anàlisi cuidados de fonts d'error, i amb l'ajut dels resultats de simulació, s'obté una estimació de la precisió assolible per al sistema. Dins de les fonts experimentals d'error, en podem distingir dos grups, un grup de factors que afecten de forma similar a tots els graons de temperatura que conformen la resposta del sensor (mode comú), i un conjunt de fonts experimentals que afecten de forma no correlada els diferents "graons" de la resposta del sensor (errors diferencials). Son aquests últims errors els que limiten més la precisió del sistema, ja que els errors fortemet correlats poden ser rebutjats de forma força efectiva per l'algoritme PLS. Es determina que una disminució de les fonts d'error experimental diferencials permet calcular calibracions PLS més precises, amb un major nombre de variables latents. La figura C5.3 mostra la precisió assolible estimada per a la predicción del poder calorífic superior en funció del factor de reducció (o increment) de les fonts d'error diferencials, per a models PLS de distint nombre de variables latents.

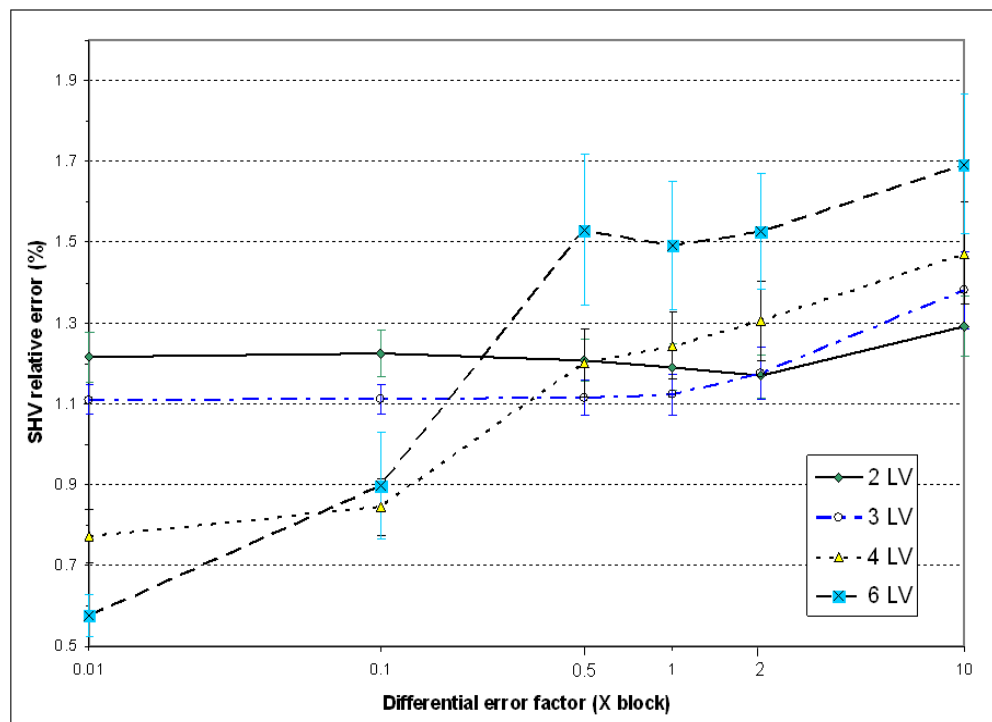


**Figura C5.3. Estimació de la precisió assolible en la determinació del poder calorífic superior, en funció d'un factor modulador aplicat a les fonts d'error diferencial. Les diferents línies mostren calibracions PLS amb diferent nombre de variables latents.**

# C6 DISSENY DE SENSORS QUÍMICS INTEL·LIGENTS: EL PROTOTIP D'ANALITZADOR DE GAS NATURAL

## C6.1 DISSENY DE L'INSTRUMENTACIÓ ELECTRÒNICA

A partir dels resultats anteriors i els conceptes presentats sobre estàndards de sensors intel·ligents es dissenyà un prototip d'analitzador de gas natural basat en IEEE-1451.2 i BS-7986. La figura C6.1 presenta el diagrama de blocs hardware del prototip.

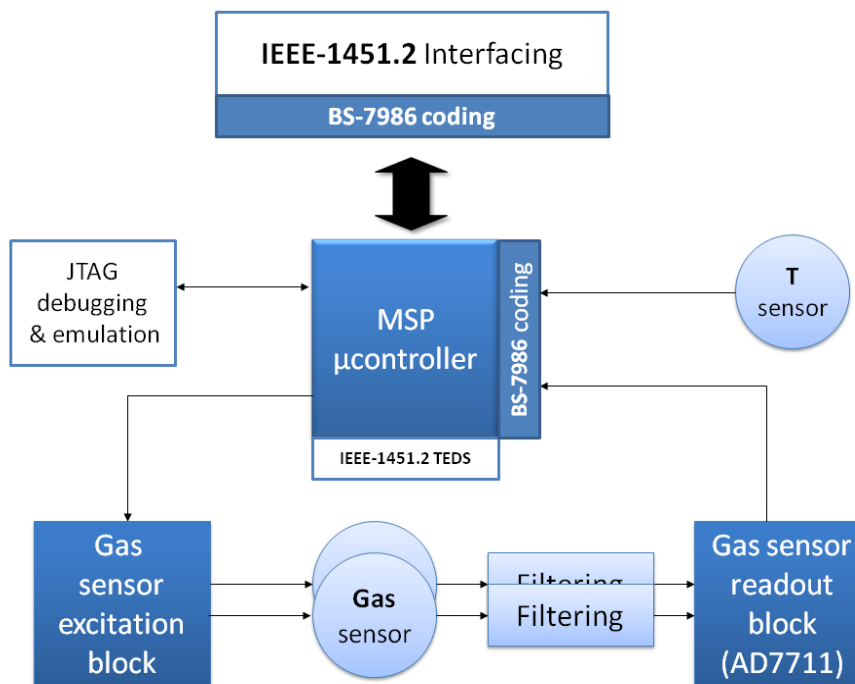


*Figura C6.1 Diagrama de blocs del prototip d'analitzador de gas natural (NGA)*

El prototip presenta dos sensors termoelèctrics, un és emprat per les mesures i l'altre hi és present com a sensor redundant de substitució, hi ha present un bloc d'excitació d'alta repetibilitat així com electrònica de lectura d'alta resolució basada en un conversor analògic-digital AD7711. Es disposa a més d'un sensor de temperatura de Sensirion allotjat a l'interior de la càmera de mesura.

## C6.2 IMPLEMENTACIÓ COMBINADA DE IEEE-1451.2 I BS-7986

---

En aquest treball es proposa una estructura de dades que combina els estàndards IEEE-1451.2 i BS-7986. Aquesta combinació ja ha estat suggerida prèviament, en particular per Karatzas et al. [Karatzas2007]. La implementació realitzada té forces analogies amb la proposta de Karatzas et al. Però amb certes particularitats que s'originen per les particularitats dels sensors químics (especialment sistemes de matrius de sensors) i d'haver mantingut al màxim la estructura básica de IEEE-1451.2 per assegurar el compliment amb l'estàndard. La figura C6.2 presenta un diagrama de blocs de les estructures de dades, oferint-ne dues visions, una desde el punt de vista de la proposta de Karatzas et al. [Karatzas2007] i l'altre desde el punt de vista del contexte de IEEE-1451.2.

A la figura C6.2 apareixen un seguit de blocs que s'expliquen breument a continuació:

**Sensor interface block:** cada sensor presenta una interfície firmware que es comunica amb el hardware de sensat, obtenint-ne les mesures, i proporcionant un nivell basic de processat de senyal.

**Sensor model block:** a [Karatzas2007] el bloc anomenat *Sensor Model Provider* (SMP) s'encarrega de proporcionar un model teòric per a un sensor o tipus de sensors. Aquest model es troba emgatzemat en aquest bloc i es proporciona als altres blocs quan convé. De forma similar, En aquest cas aquest bloc allotja un model basat en dades històriques i la seva correlació. Aquest és un primer nivell de detecció de falle, basat en un algorisme univariant com és el càlcul de la correlació.

**Fault detection block:** El bloc de detecció de falls realitza la detecció de dades defectuoses en base al model proporcionat pel bloc anterior. S'hi assignen codis de qualitat d'acord amb BS-7986. Aquest bloc també seria l'encarregat d'implementar la correcció de les lectures, i assingar els codis BS-7986 corresponents a la mateixa. També s'encarrega del calcul de la incerteza validada VU.

**Internal fusion block:** El bloc encarregat de combinar els diferents sensors (el sensor termoelèctric actua com una matriu virtual de sensors) en una sortida s'anomena Internal fusion block. En aquest cas es efectua una regressió PLS. La regressió multivariant projecta els valors dels sensors (espai d'entrada) en un valor d'una propietat mesurada, en aquest cas el poder calorífic superior (espai de sortida).

Fins aquí s'han descrit els blocs corresponents al costat esquerra de la figura C6.2. La part dreta recull la correspondència amb blocs de l'estàndard IEEE-1451.2 i es descriuen a continuació.

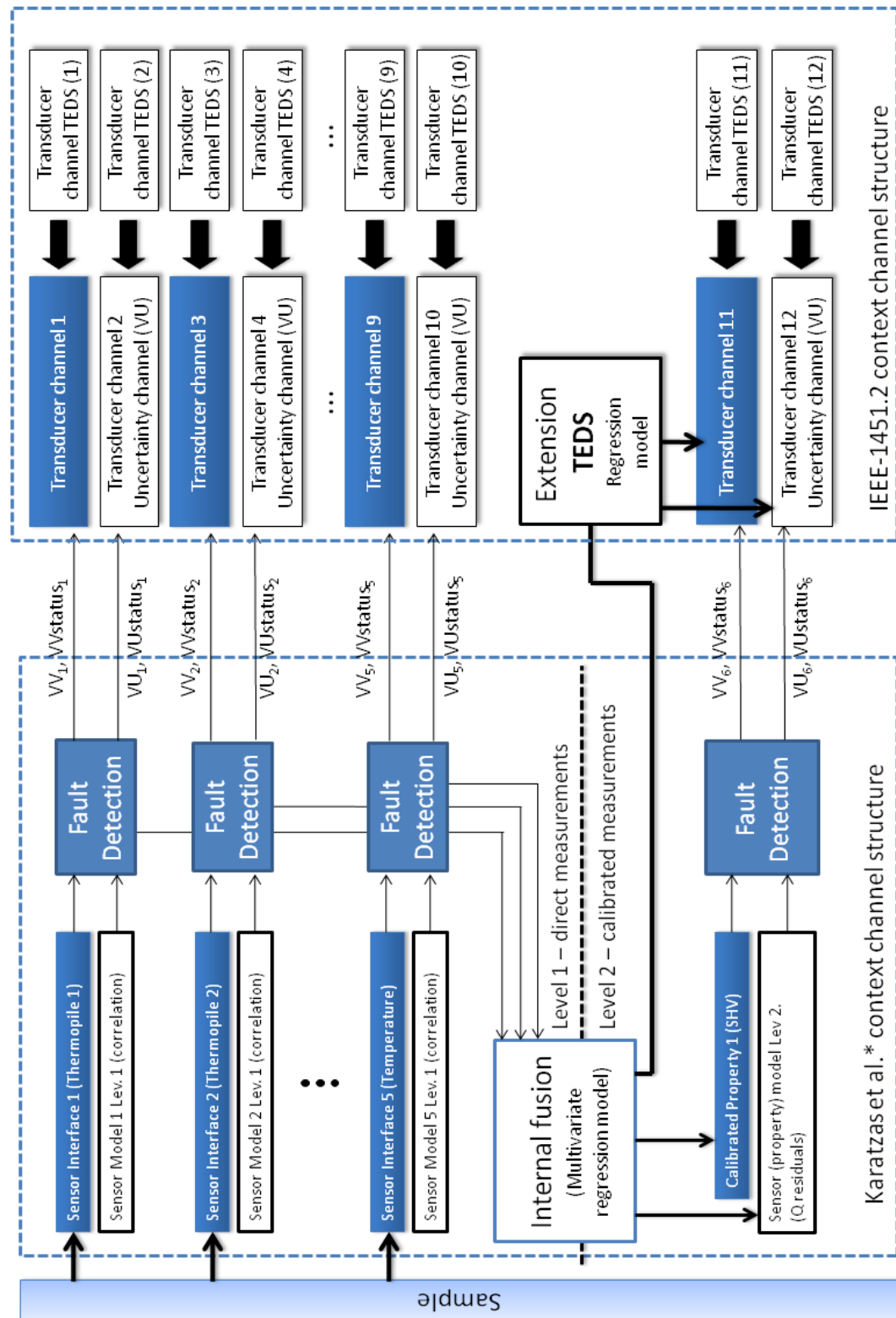


Figura C6.2 Digrama de blocs de l'estructura de dades del prototip mostrant la comparació amb la proposta de Karatzas et al. [Karatzas2007] i l'estàndard IEEE-1451.2 [IEEE1997]

**Transducer channels:** Els blocs constitutius del IEEE-1451.2 son els *transducer channels*, aquests son instàncies normalment associades a sensors o actuadors que interactuen amb fenòmens externs. Tot i així un canal d'aquest tipus també pot contenir informació corresponent a variables internes o combinacions de mesures externes. En aquest cas, els *Transducer channels* 2, 4, 6, 8, 10, 11 and 12 no corresponen a sensors individuals. El canal 11 és una combinació de mesures d'altres canals per calcular una propietat calibrada. Els altres canals(2, 4, 6, 8, 10 and 12) contenen la incertesa validada estimada per el bloc de detecció de falles, d'acord amb la terminologia de IEEE\_1451.2 aquests canals son *sensors virtuals*. Les lectures dels *transducer channels* es proporcionan a la interfície TII sota demanda del NCAP. Les lectures s'actualitzen després de cada comanda de *trigger* ordenada per el NCAP.

**Transducer channel TEDS:** Cada *transducer channel* té associats un nombre de paràmetres i especificacions que es troben formalment definits a les *transducer channel TEDS* (veure taula 30 a [IEEE1997]). A més dels paràmetres tècnics hi ha també unes TEDS d'identificació del canal que contenen cadenes de caràcters útils per a informació de l'usuari. Aquest bloc representa totes les TEDS associades a un *transducer channel*, no només les *transducer channel TEDS*.

**Extension TEDS:** contenen en aquest cas la informació corresponent a la calibració dels canals, en un format propi, més convenient que l'ofert per l'estàndard IEEE-1451.2 a les *calibration TEDS*.

**System Meta TEDS block:** La informació global comuna a tots els sensors s'emmagatzema en aquestes TEDS. També es troben combinades amb unes TEDS d'identificació, de manera similar als canals de transductors.

## C6.3 COMUNICACIONES

---

El prototip dissenyat és un mòdul de sensors (STIM) basat en IEEE-1451.2. Les comunicacions en aquest estàndard es realitzen mitjançant IEEE-1451.2, que contempla una interfície particular anomenada TII. El mòdul de sensors està dissenyat per ésser comandat a través d'aquest TII per un mòdul superior de comunicacions anomenat NCAP. En aquesta implementació, com és habitual en sistemes IEEE-1451.2, el NCAP és un PC. Per a poder comandar el STIM s'ha implementat un adaptador de USB a TII i s'ha realitzat un complet software de comunicacions que permet adquirir i emmagatzemar dades de l'STIM. La figura C6.3 presenta una captura de pantalla del programa.

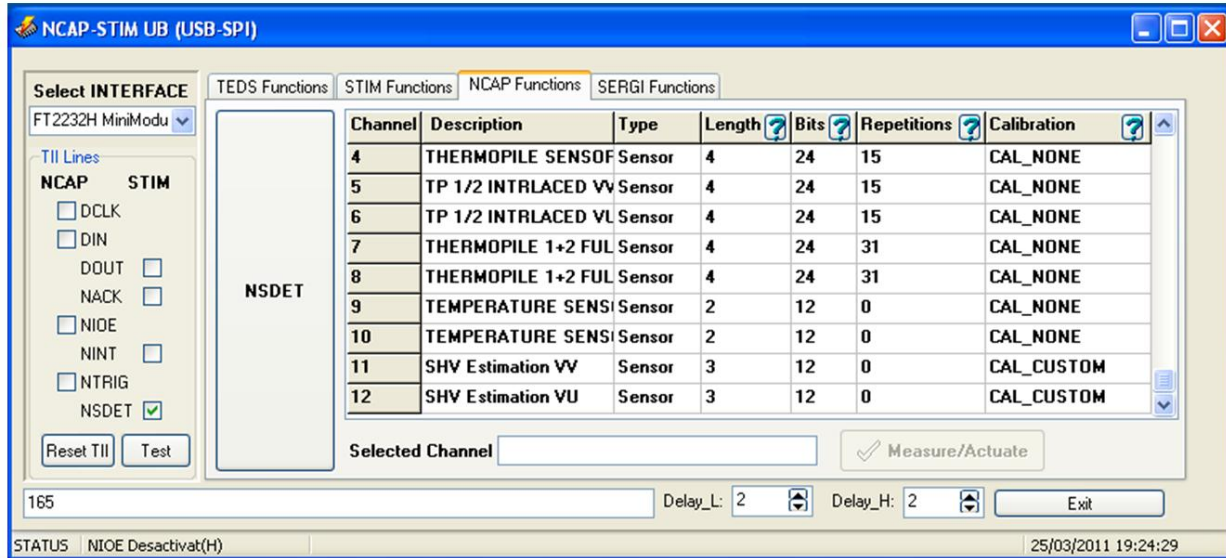


Figura C6.3 captura de pantalla del programa de comunicacions i adquisició de dades NCAP-PC

## C6.4 EXPERIMENTAL

El prototip realitzat incorpora una càmera de mesura a la seva part central tal com es pot observar a la figura C6.4. A l'interior de la mateixa es troben els sensors que realitzen la mesura.

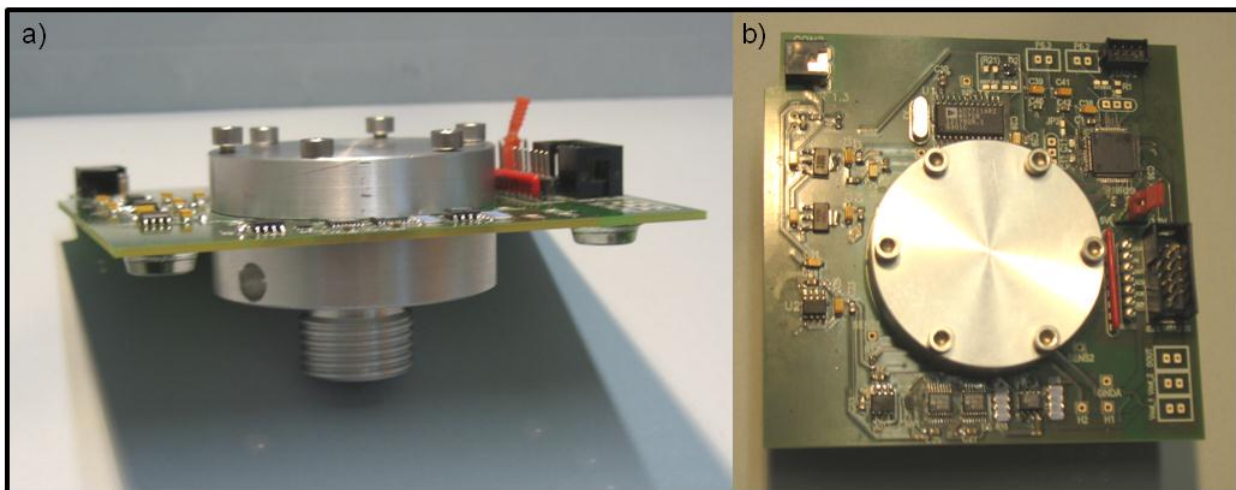
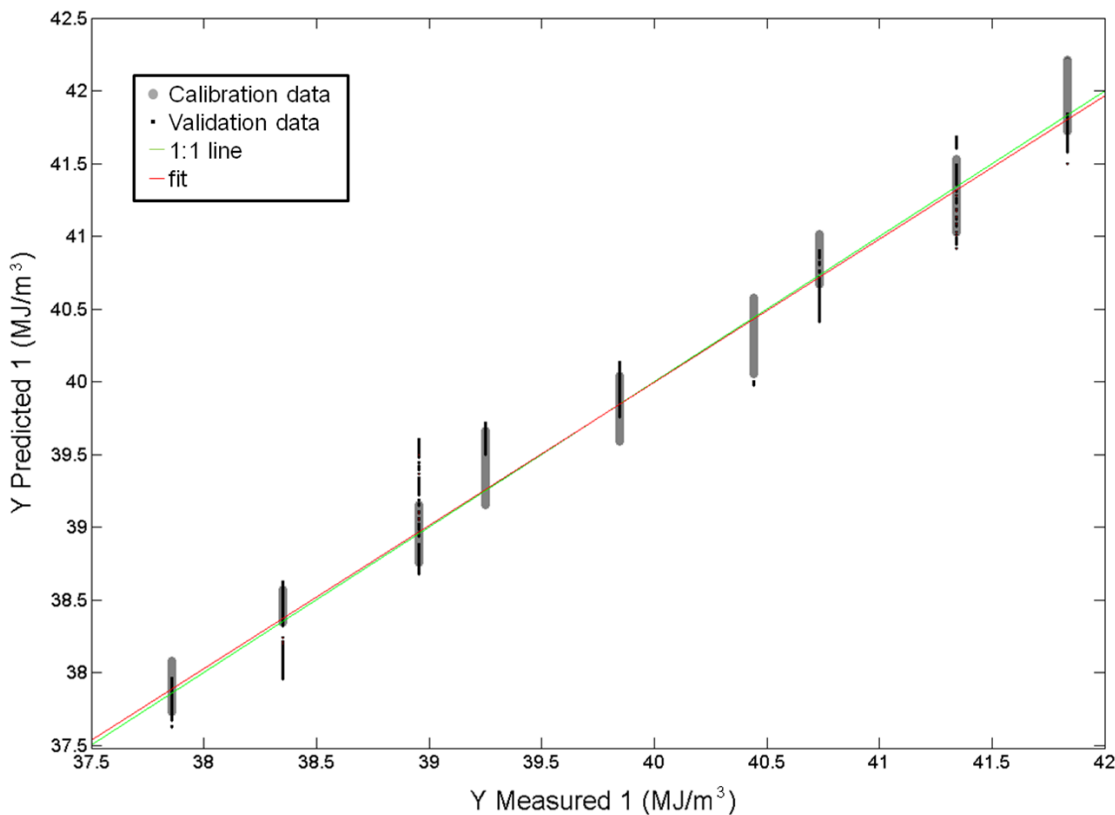


Figura C6.4 Vista lateral (a) i superior (b) del prototip d'analitzador de gas natural.

Per tal de comprobar les especificacions del sistema es realitzen un conjunt de mesures experimentals, recuperant les precisions esperades d'acord amb els estudis anteriors. La gràfica C6.5 mostra els resultats de la calibració per a mesures de validació realitzades dos mesos més tard que les mesures de calibració.



**Figura C6.5 Resultats de calibració i validació per al prototip STIM d'analitzador de gas natural**

Aquests resultats satisfactoris permeten confirmar les especificacions inicials preteses per al prototip i que es troben resumides a la taula C6.1. A més de les comunicacions, el funcionament hardware i la precisió de la calibració, també es testegen els sistemes de detecció d'errades en els sensors, demostrat que és factible la seva implementació conjunta en una estructura conjugada IEEE-1451.2 + BS-7986.

**TAULA 6.1 ESPECIFICACIONS DEL PROTOTIP D'ANALITZADOR DE GAS NATURAL**

<b>Measured Properties</b>	$H_s$ ( $W$ , $\rho$ , $[CH_4]$ , $[C_2H_6]$ , $[N_2]$ , $[C_3H_8]$ , others) <sup>1</sup> )
<b>Ranges of operation</b>	$H_{s(25/0)}$ : 34 – 49 MJ/m <sup>3</sup> $W$ : 43 – 61 MJ/m <sup>3</sup> $d$ : 0.52 – 0.75 Kg/m <sup>3</sup> $[N_2]$ : 0 – 11%* $[CO_2]$ : 0 – 3.5% $[CH_4]$ : 65 – 100 % $[C_2H_6]$ : 0 – 22 % $[C_3H_8]$ : 0 – 3.5%
<b>Communications:</b>	IEEE-1451.2 interface (with smart sensor features)
<b>Fault detection:</b>	BS-7986 coded fault detection
<b>Accuracy:</b>	$H_s$ <1.3% (SNR of sensor readings > 60dB)
<b>Noise rejection:</b>	<i>Heater noise in <math>V_{out}</math>:</i> < 40 $\mu$ V for all steps <i>Voltage reading noise:</i> < 40 $\mu$ V for all steps
<b>Size of prototype PCB:</b>	10 cm x 10 cm
<b>Power consumption:</b>	14-24V - 60 mA max. (0.85 W)
<b>Calibration stability:</b>	>2 months
<b>Analysis time:</b>	<5s

<sup>1</sup> Other properties shall be measured by adapting the calibration

## C7 CONCLUSIONS

---

La recerca presentada ha abarat dos aspectos principals. En primer lloc s'han presentat un sguit de conceptes sobre el disseny òptim de sensors químics intel·ligents. Aquests conceptes s'han basat en la implementació combinada dels estàndards IEEE-1451.2 i BS-7986. S'ha descrit la funcionalitat bàsica d'ambdos estàndards i s'ha exemplificat la seva implementació combinada al capítol 6.

La implementació combinada al capítol 6 ilustra una gamma extensiva de característiques dels sensors intel·ligents:

- Detecció de falles multinivell i auto-avaluació de la qualitat de les mesures
- Auto-identificació a xarxes.
- Connexió en calent a un sistema mitjançant TII.
- Substitució de sensors facilitada per la informació de les TEDS.
- Alta immunitat a errors esporàdics gràcies a la redundància de les lectures dels sensors.

Les línies de treball futur podrien incloure el test extensiu dels algoritmes de detecció d'errades, i la implementació de correcció de dades en temps real, aprofitant l'alta redundància a nivell de sensor. Addicionalment, caldia assegurar el compliment del nou estàndard 1451.2 quan aquest entri en actiu, i la compatibilitat amb 1451.0. Això permetria l'auto-calibració del sistema sense intervenció del NCAP ja que les TEDS de calibració i les rutines de calibració estarien allotjades al mateix STIM.

Tots aquests conceptes han estat aplicats a una proposta d'implementació en una exigent aplicació industrial: l'anàlisi del gas natural.

En segon lloc, l'aplicació d'anàlisi de gas natural ha ofert la oportunitat de millorar alguns aspectes de l'estat de l'art en anàlisi de gas natural, tot emprant tecnologia MEMS. El capítol 4 mostrava l'estudi preliminar del comportament del sensor operat amb una excitació variable del calefactor, i la seva sensibilitat al gas natural, mitjançant simulació per elements finits (FEM). Els resultats indicaven que la possibilitat d'emprar el sensor per a l'aplicació d'anàlisi de gas natural, resultats que es confirmen en aplicar la calibració multivariant tal com s'explica en el capítol 5.

Es demostra en el capítol 5 que a partir de les mesures del sensor es pot estimar el poder calorífic del gas natural i altres propietats amb alta precisió (1% del valor mesurat per al poder calorífic, 0,8% per a la densitat, 1,5% per a l'índex de Wobbe). Addicionalment, es realitza un estudi en profunditat de les fonts d'error que afecten el sensor, i s'elabora una estimació dels límits a la precisió del sensor. Aquest estudi revela que la tecnologia no és apropiada per les aplicacions de màxima precisió ja que s'estimen els límits de precisió en el 0,5% del valor mesurat.

El capítol 6 confirma de nou les precisions estimades prèviament en un prototip funcional d'analitzador de gas natural. Les mesures experimentals del capítol 6 confirmen la extraordinaria estabilitat del sensor que confirma la validesa de les calibracions durant un mínim de dos mesos, i aparentment la estabilitat podria ser força major ja que no es va observar degradació significativa.

El treball futur relacionat amb el sensor podrà incloure un estudi de la estabilitat al llarg de períodes més llargs de temps, la optimització de les formes d'ona d'excitació del calefactor i el disseny de dispositius més ràpids amb una optimització i reducció de la geometria del sensor.

En general, el nou instrument proposat millora les especificacions de tamany, consum electric, rapidesa d'anàlisi i, potencialment, cost.

Finalment apuntar que el concepte sensor presentat pot ser aplicat a l'anàlisi de moltes altres mescles de gasos amb variacions en el rang del tant per cent com ara: biogàs, capnometria de l'alè humà, anàlisi d'atmosferes protectores per alimentació, control de proporció aire-gas en cremadors, anàlisi de productes de la combustió o fins i tot anàlisi estimatiu in-situ de la composició d'atmosferes extra-terrestres.